Investigation of the dynamic interaction between the human body and car seat using a unique simulation technique

by

Purnendu Mondal

A thesis submitted in partial fulfilment of the requirements for the degree of Doctor of Philosophy

University of East London
School of Architecture, Computing and Engineering
May 2020

Abstract

Numerical simulations and mathematical models have been developed over last many years on the certain portions of human body, car seat or automobile to characterise, monitor and assess the level of vibration and its effects on the human occupant inside the automotive. Though, the numerical simulations can define the level and nature of vibration and its transmissibility up to a certain stage, vibration measurement techniques have also been gaining importance for last several years to fill the limitations of the theoretical models. Efforts have also been made to carry out vibration related investigations using combined numerical simulation and measurement procedure for the car seat and the seated human body inside car, though the numbers of case studies carried out with the combination of simulation and measurement procedure are very less. Some technologies have been achieved to judge the level of vibration inside the car seat and its human occupant, though those technologies cover only effects of vibration, dynamics or measurement techniques on specific portions of the car or the human body without considering all the real life factors, e.g., human gender, shape of the human portions, size specific stiffness properties, in-vehicle operating conditions and damping factors. Approaches to provide a comprehensive solution to estimate the level of vibration without real life testing have not been carried out by the existing technologies very well. More than that the existing technologies investigate only particular modules of the entire human-car dynamic systems, e.g., a specific human part, seat and human interaction, vibration transmission from seat to human body or the vibration measurement technique.

So, there is enormous scope of further improvement and the aim of this research work is to provide a unique simulated system considering all the critical real life factors. Outcome of this simulation study will evaluate the vibration levels inside the segments of seated human body inside a car and car seat omitting the necessity of real-life practical testing and provide the solution by linking module-wise investigations of human body and car seat. Initiative has been taken to fill up the gaps in the existing technologies and

Abstract

offer a novel study on the comprehensive simulation model of the combined human body and car seat bio-dynamic system to optimize the health, safety and comfort levels of the car seated human body.

Present research work covered the tasks of establishing the simulations for non-linear bio-dynamic model of the seated human body, feasibility and behaviour inspection of polyurethane foam cushions, contact mechanism assignment between the human body and the car seat and establishing the simulation of car seated human occupant under the real life environment. Vertical displacements, vertical accelerations and frequencies at designated points of human body and car seat have been extracted from the simulation outcome and the obtained results have been validated though real-life vibration testing data. This unique simulation methodology can successfully be implemented to predict the final vibration levels inside the car seat and the car seated human body to optimize the health, safety and comfort of the human-car seat system. The outlined novel technique contributed knowledge to the entire human body and car seat dynamic system rather than focusing only on a very specific portion of the system.

An industrial guideline has been presented to implement this unique simulation methodology in similar sectors, which will lead various industries to avoid time consuming and expensive bio-dynamic vibration testing methods and help to understand the impact of vibration on the in-vehicle human body in a better way.

Acknowledgments

I would like to express my profound appreciation to Dr. Subramaniam Arunachalam, Director of Studies and Professor Hassan Abdalla, second supervisor for their kind assistance and support throughout the whole period of this research.

I would like to thank the University of East London for providing the comfortable environment and the computing facilities to accomplish this research in the School of Architecture, Computing and Engineering (ACE).

Special thanks are dedicated to Mr. Ian Black from m+p International (UK) Ltd, for providing practical test data to validate the simulation results. I am indebted to m+p International (UK) Ltd for all their helps and supports.

Declaration of originality

I hereby declare that the work presented in this PhD thesis, is my own original work. Information derived from other research works, have been appropriately cited.

Purnendu Mondal

May 2020

Table of Contents

List of Figures

List of Tables

CHAPTER 1
INTRODUCTION

Over last many years, interaction between the dynamic automotive and its occupant playing important role to characterise the levels of safety and comfort of the vehicle system. Parts of the system or subsystem of the aviation, automotive, railway etc. industries are exposed to unwanted vibration cause of the movement and it is necessary to investigate the dynamic behaviour of the transportation medium under normal and extreme operating conditions.

One of the primary means of transportation system worldwide is the automobile and any kind of automobile must offer highest standard of the safety and comfort levels for the occupants inside. The health, safety and comfort levels of the automotive systems are mainly analysed through the complex mechanical phenomenon between the moving object and human occupant, which demands a robust dynamic study. Automotive seats are mainly made of polyurethane foam, which exhibits non-linear viscoelastic and hyper-elastic material properties. So, the overall system of human body, moving vehicle and foam seat constitute a complicated dynamic system with nonlinearities inside.

Health, safety and comfort of the dynamic vehicle, human body and transportation seat are mainly determined by the level of the vibration generated inside the system and random level of vibration plays the key role for producing uneven stresses inside the human body and automotive seat through deformation and harmonic excitation. Thus, a comprehensive evaluation is needed to characterise the level of vibration inside the

automotive seat and seated human body depending on the nature of the dynamic nonlinearity. This project will outline a computer based model of the car seated human body to evaluate the vibration data inside the car seat and its occupant.

Few technologies to judge the level of vibration are existing in the market to characterise the dynamic behaviour of the car seat and human body, but most of these technologies are based on the practical measurement tests. Many research studies were also conducted based on the computer simulation process in the past many years, though most of those researches covered only a particular portion of the human body or the car seat. Moreover, those research works collected the major parameters like stiffness values, damping levels etc. from the past researches or available data source, instead of evaluating the case specific parameter values. All the latest computer based technologies provided solution to predict the level of vibration inside part of car seat or human body in conjunction with practical experiment, but the number of research works to estimate vibration based on simulation only, are almost negligible. Both the existing experimental and simulation technologies provide the vibration data only for a very specific modules of car seat and human body system like particular human body portion, seat to body vibration transmission, human-seat interaction, pressure distribution on the car seat cushion or vibration measurement methodology. Research approaches to take into account the entire human body and car seat, are very less in number.

This research work aims to provide a comprehensive solution with a novel finite element simulation methodology to predict the final levels of vibration at different points of car seat and its human occupant in dynamic environment without conducting any practical experiment or measurement. This novel simulation technique will improve the latest technology for in-vehicle vibration assessment using dynamic interaction between the human and automotive seat subjected to real life environmental conditions. Furthermore, this technique will co-relate the damping values, three dimensional stiffness and frequencies inside the human portions to the age and shape specific human segments. This research study will make another unique effort to represent the human body using

ellipsoidal segments to define the three dimensional stiffness for each part of human body, hence, necessity of modelling the time consuming real anatomical shapes of the human structures will be omitted. For the calculation of the three dimensional stiffness, both the human muscle and bone properties will be taken into account. This unique study will establish a novel idea about the entire human body and automotive seat system, rather than concentrating only to a specific segment, hence, will fill up the gap in the latest relevant technologies and avoid the cost burdening and time consuming practical test methods. A cutting edge technology will be contributed by this unique study to the modern transportation industry to estimate and understand the vibration data inside automotive seat and seated human body, solely based on computer simulation method.

1.1. LITERATURE REVIEW

The purpose of this literature review is to explore some of the different variables of the vibration, analysis techniques and measurement procedures which influence the final outcome of the effect of the vibration inside the human body seated on a car seat, in terms of human health, safety and comfort levels. Literature review in this section is a part of the overall critical review conducted throughout this research study. Review in precise details for appropriate subject has been carried out in the respective sections as needed.

1.1.1. Numerical Simulation relating to Vibration

Over past few decades, vibration along with its effect on the car seat and occupant human body has been getting characterised, measured and assessed either by numerical model or computerized simulation process. Finite element analysis of the whole vehicle using dynamic environment in ABAQUS (Hellman, 2008) stated that because of the high cost involved with the production process of a new vehicle model, computerized simulation methods for dynamic analyses are gaining more importance for the development of the automobile system.

1.1.1.1. Multi Degrees of Freedom Bio-Dynamic Model of Seated Human inside a Car

Numerical algorithm along with multiple Degrees of Freedom (DOF) theory was applied during the biodynamic study of the car seated human body using one number of seven DOF model and two numbers of four DOF models (Abbas et al., 2010) to understand the vibration transmissibility.

The same study considered some optimized parameter values for the simulation like stiffness values, frequencies, damping coefficients etc. mainly for finding the responses due to vertical vibration and recommended that the consideration of full vehicle body would be beneficial for finding more accurate resonance frequency of the system.

Biodynamic research for the vibration transmissibility on the human body seated inside a car (Abbas *et al.*, 2010) using mathematical algorithm was conducted using one number of seven degrees of freedom model and two number of four degrees of models, which found the limits of the vibration transmissibility. The degrees of freedom systems are shown in Fig. 1.

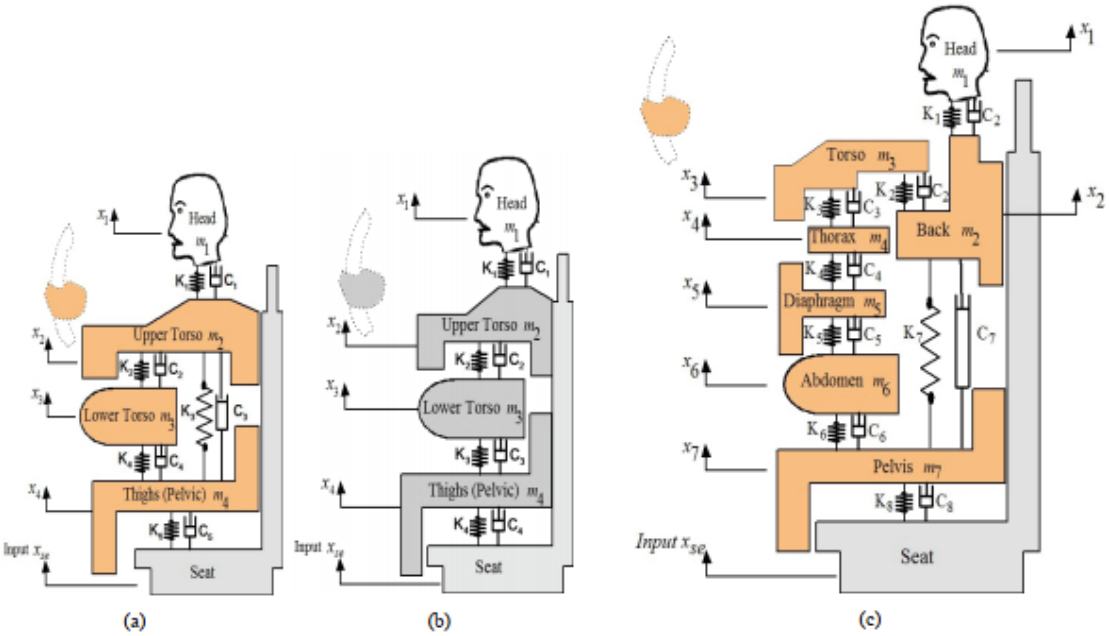

Fig. 1. Biodynamic Model with 4- DOF (left and middle) and 7-DOF (right) (Abbas *et al.*, 2010)

That study further evaluated some optimized factors for the analysis like damping-coefficients, stiffness values etc. under the effects of vertical vibration. That theoretical research was useful for biodynamic responses of the human body exposed to vertical vibration and recommended to consider the entire car body to find more appropriate ranges of natural frequency of the human-seat structure. The optimized parameters were presented through graph and table as shown in Fig. 2.

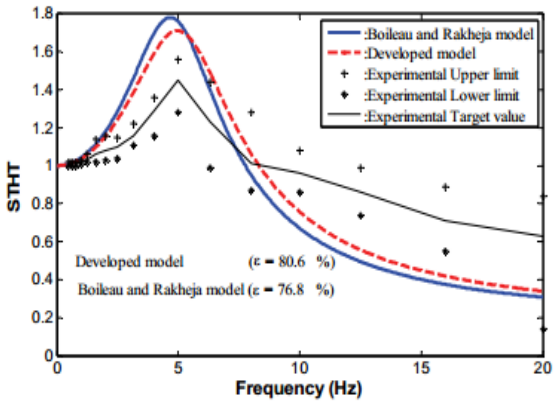

Mass (kg)	Damping coefficient (N.s/m)		Spring constant (N/m)	
	Before	After	Before	After
m_1 = 5.31	c_1 = 400	c_1 =460	k_1 = 310000	k_1 = 356370
m_2 = 28.49	c_2 = 4750	c_2 =5400	k_2 = 183000	k_2 = 208570
m_3 = 8.62	c_3 = 4585	c_3 =5190	k_3 = 162800	k_3 = 187110
m_4 = 12.78	c_4 = 2064	c_4 =2370	k_4 = 90000	k_4 = 103480

Fig. 2. Optimized parameters for human-seat system under the effect of vertical vibration (Abbas *et al.*, 2010)

1.1.1.2. Car Seat in contact to Human Body and Vibration Transmissibility

Kinematics study of the car seat in the pre-stressed condition (Williamson, 2005) made a conclusion that the contact mechanism between the human body and car seat and its establishment would be the most significant part to obtain effective results from the computer simulation. Similar type of research work on the human body and car (Burdzik and Konieczny, 2014) found the vibration and acceleration values at different locations of a car and concluded that the vibration distribution would be the major issue inside the car. Vibration transmissibility was numerically interpreted in between the automotive seat and human body (Mansfeld and Griffin, 2000). Responses of the human body against the vibration exhibited the nonlinearities with different vibration magnitudes. The same study showed that the vibration magnitude would increase while lowering the frequency level.

Car seat resonating characteristics were investigated using vibration energy theorem (Batt, 2013) which stated that the loss in energy of the car seat system would mainly occur cause of upper human part movement and not all the car seats would be appropriate to absorb the vibration energy close to the primary natural frequency. Study on the car seated human body for vibration analysis (Kitazaki and Griffin, 1998) suggested that the forces responsible for the entire human body vibration could not be accurately predicted unless the human motion and postures be not taken under consideration. That analysis could further be improved by taking into account the nonlinear biodynamic responses to the human body vibration.

Locations of the minimum and maximum level of vibrations in a car seat at the human-seat interface with respect to variable frequency (Tang *et al.*, 2010) were shown using finite element analysis. That finite element method was useful for predicting the vibration transmissibility in the two dimensional environment and could further be developed to advance level by using three dimensional format.

1.1.1.3. Harmonic Vibration and Frequency

Car bonnet was simulated using finite element method for harmonic frequency (Nesaragi *et al.*, 2014) analysis to show the amplitude of vibration with respect to frequency. The frequency range was considered from 1 Hz to 100 Hz, while the engine was assumed to be in ideal condition and the operating speed of engine had been considered as 1000 rpm. The bonnet frequency was found to be higher than 20 Hz, well distant from the engine frequency of 16 Hz. Similar simulation based analysis on the car engine parts (Nesaragi *et al.*, 2014) had chosen the damping co-efficient and stiffness values from the engineering data book and described that the mounting locations of the sensors during vibration measurement would play very important role for assessing the vibration levels inside the structure.

1.1.1.4. Vibration generated inside Human Body Portions

Human spinal segments were investigated (Guo *et al.*, 2011) for vibration analysis to find out the natural frequencies and found that the amplitudes of vibration at different points of a same human spine were different. Similar kinds of statements were made from the investigation on the vibration characterizing of human portions (Goel *et al.*, 1994) and dynamic study of human intervertebral lumbar joints (Kasra *et al.*, 1992).

1.1.1.5. Vibration inside Car Body or Portions

Lumped mass parameter method was implemented to one fourth of a car model for vibration analysis (Thite, 2012) using the Maxwell's theorem. That study co-related the damping co-efficient, damping ratio and stiffness parameter and found the vibration responses with respect to variable damping and series stiffness parameters. It was concluded that the series stiffness would be beneficial for reducing the level of damping inside the car.

1.1.2. Vibration Measurement

Mathematical or numerical simulation method for judging the level, nature and transmissibility of vibration is based on the theoretical concepts, hence, got some limitation from practical point of view. Vibration measurement techniques are more practical based on exact real life scenarios and can fill the limitations of the theoretical concepts. So, in the modern industries, vibration measurement techniques also got huge importance to monitor and characterise the vibration level inside the dynamic structures.

1.1.2.1. Vibration Measurement and Resonant Frequencies

The significance of the vibration measuring system for the human body and the car seat assembly was examined (Ittianuwat *et al.*, 2014) in compliance with the international standard of vibration ISO 2631-1 (1997). A comparative study was carried out further by

measuring vibrations at different locations with respect to different mode shapes and natural frequencies.

1.1.2.2. Vibration Transmissibility Measurement using Accelerometer and Mode Shape

The common practice for real life vibration measurement in car seat is to mount the sensors or accelerometers at the central locations of the seat cushion and backrest. But research showed (Tamaoki *et al.*, 2012) that the vibration transmissibility measured as the central location was based only on the fundamental frequencies in the range of 1 Hz to 10 Hz and the measured transmissibility of vibration from the seat to human body was not accurate enough. Another experimental study (Lo *et al.*, 2013) explored the structural dynamics of the coupling of the car seat and human body and found the fundamental frequency was ranged in between 10 Hz and 50 Hz. That analysis further found three natural frequencies for three respective mode shapes, below 80 Hz. Experiment was carried out to find out the relation between natural frequency and transmissibility of the car seated human body (Cho and Yoon, 2001) and extracted one fundamental mode shape of the human body at 4.2 Hz, while two mode shapes appeared for the head at 4.2 Hz and 7.7 Hz.

1.1.2.3. Vibration Peak Transmissibility with varying Weight, Posture and Car Speed

Observation made on an experimental car (Ford Focus, V817 LAR, Zetec, and 2.0L) at a speed of 35 miles/ hour to 45 miles/ hour to investigate the vibration transmission (Qiu and Griffin, 2004) from the seat to human body. Two number of sample masses of 70 kg and 80 kg were used in the fourth gear of the running car and the primary peak transmissibility occurred in-between 4 Hz and 5 Hz. Results from that study showed that a single input and single output system would be sufficient for examining the vertical vibration transmission, but not for the horizontal vibration transmission. Study on the car seat backrest for fore-aft vibration transmissibility (Abdul and Griffin, 2007) and nonlinear vertical vibration transmission of the car seat (Tufano and Griffin, 2012)

reported that vertical inclination and position would play vital role for determining the vibration transmissibility from seat to human object.

1.1.2.4. Estimation of Stiffness and Damping values for Human Body and Car Seat

Essential factors like stiffness and damping values were estimated during the analysis of human-seat assembly (Cho and Yoon, 2001) using a multi degrees of freedom model. The used estimated values are presented in Table 1.

Table 1. Estimated biomechanical parameters of Multi-DOF model (Cho and Yoon, 2001)

Mass (kg) and Inertia (kg m^2)	Stiffness (kN/m)	Damping (Ns/m)
m_1 15.3±2.5	k_{v1} 72.0±25.3	c_{v1} 29.4±14.4
m_2 36.0±6.0	k_{h1} 46.3±10.9	c_{h1} 447.0±167.1
m_3 5.5±0.9	k_{v2} 2.3±0.8	c_{v2} 0.4±0.8
I_1 0.9±0.20	k_{h2} 20.2±7.1	c_{h2} 446.0±165.4
I_2 1.10±0.25	k_{t1} 17.2±4.6	c_{t1} 380.6±77.5
I_3 0.03±0.00	k_{t2} 25.0±18.4	c_{t2} 182.1±40.1
	k_{r1} 0.0±0.0	c_{r1} 2576.5±1006.4
	k_{r2} 0.1±0.0	c_{r2} 1.3±1.7

1.1.2.5. Compact Vibration Measurement System inside Human Body and Car Portions

Practical testing on the vibration measurement system (Stein *et al.*, 2011) on a moving car (Skoda sedan) for academic purpose was conducted using a compact testing set up consisted of few accelerometers, data acquisition system and a laptop. That experiment was not as per the guidelines of vibration standard ISO 8041, though the entire system showed the process of measuring the vibration in cost-friendly way without the requirement of any special equipment. Another related experiment was conducted on the physical car to measure the vibration levels (Lakušić *et al.*, 2011) at heel and chassis. In

between the time interval of 0 second and 48 second, the vibration values for wheel and chassis were measured as 21.2 mm/s and 6.1 mm/s, respectively and in-between the time interval of 48 second and 112 second, the vibration values for wheel and chassis were measured as 12.7 mm/s and 4.5 mm/s, respectively.

1.1.3. Combined Numerical Simulation and Measurement of the Vibration for both the Human Body and Car Seat

Numbers of research case studies to investigate the car seat and the human body using combined simulation process and testing method, are found to be very rare. Effort had been made to explore the literatures covering both the topics relevant to this study.

A comprehensive investigation had been conducted on the car seat and human object (Verver, 2004) for the comfort analysis of the human body. That elaborative study used finite element method for analyzing the human and seat assembly and mainly focused on the vibration transmissibility. From the simulation result, it was concluded that the acceleration transmission from seat to human body was strongly reliant on the human body posture. During the stage of experimental process, the vibration transmissibility for seat to human body and seat pressure distribution were evaluated, though the international standard for seat pressure ISO 2631 was not followed and no seat frame and cushion springs were taken into account. The outcome of that study recommended to conduct a more in-depth investigation on the human model for accurate analysis of vertical vibration. Dynamic behaviour of seat were examined to estimate the car seat transmissibility (Zhang, 2014) using the mechanical modelling and measurement methods. Seat foam properties, human shape, damping and stiffness were included inside the finite element simulation and it was reported that the thickness of the automotive seat cushion would be one of the primary factors to affect the vibration transmission from the seat to the occupant. That study further investigated the sitting posture and suggested for more comprehensive investigation on the contact condition between seat and human.

Both the research works were restricted to the experiment and finite element simulation without carrying out any sort of real life vibration testing.

Human body vibration responses with respect to various sitting postures were evaluated using real testing method (Ruetzel and Woelfel, 2005) to provide a set of frequency and damping data against the human body mass. Damping, frequency and mass data were interlinked by two number case studies with 95 kg and 50 kg human masses. Later a simulation model was established using the finite element tool to compare the results obtained from the testing. That study advised for further research to optimize the characteristics of vibration with respect to human sitting posture.

1.1.4. Matrix based comparative study on Literature Review

Based on whether the investigation type is analysis or testing based, the most important key research literatures have been identified and a matrix based comparison model has been developed in Table 2 with the importance levels assigned depending on the chosen elements. In this matrix based study, each literature has been allocated with a score between 2 and 10 depending on the number of key element considered during the relevant research work, which helps to obtain a clear view on the existing technologies and their specific areas of the work on the human body and car interfaces.

Table 2. Comparative study of literature review on human body and car seat

	Title of the literature	Type of project		Significant research elements considered									No. of elements	Brief view
		Analysis and simulation	Testing	Car body or part	Car seat	Human body	Stiffness	Damping	Vibration	Vibration transmission	Real life test	Lab test	2-5=Low 6-8= Medium 9-10= High	
1	Abbas *et al.*, 2010	√			√	√	√	√	√				6	Development of the biodynamic model of the seated human using multi dof theory and mathematical algorithms.
2	Tang *et al.*, 2010	√			√	√	√	√	√	√			7	Finite element simulation of the human body and car seat.
3	Ruetzel, and Woelfel, 2005	√	√		√	√	√	√	√	√		√	9	Case study of the whole body vibration characteristics with respect to specific parameters. Experimental data of modal analysis.

	Title of the literature	Type of project		Significant research elements considered									No. of elements	Brief view
		Analysis and simulation	Testing	Car body or part	Car seat	Human body	Stiffness	Damping	Vibration	Vibration transmission	Real life test	Lab test	2-5=Low 6-8= Medium 9-10= High	
4	Qiu and Griffin, 2004		√		√				√	√	√		5	Experimental set up for vibration transmissibility from car to seat. Numerical algorithm of the practical measurement.
5	Stein *et al.*, 2011		√	√	√				√		√		5	Real life experiment to gather field vibration data using accelerometers and acquisition system.
6	Ittianuwat, *et al.*, 2014		√		√				√	√		√	5	Experimental set up for measuring the vibration transmissibility of the car seat at more than one location.

	Title of the literature	Type of project		Significant research elements considered									No. of elements	Brief view
		Analysis and simulation	Testing	Car body or part	Car seat	Human body	Stiffness	Damping	Vibration	Vibration transmission	Real life test	Lab test	2-5=Low 6-8= Medium 9-10= High	
7	Lakušić *et al.*, 2011		√	√					√			√	4	On road testing using sensors and accelerometers.
8	Hong *et al.*, 2003		√		√	√		√	√			√	6	Set up for improving the car seat properties for increasing the level of comfort.
9	Cho, *et al.*, 2001		√		√	√	√	√	√	√		√	8	Experimental set up to develop a biomechanical model of human on a seat.
10	Paddan and Griffin, 2002		√		√	√	√	√	√			√	7	Measurement of seat effective amplitude transmissibility value in different vehicles and prediction of whole-body

	Title of the literature	Type of project		Significant research elements considered									No. of elements	Brief view
		Analysis and simulation	Testing	Car body or part	Car seat	Human body	Stiffness	Damping	Vibration	Vibration transmission	Real life test	Lab test	2-5=Low 6-8= Medium 9-10= High	
														vibration influenced by seat dynamics.
11	Kim *et al.*, 2003	√	√		√	√	√	√	√			√	8	Numerical and experimental set up to predict the vibration response of mannequin occupied car seats.
12	Cheung and Zhang, 2006	√				√	√						3	Simulation of the human foot.
13	Silber and Then, 2009	√				√							2	Analysis during human motion and movement.
14	Pick and Cole, 2005		√			√					√		3	Electromyography of the human muscles while driving.

	Title of the literature	Type of project		Significant research elements considered									No. of elements	Brief view
		Analysis and simulation	Testing	Car body or part	Car seat	Human body	Stiffness	Damping	Vibration	Vibration transmission	Real life test	Lab test	2-5=Low 6-8= Medium 9-10= High	
15	Konieczny, 2016		√	√			√	√	√			√	6	Testing of the car absorber in an efficient way.
16	Nesaragi *et al.*, 2014	√		√			√	√	√				5	Vibration and noise analyses of car bonnet.
17	Guo *et al.*, 2011	√				√			√				3	Modal analysis for human spine.
18	Ezenwa and Yeoh, 2011	√				√	√	√	√				5	Multiple vibration displacements at multiple vibration frequencies on human femur.
19	Thite, 2012	√		√			√	√	√				5	Vibrational analysis of quarter car model.
20	Hellman, 2008	√		√			√	√	√				5	Complete vehicle dynamics are

	Title of the literature	Type of project		Significant research elements considered									No. of elements	Brief view
		Analysis and simulation	Testing	Car body or part	Car seat	Human body	Stiffness	Damping	Vibration	Vibration transmission	Real life test	Lab test	2-5=Low 6-8= Medium 9-10= High	
														analysed.
21	Verver, 2004	√	√	√	√	√	√	√	√	√		√	10	Complete investigation of human and car body interactions has been carried out.
22	Williamson, 2005	√			√	√	√		√				5	Analysis on the interaction between human and car seat.
23	Burdzik and Konieczny, 2014		√	√					√		√	√	5	Many point vibration measurement inside car using lab and road testing.
24	Batt, 2013	√	√		√		√	√	√			√	7	Harmonic excitation inside the car seat material.

	Title of the literature	Type of project		Significant research elements considered									No. of elements	Brief view
		Analysis and simulation	Testing	Car body or part	Car seat	Human body	Stiffness	Damping	Vibration	Vibration transmission	Real life test	Lab test	2-5=Low 6-8= Medium 9-10= High	
25	Kitazaki and Griffin, 1998	√	√		√	√	√	√	√			√	8	Resonance behaviour of the seated human body has been modelled numerically.
26	Mansfeld. and Griffin, 2000	√			√	√	√	√	√	√			7	Numerical interpretation of the vibration transmissibility in between the human body and car seat.
27	Shan *et al.*, 2012		√		√		√	√	√	√		√	7	Vibration characterization of seat foam material.
28	Fang, 2013	√					√	√	√	√		√	6	Simulation on the vibration transmission inside engine components with small experimental set

	Title of the literature	Type of project		Significant research elements considered									No. of elements	Brief view
		Analysis and simulation	Testing	Car body or part	Car seat	Human body	Stiffness	Damping	Vibration	Vibration transmission	Real life test	Lab test	2-5=Low 6-8= Medium 9-10= High	
														up.
29	Singh *et al.*, 2003	√	√		√		√	√	√			√	7	Estimation of dynamic properties of the car seat using numerical modelling and experimental set up.
30	Pattern *et al.*, 1998	√	√		√		√	√	√			√	7	Establishing vibration model of the car seat using numerical modelling and experimental set up.
31	Zhang, 2014	√	√	√	√	√	√	√	√	√		√	10	All the areas of the car, seat and human body interactions have been investigated.

	Title of the literature	Type of project		Significant research elements considered									No. of elements	Brief view
		Analysis and simulation	Testing	Car body or part	Car seat	Human body	Stiffness	Damping	Vibration	Vibration transmission	Real life test	Lab test	2-5=Low 6-8= Medium 9-10= High	
32	Sitnik *et al.*, 2013		√	√					√		√		4	Laser doppler vibrometry and digital signal have been used on a non-moving car to find out the vibration magnitude.

1.1.5. Research Gap in the Existing Technologies and Aims & Objectives of the Current Research Work

From the critical review of the relevant literatures, it is inevitably clear that over past many years, segments of automotive structures, car seats and human bodies have been examined through the computerized simulation process to judge the level and nature of vibration and associated effects on the health and safety of the human being. Aside of simulation techniques, efforts have also been taken to monitor and characterise the level of vibration using some measurement techniques and experimental methods. Both the simulation technique and the measurement process got the distinct advantages and disadvantages, though the usability of a certain method completely depends on the application of the dynamic object of interest. In few cases, approaches have been taken to combine the simulation and testing methods for evaluating the vibration inside human body and car seat, though the existing numbers of research tasks with combined simulation and testing are significantly less.

Technologies are available in the academic areas and industries to investigate the dynamic nonlinear interaction between the automotive seats and the human occupant, though most of the existing technologies cover only a very specific portion of the entire human-car system or a very particular module of the vibration science. Typical considerations by these present technologies for the human-seat system are mainly based on an exact human part, seat-human contact interface, seat pressure distribution, human and seat modal analysis, human and seat postures, seat to head transmissibility, frequency response and power spectrum density, etc. Moreover, stiffness values of the human portions have been taken from past research work, rather than trying to evaluate for a definite case scenario. Simulation methods of these technologies also neglected the real life conditions coming from dynamic vehicle.

Initiatives to deliver a complete solution to predict and assess the vibration inside human-car system without the need of real testing operation, have not been conducted by the available techniques so well. So, enormous scope of future improvement in the field of vibration measurement using computer based simulation technique is there and this research project aims to provide a unique simulation methodology to predict the final vibration level inside human and car seat by taking into account the car seat, human body, calculated stiffness of each segment of the human body, damping parameters, ellipsoidal bodies to represent human segments and acceleration-displacement-frequency functions with respect to time. The outcome of this research will help to assess and monitor the human health, safety and comfort against the automotive vibration, which will eventually eliminate the necessity of the time consuming and expensive testing method in the modern transportation industries. This study will conduct module-wise analyses of the car-human system and propose a comprehensive novel simulation technique to estimate vibration data inside the entire human body and car seat assembly by interconnecting all the module based investigation.

The industrial market for estimating the accurate level of vibration inside the automotive-human system has been growing worldwide in exponential rate and already a number of organizations with excellent infrastructure are pre-existing in the market for providing the vibration related solutions to the portions of the automotive and its occupant. Hence, a cutting edge technique will be contributed to the modern industries by this unique simulation methodology and this research study will fill the technical gaps existing in present vibration measuring technologies by providing a comprehensive solution to predict the level of vibration at various locations of the entire human body and car seat.

So, based on the discussion in this section, the objectives of this research project are listed next.

1. To carry out literature review to understand the health, safety and comfort levels of a seated human body whilst driving.

2. To carry out a critical analysis of existing simulation techniques used in vibration study of the car seat and human body.

3. Develop simulated models for seated human body, non-linear behaviour of car seat and combination of both.

4. Validate the simulation model by comparing simulated results to real-life test data.

5. Propose guidelines to implement the developed simulation model in similar industries, preferable automobile.

1.1.6. Research Questions

a. What will be the best technique to carry out simulation for the entire human-car seat system to achieve real life results?
b. How the health, safety and comfort levels of the car seated human body can be optimized?
c. How accurate will the simulation data be with respect to test data?
d. What will be the limitations of the finite element simulation to represent different phases?
e. How the project outcome can be implemented to the similar industries?

1.2. PROPOSAL OF A NOVEL TECHNIQUE AND RESEARCH METHODOLOGY

The steps for this unique methodology will be critical literature review followed by computerized simulation of car seated human body, simulation set up of car seat, establishing contact mechanism between car seat and human body, simulation of combined human body and car seat to get desired output, collection of testing data from similar real life environment, validation of simulation results with testing data and finally outlining a guideline to implement this technique in similar industries. All the phases are summarized in Fig. 3.

Fig. 3. All the phases of the research study

1.2.1. Literature Review

Literature review on the existing technologies has been carried out critically for defining research gap and proposed plan of work. Further explorations and review of literatures have been conducted throughout the span of this research study.

1.2.2. Biodynamic Simulation of Car-Seated Human Body

The most convenient way to understand the impact of the vibration on human body is to evaluate the fundamental frequencies and relevant mode shapes of the dynamic system and constructing the numerical model is the classic approach for extracting these natural

frequencies and associated mode shapes. From the main structure the assembly and sub-assembly of interest can be isolated and the equations of motion based on stiffness and damping can be established. From the set of equations generated, modal matrix can be obtained through repetitive iteration process, which eventually will be the sign of the biodynamic responses of the system. Cause of the human limitation of solving very complex numerical equations, computerized tools are more preferable choice for analyzing the robust structures.

For the biodynamic simulation of the human body, stiffness, damping, human muscle and bone properties and real life loading condition will be taken into account which will yield a complicated non-linear simulation set up. The simulation can be structured by using either the finite element tool like ABAQUS CAE, ANSYS Workbench, etc. or numerical computational programming tool like MATLAB.

Existing techniques for the human biodynamic analysis will be explored and the most convenient and justified technique for this project will be implemented to the simulation process.

1.2.3. Simulation for Non-Linear Mechanical Behaviour of Car Seat

Car seats are primarily made of polyurethane foam material, though different types of materials can be used, too. These materials are non-linear in nature and exhibit hyper-elastic and viscoelastic behaviour. The best possible material properties and simulation technique will be explored and will be applied to the simulation of the car seat for this project using preferable finite element tool like ABAQUS CAE, ANSYS Workbench, etc.

1.2.4. Determine the Contact Mechanism between Human and Seat in the Analysis Environment

Establishing the contact interface between the car seat and human body and defining the appropriate dynamic contact formulation will be the main aim of this phase. Different kinds of contact formulations are available in the applied mechanics science, though many of these formulations are not useable cause of the limitations of software and computer system.

After exploring the past research works on the relevant contact interfaces and understanding the timeframe for solving the analysis in accessible computer system, most suitable contact mechanism will be chosen for this project.

1.2.5. Simulation of combined Human Body and Car Seat under Real Life Scenario

Once the biodynamic model for the human body and the non-linear simulation of the car seat will be established, the human and seat model will be combined together in the analysis environment and all the possible real life input condition will be implemented. Output from the this simulation will the vibration data at the designated points of the human body and cat seat by means of acceleration, displacement or frequency. The type of the output and the data to be extracted from the result, will be decided depending on the facility available inside the analysis tool. This phase will give an idea of the level of vibration occurring inside car seated human, hence, the health, safety and comfort levels will be assessed.

1.2.6. Collecting and Processing Test Data

Test data will be gathered for the car seat-human set up ideally identical to the simulation. In case, the test data received from an environment different from simulation set up, the computerized simulation has to be amended to match to the test condition.

Test set up and output data from testing are expected to be as shown in Table 3.

Table 3. Estimated experimental set up and output

Parameter	Value/ Designated point
Vehicle speed	Around 35 mile/ hour
Human body mass	In the range of 70 kg to 80 kg
Expected output	Acceleration with respect to time and frequency.
Duration of testing	In the range of 0 second to 60 seconds
Locations of vibration measurements	For occupant body- Head (preferable forehead), Chest (at front center), Upper arm (at middle), Lower arm (at middle), Waist (back center), Thigh (at middle), Leg (at middle) For car seat- Headrest (at center), Backrest (at center), Cushion (at center)

"m+p International (UK) Ltd" is a renowned international organization for measuring noise, assessing vibration and data acquisition systems. The testing data for the human body and car seat will be collected from them.

1.2.7. Comparison between Simulation Results and Test Data

Simulation results will be validated by the testing data. The formats of the testing data received and the simulation results should be matching to each other in terms of parameter, unit, duration, etc. In case of mismatch, the simulation results can be adjusted to match to the simulation output parameters. Raw data received from the testing can be processed to a convenient format, if needed.

A comparison table or matrix will be prepared to represent the contrast between test data and simulation results.

1.2.8. Developing Industrial Guideline to Implement the Unique Simulation Technique to Relevant Sectors

Though this simulation project is based on the seat and human object inside a car, the unique simulation method outlined in this project work can also be used as a generic guideline for the transportation seat and its occupant for other similar industries. So, a comprehensive instruction manual will be presented which can be implemented to other relevant transportation industries for judging the level of vibration and optimizing the human occupant's health, comfort and safety.

CHAPTER 2
BIO-DYNAMIC MODEL FOR SEATED HUMAN BODY INSIDE A CAR

A human body can be considered as a complex mechanical system, the biodynamic behaviour of which differ in many aspects. Biodynamic responses of the different systems have been proposed with many different models and for different purposes. For a better understanding of the biodynamic responses along with whole body vibration, simulation model development became well accepted method for last many years. This method became more reliable to judge the human body dynamics cause of rapid improvement in the computer technologies, especially in the fields of Computer Aided Design (CAD) and Computer Aided Engineering (CAE).

Biodynamic model may not necessarily take into account all the real life input parameters, but should identify and implement the factors with highest priority. A wide range of human biodynamic models has been explored for many years based on different postures and input functions. The simulation modeling techniques for human dynamics mainly have been classified in few categories like lumped mass model, finite element model and multi-body dynamics model. Kinematic studies consider only the motion without any accountable force, hence, kinematic models are not considered during the current study. Different categories of biodynamic model for establishing simulation are shown in Fig. 4.

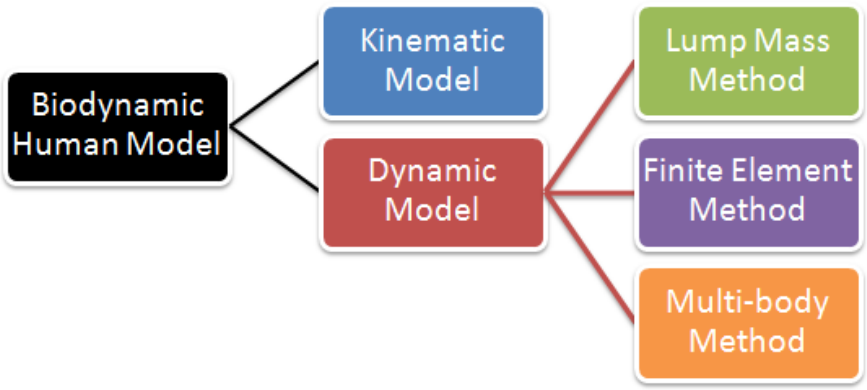

Fig. 4. Methods for biodynamic human modelling

This chapter describes the research activities carried out on the human model exposed to the whole body vibration using lumped mass method, finite element technique and multi-body dynamics. Experimental studies have been carried out on lumped mass and finite element methods along with finding limitations of different techniques. Based on the limitation and identifying the potential areas of further development, a unique technique for biodynamic simulation has been proposed and elaborated in this chapter.

2.1. LUMPED MASS MODEL

Mathematical formulation of the human body dynamics can be simplified using lumped mass parameters to describe the whole model into one or two dimensional spatial area. This model consists of rigid body masses connected through springs and dampers. Lumped models are very useful in judging the human body response in the vertical direction and widely used for validating the experimental results.

A very basic lump mass system with masses and stiffness elements is shown in Fig. 5.

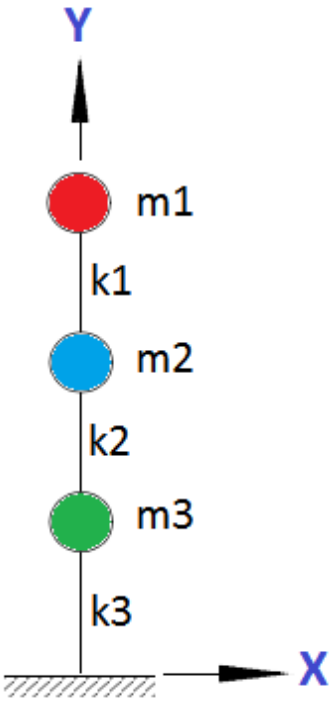

Fig. 5. Simple lump mass model

The basic procedure of this method is to set up the equations of the motion of the whole system and solving the parameters using an iterative process. The outputs obtained from this technique are natural frequencies, mode shapes and eigen values of the system.

2.1.1. Past works on Lumped Mass Model related to Human Body Dynamics

Over the last few decades, numerous numbers of bio-dynamic researches have been carried out on the human postures using lumped mass method.

A seated human body with 15 degrees of freedom (DOF) shown in Fig. 6, was established by utilizing the anthropometric data and using lump mass parameters (Nigam and Malik, 1987), where 15 rigid body masses were considered along with 14 functional joints. The outputs were mainly the natural frequencies in the vertical direction which were hugely matching with the permissible range of frequencies for the human portions.

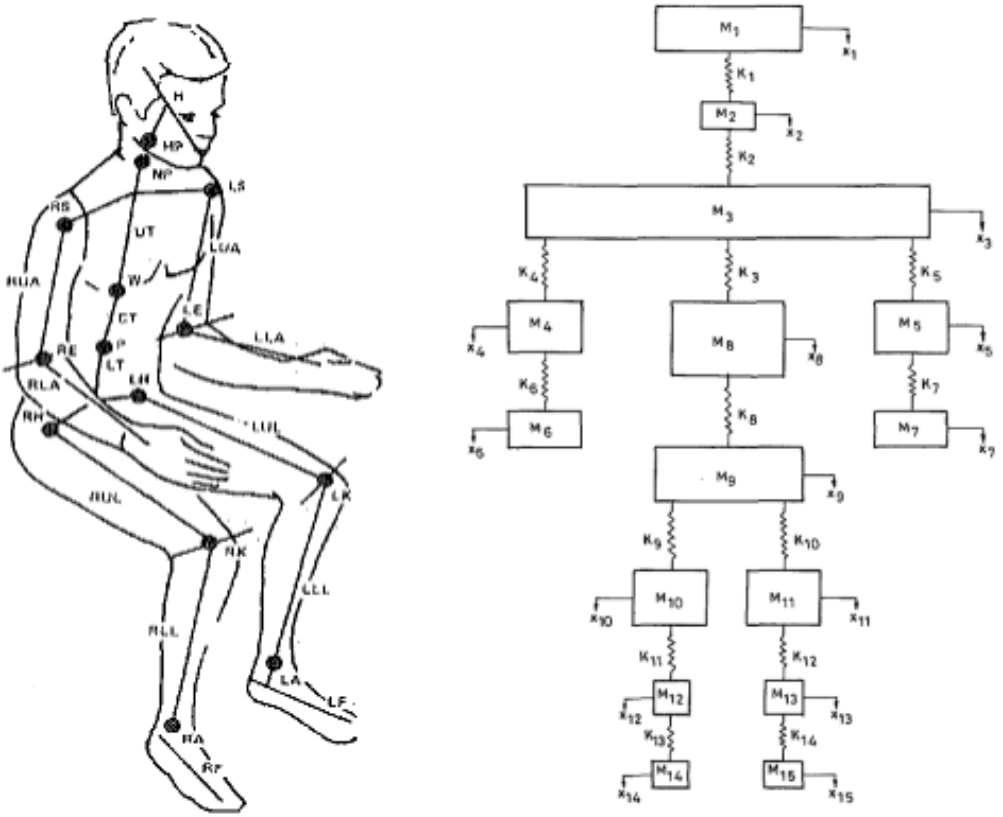

Fig. 6. 15 DOF lumped mass model (Nigam and Malik, 1987)

Dynamic ride quality was investigated (Kim *et al.*, 2001) considering the level of vibrations inside the human body and SEAT (seat effective amplitude transmissibility) values. Three linear axes at feet, three linear axes on seat and 2 linear axes on backrest of the seat were considered. That investigation observed that the level of vibration inside human body was greatly influenced by the sitting posture.

Lumped masses connected through dampers and springs, were used as a dynamic human model (Kim *et al.*, 2005) to fit the data of apparent masses. Vertical vibration and vibration transmissibility were successfully extracted from this model.

Biomechanical model of seated human body was proposed (Cho and Yoon 2001) using 1 DOF, 2 DOF, 3 DOF and 9 DOF lumped mass models to describe the whole body vibration and the ride quality through vibration transmission. The 9 DOF model showed justified results for the first two mode shapes. All the lumped mass models are shown in Fig. 7.

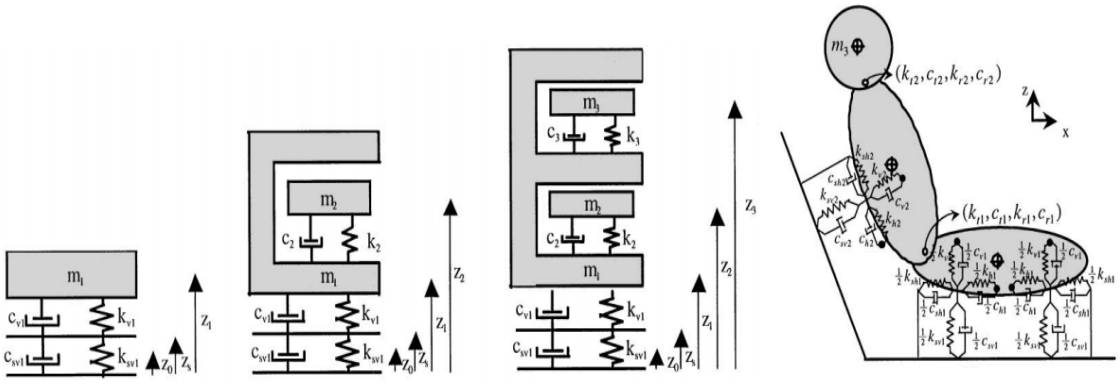

Fig. 7. 1, 2, 3 and 9 DOF Lumped Mass Models (Cho and Yoon, 2001)

During the study of seated human exposed to the whole body vibration (Zengkang *et al.*, 2001), a lumped mass model was developed as shown in Fig. 8, to represent seat-to-head transmissibility (STHT), driving-point mechanical impedance (DPMI) and apparent mass (APM). That method considered both the vertical and fore-aft directions.

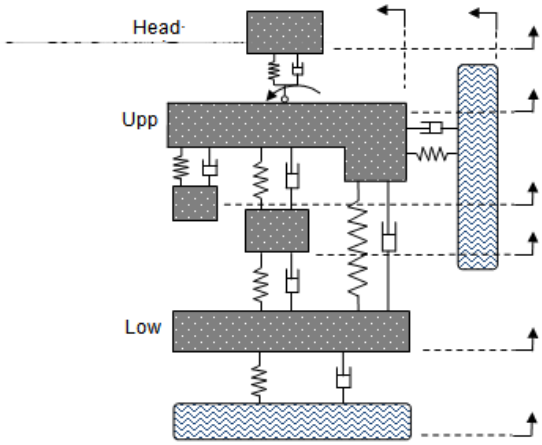

Fig. 8. Lumped Mass Model for seated human in both vertical and fore-and-aft directions (Zengkang *et al.*, 2013)

A four-DOF vertical model had been constructed (Wan and Schimmels, 1995) to find the highest average of goodness-of-fit and another four-DOF lumped model had been developed (Boileau and Rakheja, 1998) to analyse the vertical vibration. A two-DOF lumped model had been established (Stein *et al.*, 2005) for judging the fore-aft vibration and a four-DOF model was presented (Qiu and Griffin, 2011) to show the fore-aft vibration with apparent mass. All the models are shown in Fig. 9.

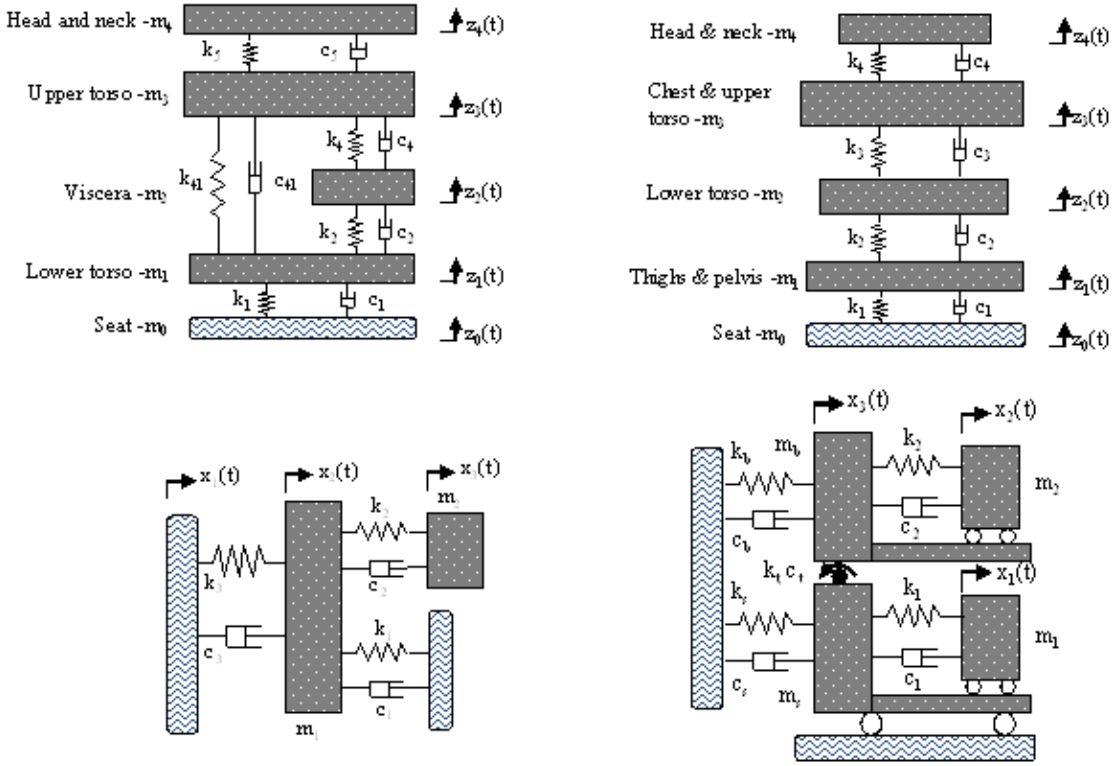

Fig. 9. Lumped Mass Models used for comparative studies (Zengkang *et al.*, 2013)

Top Left - Four-DOF vertical model (Wan and Schimmels, 1995)

Top Right- Four-DOF model (Boileau and Rakheja, 1998)

Bottom Left- Two-DOF model (Stein *et al.*, 2005)

Bottom right- Four-DOF model (Qiu and Griffin, 2011)

Vertical mass of seated subjects was represented (Fairley and Griffin, 1989) using a single DOF lumped mass model where the sprung, unsprung and foot interaction were simulated using different masses (m_1, m_2 and m_3, respectively). The arrangement of that model is shown in Fig. 10.

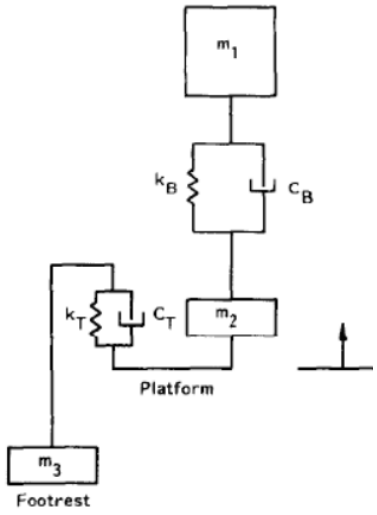

Fig. 10. Single DOF Model for mean vertical apparent mass subject (Fairley and Griffin, 1989)

Stiffness and damping values were defined (Wei and Griffin, 1998) using a 1 DOF Model with complex dynamic stiffness. In the same study, another 2 DOF model was considered to define the apparent mass and estimate the seat transmissibility. Though, both the models as shown in Fig. 11, were giving good results, the 2 DOF model predicted the outputs in more accurate way.

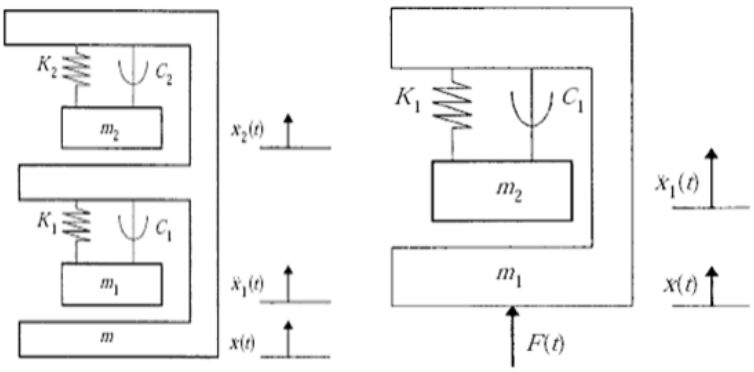

Fig. 11. 2 DOF (Left) and 1 DOF (Right) Models (Wei and Griffin, 1998)

A 7 DOF lumped mass model considered (Muksian and Nash, 1974) the human pelvis, back, abdomen, thorax, torso and head, which stated that the vibration response of the seated human in the vertical direction was non-linear in nature. The set-up is shown in Fig. 12. The same lumped model extended the research and made a conclusion that the outputs were matching to experimental data up to 6 Hz considering linear damping elements and above 6 Hz considering non-linear damping elements.

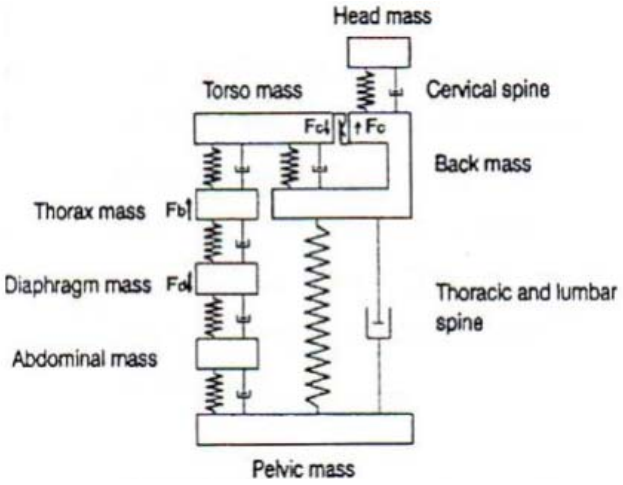

Fig. 12. 7 DOF Non-Linear Lumped Mass Model (Muksian and Nash, 1974)

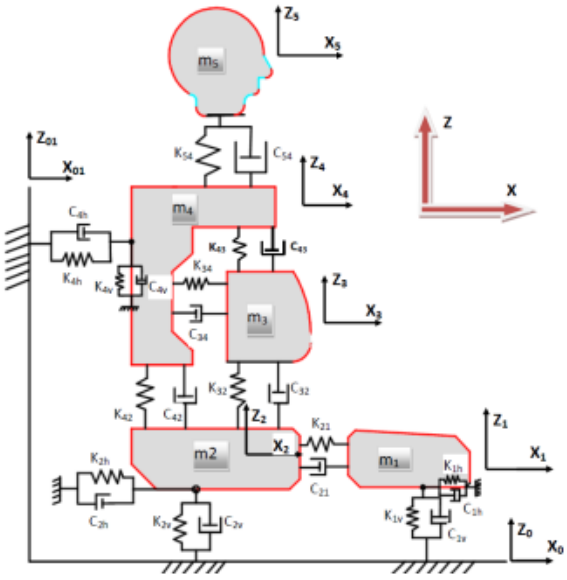

Parameters	Representation
m_1	Upper Leg(left + right)
m_2	Pelvic
m_3	Viscera (Soft abdominal body parts)
m_4	Upper Torso (Including hands)
m_5	Head and neck
c_{4h}, c_{4v}	Back horizontal and vertical dampers
c_{2v}, c_{2h}	Pelvic vertical and horizontal dampers
c_{1v}, c_{1h}	Upper leg vertical and horizontal dampers
k_{4h}, k_{4v}	Back horizontal and vertical springs
k_{2v}, k_{2h}	Pelvic vertical and horizontal springs
k_{1h}, k_{1v}	Upper leg vertical and horizontal springs
c_{21} up to c_{54}	The respective dampers between body segments
k_{21} up to c_{54}	The respective springs between body segments

Fig. 13. 9 DOF two dimensional Lumped Mass Model (Harsha *et al.*, 2014)

A seated human body was depicted with a 9 DOF lumped mass model (Harsha *et al.*, 2014) where the whole body was exposed to low frequency environment. Twelve numbers of male subjects were considered mainly in three sitting postures under three magnitudes of vibration (0.4, 0.8 and 1.2 m/s^2 rms) in frequency range of 1 to 20 Hz. The results suggested that more the numbers of factors would be considered, more the accurate design and analysis could be carried out. The typical arrangement for that experiment and the parameters are shown in Fig. 13.

International standard on mechanical vibration and shock (ISO 5982, 2001) gives a guideline on selecting specific values of different parameters to characterise biodynamic response of seated human body under vertical vibration. It suggests that a 3 DOF lumped mass model can be taken under consideration as displayed in Fig. 14, to describe the apparent mass and transmissibility related dynamic problems. This standard helps to define the ideal values of driving-point impedance, apparent mass and transmissibility.

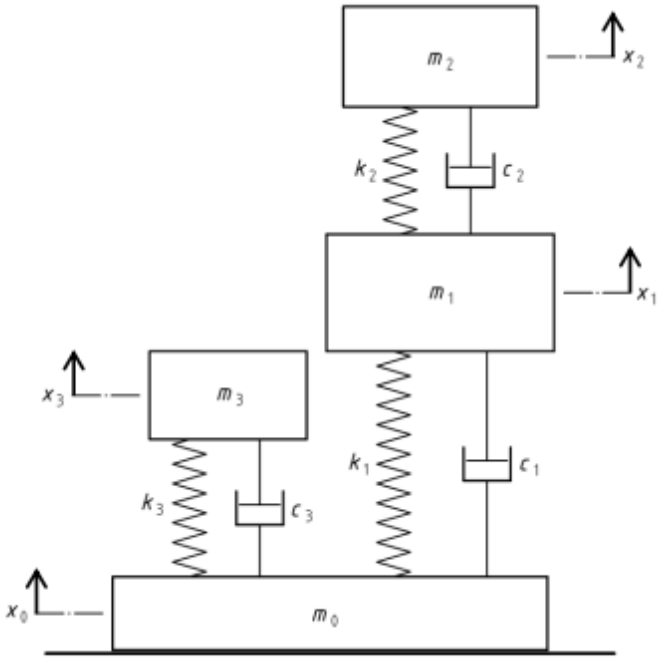

Fig. 14. 3 DOF Lumped Mass Model as per International standard on mechanical vibration and shock (ISO 5982, 2001)

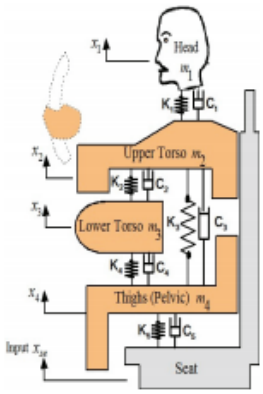

$$
\begin{cases}
m_1\ddot{x}_1 = -c_1(\dot{x}_1 - \dot{x}_2) - k_1(x_1 - x_2) \\
m_2\ddot{x}_2 = c_1(\dot{x}_1 - \dot{x}_2) + k_1(x_1 - x_2) - c_2(\dot{x}_2 - \dot{x}_3) \\
-k_2(x_2 - x_3) - c_3(\dot{x}_2 - \dot{x}_4) - k_3(x_2 - x_4) \\
m_3\ddot{x}_3 = c_2(\dot{x}_2 - \dot{x}_3) + k_2(x_2 - x_3) \\
-c_4(\dot{x}_3 - \dot{x}_4) - k_4(x_3 - x_4) \\
m_4\ddot{x}_4 = c_4(\dot{x}_3 - \dot{x}_4) + k_4(x_3 - x_4) + c_3(\dot{x}_2 - \dot{x}_4) \\
+k_3(x_2 - x_4) - c_5(\dot{x}_4 - \dot{x}_{se}) - k_5(x_4 - x_{se})
\end{cases}
$$

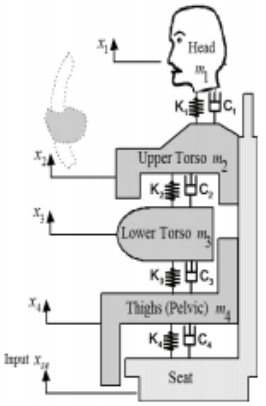

$$
\begin{cases}
m_1\ddot{x}_1 = -c_1(\dot{x}_1 - \dot{x}_2) - k_1(x_1 - x_2) \\
m_2\ddot{x}_2 = c_1(\dot{x}_1 - \dot{x}_2) + k_1(x_1 - x_2) - c_2(\dot{x}_2 - \dot{x}_3) \\
-k_2(x_2 - x_3) \\
m_3\ddot{x}_3 = c_2(\dot{x}_2 - \dot{x}_3) + k_2(x_2 - x_3) - c_3(\dot{x}_3 - \dot{x}_4) \\
-k_3(x_3 - x_4) \\
m_4\ddot{x}_4 = c_3(\dot{x}_2 - \dot{x}_4) + k_3(x_2 - x_4) - c_4(\dot{x}_4 - \dot{x}_{se}) \\
-k_4(x_4 - x_{se})
\end{cases}
$$

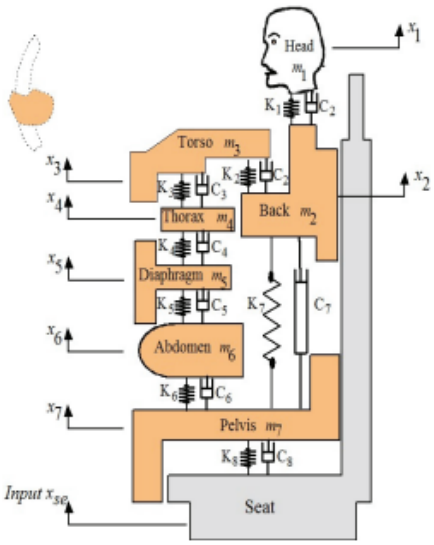

$$
\begin{cases}
m_1\ddot{x}_1 = -c_1(\dot{x}_1 - \dot{x}_2) - k_1(x_1 - x_2) \\
m_2\ddot{x}_2 = c_1(\dot{x}_1 - \dot{x}_2) + k_1(x_1 - x_2) - c_7(\dot{x}_2 - \dot{x}_7) \\
-k_7(x_2 - x_7) - c_2(\dot{x}_2 - \dot{x}_3) - k_2(x_2 - x_3) \\
m_3\ddot{x}_3 = c_2(\dot{x}_2 - \dot{x}_3) + k_2(x_2 - x_3) - c_3(\dot{x}_3 - \dot{x}_4) \\
-k_3(x_3 - x_4) \\
m_4\ddot{x}_4 = c_3(\dot{x}_3 - \dot{x}_4) + k_3(x_3 - x_4) - c_4(\dot{x}_4 - \dot{x}_5) \\
-k_4(x_4 - x_5) \\
m_5\ddot{x}_5 = c_4(\dot{x}_4 - \dot{x}_5) + k_4(x_4 - x_5) - c_5(\dot{x}_5 - \dot{x}_6) \\
-k_5(x_5 - x_6) \\
m_6\ddot{x}_6 = c_5(\dot{x}_5 - \dot{x}_6) + k_5(x_5 - x_6) - c_6(\dot{x}_6 - \dot{x}_7) \\
-k_6(x_6 - x_7) \\
m_7\ddot{x}_7 = c_6(\dot{x}_6 - \dot{x}_7) + k_6(x_6 - x_7) + c_7(\dot{x}_2 - \dot{x}_7) \\
+k_7(x_2 - x_7) - c_8(\dot{x}_7 - \dot{x}_{se}) - k_8(x_7 - x_{se})
\end{cases}
$$

Fig. 15. Representation of a human body with different configurations (Abbas *et al.*, 2010)

Top - Four-DOF model (Wan and Schimmels, 1995)

Middle- Four-DOF model (Boileau and Rakheja, 1998)

Bottom - Seven-DOF model (Patil *et al.*, 1978)

Study performed on development of the biodynamic model of the seated human using multi Degrees of Freedom theory and mathematical algorithms (Abbas *et al.*, 2010), which evaluated the range of vibration transmissibility based on the optimized frequency, stiffness and damping co-efficient. That study also performed a comparative study on how the different researches split up the human body and body portions into different segments to construct most efficient lump mass model. Based on the different model set ups, different sets of characteristics equations were set up to solve the dynamic parameters related to vibration responses. The same research work studied a 4 DOF model (Wan and Schimmels, 1995), another 4 DOF model with slightly different arrangement (Boileau and Rakheja, 1998) and a 7 DOF model (Patil *et al.*, 1978) with different lump mass arrangements to show how the solving equations of motions could be derived differently. Fig. 15 is representing all the models described in that investigation.

2.1.2. Experimental Simulation work carried out on human bio-dynamics based on Lumped Mass Method to find out Natural Frequencies and Mode Shapes

The basic principle of lumped mass model is to consider the human portions as concentration point masses and then to connect these masses with the help of spring and damping elements, followed by constructing the set of characteristic equations using Newton's second law. The set of equations can be solved in a manual iterative way or by some mathematical software tool to get the mode shapes and natural frequencies of the system. The equation set up can be changed based on whether the system is influenced by free or forced vibration.

To understand how the lumped system works theoretically, a very basic human upper body consists of head and torso had been considered as shown in Fig. 16. To reduce the complexity in solving the equations during this experimental work, all other portions of

the human body had been ignored. The equivalent lumped mass system is also shown in Fig. 16. The stiffness values k_1 and k_3 can be considered as 0, while the stiffness value k_2 is the stiffness between the human head and human torso.

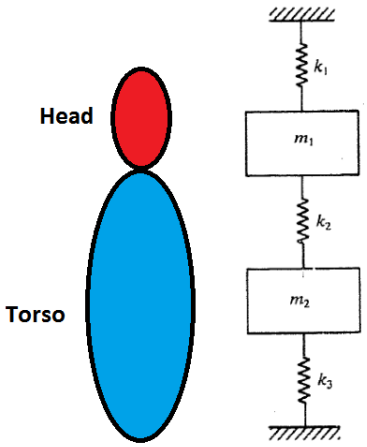

Fig. 16. Human head and torso represented through lumped mass model

The masses of the head and torso are considered as 4.30 kg (42.169 N) and 29.03 kg (284.687N), respectively while axial stiffness values for head and torso are considered as 623633236.74 N/m and 1545963178.02 N/m, respectively. The lengths of the head and torso are taken as 15.66 cm and 29.90 cm, respectively. The details of these assumed data are elaborated in the CHAPTER 3.

Starting from the equations of motion, the system has been solved using characteristics equations. This small experimental work has been carried out using analytical software tool Mathcad. First two natural frequencies and modes shapes have been evaluated.

The equations of motion are formed and presented in Equations 2.1 and 2.2.

$$m_1 \cdot \frac{d^2}{dx_1^2} x_1 + k_1 \cdot x_1 - k_2\left(x_2 - x_1\right) = 0 \quad \ldots \qquad \text{(Eq. 2.1)}$$

$$m_2 \cdot \frac{d^2}{dx_2^2} x_2 + k_2 \cdot (x_2 - x_1) + k_3 \cdot x_2 = 0 \quad .... \qquad \text{(Eq. 2.2)}$$

Where,

m_1, m_2= Masses of head and torso, respectively.

k_1, k_2, k_3= Stiffness parameters of the interconnected portions as shown in Fig. 16. For the completeness of the fundamental equations of motion, all three stiffness parameters have been displayed in the equations, though k_1 and k_3 have been assumed to be zero considering the practical feasibility.

x_1, x_2= Displacements of head and torso, respectively and functions of amplitudes as defined in Equations 2.3 and 2.4.

$$x_1 = A_1 \cdot \sin(\omega t) \qquad \text{(Eq. 2.3)}$$

$$x_2 = A_2 \cdot \sin(\omega t) \qquad \text{(Eq. 2.4)}$$

Where,

A_1, A_2= Amplitudes head and torso, respectively.

The characteristics equations can be re-written as shown in Equations 2.5 and 2.6.

$$m_1 \left(-A_1 \cdot \omega^2 \cdot \sin(\omega t)\right) + k_1 \cdot A_1 \cdot \sin(\omega t) - k_2 \left(A_2 - A_1\right) \cdot \sin(\omega t) = 0 \quad ..... \qquad \text{(Eq. 2.5)}$$

$$m_2 \cdot \left(-A_2 \cdot \omega^2 \cdot \sin(\omega t)\right) + k_2 \left(A_2 - A_1\right) \cdot \sin(\omega t) + k_3 \cdot A_2 \cdot \sin(\omega t) = 0 \quad ..... \qquad \text{(Eq. 2.6)}$$

After simplifications, the polynomial expression for the natural frequencies is obtained and shown in Equation 2.7.

$$p(\omega) := \left(k_1 + k_2 - m_1 \cdot \omega^2\right)\left(k_2 + k_3 - m_2 \cdot \omega^2\right) - \left(-k_2\right) \cdot \left(-k_2\right) \qquad \text{(Eq. 2.7)}$$

Where,

ω= Natural frequency.

Solving Equation 2.3, the first two natural frequencies are obtained as 0 and 3478.344 Hz, while the ratios of amplitudes for first two mode shapes are found to be 1 and -6.751. The associated mode shapes have been extracted and mathematically displayed in Equations 2.8 and 2.9.

$$M_1 := \begin{pmatrix} 0 \\ 1 \\ 1 \\ 0 \end{pmatrix} m \qquad \text{(Eq. 2.8)}$$

$$M_2 := \begin{pmatrix} 0 \\ -6.751 \\ 1 \\ 0 \end{pmatrix} m \qquad \text{(Eq. 2.9)}$$

The obtained first two mode shapes are shown in Fig. 17 and give clear idea about final configurations.

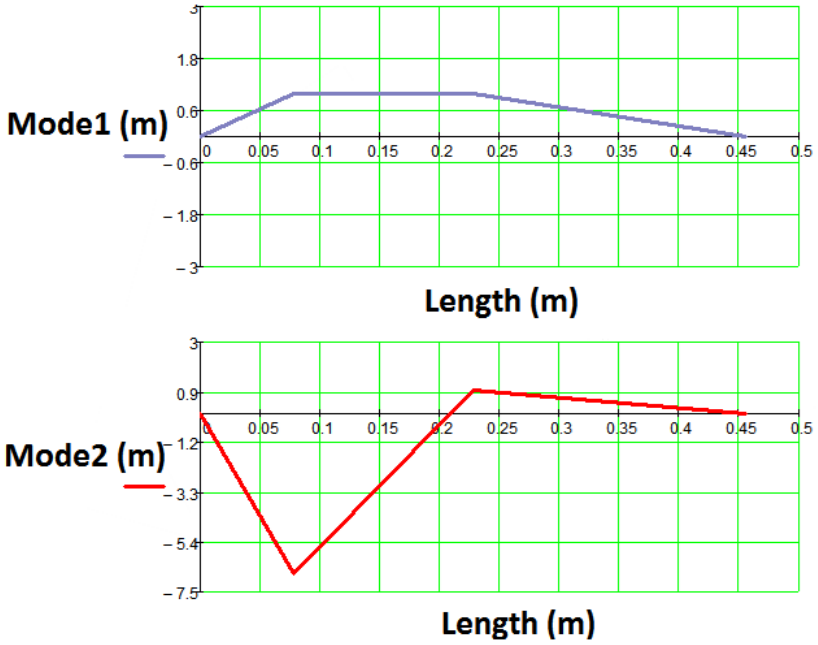

Fig. 17. Mode shapes

2.1.3. Discussion

The experimental work on the lumped mass method became successful in obtaining the natural frequencies and the mode shapes. So, it can be concluded that the lumped mass model is the simplest way to carry out the modal analysis for one or two directional systems. Especially, this method is very useful for analyzing the vertical response under the influence of whole body vibration. Vibration transmissibility can also be well defined using this method.

The real problem for this method is the complicacy in defining equations while the numbers of degrees of freedom are increased. The problem gets too complicated, while the three dimensional environment is considered.

From the experimental work it is clear that the analytical lumped mass method became outdated cause of the human capability to solve numerous number of equations manually. For the simple structures e.g., beam and single body structures, this analytical method can be very quick and efficient, but for the higher number of degrees of freedom systems, ample equations need to be solved either by coding programs, for example FORTRAN or by using the graphical interfaced mathematical tool like MATLAB.

Also, this method assumes the human portions to be rigid point masses, which actually is not realistic. The mass of the human body is non-equally distributed and the mechanical properties for each segment are different. The stiffness, damping co-efficient and density also vary with the different parts of human body, which are not covered by lumped mass method.

Last many years, many research works have been carried out on many fields of human bio-dynamics based on lumped mass method. So, chances to obtain an innovative solution using this method are very less. Cause of the very fast development of computer

aided technologies with visual interfaces; many other advanced techniques are already existing to solve dynamic problems in more accurate way than lumped mass method.

2.2. FINITE ELEMENT MODEL

In finite element method, the entire system is divided into finite numbers of volumetric segments and stress distributions along with deformations can be described very efficiently. The small volumetric portions are interconnected through 'points', which are commonly known as 'nodes' in finite element method. The stress and the deformation levels are functions of the linear or non-linear material properties defined inside the body. While implementing this method to human bio-dynamics, this method assumes that human body can be defined by a finite number of elements and the mechanical properties of these elements are obtained either from experimental or testing data. The more accurate element properties are defined, more accurate the results from this method are received. The body is subdivided into several elements containing nodes and the stress and strain levels are judged based on the nodal displacements. A typical solid body made of elements and nodes is represented in Fig. 18.

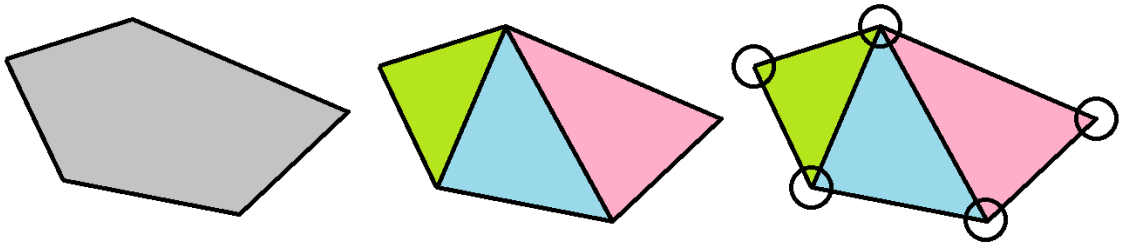

Fig. 18. Concepts of body, element and node in finite element modelling

There are many software tools available for finite element analysis of complicated structures. The most popular and capable two finite element software tools used worldwide are ANSYS and ABAQUS. The approach of finite element analysis tools can be classified as Explicit and Implicit types.

In the Explicit approach, after each incremental step the stiffness matrix is updated by the system and a new stiffness matrix is formed to calculate the next step. This approach is very useful if the increment levels are small. But as a result of many small increments, obtaining solution is very much time consuming.

Implicit approach is same like Explicit with the addition of Newton-Raphson iterations after each step. So, it is useful for big incremental steps and the problem can be solved quicker than that of in explicit approach.

Field variables calculated at the nodes, can be interpreted by the formula of shape functions. An example of simple three node element is shown in Fig. 19.

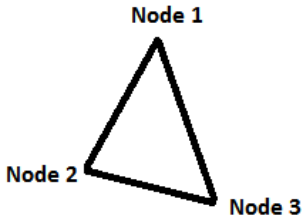

Fig. 19. Simple three node element

Equation 2.6 shows the field variables.

$$\varphi(x, y) = N1(x, y)\, \varphi\, 1 + N2(x, y)\, \varphi\, 2 + N3(x, y)\, \varphi\, 3 \quad (2.6)$$

Where, φ 1, φ 2, and φ 3 are the field variable nodal values, and N1, N2, and N3 are the shape functions.

2.2.1. Past works on Finite Element Model related to Human Body Dynamics

Finite element method was invented during the middle of last century from the necessity of solving complicated structural problems and over the time this method became popular worldwide cause of its interface with computerized visual effects.

One of the oldest human body analyses using finite element was developed in 1970s, to represent the human brain and skull (Shugar, 1977) as shown in Fig. 20. Linear elastic and visco-elastic material properties were used and the results were compared to the experimental data.

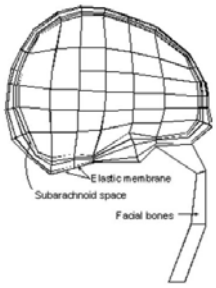

Fig. 20. Finite element model for human brain and skull (Shugar, 1977)

Fig. 21 shows the 3D model in finite element, which was constructed (DeMasi *et al.*, 1991) to simulate the car crash and its effect on the human brain. The study was further extended to investigate the padded and unpadded automobile A-Pillar at a speed of 25 miles per hour. Using the very accurate programming code, the most realistic impact on the human brain was estimated.

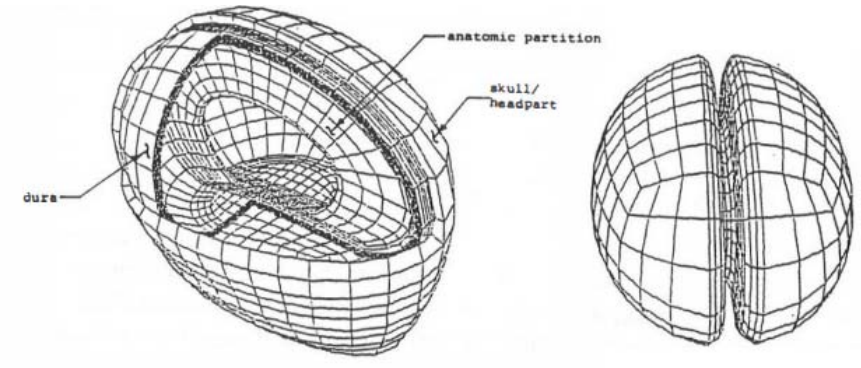

Fig. 21. Finite element model for human brain (DeMasi *et al.*, 1991)

Many studies were carried out for designing the car seat only considering the interaction between human soft tissue and seat cushion, but without considering the pressure distribution inside the car seat. Human buttocks and thigh had been modelled in finite element to investigate the dynamic interaction between the seat cushion and human

muscles during the studies of human soft tissue and seat (Setyabudhy *et al.*, 1997), body-chair interaction using experimental–numerical investigation (Brosh and Arcan, 2000), stresses in soft body tissues of a sitting person (Chow and Odell, 1978) and three-dimensional computer modelling of human buttocks (Todd and Thacker, 1994). Similar kind of study (Moens and Horvath, 2002) was carried out on human buttocks for designing the seat parameters.

A modal analysis was performed to extract seven mode shapes under the frequency of 10 Hz (Kitazaki and Griffin, 1997). The human spine was considered to be constructed by rigid bodies while the inter-vertebral discs were made of deformable elements. The model is shown in Fig. 22. The study showed how changing the posture could increase the pressure between the thigh and seat cushion.

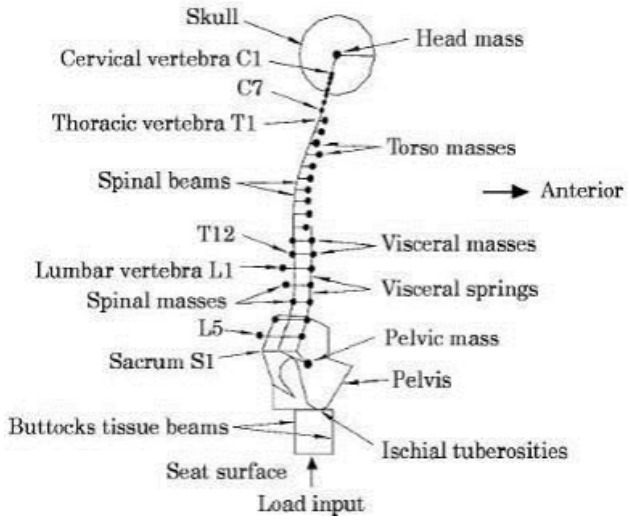

Fig. 22. Finite element model for modal analysis of human body (Kitazaki and Griffin, 1997)

An advance approach was initiated to construct three dimensional human body by taking into account the spine, skull, ribs, pelvis, muscles and skin (Hubbard *et al.*, 1993). Then several other models depending on small, medium and big sizes had been created in computer modeling software. The spine was defined as deformable body while the skull, rib and pelvis were defined as rigid bodies. Muscles and skin were also incorporated into

the whole system using the best possible material properties. The muscles, skins, rigid bodies and deformable bodies were configured to give the real shape of human structure. These models were taken into a new investigation (Frost *et al.*, 1997) and configured into different positions to study the comfort level inside human body in relation to the sitting posture inside a car. That study further developed the new design of the automotive seat in articulated position.

The transmissibility between the human and seat interface was estimated using a finite element model (Zheng *et al.*, 2012) for whole human body considering feet, leg, thigh, arm, hand torso, pelvis, head and neck. The constructed assembly for that research work is shown in Fig. 23. That model was able to predict the apparent masses and transmissibilities of vertical human spine along the fore-aft axis. The properties of the soft tissues of the human body had also been considered for that model to be accurate in modeling the whole human body.

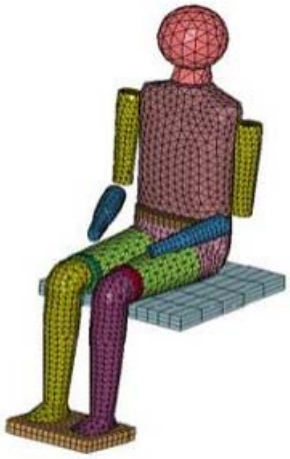

Fig. 23. Finite element model for whole human body (Zheng *et al.*, 2012)

Similar sort of investigation was carried out (Liu *et al.* 2012) during the finite element study of mass and transmissibility of the human body sitting on a rigid seat and exposed to vertical vibration. The average values of human weight and height were considered as

68.5 kg and 1.74 meter, respectively. Feet, legs, thighs, pelvis portion, arms, torso, neck and head were taken into account for whole body modeling.

3D anatomy of the seated human buttocks, as displayed in Fig. 24, was investigated (Sonenblum *et al.*, 2015) through finite element method for the deformation analysis only. The study was not validated by complete 3D assessment of deformation under load.

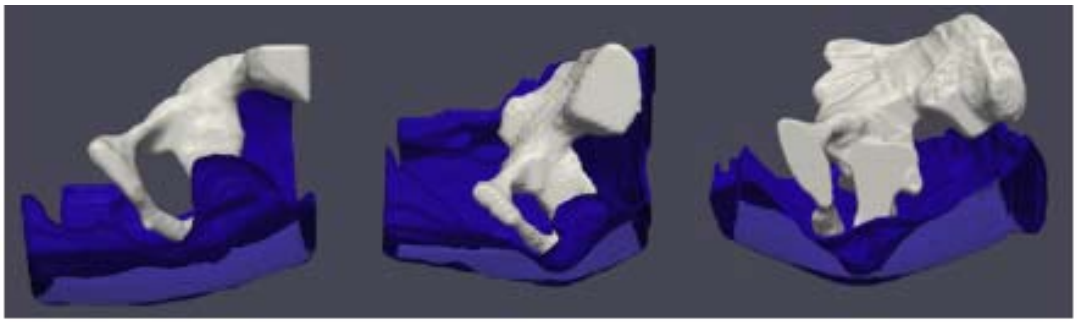

Fig. 24. Finite element model for deformation of buttocks (Sonenblum *et al.*, 2015)

During another buttocks analysis (Todd and Thacker, 1994) using finite element 3D modelling, the pressure distribution at the contact interface between human buttocks and cushion was estimated. Von-Mises stresses and displacements were found efficiently from that study. Minimum principal stresses at the buttock-cushion interface for male and female were found as 15 kPa and 17 kPa, respectively. The obtained stress and displacement plots are shown in Fig. 25.

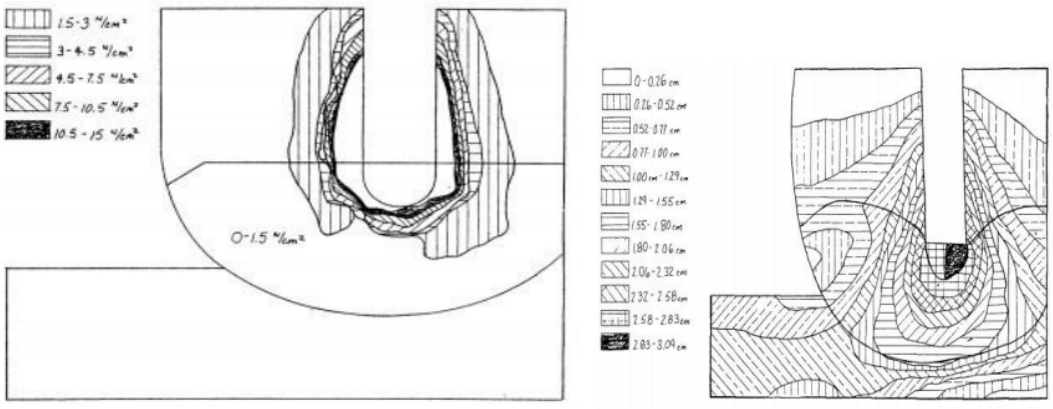

Fig. 25. VM stress and displacements on seat-buttocks interface (Todd and Thacker, 1994)

Fig. 26 represents the similar kind study (Wagnac *et al.*, 2012) where the pressure distribution at the interface of human buttocks and seat cushion was evaluated using the 3D finite element modelling.

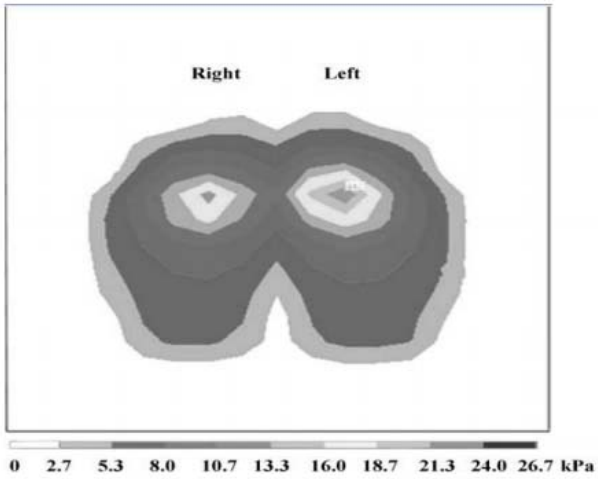

Fig. 26. **P**ressure distribution at seat-buttocks interface (Wagnac *et al.*, 2012)

Global Human Body Models Consortium (GHBMC) is a world famous organization to gather all the significant developments on the human body solid modelling into a single place. 3D models of 50th percentile male body in detailed and simplified versions existing in their database is presented in Fig. 27.

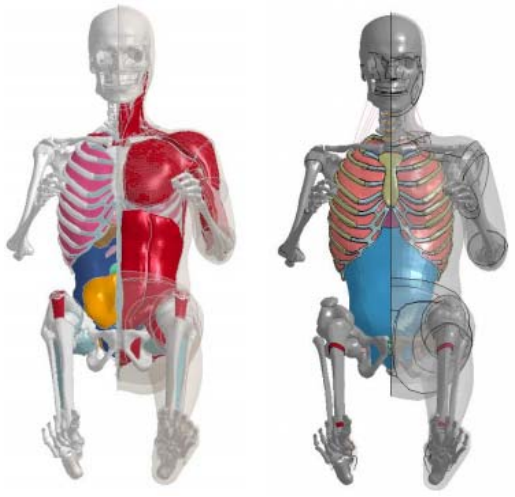

Fig. 27. 50th percentile male models from GHBMC database (left-detailed, right-simplified)

2.2.2. Experimental Simulation work carried out on Human Bio-Dynamics based on combined Lumped Mass and Finite Element Methods to find out Natural Frequencies and Mode Shapes

From the experimental work on lumped mass method in Section 2.1, it is clear that lumped mass parameter is efficient for judging the frequency related problems for human bio-dynamics in two dimensional environment, while finite element method is more useful for analyzing portions of the human body in three dimensional space. Based on the literature surveys on the finite element and lumped mass methods, an experimental three dimensional finite element model has been established to portray the entire human body with lumped mass parameters in finite element environment. The aim of this experimental task is to gain knowledge on the feasibility of using lumped mass parameter and finite element methods together.

2.2.2.1. Three Dimensional Model Set Up of Human Body

Grabcad is an open source platform for the engineers and scientists to share and access different kinds of three dimensional models for the use of technological developments. The database was explored and a raw 3D CAD model of seated human body inside a car (Rhimi, 2015) was chosen for the experimental work.

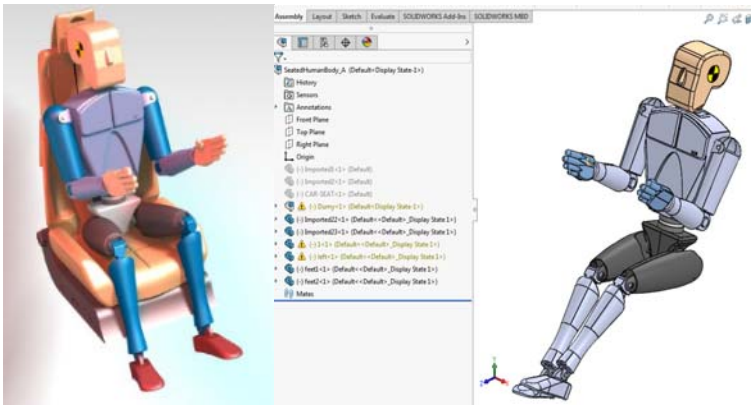

Fig. 28. Raw model collected from Grabcad database (Left) and modified model for experimental work (Right)

The model later was adjusted with proper scaling factor to define a 62 kg male mass body in the simulated system. University of East London got the access to the advanced 3D CAD modeling tool Solidworks. So, the entire CAD related works have been carried out using Solidworks. The raw CAD data collected from the open database of Grabcad and modified model used in experimental work, have been shown with a screenshot in Fig. 28.

2.2.2.2. Locating the Co-Ordinates of Lumped Masses in 3D Space

The preliminary model was only a single solid body in IGES (Initial Graphics Exchange Specification) format without any part or sub-assembly associated with it. The configuration was also not suitable for proper driving position. The model was taken to Solidworks and sub divided into different parts and sub-assemblies as needed. Later, a proper driving position was imposed to the entire model. The model parts were also moved, rotated and scaled to fit to a 62 kg male mass body. The details of the human body dimensions considered, are explained in CHAPTER 3.

Once the CAD model was finalized, the entire model was taken to Solidworks drawing layout and the dimensions of all the necessary joints had been measured in the 3D space with respect to the designated origin point. For better understanding and ease in future work, the intersection of human body vertical central plane and pivot axis of the car seat has been taken as the origin point. The measured dimensions along with the orientations of car seated human body are detailed in Fig. 29.

The co-ordinates of all the necessary joints were measured in X, Y, Z format with respect to the origin and gathered in Table 4. For simplicity, the entire human body had been considered as symmetrical on both the sides of the human vertical plane.

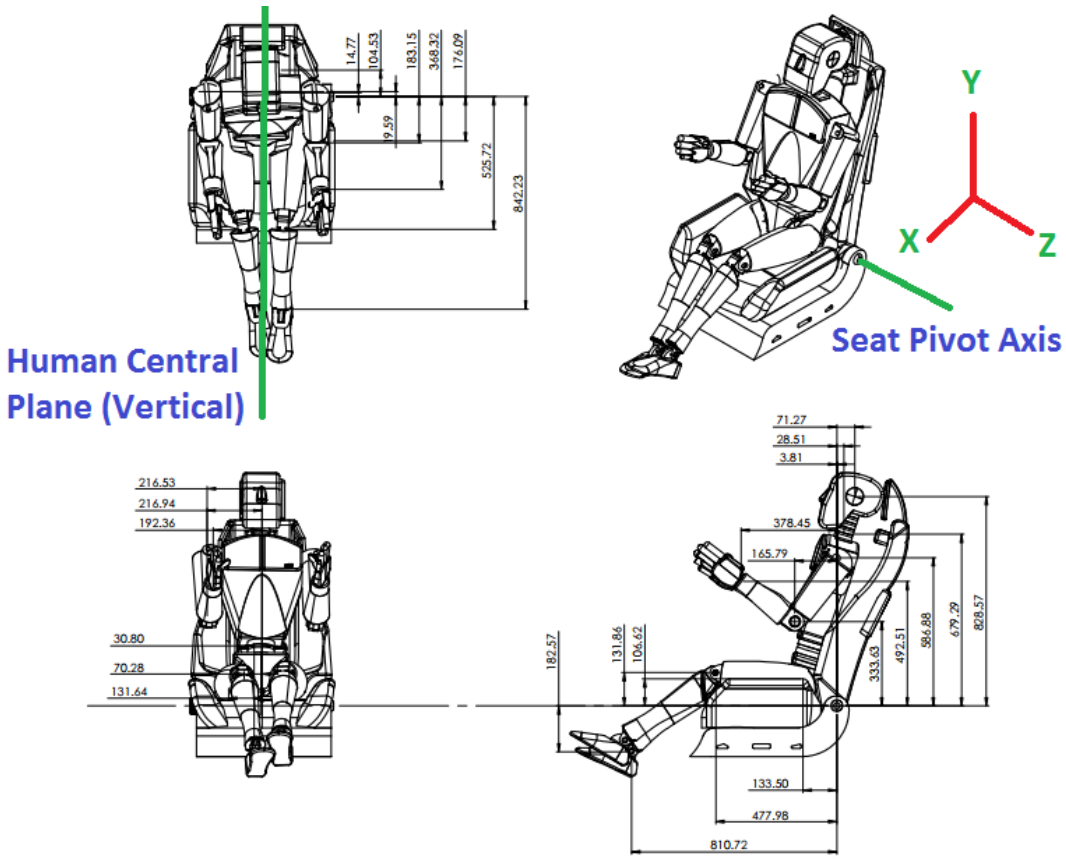

Fig. 29. Dimensions of male mass body in 3D space

Table 4. Measured co-ordinates of human joints

Body Segment	Co-Ordinate with respect to origin (X, Y, Z) in m Left	Co-Ordinate with respect to origin (X, Y, Z) in m Right
Hip	-.1335, .10662, .13164	-.1335, .10662, -.13164
Waist	-.1235, .10850, 0	
Knee	-.47798, .13186, .07028	-.47798, .13186, -.07028
Ankle	-.81072, -.18257, .03080	-.81072, -.18257, -.03080
Neck	.02851, .67929, 0	
Head	.07127, .82857, 0	
Shoulder	.00381, .58688, .21694	.00381, .58688, -.21694

Body Segment	Co-Ordinate with respect to origin (X, Y, Z) in m Left	Co-Ordinate with respect to origin (X, Y, Z) in m Right
Elbow	-.16579, .33363, .21653	-.16579, .33363, -.21653
Wrist	-.37845, .49251, .19236	-.37845, .49251, -.19236

2.2.2.3. Mounting the Co-Ordinates of Lumped Masses in Finite Element Environment

ABAQUS, one of the advanced finite element packages, is available at the engineering department of University of East London. All the pointed measured for the human joints, had been mounted in the three dimensional space of ABAQUS environment. All the points of the human joints in 3D space are shown in Fig. 30.

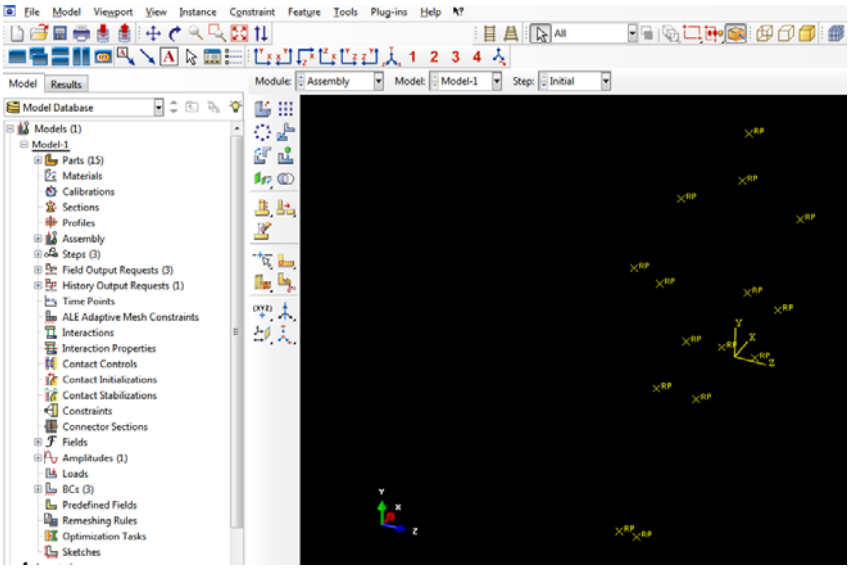

Fig. 30. Human joint locations mounted in 3D space of ABAQUS

2.2.2.4. Parts, Assembly and Properties

All the co-ordinate points had been assigned with the rigid masses. The assigned values of masses were based on the volumetric information from the Solidworks CAD model. As an assumption of this experiment, the entire human body had been considered to be

made of material with uniform density. Considering a male human body of 62 kg mass, the volumetric percentages and masses of human segments were calculated. The calculated masses of different human portions along with all the segmental parameters are given in Table 5.

Table 5. Calculated mass of each human body segment

Segment	Volume (mm^3)	Total Volume (mm^3)	% of Total Volume	Total Mass (Kg)	Mass of Segment (Kg)
Head	2229970.07	30991651.97	7.20	62.00	4.46
Neck	130349.30		0.42		0.26
Upper Arm	1865987.58		6.02		3.73
Lower Arm	1325566.16		4.28		2.65
Hand	451071.59		1.46		0.90
Torso	15290604.99		49.34		30.59
Pelvis	2305471.46		7.44		4.61
Thigh	4259950.45		13.75		8.52
Leg	2104915.09		6.79		4.21
Foot	1027765.28		3.32		2.06

As the masses could only be introduced to the system through lumped masses, the calculated segmental masses were required to be refined to average values. Except hands and feet, all the other body component masses had been averaged at the respective intersection points. All the rigid masses were taken to assembly level and no material properties were assigned as the bodies were rigid for the experimental work. The calculated masses are shown in Table 6.

Table 6. Calculated mass of lumped mass point

Segment	Mass (Kg)	Total Mass (Kg)
Head	2.23	62.00

Segment	Mass (Kg)	Total Mass (Kg)
Neck	2.36	
Shoulder	2.00	
Elbow	3.19	
Wrist	2.23	
Waist	32.90	
Hip	6.57	
Knee	6.37	
Ankle	4.16	

2.2.2.5. Interaction and Stiffness

All the lumped masses had been connected through connector elements to give the shape of real human body. In this experimental work, only the axial stiffness values had been considered. The calculated axial stiffness values for all the segments are shown in details in CHAPTER 3. The connectors and stiffness parameters are shown in Fig. 31 and Table 7, respectively.

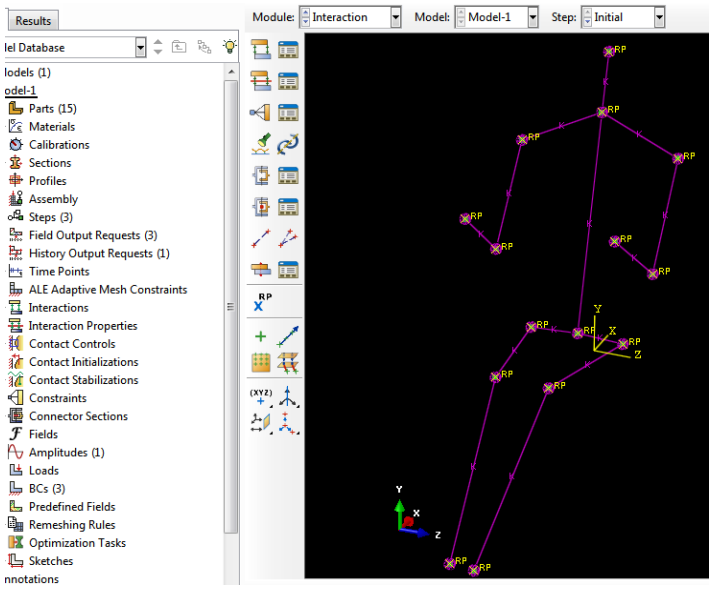

Fig. 31. Lumped masses connected through connectors

Table 7. Axial stiffness values assigned to body segments

Body Segment	Axial Stiffness (N/mm)
Head including Neck	0.36
Torso	0.90
Upper Arm	0.08
Lower Arm	0.09
Hand	0.15
Upper Leg	0.16
Lower Leg	0.11
Foot	0.11

2.2.2.6. Boundary Conditions and Steps

As the car seat had not been considered during this experimental task, the following boundary conditions were applied to the system:

a. Hand - Rotational movement around steering center was allowed, but detachment was not allowed from steering wheel position.
b. Legs - Angular movement was allowed around ankle-leg interface, but detachment was not allowed from brake and clutch positions.
c. Head - Restrained to the headrest, but lateral movement was allowed with respect to head rest.
d. Pelvis - Fixed as per the position of seat cushion.

Linear perturbation frequency analysis had been assigned for analyzing the whole body.

2.2.2.7. Results: Natural Frequencies and Mode Shapes under Free Vibration

Twelve numbers of natural frequencies along with associated mode shapes were extracted. The values of natural frequencies and maximum deformations (modal displacements) with respect to mode shapes are given in Table 8.

Table 8. Modal displacements and natural frequencies

Mode	Displacement (mm)	Frequency (cycles/time)
1	-4.43E-09	0.00
2	-3.79E-09	0.00
3	-1.34E-09	0.00
4	6.42E-11	1.28E-06
5	2.47E-10	2.50E-06
6	1.13E-09	5.34E-06
7	3.05E-09	8.79E-06
8	3.59E-09	9.54E-06
9	3.88E-09	9.91E-06
10	5.20E-09	1.15E-05
11	7.01E-09	1.33E-05
12	1.90E-08	2.19E-05

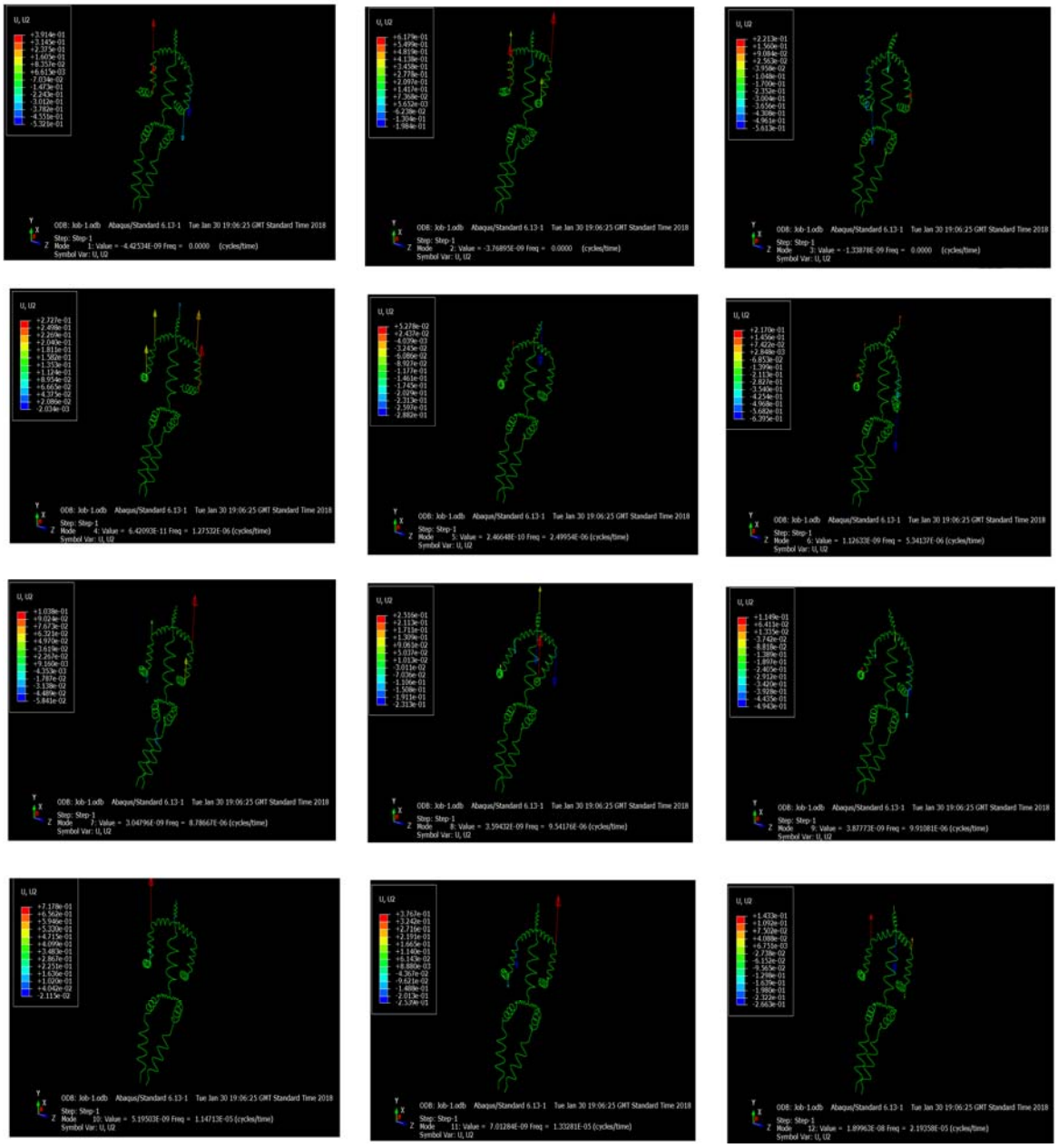

Fig. 32. Mode shapes and associated vertical displacements under the effect of free vibration

All the modal deformations are showing the final configurations under the effect of vibration. A screenshot of all the modal displacements and natural frequencies is shown in Fig. 32.

2.2.3. Discussion

The results are displaying very low level of natural frequencies, compared to the permissible vibration ranges for human body portions. Consideration of the free vibration without any external excitement is the primary reason behind this. If the car seat is associated to the finite element model of human body with proper stiffness parameters and the whole system is excited with forced vibration as per the real life scenario, the natural frequencies will be much higher than what obtained from this experimental work.

Furthermore, only uni-directional stiffness values had been considered without any damping properties. The result could be more accurate if three directional stiffness values along with damping co-efficient values were considered.

The car seat can be associated to this experimental work as another lumped mass system. But problem with this method is that the real life physical bodies cannot be represented through this system. Both the human body and car seat are practically made of distributed inhomogeneous masses instead of point masses. Generally, the stiffness values assigned in this method, are also not functions of the human shapes and sizes, hence, not realistic. This method greatly relies on experimental data or literature survey for assigning the stiffness values.

From the output of the experimental work out, it is clear that the combination of the finite element and lumped mass parameter methods can effectively be used to establish a bio-dynamic model for vibration analysis. In the experimental work, the simulation set up worked fine without any error and yielded desired results. So, this trial work can be considered as successful to take it to next stage.

2.3. MULTIBODY MODEL

Multi-body method is very effective to represent the whole human body and automotive structures as a combination of different kinematic connections to solve the complex problems. In the multi-body model method, the elements inside a system are considered to be interconnected through different joints and these joints constrain the degrees of freedom of the system to execute a certain motion or mechanism. The movement of the whole system is caused by the external forces exerted to the system by means of spring, damper, acceleration, contact, impact, impulse etc.

2.3.1. Past works on Multi-body Model related to Human Body Dynamics

Cause of the development of the computer graphics and hardware technologies, multi-body analysis became very popular worldwide for analyzing complicated dynamic problems. In past many years, different multi-body tools had been used to characterise the human body by means of rigid and flexible parts representing head, arms, hands, thorax, pelvis, thighs, legs and feet.

Two multi-body human models in seated condition had been constructed (Liang and Chiang, 2008) to study the motion of a seated human body exposed to vertical vibrations in various postures. One of the models was with backrest arrangement and the other one was without backrest. The results obtained were greatly matched to the experimental data. Similar kind of model was developed (Zheng *et al.*, 2011) as shown in Fig. 33, for a seven DOF multi-body human-seat assembly to understand the bio-dynamic responses under the effect of vertical vibration in different sitting postures. That investigation showed that the fore-aft and vertical apparent masses on the seat backrest were significantly dependent on the stiffness values of the pelvis muscle.

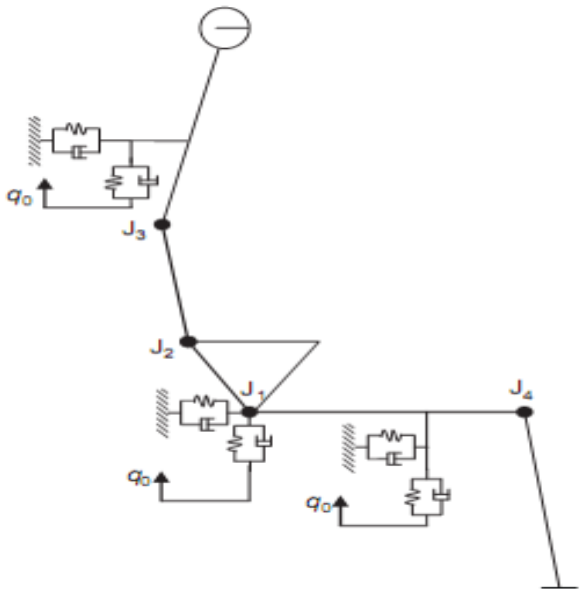

Fig. 33. 7 DOF multi-body human model with spring and damper (Zheng *et al.*, 2011)

Thirteen numbers of body segments were considered during a multi-body modeling approach (Amirouche and Ider, 1988) where spherical joints were used. The model was very efficient in determining the axial and rotary accelerations under the effect of vibration.

A non-linear, kinematic and flexible multi-body model was proposed (Bauchau *et al.*, 2011) considering non-linear material properties, constraints and high level of frequencies. That study gave an algorithm based on elastic-dynamic concept.

Vertical motions along with fore-aft and pitch movements were considered during the multi-body model study (Matsumoto and Griffin, 2001) for apparent mass and transmissibility. The multi-body set up is shown in Fig. 34.

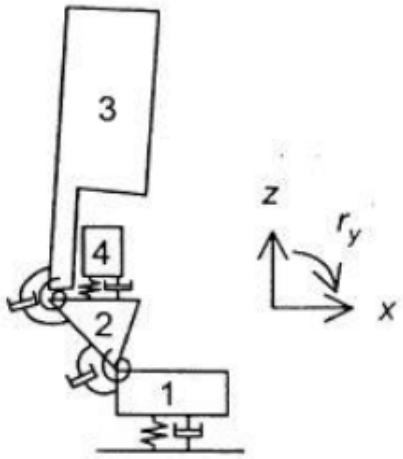

Fig. 34. Multi-body model with spring and damper for studying apparent mass and transmissibility (Matsumoto and Griffin, 2001)

Some hybrid approaches had taken into considerations the acceleration, spring, damper, seat belt, joints, muscles, tissue and contact between the human body and car seat. A homogeneous field of acceleration, air bag and seat belt were shown based on the past references during a study of complex hybrid model (Prasad, 2005). Fig. 35 is presenting that hybrid model.

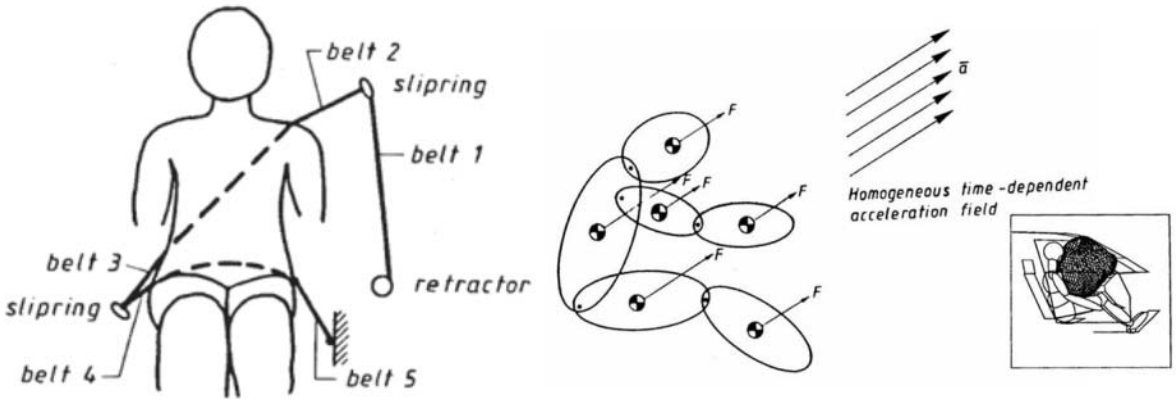

Fig. 35. Hybrid multi-body modelling for car seat and human body (Prasad, 2005)

2.3.2. Discussion

Multi-body modeling method is one of the best methods for determining the effect of vibration on the human body and automotive. The main advantage of this method is that a 3D CAD model can be imported to the multi-body environment and all the joints and contacts can be defined. If the CAD model is constructed in right way, the results from the analysis can be very accurate.

This method is very useful for optimization study where a number of same kinds of structures need to be analysed for a comparative report on the system behavior.

The problem with this method is that the 3D CAD model needs to be precise enough. If the CAD model is not accurate enough, there is very less possibility to simplify it inside the multi-body environment. So, huge amount of time to be allocated for developing the fault free CAD model. Also, numbers of effective multi-body analysis tools are limited in the present industrial market and very expensive. Hence, the running cost of multi-body analysis tool is much higher than operating finite element or lumped mass software tools.

ADAMS, MADYMO, ALASKA and PAMCRASH are the market leading multi-body analysis software tools. ANSYS and ABAQUS also started developing the tools for multi-body dynamics besides their pre-owned finite element packages. LS-DYNA and CASIMIR are the good quality multi-body analysis packages developed by ANSYS and ABAQUS, respectively.

No experimental work on this method was carried out cause of the lack of accessibility of suitable multi-body analysis tool.

CHAPTER 3

UNIQUE BIO-DYNAMIC SIMULATION MODEL DEVELOPED FOR SEATED HUMAN BODY INSIDE A CAR

After exploring the latest technologies on the human bio-dynamics and carrying out the experimental works using different methods in CHAPTER 2, it is clear that simplification must be done on the complex human body and car seat before carrying out the analysis work. Moreover, none of the existing technologies are taking into account the stiffness and damping values based on the shape and size of the human body, hence, lacking the real life feasibility, though every technology got some pros and cons. In this chapter, efforts have been made to achieve a bio-dynamic simulated model of car seated human body as per real life environment, with the considerations of human shape and size specific stiffness and damping values. This chapter elaborates a unique biodynamic simulation technique for a car seated human body.

3.1. Human Segmental Masses

Human segmental masses are defined as the percentages of the total body mass and these percentage values are variable with respect to age, gender, shape etc. Efforts have been made for last many years to standardize the human segmental mass data. Detailed (Plagenhoef *et al.*, 1983) and shorter (Leva, 1996) versions of human segmental database chosen for this research work, are presented in Table 9.

Table 9. Human segmental mass as a percentage of total body mass (left- Plagenhoef *et al.*, 1983, right - Leva, 1996)

Segment	Males (Kg)	Females (Kg)	Average (Kg)
Head	8.26	8.2	8.23
Trunk	55.1	53.2	54.15
Thorax	20.1	17.02	18.56
Abdomen	13.06	12.24	12.65
Pelvis	13.66	15.96	14.81
Total Arm	5.7	4.97	5.335
Upper Arm	3.25	2.9	3.075
Forearm	1.87	1.57	1.72
Hand	0.65	0.5	0.575
Forearm & Hand	2.52	2.07	2.295
Total Leg	16.68	18.43	17.555
Thigh	10.5	11.75	11.125
Leg	4.75	5.35	5.05
Foot	1.43	1.33	1.38

Segment	Males (Kg)	Females (Kg)	Average (Kg)
Head & Neck	6.94	6.68	6.81
Trunk	43.46	42.58	43.02
Upper Arm	2.71	2.55	2.63
Forearm	1.62	1.38	1.5
Hand	0.61	0.56	0.585
Thigh	14.16	14.78	14.47
Shank	4.33	4.81	4.57
Foot	1.37	1.29	1.33

Segment	Males (Kg)	Females (Kg)	Average (Kg)	Segment	Males (Kg)	Females (Kg)	Average (Kg)
Leg & Foot	6.18	6.68	6.43				

Initially a male human model of 62 kg mass was developed in CHAPTER 2. Because of the reason that the outside testing facility can provide the testing data for a standard 50th percentile male human body, the simulation set up in this chapter have been established with a CAD model of 50th percentile male human of typical 77.3 kg mass.

The calculated masses of all the portions of human body derived from Table 9 are shown in Table 10.

Table 10. Calculated human segmental mass data

Total Mass			77.3 Kg	
Segment	Mass - Males (Kg)	Mass – Females (Kg)	Average Mass (Kg)	Segmental Mass (Kg)
Head	8.26	8.2	8.23	6.38
Whole Trunk	55.1	53.2	54.15	42.59
Thorax	20.1	17.02	18.56	15.54
Abdomen	13.06	12.24	12.65	10.10
Pelvis	13.66	15.96	14.81	10.56
Upper Arm	3.25	2.9	3.075	2.51
Forearm	1.87	1.57	1.72	1.45
Hand	0.65	0.5	0.575	0.50
Forearm & Hand	2.52	2.07	2.295	1.95
Total Leg	16.68	18.43	17.555	12.89
Thigh	10.5	11.75	11.125	8.12

Total Mass			77.3 Kg		
Segment	Mass - Males (Kg)	Mass – Females (Kg)	Average Mass (Kg)	Segmental Mass (Kg)	
Leg	4.75	5.35	5.05	3.67	
Foot	1.43	1.33	1.38	1.11	
Head & Neck	6.94	6.68	6.81	5.36	
Trunk	43.46	42.58	43.02	33.59	
Upper Arm	2.71	2.55	2.63	2.09	Kg
Forearm	1.62	1.38	1.5	1.25	Kg
Hand	0.61	0.56	0.585	0.47	Kg
Thigh	14.16	14.78	14.47	10.95	Kg
Foot	1.37	1.29	1.33	1.06	Kg

From Table 10 , the necessary data had been extracted for the segments of interest in this research work, as needed.

3.2. Human Anthropometric Data

Dimensions of the human portions vary on the geographical locations, especially from one continent to another. Last many years plenty researches have been carried out on the anthropometric measurements of human portions at different parts of the world.

Surveys carried out for anthropometric measurement of human on Chinese elderly people (Hu *et al.*, 2007), on the workers of India, Indonesia and Jakarta (Saha, 1985), on elite Italian gymnasts (Massidda *et al.*, 2013), on Mexican adults (Macias *et al.*, 2014), on rugby players (Duthie *et al.*, 2006), on Turkish women (Cengiz, 2014), etc. Ergonomic handbook was published (Ashby, 1975) on human design factors with respect to body size and strength. Comprehensive data table on anthropometric dimensions were also

published (Majumder, 2014) based on the principal component analysis. Basics of the human body measurements were described in international standards PD ISO/TR 7250-2:2010 and BS EN ISO 7250:1998.

From all the mentioned references for human anthropometric data, the necessary dimensions for all the segments of a 50th percentile male human body have been extracted. Though different geographical databases have been consulted, attention has been paid to collect the dimensions from European data archives. Some of the dimensions were not available in the database, hence, have been calculated from the dimensions of other segments. All the extracted and calculated dimensions are summarized in Table 11.

Table 11. Extracted and calculated dimensions for seated 50th percentile male human body

Parameter measured	Dimensions (cm)
Standing height	175.49
Shoulder height	59.80
Armpit height	Not required
Waist height	Not required
Seated height	Not required
Head length (including neck)	31.31
Head breadth (including neck)	15.50
Head to Chin Height	Not required
Neck circumference	Not required
Shoulder breadth	Not required
Shoulder to Elbow Length	36.88
Forearm hand length	26.92
Biceps circumference	24.40
Elbow circumference	27.30
Forearm circumference	22.80

Parameter measured	Dimensions (cm)
Wrist circumference	15.60
Knee height seated	Not required
Thigh circumference	46.70
Upper leg circumference	42.40
Knee circumference	35.10
Calf circumference	31.90
Ankle circumference	23.90
Ankle height outside	6.10
Foot breadth	10.00
Foot length	26.50
Neck height	Not required
Upper leg length	60.50
Thigh thickness	15.50
Lower leg length	45.00
Ground to Shoulder	144.18
Chest depth	24.50
Abdominal depth	27.50
Average torso depth	26.00
Torso height	59.80
Torso top	48.50
Torso bottom	39.00
Average torso width	43.75
Hand length (fist)	6.94
Hand width	9.03
Hand depth	2.41
Upper leg length	61.54
Lower leg length	50.39

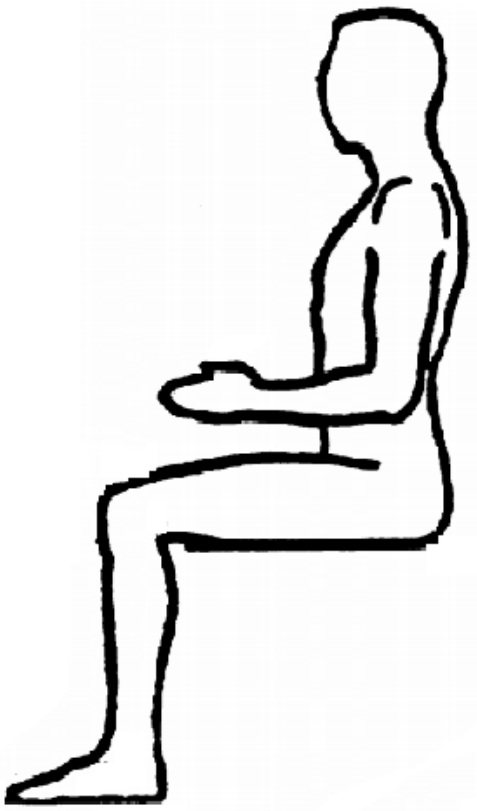

3.3. Representing the Human Segments by Ellipsoidal Bodies

Ellipsoidal bodies are one of the best options to represent the human body segments. In past, in many researches the ellipsoidal bodies had been used as human segments for carrying out the analyses in efficient way. The main advantage of presenting human portions by ellipsoidal segments is that the designated body can be assigned with the calculated stiffness parameters along the axes of the ellipsoids instead of hypothetical data. Moreover, the real anatomical geometry of the human portion is not mandatorily required for vibration related analysis, hence, simplified ellipsoidal human portions will fulfill the aspects of this simulation phase.

During the study on deformations of legs and arms (Hyun *et al.*, 2003), the displacement of the human body was shown as a portion of the movement of ellipsoidal cross-sectional. The mathematical relationship between the scalar parameters showed how the numerical system worked for the displacement of the body.

Representation of human portions through ellipsoidal bodies and the scalar displacement on the designated elliptical cross-section are pictorially explained in Fig. 36.

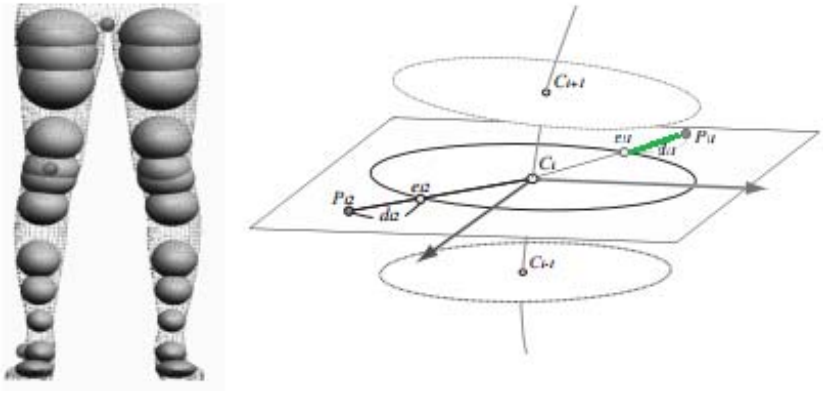

Fig. 36. Representing human limbs as ellipsoids and the scalar displacements (Hyun *et al.*, 2003)

Fig. 36 is showing the original and displaced points on an ellipsoidal cross sectional area. The deviation of the displaced point from the original point is shown with green line and can be formulated by the Equation 3.1.

$$D(u_{ij}, v_i) = d_{ij} = ||p_{ij} - e_{ij}||, \quad \text{(Eq. 3.1)}$$

$i = 1,...,M,$

$j = 1,...,N_i$

Where,

(u_{ij}, v_i) = Surface parameter for the point e_{ij} on the sweep surface of C_i,

M = Number of cross-sections,

N_i = Number of data points on the cross-section.

During the academic study of mathematical validation of eigen values and eigen vectors of different human body segments in sitting posture (Bansal, 2013), the human portions were considered as truncated ellipsoids.

Noting down all the advantages, in the current research work, the human segments are represented through ellipsoidal bodies and the parameters of human portions have been calculated without any estimation or hypothesis. A typical example of representing human portions by three dimensional ellipsoidal bodies, is given in Fig. 37.

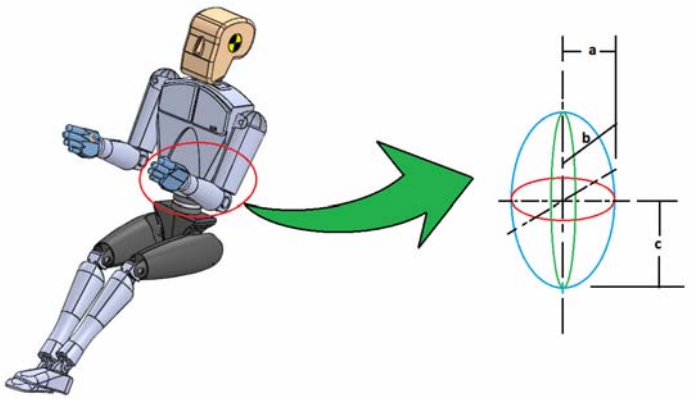

Fig. 37. Representing human hand as an ellipsoid – a, b, c are the half lengths of ellipsoidal axes

The ellipsoidal dimensions and masses are calculated from the data provided in Table 10 and Table 11 and presented in Table 12.

Table 12. Calculated dimensions and masses of ellipsoids representing the human portions

Body Segment	Ellipsoid Parameters (cm)			Mass (Kg)	Quantity
	a	b (depth)	c		
Head including Neck	7.75	7.75	15.66	5.36	1
Torso	21.88	13.00	29.90	36.19	1
Upper Arm	3.88	3.88	18.44	2.51	2
Lower Arm	3.63	3.63	13.46	1.45	2
Hand	4.52	1.21	3.47	0.50	2
Upper Leg	6.75	7.75	30.25	8.12	2
Lower Leg	5.08	5.08	22.50	3.67	2
Foot	5.00	3.05	13.25	1.06	2

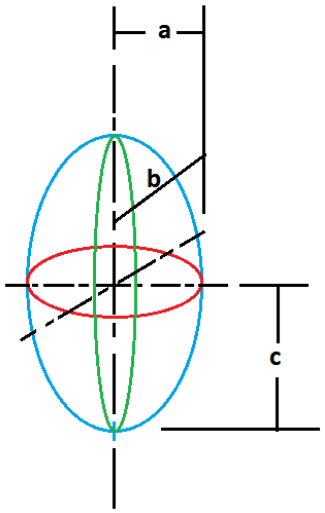

3.4. Preparation of CAD Assembly and Sitting Configuration for 50th percentile Male Human constructed by Ellipsoidal Bodies

3.4.1. Human Sitting Posture

International standards ISO/TC 159/SC 1, ISO/TC 159/SC 3 and ISO/TC 159/SC 4 describe the general ergonomics principles, anthropometry with biomechanics and ergonomics of human-system interaction, respectively and the angles between the different segments of the human body can be obtained from these standards.

To make this research work feasible, a real life male human of 77 kg mass has been considered in sitting position inside a car. Fig. 38 is showing the picture taken of that

male human body in seated condition inside car. Later, the picture was projected to the Solidworks drafting format to measure all the angular dimensions.

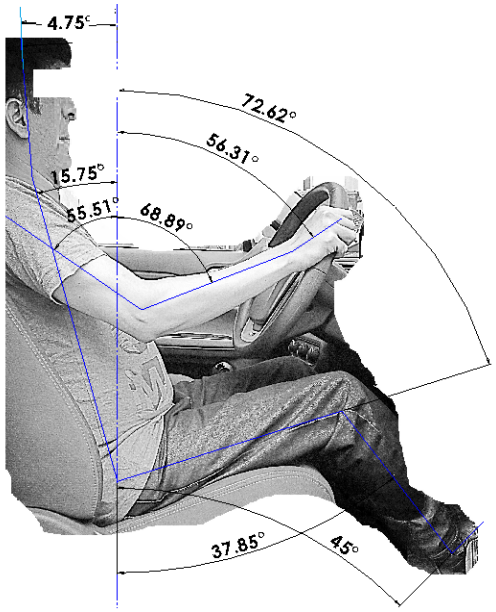

Fig. 38. Male human driver of 77 kg mass seated on a car seat

The distance between two hands or the diameter of the steering wheel has been taken from standard automobile size of category AX – 15" x 3 ½". The available steering sizes are shown in Fig. 39 in wheel diameter x grip diameter format.

Fig. 39. Standard car steering wheel dimensions in wheel diameter x grip diameter format (Carsoda. 2017)

The gap between the feet depends on the distances between accelerator, brake and clutch, which are also varied from one manufacturer to other. For this simulation modelling, standard gap of 3 inches has been considered between the feet.

3.4.2. Human Body Modelling

Based on all the dimensions gathered, a 3D parametric assembly of seated male human driver has been constructed in Solidworks and shown in Fig. 40. As the assembly is in parametric form, the posture can be altered quickly at later stage, if required.

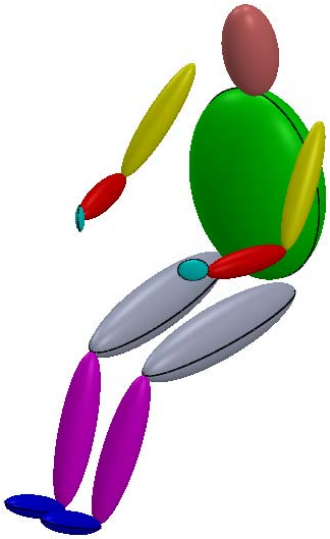

Fig. 40. Established 3D parametric CAD assembly in Solidworks

3.5. Setting up Simulation Model in Finite Element Environment for 50th percentile Male Human constructed by Ellipsoidal Bodies

The CAD assembly has been taken into the environment of ABAQUS, the finite element tool. The imported assembly in ABAQUS is presented in Fig. 41.

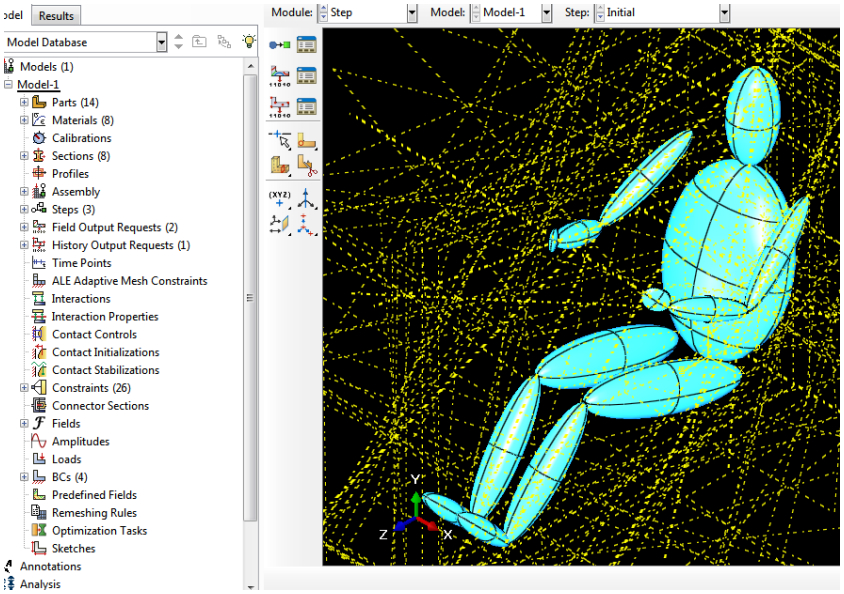

Fig. 41. Human model imported into finite element environment

3.5.1. Densities of the Body Segments

The volumes, densities and ratios of two lateral axes for all the human segments have been calculated from the values in Table 12 and recorded in Table 13.

Table 13. Calculated ratios of two lateral axes, volumes and densities for the ellipsoids representing the human portions

Body Segment	Ratio a/b	Volume (mm^3)	Density (Kg/mm^3)	Density ($tonne/mm^3$)
Head-Neck	1	3937886.096	1.36231E-06	1.36231E-09
Torso	0.594286	35609778.75	1.01635E-06	1.01635E-09
Upper Arm	1	1165068.28	2.15631E-06	2.15631E-09
Lower Arm	1	742549.7612	1.94668E-06	1.94668E-09
Hand	0.266888	79064.39451	6.35495E-06	6.35495E-09
Upper Leg	1.148243	6626766.667	1.22481E-06	1.22481E-09
Lower Leg	1	2429823.305	1.51112E-06	1.51112E-09
Foot	0.61	846237.75	1.25143E-06	1.25143E-09

3.5.2. Evaluating Axial and Lateral Young's Moduli of the Human Body Segments

Human muscle and bone properties are not known as elastic or homogeneous in natures, in fact they can be termed as non-linear in natures. Especially the tissues, muscles and skin exhibit the visco-elastic and hyper-elastic material properties. So, defining the Young's Modulus (YM) for the human bone-muscle structure is a great challenge. Generally, the analytical studies on the human bone-muscle structures consider the YM values from past references or practical experimental data.

Soft biological tissues were examined through mechanical indentation and tensile measurement (McKee *et al.*, 2011) for estimating the YM values. That study obtained the YM values of tissues, muscles and tendons in the range of 3 to 8 kPa. Another testing study on the biomaterial (Crichton *et al.*, 2013) showed that the YM values were hugely dependent on the indentation depth. For the highest probe depth, the minimum YM value of the skin was evaluated as 420 kPa.

Mechanical properties of the bones with variable age and gender were showed (Mirzaali*, et al.*, 2016) through the testing of bone specimens. The maximum YM value obtained from that investigation was 20.04 GPa. Finite element investigation on 3D model of human bone (Zhang*, et al.*, 2013) considered the YM value as 15 GPa.

For this simulation modelling work, the values of YM for muscle and bone materials have been chosen as 8 kPa and 20.04 GPa, respectively.

The combined structure of human bone and muscle can be represented through silicon, fiber or composite material. Composite structures got distinct advantage for calculating the accurate value of stress generated in the fiber-matrix structure inside it. A simple composite material formation has been shown in Fig. 42.

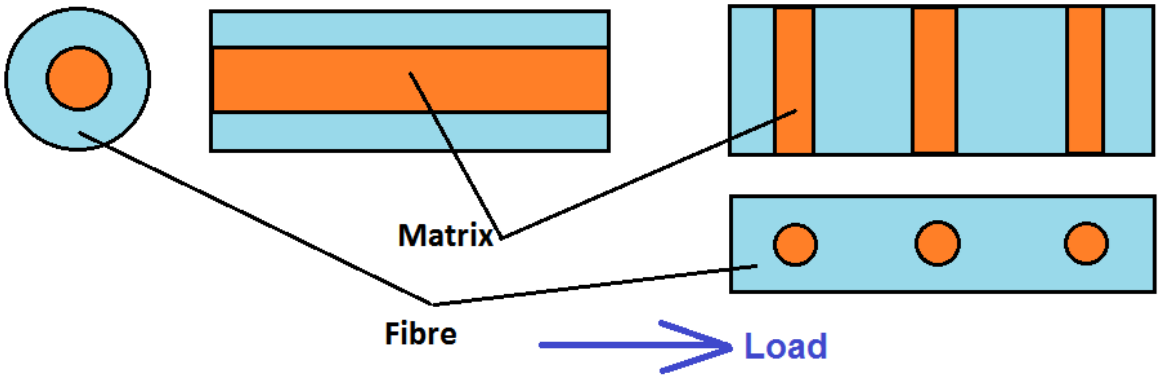

Fig. 42. Matrix and fibre structure inside composite (left- axial, right- transverse)

For axial direction,

$$F_{Comp} = F_{Fibre} + F_{Matrix} \quad \text{(Eq. 3.2)}$$

Where, F_{Comp} is the total force on the composite structure, F_{Fibre} is the force on the fibre portion and F_{Matrix} is the force on the matrix portion.

For transverse direction,

$$d_{Comp} = d_{Fibre} + d_{Matrix} \quad \text{(Eq. 3.3)}$$

Where, d_{Comp} is the total deformation of the composite structure, d_{Fibre} is the deformation of the fibre portion and d_{Matrix} is the deformation of the matrix portion.

The equations of the Axial and Transverse Young's Moduli can be written as:

$$E_{Comp.Axial} = E_{Fibre} \times f_{Fibre} + E_{Matrix} \times \left(1 - f_{Fibre}\right) \quad \text{(Eq. 3.4)}$$

$$E_{Comp.Transverse} = \frac{E_{Fibre} \times E_{Matrix}}{E_{Fibre} \times \left(1 - f_{Fibre}\right) + E_{Matrix} \times f_{Fibre}} \quad \text{(Eq. 3.5)}$$

Where, E_{Fibre} is the Young's Modulus of fibre portion and E_{Matrix} is the Young's Modulus of matrix portion.

In the database of advanced human nutrition (Wildman, 2000), it is found that the male human body consists of 15% bone and 85% fat, organ and muscle. These percentages have been used to evaluate the axial and lateral YM values of bone muscle structure.

Percentage of tissue:

$f_t := 0.85$

Percentage of bone:

$f_b := 0.15$

Young's Modulus of tissue:

$E_t := 8 \times 10^3 Pa$

Young's Modulus of bone:

$E_b := 20.04GPa$

Axial Young's Modulus of bone muscle structure:

$$E_a := E_t \cdot f_t + E_b \cdot f_b \qquad \text{(Eq. 3.6)}$$

$E_a := 3.006\ GPa$

Lateral Young's Modulus of bone muscle structure:

$$E_l := \frac{E_b \cdot E_t}{\left(E_b \cdot f_t + E_t \cdot f_b\right)} \qquad \text{(Eq. 3.7)}$$

$E_l := 9.412\ kPa$

3.5.3. Evaluating Axial and Lateral Stiffness Values of the Human Body Segments

From the relationship between force, stress, strain, area and stiffness, the axial and transverse stiffness values have been derived.

Axial stiffness value of ellipsoid (along c-axis of the ellipsoid in Table 12):

$$K_{Axial} = \frac{\pi \cdot E_a \cdot a_i \cdot b_i}{c_i} \qquad \text{(Eq. 3.8)}$$

Transverse stiffness value of ellipsoid (along b-axis of the ellipsoid in Table 12):

$$K_{Trans.b} = \frac{\pi \cdot E_a \cdot a_i \cdot c_i}{b_i} \qquad \text{(Eq. 3.9)}$$

Transverse stiffness value of ellipsoid (along a-axis of the ellipsoid in Table 12):

$$K_{Trans.a} = \frac{\pi \cdot E_a \cdot b_i \cdot c_i}{a_i} \qquad \text{(Eq. 3.10)}$$

The axial and lateral stiffness values of each of the human segments have been calculated and given in Table 14.

Table 14. Evaluated values of stiffness for all the segments

Body Segment	Axial Stiffness (kN/m) – c-Axis	Lateral Stiffness (kN/m) – b-Axis	Lateral Stiffness (kN/m) – a-Axis
Head including Neck	362249.86	4.63	4.63

Body Segment	Axial Stiffness (kN/m) – c-Axis	Lateral Stiffness (kN/m) – b-Axis	Lateral Stiffness (kN/m) – a-Axis
Torso	898003.69	14.87	5.25
Upper Arm	77246.85	5.45	5.45
Lower Arm	92403.13	3.98	3.98
Hand	148038.00	3.84	0.27
Upper Leg	163268.40	7.79	10.27
Lower Leg	108208.38	6.65	6.65
Foot	108670.55	6.42	2.39

The calculated stiffness parameters are falling within the ranges described in past studies and literatures.

3.5.4. Poisson's Ratio

Poisson's ratio is the ratio of lateral strain to axial strain and theoretical value of it falls in the range of 0 to 0.5. For the value of 0, the material is known as completely compressible, while for the value of 0.5, the material is known as completely incompressible. Most of the soft tissues are assumed to be fully incompressible in nature and usually the Poisson's ratio for fully incompressible materials is considered in between 0.45 and 0.49 (Chen *et al.*, 1996). The study on measuring the Young's Modulus (Chen *et al.*, 1996) for the soft human tissue considered the Poisson's Ratio value as 0.49. Another similar study on computational modelling of human tissue in finite element (Spyrou and Aravas, 2011) used the Poisson's ratio value of 0.49995.

The human muscles are viable to be deformed more and faster than the bones inside. Considering this fact, in many investigations in the past, the bones had been considered as rigid bodies.

For this simulation study, the Poisson's ratio values for all the ellipsoidal human segments have been considered as 0.49.

3.5.5. Damping Co-efficient and Damping Ratio

There are no specific values for damping parameters for the human bone-muscle structures, though depending on the aspect of a particular research work, human segments can be assigned with unique values of damping coefficients.

For a human body of 75 Kg mass exposed to whole-body vibration in both vertical and fore-and-aft directions (Zengkang *et al.*, 2013), the damping coefficients for lower torso, arms, upper torso and hands were taken as 2376.4 Ns/m, 145.8 Ns/m, 1797.7 Ns/m and 1797.7 Ns/m, respectively. For a human body of 90 Kg mass, whole body vibration analysis (Kamalakar *et al.*, 2017) was carried out and the damping coefficients for head-neck, chest-upper torso, lower torso and pelvis-thigh were considered as 620 Ns/m, 8550 Ns/m, 5685 Ns/m and 3564 Ns/m, respectively. Response of a seated human body of 80 Kg mass (Muksian *et al.*, 1974) was investigated where the damping coefficients for head, back, torso, thorax and abdomen were considered as 3575.506 Ns/m, 3575.506 Ns/m, 3575.506 Ns/m, 291.878 Ns/m and 291.878 Ns/m, respectively.

From the closest matching human mass criteria, the damping coefficients for human segments used in this research work have been selected as 620 Ns/m, 1797.7 Ns/m, 145.8 Ns/m, 145.8 Ns/m, 1797.7 Ns/m, 2376.4 Ns/m, 2376.4 Ns/m and 2376.4 Ns/m for head, torso, upper arms, lower arms, hands, thighs, legs and feet, respectively.

If ζ= Damping ratio, a system can be defined as:
Overdamped for $\zeta>1$, where system comes back to equilibrium without oscillation and with decay.
Critically damped for $\zeta=1$, where system comes back to equilibrium without oscillation as soon as possible.

Underdamped for $\zeta<1$, where system oscillation occurs before coming back to equilibrium.

Undamped for $\zeta=0$, where system has no damping effect.

The relationship between damping ratio, damping coefficient, mass and stiffness is shown in Equation 3.11.

$$\zeta = \frac{c}{2\sqrt{m \cdot k}} \qquad \text{(Eq. 3.11)}$$

Where,

c= damping coefficient, m= mass and k= stiffness.

Damping ratios for the human muscles and bones had been investigated for many years. For the index finger joints (Gottlieb and Agarwal, 1978) the damping ratio was found to be in the range of 0.20±0.40. For the joints in human elbow, the obtained damping ratio was in the range of 0.2-0.6 (Bennett *et al.*, 1992). For ankle joints inside human body, the damping ratio was found to be in the range of 0.25-0.45 (Hunter and Kearney 1982). Similar kinds of earlier studies on ankle joints found the damping ratio in the range of 0.35±0.10 (Gottlieb and Agarwal, 1978). Study on the human joints (Lacquaniti *et al.*, 1982) reported damping ratio in the range of 0.08-0.21. After careful observation of the past works carried out on damping ratio for human organs, a damping ratio value of 0.2 has been chosen for this simulation work.

3.6. Analysis Details in ABAQUS for 50th percentile Male Human constructed by Ellipsoidal Bodies

3.6.1. Interaction

All the adjacent human segments have been interconnected by means of 'Tie' constrains. This is the most suitable constraining technique used for the human body simulation to connect different parts. The segments, which apparently seem to be floating in the space,

are actually connected through 'Tie' constrains. Fig. 43 is showing these constrains through red coloured lines.

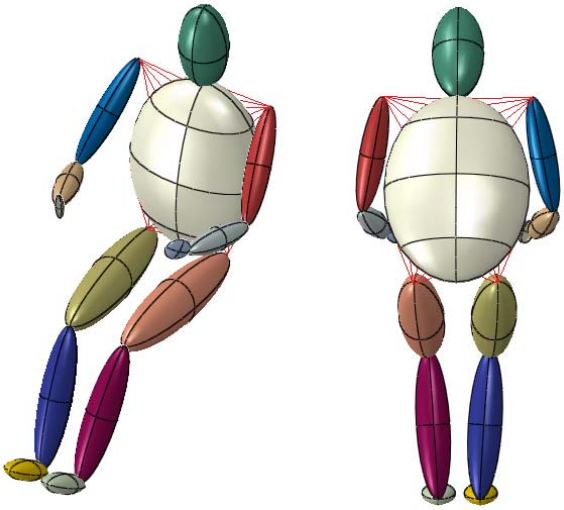

Fig. 43. 'Tie' constrains (red coloured lines) (left- isometric view, right- back view)

3.6.2. Analysis Steps

3.6.2.1. Step 1: Initial

First step is the base state of the simulation, where material properties and boundary conditions have been assigned to the human body segments.

3.6.2.2. Step 2: Linear perturbation

Second step is for the linear perturbation, where the system solves the natural frequencies.

A complex analysis can be split into different linear and non-linear steps. The linear perturbation step provides the linear response of the very initial stage without showing the responses of the non-linear steps in the system. From the theoretical concepts outlined in ABAQUS user's manual version 6.3, this fact can be explained.

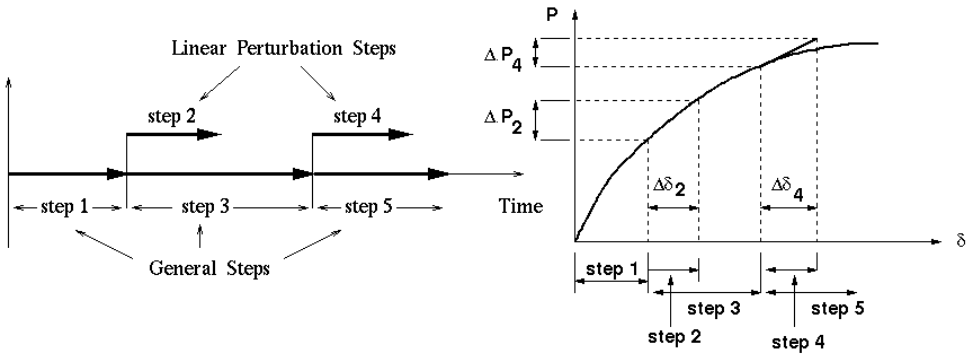

Fig. 44. Concept of linear perturbation theory in ABAQUS (ABAQUS User's manual version 6.3)

In Fig. 44, the steps 1, 2, 3 and 4 can be static loading, frequency, static loading and frequency, respectively. A general analysis will show the responses of all the steps at the end of analysis, while a linear perturbation analysis will display the responses due to step 2 and 4 only. Step 2 will not have any effect on the result of step 3 as step 2 is a linear perturbation step.

3.6.2.3. Step 3: Modal Dynamics

Third step is for modal dynamics. Modal dynamics step is very useful to understand the system behavior when the eigen frequencies or natural frequencies are obtained prior to this step. This step also considers the damping of the system and calculates the responses with respect to mode shapes of the system. Fig. 45 is showing the theoretical perception behind the frequency related modal analysis inside the finite element tool ABAQUS.

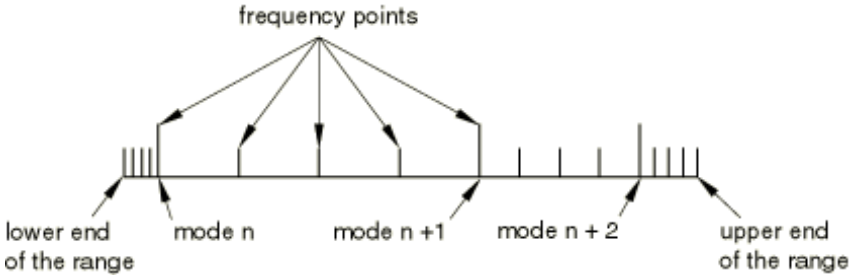

Fig. 45. Concept of frequency range for modal dynamics analysis (ABAQUS user's manual version 6.3)

3.6.3. Boundary Conditions

As the car seat has not been considered in this stage, the following boundary conditions have been applied to the human portions:

a. Hand - Rotational movement around steering center is allowed, but detachment is not allowed from steering wheel position.
b. Legs - Angular movement is allowed around ankle-leg interface, but detachment is not allowed from brake and clutch positions.
c. Head - Supported to the headrest position, but lateral movement is allowed without detachment from headrest position.
d. Thighs – Bottom surfaces are fixed with respect to the seat cushion position.

3.6.4. Acceleration and Load

The load in a moving vehicle primarily comes from the acceleration, which is a function of change of speed within a certain time frame. For a racer type car, the measured acceleration was 28 m/sec^2 (Zitzewitz, 1995), while Aston Martin DBS 2008 defined the acceleration for their car as 6.5 m/sec^2. For the Jaguar XK coupe (Wardell, 2007), Ferrari Enzo (Ferrari Enzo Technical Specifications, 2002) and Bugati 2006 (Albee Digital, 2006), the measured acceleration values were 4.5 m/sec^2, 7.6 m/sec^2 and 11.59 m/sec^2, respectively. During the study on speed and acceleration characteristics of different types of vehicles on multi-lane highways (Mehar *et al.*, 2013), the acceleration values at 60 km/hour and 40 km/hour were calculated as 1.083 m/sec^2 and 0.861 m/sec^2, respectively.

For a passenger car operating in the rural area, the acceleration values were defined (Brooks, R. M., 2012) by Equations 3.12 and 3.13 containing the speed factor and constants.

$$a_{av} = a \cdot e^{bv} \quad \text{(Eq. 3.12)}$$

$$a_{max} = c + d \cdot v \quad \text{(Eq. 3.13)}$$

Where,

a_{av} = average acceleration, m/sec^2

a_{max} = maximum acceleration, m/sec^2

v = speed of the vehicle, m/sec

a, b, c, d = constants

For this simulation phase, the value of acceleration has been taken as 0.861 m/sec^2 or 3.1 km/hour.sec to calculate the force.

Solution of a system under forced vibration is based on the Equations 3.14 and 3.15.

$$m\,a + cv + kd = F_0 \sin(\omega t) \quad \text{(Eq. 3.14)}$$

$$d = A \sin(\omega t - \alpha) \quad \text{(Eq. 3.15)}$$

Where, m= mass, a= acceleration, c= damping co-efficient, v= velocity, k= stiffness, d= displacement, F_0= force, ω= frequency, t= time, A= amplitude, α= phase angle.

The force has been applied to the human body in the modal dynamics step to know the behavior of the system under the effect of vibration. In absence of car seat, this external force has been identified as suffice to characterise the simulated system and monitor the simulation performance.

3.6.5. Element type and Mesh

Ten-node tetrahedral element - C3D10 has been used for generating meshed human body. The C3D10 element is suitable for generating mesh for general purpose by utilizing four

integration points. The meshed human body is shown in Fig. 46. Mesh refinement has been optimized based on the capability of the computer hardware system.

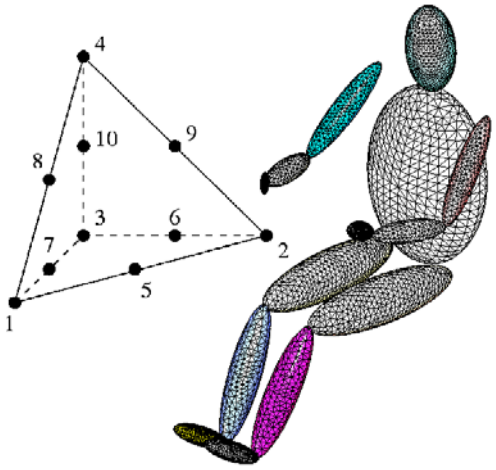

Fig. 46. 10-node tetrahedral element and meshed human body

3.7. Results

A 64 bit standard laptop with RAM of 6 GB, Windows XP operating system and two number of dual-core 2.1 GHz Intel(R) Pentium(R) CPU B950 had been used to complete the simulation task. The simulation was set to run for 10 seconds. The ABAQUS solver took around 5 wall clock hours to run the simulation and yield results. The natural frequencies, acceleration responses and displacement values at the points of interest have been extracted from the result.

3.7.1. Natural Frequencies

First one hundred number of natural frequencies have been extracted from the system. Few of the deformed configurations along with associated natural frequencies are shown in Fig. 47.

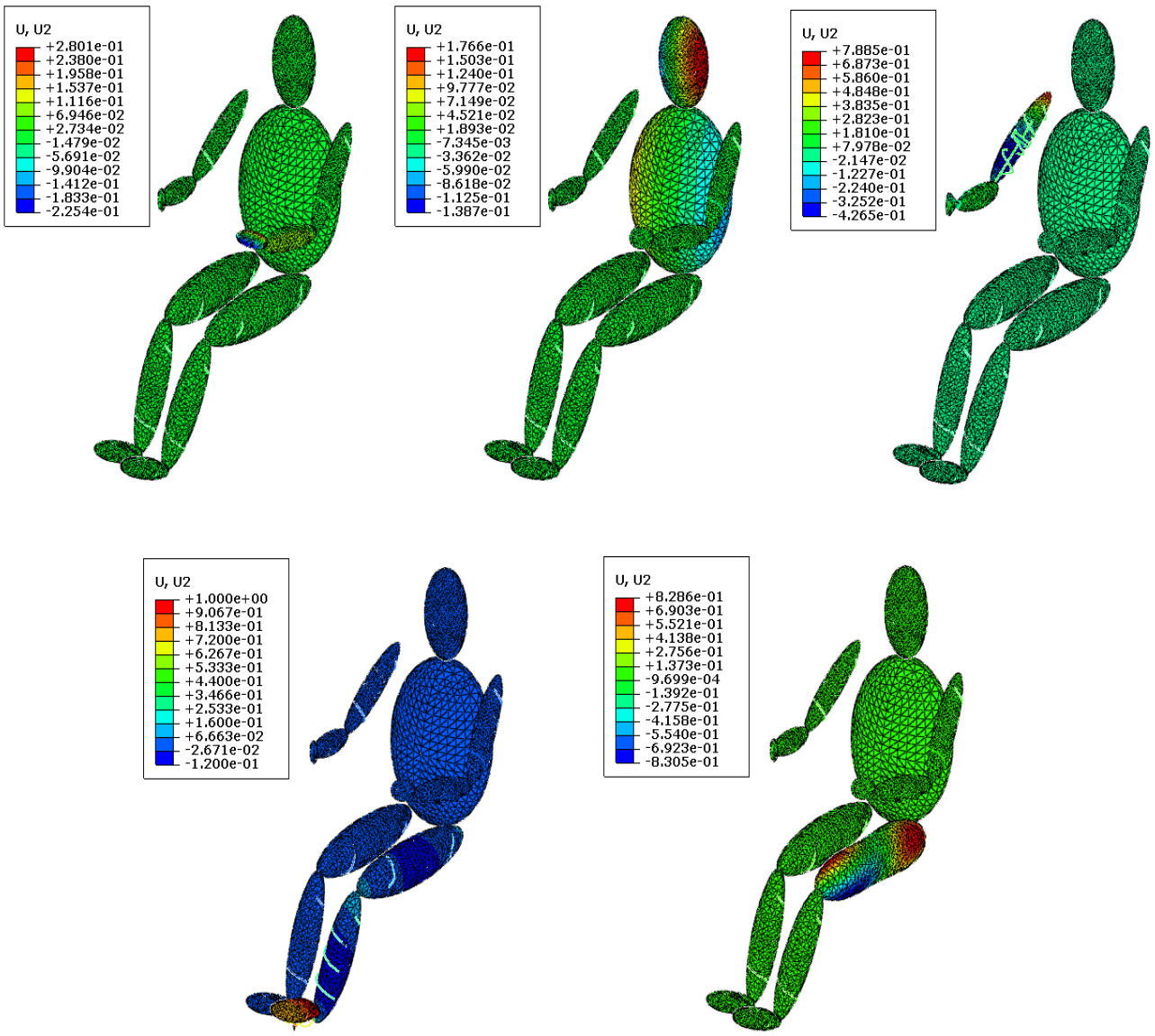

Fig. 47. Deformed shapes for the natural frequency numbers 1, 25, 50, 75 and 100 (ordered from top left to bottom right horizontally)

The obtained natural frequencies for different modes are shown in Fig. 48.

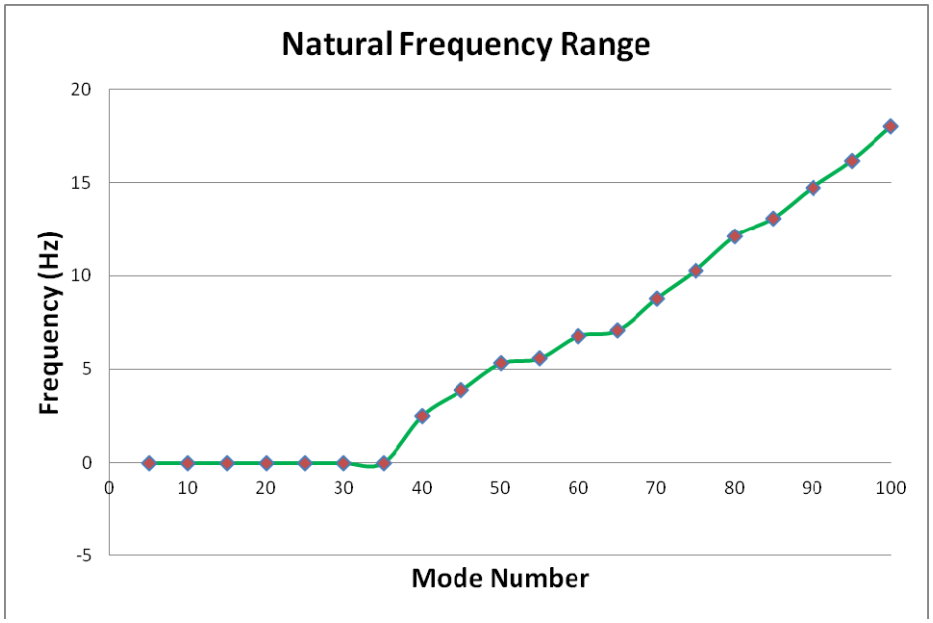

Fig. 48. Natural frequencies with respect to modes

3.7.2. Acceleration responses at the points of interest

This research work intends to focus on the vertical vibration. Hence, vertical acceleration responses with respect to simulation time at the designated points of head, chest, waist, upper arm, lower arm, thigh and leg have been measured from the simulation result and detailed in Table 15.

Table 15. Measured values of vertical accelerations for all the segments

Time (Sec)	Acceleration (mm/sec^2)						
	Head	Chest	Waist	Upper Arm	Lower Arm	Thigh	Leg
0.0	0.00	0.00	0.00	0.00	0.00	0.00	0.00
0.1	-0.97	1.34	1.19	0.27	1.70	1.70	-0.18
0.2	5.42	3.04	3.16	0.00	2.18	2.18	-0.17
0.3	-1.24	0.28	0.10	-0.17	1.23	1.23	0.15
0.4	-4.41	-0.04	-0.45	-0.16	0.65	0.65	0.52

Time (Sec)	Acceleration (mm/sec^2)						
	Head	Chest	Waist	Upper Arm	Lower Arm	Thigh	Leg
0.5	9.16	3.68	3.93	0.14	1.33	1.33	0.68
0.6	-2.71	0.97	0.77	0.11	1.62	1.62	0.49
0.7	-3.26	-0.47	-0.75	-0.25	1.23	1.23	0.60
0.8	6.17	2.54	2.74	-0.34	0.61	0.61	0.96
0.9	-0.49	2.10	2.07	0.24	2.10	2.10	1.31
1.0	-0.30	0.17	0.01	0.09	1.64	1.64	1.66
1.1	-1.29	0.59	0.34	0.16	0.53	0.53	1.91
1.2	4.94	3.22	3.36	0.15	1.13	1.13	2.19
1.3	1.14	1.22	1.09	-0.14	2.19	2.19	2.17
1.4	-6.61	-0.88	-1.39	0.02	1.72	1.72	2.11
1.5	8.09	3.20	3.54	0.12	0.61	0.61	2.35
1.6	0.88	2.03	2.03	-0.05	0.70	0.70	2.43
1.7	-5.22	-0.82	-1.21	0.00	1.98	1.98	2.22
1.8	4.73	1.85	1.99	-0.12	1.63	1.63	1.78
1.9	1.19	2.71	2.67	-0.36	0.55	0.55	1.79
2.0	0.79	0.65	0.47	0.10	1.38	1.38	2.27
2.1	-2.80	-0.06	-0.37	0.23	1.73	1.73	2.12
2.2	3.00	2.91	2.95	0.12	1.25	1.25	1.29
2.3	5.18	2.16	2.30	-0.08	0.81	0.81	0.49
2.4	-7.43	-1.26	-1.71	-0.04	1.75	1.75	0.56
2.5	4.24	2.35	2.48	0.16	2.09	2.09	1.02
2.6	4.53	2.94	3.09	0.29	0.92	0.92	0.76
2.7	-4.63	-0.61	-0.97	-0.25	0.15	0.15	0.14
2.8	2.28	1.13	1.03	0.04	2.19	2.19	-0.12
2.9	1.21	2.87	2.79	-0.10	1.80	1.80	0.19
3.0	2.68	1.28	1.28	-0.29	0.79	0.79	0.32

Time (Sec)	Acceleration (mm/sec^2)						
	Head	Chest	Waist	Upper Arm	Lower Arm	Thigh	Leg
3.1	-2.48	-0.39	-0.67	-0.01	0.71	0.71	-0.25
3.2	-0.38	2.15	2.07	0.28	1.68	1.68	-0.59
3.3	7.53	2.94	3.28	-0.04	1.72	1.72	-0.32
3.4	-5.80	-0.99	-1.41	-0.11	1.12	1.12	0.25
3.5	0.71	1.36	1.26	-0.02	0.88	0.88	0.52
3.6	6.20	3.45	3.65	0.36	2.39	2.39	0.37
3.7	-3.75	0.02	-0.38	0.06	1.04	1.04	0.53
3.8	1.12	0.48	0.35	0.01	0.51	0.51	0.87
3.9	1.23	2.55	2.57	-0.09	1.61	1.61	1.16
4.0	2.80	1.90	1.92	-0.19	2.03	2.03	1.37
4.1	-1.49	-0.30	-0.48	0.00	1.07	1.07	1.52
4.2	-2.20	1.21	1.09	-0.03	0.52	0.52	1.84
4.3	8.46	3.48	3.74	-0.03	1.10	1.10	2.06
4.4	-4.48	-0.22	-0.64	0.07	2.37	2.37	2.31
4.5	-2.08	0.35	0.12	-0.16	1.22	1.22	2.58
4.6	8.08	3.50	3.72	0.02	0.66	0.66	2.48
4.7	-3.14	0.84	0.53	0.29	1.73	1.73	2.15
4.8	-0.80	-0.02	-0.12	0.14	1.69	1.69	1.78
4.9	2.01	1.94	1.97	0.12	0.98	0.98	1.90
5.0	3.22	2.49	2.55	-0.26	1.00	1.00	2.26
5.1	-0.93	0.19	0.06	-0.11	1.86	1.86	2.11
5.2	-4.17	0.26	-0.11	0.19	1.58	1.58	1.65
5.3	9.11	3.64	3.89	-0.04	0.41	0.41	1.21
5.4	-1.83	0.84	0.63	-0.30	0.77	0.77	1.10
5.5	-5.46	-0.57	-0.99	0.14	2.48	2.48	1.00
5.6	8.26	3.06	3.34	-0.13	1.48	1.48	0.57

Time (Sec)	Acceleration (mm/sec^2)						
	Head	Chest	Waist	Upper Arm	Lower Arm	Thigh	Leg
5.7	-0.69	1.77	1.74	-0.07	0.64	0.64	0.28
5.8	-1.99	-0.17	-0.37	0.29	1.04	1.04	0.18
5.9	0.93	1.22	1.10	0.28	2.10	2.10	0.18
6.0	3.28	2.89	2.98	-0.12	1.49	1.49	0.06
6.1	1.79	1.00	0.90	-0.09	0.84	0.84	-0.13
6.2	-6.12	-0.56	-1.09	-0.06	1.17	1.17	-0.09
6.3	6.77	3.25	3.49	0.28	2.13	2.13	-0.20
6.4	2.42	1.95	2.00	-0.10	0.48	0.48	-0.36
6.5	-6.58	-1.08	-1.53	-0.25	0.87	0.87	-0.23
6.6	5.74	2.31	2.53	-0.08	1.94	1.94	0.27
6.7	1.13	2.58	2.58	-0.06	1.80	1.80	0.82
6.8	-0.95	0.11	-0.13	0.06	0.74	0.74	0.82
6.9	0.08	0.56	0.39	0.23	0.82	0.82	0.77
7.0	1.22	2.84	2.77	0.05	1.69	1.69	1.18
7.1	4.52	1.82	1.88	0.00	2.43	2.43	1.68
7.2	-5.60	-1.00	-1.38	-0.08	0.57	0.57	1.77
7.3	3.16	2.46	2.55	0.12	0.84	0.84	1.46
7.4	5.11	2.89	3.07	0.17	1.88	1.88	1.70
7.5	-6.05	-1.01	-1.40	-0.06	1.30	1.30	2.52
7.6	3.72	1.51	1.53	-0.16	0.85	0.85	2.88
7.7	2.10	3.04	3.00	-0.38	1.31	1.31	2.41
7.8	-0.67	0.61	0.42	0.12	1.75	1.75	1.72
7.9	0.24	0.10	-0.08	0.29	1.35	1.35	1.86
8.0	-0.12	2.36	2.27	-0.15	0.43	0.43	2.37
8.1	5.71	2.52	2.75	-0.05	1.57	1.57	2.26
8.2	-4.85	-0.91	-1.27	0.18	2.57	2.57	1.70

Time (Sec)	Acceleration (mm/sec^2)						
	Head	Chest	Waist	Upper Arm	Lower Arm	Thigh	Leg
8.3	0.34	1.48	1.42	-0.06	0.90	0.90	1.29
8.4	7.67	3.54	3.84	0.21	0.52	0.52	1.45
8.5	-5.76	-0.44	-0.93	0.12	1.45	1.45	1.54
8.6	1.04	0.69	0.53	-0.01	2.07	2.07	1.04
8.7	4.08	3.04	3.16	-0.27	1.00	1.00	0.44
8.8	-0.16	1.25	1.09	-0.23	0.73	0.73	0.05
8.9	-0.77	-0.11	-0.29	0.13	1.50	1.50	0.02
9.0	-1.21	1.58	1.53	0.26	1.84	1.84	0.06
9.1	7.44	3.09	3.36	-0.31	0.48	0.48	0.05
9.2	-3.64	-0.28	-0.63	-0.09	1.47	1.47	0.04
9.3	-3.59	0.43	0.15	0.19	2.06	2.06	-0.17
9.4	9.77	3.75	4.05	0.10	1.51	1.51	-0.28
9.5	-3.46	0.50	0.13	0.16	0.45	0.45	-0.19
9.6	-2.38	-0.07	-0.28	0.16	1.21	1.21	0.07
9.7	4.43	2.57	2.70	-0.21	2.03	2.03	0.31
9.8	1.41	1.95	1.93	-0.06	1.79	1.79	0.36
9.9	-0.44	0.09	0.01	-0.05	0.07	0.07	0.72
10.0	-3.33	0.69	0.42	0.01	1.31	1.31	1.27

The acceleration responses of all the human segments have been outlined through graphs in Fig. 49, Fig. 50, Fig. 51, Fig. 52, Fig. 53, Fig. 54 and Fig. 55.

3.7.2.1. Response at Head

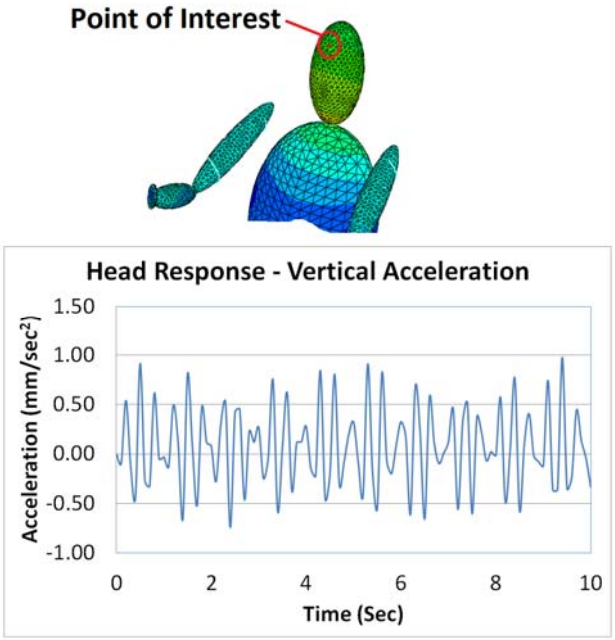

Fig. 49. Acceleration response at head

3.7.2.2. Response at Chest

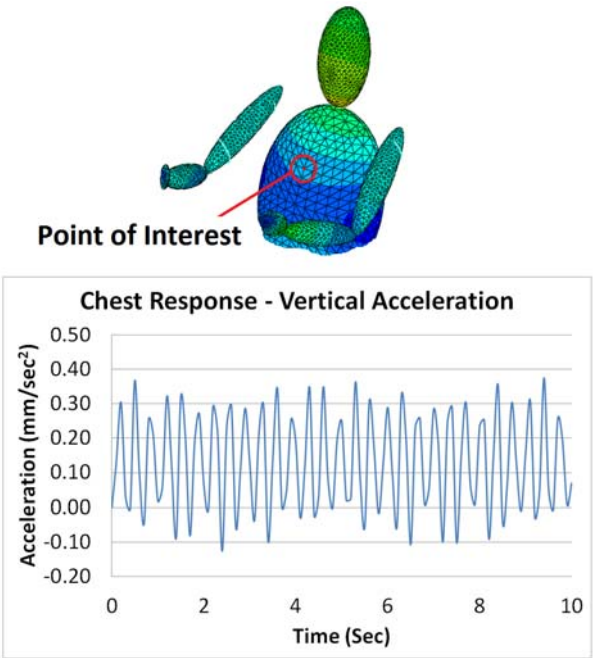

Fig. 50. Acceleration response at chest

3.7.2.3. Response at Waist

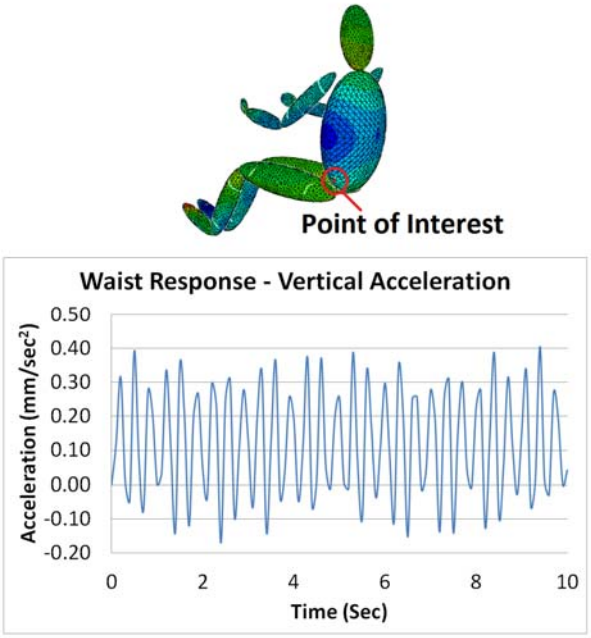

Fig. 51. Acceleration response at waist

3.7.2.4. Response at Upper Arm

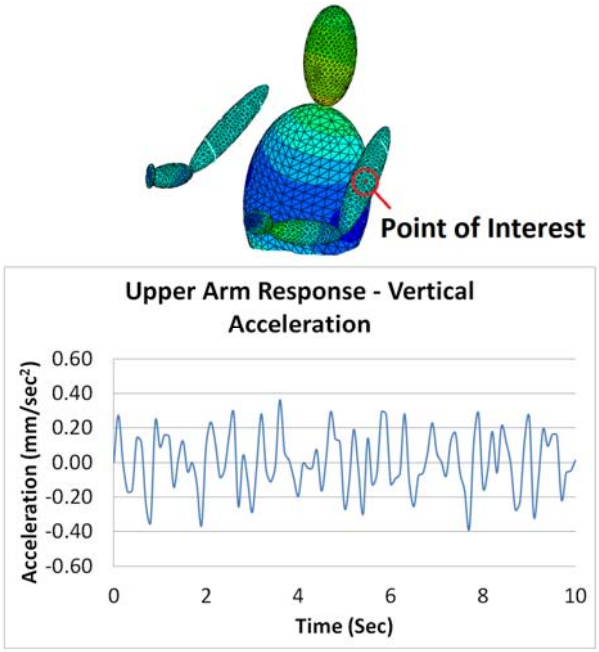

Fig. 52. Acceleration response at upper arm

3.7.2.5. Response at Lower Arm

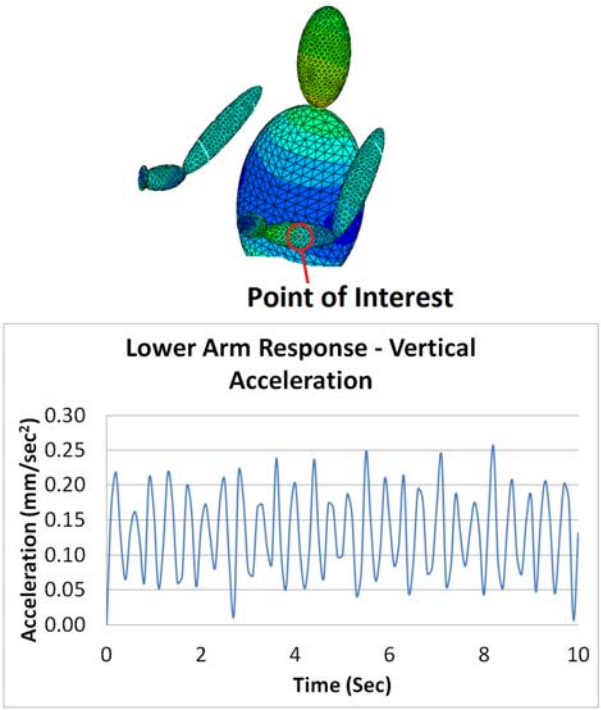

Fig. 53. Acceleration response at lower arm

3.7.2.6. Response at Thigh

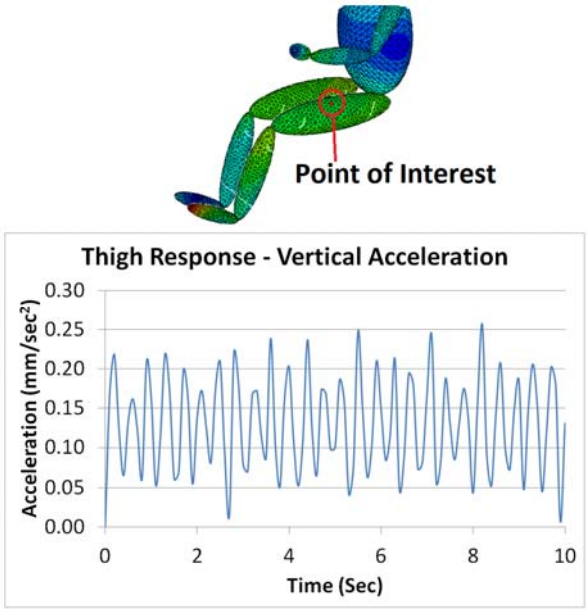

Fig. 54. Acceleration response at thigh

3.7.2.7. Response at Leg

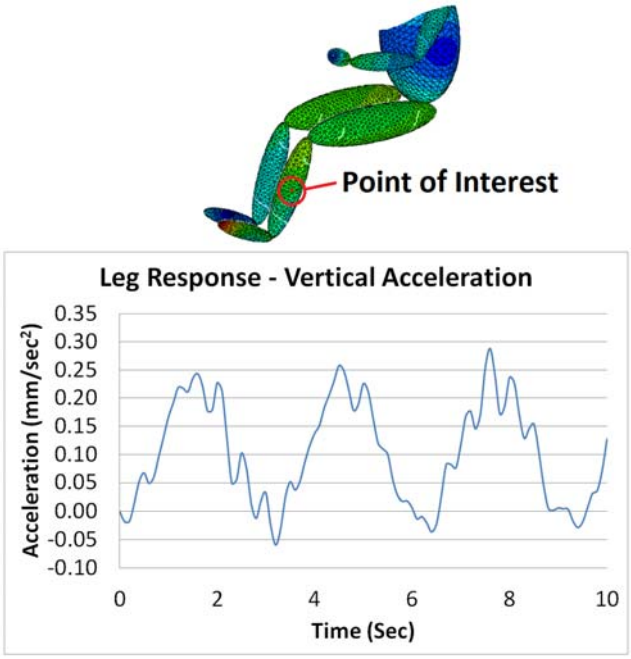

Fig. 55. Acceleration response at leg

3.7.3. Displacement responses at the points of interest

The measured vertical displacement values with respect to simulation time at the designated points of head, chest, waist, upper arm, lower arm, thigh and leg are shown in Table 16.

Table 16. Measured values of vertical displacements for all the segments

Time	Displacement (mm)						
(Sec)	Head	Chest	Waist	Upper Arm	Lower Arm	Thigh	Leg
0.0	0.0000000	0.0000000	0.0000000	0.0000000	0.0000000	0.0000000	0.0000000
0.1	0.0000043	0.0000061	0.0000062	0.0000007	0.0000008	-0.0000004	0.0000049
0.2	0.0000173	0.0000246	0.0000248	0.0000026	0.0000032	-0.0000017	0.0000197

Time (Sec)	Displacement (mm)						
	Head	Chest	Waist	Upper Arm	Lower Arm	Thigh	Leg
0.3	0.0000389	0.0000553	0.0000557	0.0000059	0.0000072	-0.0000038	0.0000443
0.4	0.0000692	0.0000983	0.0000991	0.0000104	0.0000129	-0.0000067	0.0000787
0.5	0.0001081	0.0001536	0.0001548	0.0000163	0.0000201	-0.0000104	0.0001230
0.6	0.0001557	0.0002211	0.0002229	0.0000234	0.0000290	-0.0000150	0.0001772
0.7	0.0002119	0.0003010	0.0003034	0.0000319	0.0000394	-0.0000205	0.0002411
0.8	0.0002768	0.0003931	0.0003963	0.0000417	0.0000515	-0.0000267	0.0003149
0.9	0.0003503	0.0004975	0.0005016	0.0000528	0.0000652	-0.0000338	0.0003986
1.0	0.0004324	0.0006142	0.0006192	0.0000651	0.0000805	-0.0000418	0.0004921
1.1	0.0005232	0.0007432	0.0007492	0.0000788	0.0000974	-0.0000505	0.0005954
1.2	0.0006227	0.0008845	0.0008916	0.0000938	0.0001159	-0.0000601	0.0007086
1.3	0.0007308	0.0010381	0.0010465	0.0001101	0.0001360	-0.0000706	0.0008316
1.4	0.0008476	0.0012039	0.0012136	0.0001277	0.0001578	-0.0000818	0.0009645
1.5	0.0009730	0.0013821	0.0013932	0.0001465	0.0001811	-0.0000939	0.0011072
1.6	0.0011070	0.0015725	0.0015852	0.0001667	0.0002061	-0.0001069	0.0012598
1.7	0.0012497	0.0017752	0.0017895	0.0001882	0.0002326	-0.0001207	0.0014221
1.8	0.0014011	0.0019902	0.0020062	0.0002110	0.0002608	-0.0001353	0.0015944
1.9	0.0015611	0.0022174	0.0022353	0.0002351	0.0002906	-0.0001507	0.0017764
2.0	0.0017297	0.0024570	0.0024768	0.0002605	0.0003220	-0.0001670	0.0019684
2.1	0.0019070	0.0027088	0.0027307	0.0002872	0.0003550	-0.0001841	0.0021701
2.2	0.0020929	0.0029729	0.0029969	0.0003152	0.0003896	-0.0002021	0.0023817

Time (Sec)	Displacement (mm)						
	Head	Chest	Waist	Upper Arm	Lower Arm	Thigh	Leg
2.3	0.0022875	0.0032493	0.0032756	0.0003445	0.0004258	-0.0002209	0.0026032
2.4	0.0024908	0.0035380	0.0035666	0.0003752	0.0004636	-0.0002405	0.0028344
2.5	0.0027027	0.0038390	0.0038700	0.0004071	0.0005031	-0.0002610	0.0030756
2.6	0.0029232	0.0041523	0.0041858	0.0004403	0.0005441	-0.0002822	0.0033265
2.7	0.0031524	0.0044778	0.0045140	0.0004748	0.0005868	-0.0003044	0.0035874
2.8	0.0033902	0.0048156	0.0048545	0.0005106	0.0006311	-0.0003273	0.0038580
2.9	0.0036367	0.0051658	0.0052075	0.0005478	0.0006769	-0.0003511	0.0041385
3.0	0.0038918	0.0055282	0.0055728	0.0005862	0.0007244	-0.0003758	0.0044288
3.1	0.0041556	0.0059028	0.0059505	0.0006259	0.0007735	-0.0004012	0.0047290
3.2	0.0044280	0.0062898	0.0063406	0.0006670	0.0008242	-0.0004275	0.0050390
3.3	0.0047091	0.0066891	0.0067431	0.0007093	0.0008766	-0.0004547	0.0053589
3.4	0.0049988	0.0071006	0.0071579	0.0007529	0.0009305	-0.0004826	0.0056886
3.5	0.0052972	0.0075244	0.0075852	0.0007979	0.0009860	-0.0005114	0.0060281
3.6	0.0056042	0.0079605	0.0080248	0.0008441	0.0010432	-0.0005411	0.0063775
3.7	0.0059199	0.0084089	0.0084768	0.0008917	0.0011020	-0.0005716	0.0067368
3.8	0.0062442	0.0088696	0.0089412	0.0009405	0.0011623	-0.0006029	0.0071058
3.9	0.0065772	0.0093425	0.0094180	0.0009907	0.0012243	-0.0006350	0.0074848
4.0	0.0069188	0.0098278	0.0099072	0.0010421	0.0012879	-0.0006680	0.0078735
4.1	0.0072691	0.0103253	0.0104087	0.0010949	0.0013531	-0.0007018	0.0082721
4.2	0.0076280	0.0108351	0.0109226	0.0011490	0.0014199	-0.0007364	0.0086806

Time	Displacement (mm)						
(Sec)	Head	Chest	Waist	Upper Arm	Lower Arm	Thigh	Leg
4.3	0.0079955	0.0113572	0.0114489	0.0012043	0.0014883	-0.0007719	0.0090989
4.4	0.0083717	0.0118916	0.0119876	0.0012610	0.0015584	-0.0008082	0.0095270
4.5	0.0087566	0.0124382	0.0125387	0.0013190	0.0016300	-0.0008454	0.0099650
4.6	0.0091501	0.0129972	0.0131022	0.0013782	0.0017033	-0.0008834	0.0104128
4.7	0.0095523	0.0135684	0.0136780	0.0014388	0.0017781	-0.0009222	0.0108704
4.8	0.0099631	0.0141519	0.0142663	0.0015007	0.0018546	-0.0009618	0.0113379
4.9	0.0103825	0.0147477	0.0148669	0.0015639	0.0019327	-0.0010023	0.0118153
5.0	0.0108106	0.0153558	0.0154799	0.0016284	0.0020124	-0.0010437	0.0123025
5.1	0.0112473	0.0159761	0.0161053	0.0016942	0.0020937	-0.0010858	0.0127995
5.2	0.0116927	0.0166088	0.0167430	0.0017613	0.0021766	-0.0011288	0.0133064
5.3	0.0121468	0.0172537	0.0173932	0.0018297	0.0022612	-0.0011726	0.0138231
5.4	0.0126095	0.0179109	0.0180557	0.0018994	0.0023473	-0.0012173	0.0143497
5.5	0.0130808	0.0185804	0.0187306	0.0019704	0.0024350	-0.0012628	0.0148861
5.6	0.0135608	0.0192622	0.0194179	0.0020427	0.0025244	-0.0013091	0.0154323
5.7	0.0140494	0.0199563	0.0201176	0.0021163	0.0026154	-0.0013563	0.0159884
5.8	0.0145467	0.0206626	0.0208297	0.0021912	0.0027080	-0.0014043	0.0165543
5.9	0.0150526	0.0213812	0.0215541	0.0022674	0.0028022	-0.0014531	0.0171301
6.0	0.0155672	0.0221121	0.0222909	0.0023449	0.0028980	-0.0015028	0.0177157
6.1	0.0160905	0.0228553	0.0230401	0.0024238	0.0029954	-0.0015533	0.0183112
6.2	0.0166223	0.0236108	0.0238017	0.0025039	0.0030944	-0.0016046	0.0189165

Time	Displacement (mm)						
(Sec)	Head	Chest	Waist	Upper Arm	Lower Arm	Thigh	Leg
6.3	0.0171629	0.0243786	0.0245757	0.0025853	0.0031950	-0.0016568	0.0195317
6.4	0.0177120	0.0251586	0.0253621	0.0026681	0.0032973	-0.0017098	0.0201567
6.5	0.0182699	0.0259509	0.0261608	0.0027521	0.0034011	-0.0017636	0.0207915
6.6	0.0188363	0.0267556	0.0269720	0.0028374	0.0035066	-0.0018183	0.0214362
6.7	0.0194114	0.0275724	0.0277955	0.0029241	0.0036137	-0.0018738	0.0220907
6.8	0.0199952	0.0284016	0.0286314	0.0030120	0.0037224	-0.0019302	0.0227551
6.9	0.0205876	0.0292431	0.0294796	0.0031013	0.0038327	-0.0019873	0.0234293
7.0	0.0211887	0.0300968	0.0303403	0.0031919	0.0039446	-0.0020453	0.0241134
7.1	0.0217984	0.0309629	0.0312133	0.0032837	0.0040582	-0.0021042	0.0248073
7.2	0.0224168	0.0318412	0.0320988	0.0033769	0.0041733	-0.0021639	0.0255110
7.3	0.0230438	0.0327318	0.0329966	0.0034714	0.0042900	-0.0022244	0.0262246
7.4	0.0236794	0.0336346	0.0339068	0.0035671	0.0044084	-0.0022857	0.0269481
7.5	0.0243237	0.0345498	0.0348293	0.0036642	0.0045284	-0.0023479	0.0276814
7.6	0.0249767	0.0354772	0.0357643	0.0037626	0.0046500	-0.0024109	0.0284245
7.7	0.0256383	0.0364169	0.0367116	0.0038623	0.0047732	-0.0024748	0.0291775
7.8	0.0263085	0.0373689	0.0376714	0.0039633	0.0048980	-0.0025394	0.0299403
7.9	0.0269874	0.0383332	0.0386435	0.0040656	0.0050244	-0.0026050	0.0307129
8.0	0.0276750	0.0393098	0.0396280	0.0041692	0.0051524	-0.0026713	0.0314955
8.1	0.0283712	0.0402987	0.0406248	0.0042741	0.0052821	-0.0027385	0.0322878
8.2	0.0290760	0.0412998	0.0416341	0.0043803	0.0054133	-0.0028065	0.0330900

Time	Displacement (mm)						
(Sec)	Head	Chest	Waist	Upper Arm	Lower Arm	Thigh	Leg
8.3	0.0297895	0.0423132	0.0426557	0.0044878	0.0055462	-0.0028754	0.0339021
8.4	0.0305116	0.0433389	0.0436897	0.0045966	0.0056807	-0.0029451	0.0347240
8.5	0.0312424	0.0443769	0.0447361	0.0047068	0.0058168	-0.0030156	0.0355557
8.6	0.0319818	0.0454271	0.0457949	0.0048182	0.0059545	-0.0030869	0.0363973
8.7	0.0327299	0.0464897	0.0468661	0.0049309	0.0060938	-0.0031591	0.0372487
8.8	0.0334867	0.0475645	0.0479496	0.0050450	0.0062348	-0.0032321	0.0381100
8.9	0.0342520	0.0486516	0.0490455	0.0051603	0.0063773	-0.0033060	0.0389811
9.0	0.0350261	0.0497510	0.0501539	0.0052770	0.0065215	-0.0033807	0.0398621
9.1	0.0358087	0.0508627	0.0512745	0.0053949	0.0066673	-0.0034562	0.0407529
9.2	0.0366001	0.0519866	0.0524076	0.0055142	0.0068147	-0.0035326	0.0416536
9.3	0.0374000	0.0531229	0.0535531	0.0056348	0.0069636	-0.0036098	0.0425641
9.4	0.0382086	0.0542714	0.0547109	0.0057566	0.0071143	-0.0036878	0.0434845
9.5	0.0390259	0.0554322	0.0558811	0.0058798	0.0072665	-0.0037667	0.0444147
9.6	0.0398518	0.0566053	0.0570637	0.0060043	0.0074203	-0.0038464	0.0453547
9.7	0.0406864	0.0577906	0.0582587	0.0061301	0.0075758	-0.0039269	0.0463046
9.8	0.0415296	0.0589883	0.0594661	0.0062572	0.0077329	-0.0040083	0.0472644
9.9	0.0423815	0.0601982	0.0606858	0.0063856	0.0078915	-0.0040904	0.0482340
10.0	0.0432420	0.0614204	0.0619180	0.0065153	0.0080518	-0.0041735	0.0492134

The displacement values of all the human segments have been outlined graphically in Fig. 56.

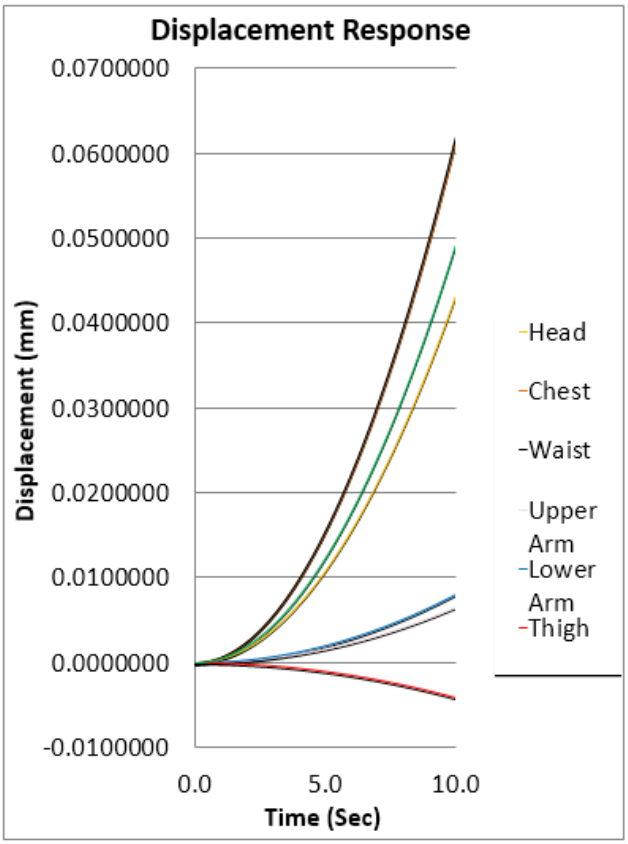

Fig. 56. Displacement values at different human segments

3.7.4. Frequencies at the points of interest

The frequencies of the human segments have been calculated and given in Table 17.

Table 17. Calculated values of frequencies for all the segments

Time (Sec)	Frequency (Hz)						
	Head	Chest	Waist	Upper Arm	Lower Arm	Thigh	Leg
0.0	0.00	0.00	0.00	0.00	0.00	0.00	0.00
0.1	23.87	23.50	22.11	32.68	73.26	101.71	9.55

Time (Sec)	Frequency (Hz)						
	Head	Chest	Waist	Upper Arm	Lower Arm	Thigh	Leg
0.2	28.19	17.70	17.99	0.77	41.45	57.55	4.70
0.3	9.00	3.59	2.15	8.54	20.77	28.84	2.93
0.4	12.70	1.00	3.38	6.21	11.34	15.74	4.10
0.5	14.65	7.79	8.02	4.73	12.94	17.97	3.73
0.6	6.64	3.33	2.95	3.50	11.90	16.52	2.64
0.7	6.24	1.99	2.51	4.45	8.87	12.32	2.51
0.8	7.52	4.04	4.18	4.56	5.49	7.63	2.77
0.9	1.87	3.27	3.23	3.38	9.03	12.54	2.88
1.0	1.33	0.85	0.18	1.88	7.18	9.97	2.93
1.1	2.50	1.42	1.06	2.26	3.72	5.16	2.85
1.2	4.48	3.04	3.09	2.01	4.97	6.90	2.80
1.3	1.99	1.72	1.62	1.80	6.38	8.86	2.57
1.4	4.44	1.36	1.70	0.66	5.26	7.30	2.36
1.5	4.59	2.42	2.54	1.47	2.92	4.05	2.32
1.6	1.42	1.81	1.80	0.89	2.93	4.07	2.21
1.7	3.25	1.08	1.31	0.04	4.65	6.45	1.99
1.8	2.93	1.54	1.59	1.21	3.98	5.53	1.68
1.9	1.39	1.76	1.74	1.98	2.18	3.03	1.60
2.0	1.07	0.82	0.69	0.96	3.30	4.58	1.71
2.1	1.93	0.23	0.59	1.44	3.51	4.87	1.57
2.2	1.90	1.58	1.58	0.97	2.85	3.95	1.17
2.3	2.39	1.30	1.33	0.78	2.20	3.06	0.69
2.4	2.75	0.95	1.10	0.53	3.10	4.30	0.71
2.5	1.99	1.24	1.27	0.99	3.24	4.50	0.92
2.6	1.98	1.34	1.37	1.28	2.07	2.87	0.76

Time (Sec)	Frequency (Hz)						
	Head	Chest	Waist	Upper Arm	Lower Arm	Thigh	Leg
2.7	1.93	0.59	0.74	1.16	0.79	1.10	0.31
2.8	1.31	0.77	0.73	0.45	2.97	4.12	0.28
2.9	0.92	1.19	1.17	0.68	2.60	3.61	0.34
3.0	1.32	0.77	0.76	1.12	1.66	2.31	0.43
3.1	1.23	0.41	0.53	0.20	1.52	2.12	0.37
3.2	0.47	0.93	0.91	1.03	2.27	3.15	0.55
3.3	2.01	1.06	1.11	0.38	2.23	3.10	0.39
3.4	1.72	0.59	0.71	0.61	1.75	2.43	0.33
3.5	0.58	0.68	0.65	0.25	1.50	2.08	0.47
3.6	1.67	1.05	1.07	1.04	2.41	3.34	0.38
3.7	1.27	0.07	0.34	0.42	1.55	2.15	0.45
3.8	0.68	0.37	0.32	0.18	1.05	1.46	0.56
3.9	0.69	0.83	0.83	0.48	1.82	2.53	0.63
4.0	1.01	0.70	0.70	0.69	2.00	2.77	0.66
4.1	0.72	0.27	0.34	0.10	1.41	1.96	0.68
4.2	0.86	0.53	0.50	0.26	0.97	1.34	0.73
4.3	1.64	0.88	0.91	0.25	1.37	1.90	0.76
4.4	1.17	0.22	0.37	0.38	1.96	2.73	0.78
4.5	0.78	0.27	0.16	0.56	1.38	1.91	0.81
4.6	1.50	0.83	0.85	0.20	0.99	1.38	0.78
4.7	0.91	0.40	0.31	0.72	1.57	2.18	0.71
4.8	0.45	0.06	0.14	0.48	1.52	2.11	0.63
4.9	0.70	0.58	0.58	0.44	1.13	1.57	0.64
5.0	0.87	0.64	0.65	0.64	1.12	1.56	0.68
5.1	0.46	0.18	0.09	0.41	1.50	2.09	0.65

Time (Sec)	Frequency (Hz)						
	Head	Chest	Waist	Upper Arm	Lower Arm	Thigh	Leg
5.2	0.95	0.20	0.13	0.53	1.36	1.89	0.56
5.3	1.38	0.73	0.75	0.24	0.68	0.95	0.47
5.4	0.61	0.34	0.30	0.63	0.91	1.27	0.44
5.5	1.03	0.28	0.37	0.42	1.61	2.23	0.41
5.6	1.24	0.63	0.66	0.40	1.22	1.69	0.31
5.7	0.35	0.47	0.47	0.28	0.79	1.09	0.21
5.8	0.59	0.14	0.21	0.58	0.99	1.37	0.17
5.9	0.40	0.38	0.36	0.56	1.38	1.91	0.17
6.0	0.73	0.58	0.58	0.37	1.14	1.58	0.10
6.1	0.53	0.33	0.31	0.31	0.84	1.17	0.13
6.2	0.97	0.25	0.34	0.25	0.98	1.36	0.11
6.3	1.00	0.58	0.60	0.53	1.30	1.81	0.16
6.4	0.59	0.44	0.45	0.32	0.61	0.84	0.21
6.5	0.96	0.32	0.39	0.48	0.81	1.12	0.17
6.6	0.88	0.47	0.49	0.26	1.18	1.64	0.18
6.7	0.38	0.49	0.48	0.23	1.12	1.56	0.31
6.8	0.35	0.10	0.11	0.22	0.71	0.99	0.30
6.9	0.10	0.22	0.18	0.43	0.73	1.02	0.29
7.0	0.38	0.49	0.48	0.21	1.04	1.44	0.35
7.1	0.73	0.39	0.39	0.05	1.23	1.71	0.41
7.2	0.80	0.28	0.33	0.24	0.59	0.82	0.42
7.3	0.59	0.44	0.44	0.30	0.70	0.98	0.38
7.4	0.74	0.47	0.48	0.35	1.04	1.44	0.40
7.5	0.79	0.27	0.32	0.20	0.85	1.19	0.48
7.6	0.61	0.33	0.33	0.33	0.68	0.94	0.51

Time (Sec)	Frequency (Hz)						
	Head	Chest	Waist	Upper Arm	Lower Arm	Thigh	Leg
7.7	0.46	0.46	0.46	0.50	0.83	1.16	0.46
7.8	0.25	0.20	0.17	0.28	0.95	1.32	0.38
7.9	0.15	0.08	0.07	0.42	0.82	1.15	0.39
8.0	0.10	0.39	0.38	0.30	0.46	0.64	0.44
8.1	0.71	0.40	0.41	0.17	0.87	1.20	0.42
8.2	0.65	0.24	0.28	0.32	1.10	1.52	0.36
8.3	0.17	0.30	0.29	0.18	0.64	0.89	0.31
8.4	0.80	0.46	0.47	0.34	0.48	0.67	0.33
8.5	0.68	0.16	0.23	0.25	0.80	1.10	0.33
8.6	0.29	0.20	0.17	0.08	0.94	1.30	0.27
8.7	0.56	0.41	0.41	0.37	0.64	0.89	0.17
8.8	0.11	0.26	0.24	0.34	0.55	0.76	0.06
8.9	0.24	0.07	0.12	0.25	0.77	1.07	0.04
9.0	0.30	0.28	0.28	0.36	0.85	1.18	0.06
9.1	0.73	0.39	0.41	0.38	0.43	0.59	0.05
9.2	0.50	0.12	0.17	0.21	0.74	1.03	0.05
9.3	0.49	0.14	0.08	0.30	0.87	1.20	0.10
9.4	0.81	0.42	0.43	0.21	0.73	1.02	0.13
9.5	0.47	0.15	0.08	0.27	0.40	0.55	0.10
9.6	0.39	0.05	0.11	0.26	0.64	0.89	0.06
9.7	0.53	0.34	0.34	0.30	0.82	1.14	0.13
9.8	0.29	0.29	0.29	0.16	0.76	1.06	0.14
9.9	0.16	0.06	0.02	0.14	0.15	0.20	0.19
10.0	0.44	0.17	0.13	0.07	0.64	0.89	0.26

The frequencies of all the human segments with respect to simulation time have been outlined through graph in Fig. 57.

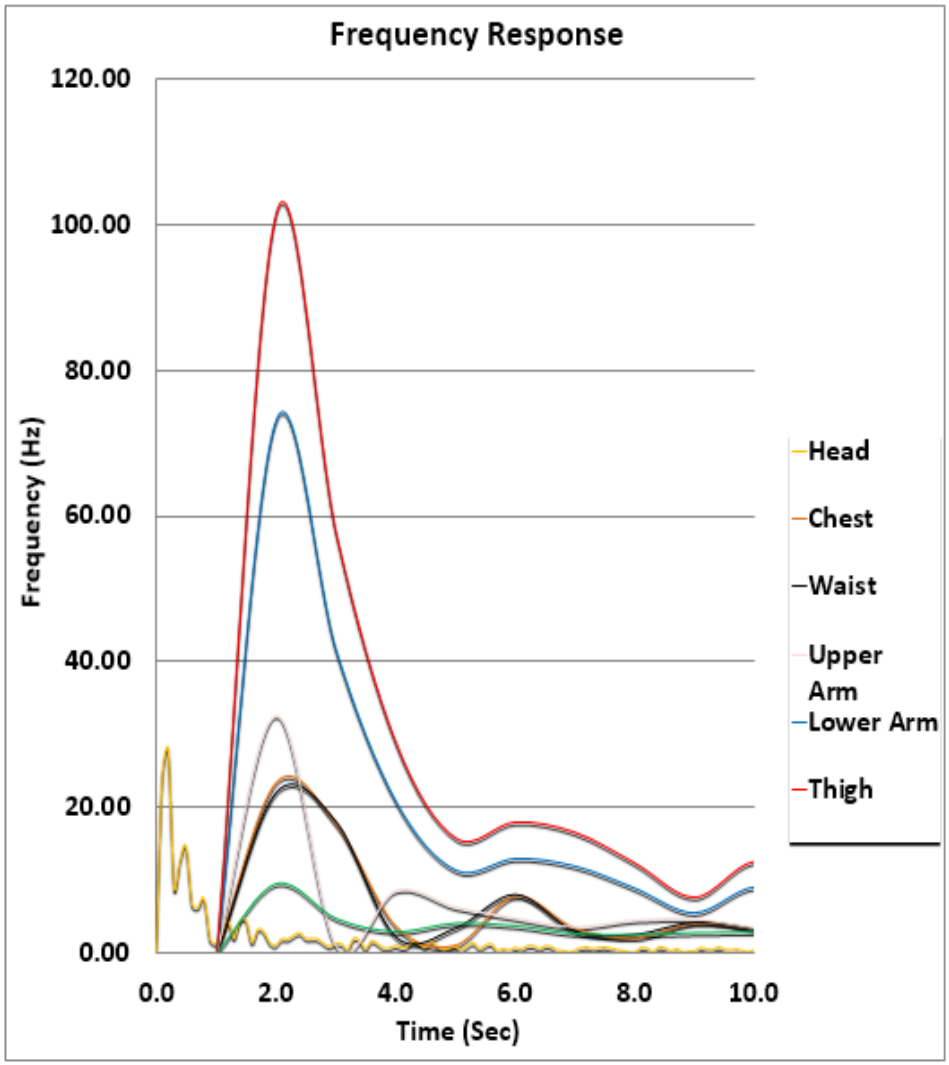

Fig. 57. Frequencies at different segments

The average frequencies of all the human segments are presented in Table 18.

Table 18. Average frequencies of human segments

Segment	Average frequency of human segment (Hz)
Head	2.06
Chest	1.20
Waist	1.21
Upper Arm	1.17
Lower Arm	3.39
Thigh	4.70
Leg	0.93

3.8. Discussion on this Unique Simulation Technique

The frequencies obtained from this simulation results, are close to the acceptable ranges of frequencies for human body portions as found in other studies. Investigation on the vibro-acoustic system (Cempel, 1989) showed the natural frequency values for head, chest, upper limbs, pelvis and muscles as 4-5 Hz, 5-9 Hz, 3 Hz, 5-9 Hz and 3-4 Hz, respectively. Analysis of the bio-dynamic model (Zengkang *et al.*, 2013) suggested that the permissible frequency values for vertical and fore-aft vibration to be 0.5-20 Hz and 0.5-12 Hz, respectively.

Forced vibration along with three directional stiffness values have been taken into account during this course of biodynamic simulation work. Moreover, the stiffness values have been calculated based on the real life human parameters. These are the reasons for obtaining the frequency values close to the allowable limits. The displacement values obtained from this simulation are higher than expected. If the car seat is associated to the finite element model with proper material properties and the whole human-seat system is excited with forced vibration, the displacement magnitudes will be more realistic.

From the outputs of the unique simulation work, it is clear that the finite element method can effectively be used to establish a comprehensive bio-dynamic model for vibration analysis using this unique technique. The boundary conditions, material properties and load conditions used in this unique simulation methodology have worked flawless and yielded realistic outputs. So, this bio-dynamic simulation set up can be taken to further advanced level in association with the car seat.

CHAPTER 4

SIMULATION MODEL DEVELOPED FOR CAR SEAT

The basic objective of the automotive seat is to provide the comfortable sitting arrangement and offer sufficient safety to human occupant. Ideal ergonomic design of the car seat is achieved by a combination of mechanical framework and foam materials. The seat base and slider rail underneath the seat are made of the metallic framework, while the cushion, backrest and headrest are made of the foam materials. The mechanical frameworks and foam materials provide the support to the seated human and safe driving condition.

Fig. 58. Car seat segments (Seat rails underneath the seat is not shown)

The elementary structures of the car seats from various manufacturers are very similar to each other and consist of seat base, seat rail, cushion, backrest and headrest. The cushion and the backrest are further sub-divided into two ends, middle and wing portions. A typical car seat and its major components are shown in Fig. 58. The car seat can be adjusted to fit with the safe human posture by means of front-back sliding movement, vertical height adjustment, backrest angular adjustment and headrest tilting adjustment.

Car seat design considers many design parameters which are related to the type of the car seat and its material properties. Car seat properties have great influence on the human health and safety and numerous number of seat design variables had been reported in the studies over the past few decades. More the number of parameters are taken into considerations, more the seat design procedure becomes complex and time consuming.

Car seat cushion, backrest and headrest are made of the polyurethane foam material and during the design process of car seat the main challenge is to assess and define the mechanical properties of this foam material. The level of vibration transmission from the seat to the human body greatly depends on the automotive seat material, hence the material modelling of the car seat should be accurate enough to match to the physical foam material properties. The most realistic way of foam material modelling is to consider it as hyper-elastic or viscoelastic material. For detailed investigation of car seat, initiative can be taken to consider both the hyper-elastic and viscoelastic material properties together.

4.1. Past works on Vibration Investigation Techniques and Material Properties of Automotive Seat

Automobile seats can be classified into suspension and foam types. In the mechanical suspension seats, the seat cushion is supported by a set of spring and damper arrangements, while in the foam seats, a full depth foam cushion along with foam

backrest is utilized. Though the foam material can be constructed by nylon, polyester, alcantara, vinyl, faux leather or leather, still the most commonly used foam material for the car seat is known as polyurethane.

A comparative study of car seat transmissibilities (Griffin, 1990) was carried out for understanding the transmissibility level of vibration from the car seat to human body for different kinds of seats. It was visible that the level of vibration transmission in case of foam cushion was higher for the frequency range of 4-8 Hz. The transmissibility obtained from that study had been graphically presented as shown in Fig. 59.

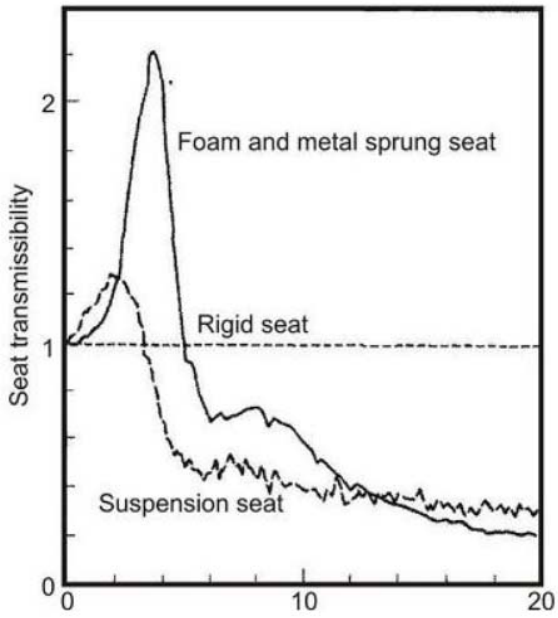

Fig. 59. Transmissibility study using different seat types (Griffin, 1990)

Material properties of the car seat are vital to assess the contact interface between the human and seat. The study on the comfort level of automotive seats (Zhao *et al.*, 1994) showed the contact interactions between the human and seat and associated acceleration transmission. Physical characteristics and subjective comforts were investigated (Park *et al.*, 1997) with respect to the pressure distribution at the seat-human contact interface. Human safety was judged during the collision investigation (Warner *et al.*, 1991), which

concluded that the seat shape and material would play very important roles for the human movements in the rear and side directions during the course of accident.

The mechanical behavior of the foam material are non-linear in nature and usually the foams are in compressed condition. For the small level of strain, the stress generated inside the foam material behaves like perfect elastic material, but with the further increment of the strain, the stress level exhibits gradual increment. At the end of the compression method, the foam material again shows the sharp increment in the stress level. The polyurethane foam material can be described as hyper-elastic elastomer with visco-elastic behavior. Study on the car seat using finite element (Haan, 2002) showed the non-linear nature of foam material along with hysteresis effects under cyclic loading, strain rate dependency and energy dissipation as presented in Fig. 60.

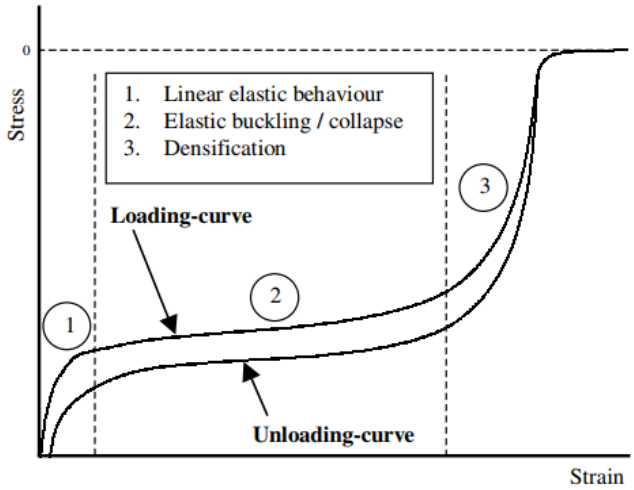

Fig. 60. Behaviour of polyurethane foam material under compression (Haan, 2002)

Similar kind of graph was obtained during the study (Singh *et al.*, 2003) of full depth foam type car seat for load deflection investigation. The process of load-deflection curve measurement is outlined in detail in the international standard ISO 2439:2008 for flexible cellular polymeric materials and determination of hardness using indentation technique.

The study on the foam material (Rusch, 1965) gave relations between the stress and strain inside the polyurethane foam as shown in Equation 4.1 and 4.2.

$$\sigma = E_f \cdot \varepsilon \cdot \psi(\varepsilon) \qquad \text{(Eq. 4.1)}$$

$$\frac{E_f}{E_o} = \frac{\varphi\left(2 + 7\varphi + 3\varphi^2\right)}{12} \qquad \text{(Eq. 4.2)}$$

Where,

σ = compressive stress

ε = compressive strain

E_f = Young's modulus of foam

E_o = Young's modulus of matrix polymer

$\psi(\varepsilon)$ = Factor reflecting the collapse of matrix

φ = Volume fraction of foam

The behaviour of the car seat polyurethane foam are complex and non-linear which exhibit hysteresis under the cyclic loading condition. Polyurethane foam can show high level of strain under the influence of low level of stress, hence, is highly capable of absorbing the energy. During the material modellings of seat cushion and soft human tissue using finite element method (Grujicic *et al.*, 2009), the Ogden model for strain energy absorption capacity of the hyper-elastic material was described with the Equation 4.3.

$$U = \sum_{i=1}^{N} \left[\frac{2\mu_i}{\alpha_i^2} \cdot \left[\lambda_1^{\alpha_i} + \lambda_2^{\alpha_i} + \lambda_3^{\alpha_i} - 3 + \frac{1}{\beta_i} \cdot \left[\left(J^{el}\right)^{-\alpha_i \cdot \beta_i} - 1 \right] \right] \right] \qquad \text{(Eq. 4.3)}$$

Where,

N = parameter defining approximate order of model

λ = principal stretch

J^{el} = elastic volume ratio

α_i, β_i, μ_i = material parameters

The same mathematical model for the strain energy absorption capacity was proposed earlier for slightly compressible hyper-elastic materials (Ogden, 1972) and highly compressible hyper-elastic materials (Mills, 2003).

Approaches had been taken in many research works to describe the material properties of the polyurethane foam by the non-linear stress-strain responses with respect to the variable strain rates. FE model of a car seat (Haan, 2002) reported that the stress-strain relationship was a function of the strain rate of the polyurethane foam material and advised for further testing to obtain more accurate strain rate related data. Modelling of polymeric foam material subjected to dynamic crash loading (Zhang *et.al.*, 1998) represented the stress-strain characteristics of polyurethane foam material under the effect of the uniaxial compression with variable strain rate. The obtained stress-strain curves are shown in Fig. 61.

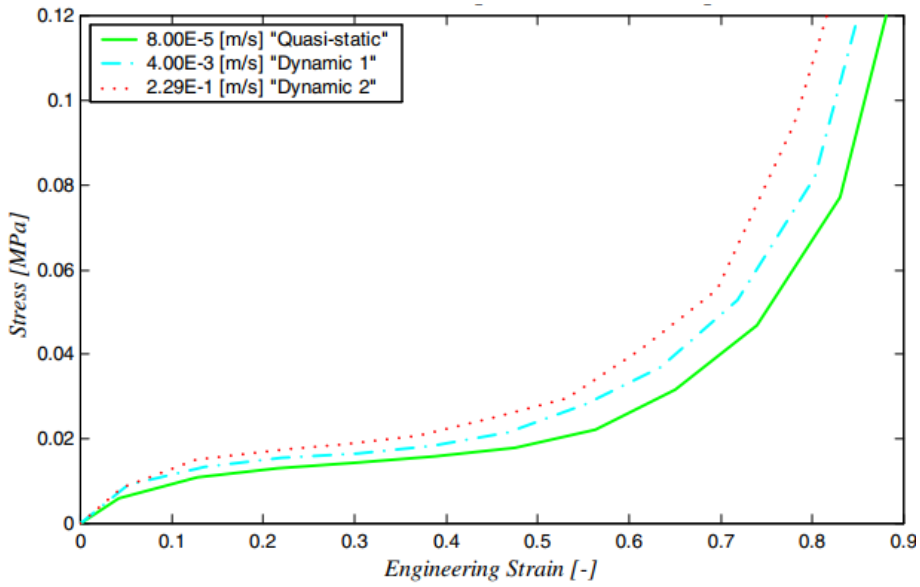

Fig. 61. Stress-strain behaviour of polyurethane foam with respect to variable strain rate (Zhang *et.al.*, 1998)

Numerical simulation of the seat cushion made of polyurethane foam (Camprubí *et.al*, 2007) revealed the relationship of the stress and strain under the effects of uniaxial compression and uniaxial indentation loads as shown in Fig. 62. The simulation data were compared to the testing data and it was found that the simulation modelling of the car seat cushion with hyper-foam material was able to predict the accurate stress-strain relationship.

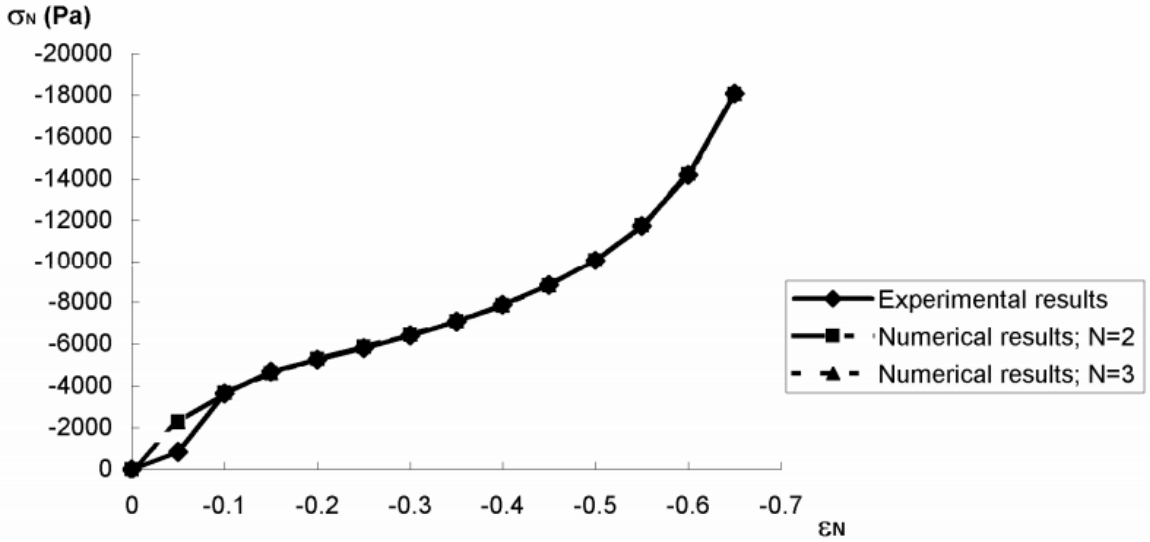

Fig. 62. Stress-strain relationship of polyurethane foam under the effect of uniaxial compression load (Camprubí *et.al*, 2007)

Besides the hyper-elastic material properties and non-linear stress-strain behaviour, polyurethane foam also exhibits visco-elastic properties. While exploring the shear modulus of the foam material for car seat cushion (Grujicic *et al.*, 2009), the time based Prony series formulation of Equation 4.4 had been used.

$$G(t) = G_o - \sum_{i=1}^{N} \left[G_i \cdot \left(1 - e^{\frac{-t}{\tau_i}} \right) \right] \qquad \text{(Eq. 4.4)}$$

Where,

$G(t)$ = time dependent shear modulus

G_o = instantaneous shear modulus

G_i = relaxation magnitud

τ_i = relaxation time

Prony series formulation is known as one of the best effective ways to analyse the visco-elastic materials in the finite element environment.

Same like the simulation modelling of the seated human body, car seat and its portions had also been modelled over last many years using the lumped mass parameter method, finite element technique and multi-body dynamic system.

A seat model was developed in the finite element environment (Kondo *et al.*, 2002) using foam and spring elements to analyse the vertical vibration of the system. Aspects of the three dimensional simulation process for the car seat were explored using LS-Dyna on dummy human model (Williamson, 2005) and the contract stress distribution between car seat cushion and human body was monitored. The outputs from LS-Dyna of that study are visually represented in Fig. 63.

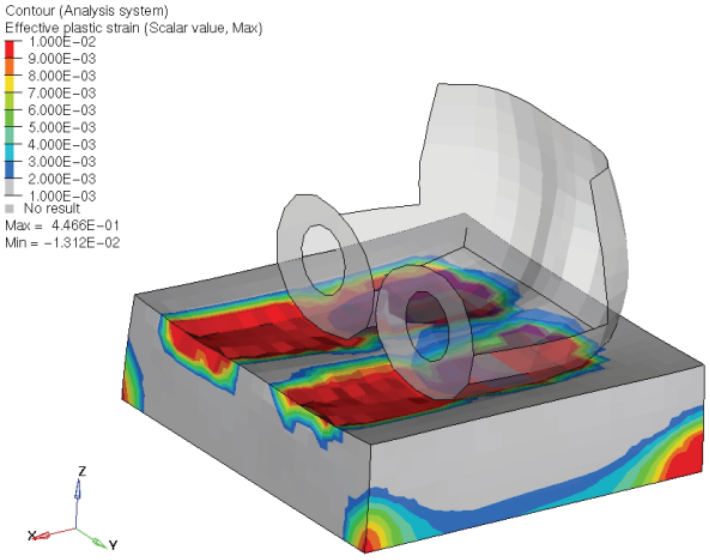

Fig. 63. Contact stress distribution at seat-human interface (Williamson, 2005)

The vibration transmitted to the backrest of a seat through the human body, was investigated through two, four and six input points (Qiu and Griffin, 2003). That study concluded that the vibration magnitudes at the four corners of the seat cushion were highly related to the acceleration of the backrest. To understand the effect of the acceleration, a seat was developed (Marshall *et al.*, 2000) in the aviation mode utilizing beam, shell and joint elements in both the multi-body and finite element environments. To estimate the vibration transmissibility of the automotive seat, a lumped mass model was developed (Cho, 2000), which was also feasible to study the impedance level inside the seat.

4.2. Preparation of CAD Assembly of the Car Seat

Design concepts of the car seat have been modified over time by the seat manufacturers based on the demands from the industrial and ergonomic aspects. “Ricaro”, a pioneer in the field of automotive seat designing, showed the shape and size changes of the seat over in the 40 years. The revolution of car seat design from 1971 to 2009, has visually been detailed in Fig. 64.

During the study of ergonomic evaluation of the car seat (Jhinkwan and Singh, 2014), effects of the car seat postures on the human body injury were overviewed. Specifications on the fit parameters (Gordon *et al.*, 1989) suggested that the minimum cushion width to be 432 mm for 95^{th} percentile female body, though larger cushion width would be beneficial considering the human clothing. Another similar kind of study (Grandjean, 1980) advised that the minimum cushion width to be in between 480 mm and 500 mm.

Fig. 64. Changes of the seat design concepts during 1971 – 2009 (Collected from Ricaro automotive seat design database)

Recommendations had also been given on the optimized length of the seat cushion. Suggested seat cushion lengths according to different investigations are 432 mm (Keegan, 1964), in-between 440 mm and 550 mm (Grandjean, 1980), and 330 mm to 470 mm (Chaffin and Anderson, 1991), depending on the human body anthropometric dimensions.

Information on the backrest of the automotive seats can be found in the detailed survey of automotive seat design recommendations for improved comfort (Reed *et al.*, 1994), which suggests the backrest width should be minimum of 360 mm, while the backrest height should be in-between 410 mm and 550 mm above the H-point.

While studying the effect of seat posture on the human ergonomics (Kovacevc *et al.*, 2010), an approximate dimension table for the seat and human body was described based on 13 number of different parameters. The details of all the dimensions from this investigation, are given in Section 5.1.

Based on all the recommendations on the optimized seat parameters, a three dimensional CAD model for the car seat has been established. University of East London got the access to the advanced 3D CAD modeling software Solidworks. Hence, the CAD related tasks have been carried out using Solidworks.

Fig. 65 is showing the overall dimensions of the established car seat model.

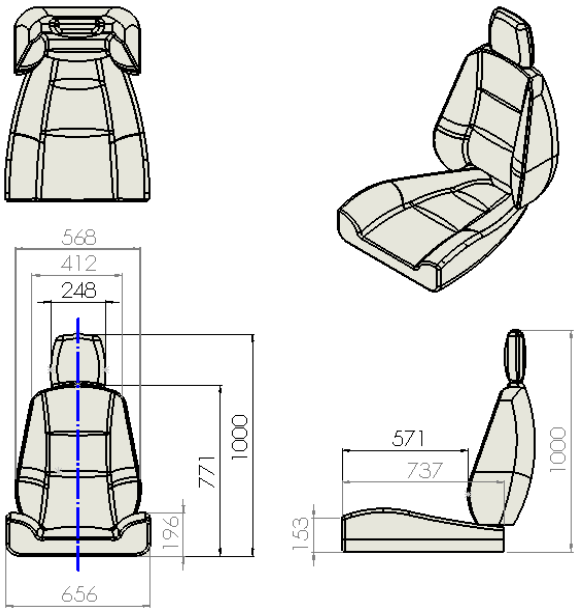

Fig. 65. Overall dimensions (mm) of the car seat model

In the next phase of this research work, the car seat will be associated to the human model established in CHAPTER 3 and suitable contacts will be assigned between the human body and car seat. As the interaction between the human body and car seat is going to be the focal point of simulation, the metallic frames of the car seat have not been modelled. The modelled car seat is shown in Fig. 66.

Fig. 66. Established three dimensional car seat model

4.3. Setting up the Simulation Model of Car Seat in Finite Element Environment

The CAD model of car seat has been taken into the finite element environment. Finite element tool ABAQUS has been used for the simulation work on the car seat. The imported model in ABAQUS is shown in Fig. 67.

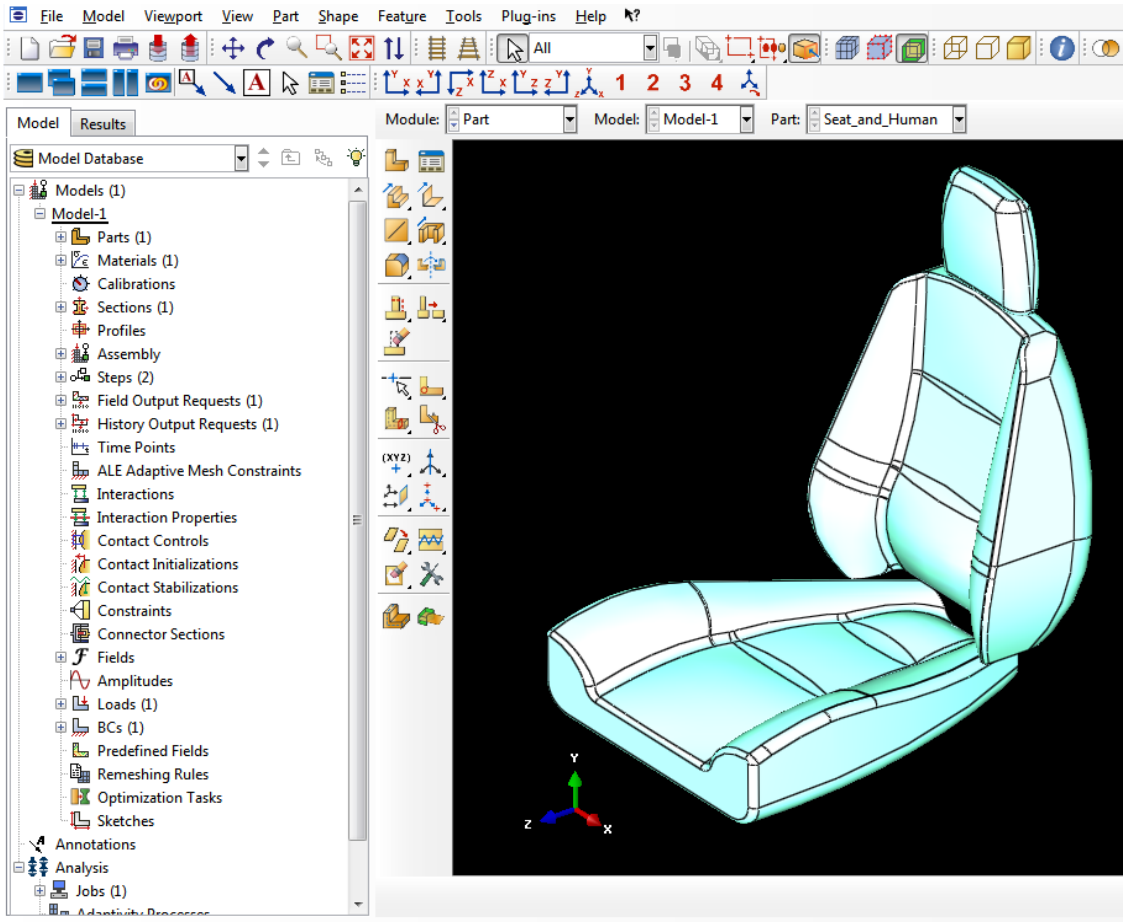

Fig. 67. Imported car seat model in finite element environment

4.3.1. Seat Foam Material

Exploring the past investigations carried out on the material properties of the car seat polyurethane foam, it is clear that the foam material can be modelled in finite element either by hyper-elastic material properties or by combination of hyper-elastic and visco-elastic properties or by stress-strain behaviour with respect to the variable strain rates. Hyper-elastic or the hyper-foam is the most suitable material for defining the foam properties, while the visco-elastic material is more suitable to investigate the behaviour of foam under shear loading. Stress-strain curve with respect to the variable strain rate is useful for examining the problems related to physical foam behaviour e.g., the contact pressure distribution or the contact interfaces between human body and seat foam layer.

Based on the second order strain energy potential function, relationships between the stress and strain were evaluated under the compressive and shear loading conditions (Grujicic *et al.*, 2009) as shown in Fig. 68. The experimental set of that study was arranged as per the guidelines of international standard ASTM D 3574 – 01 for standard test methods for flexible cellular materials.

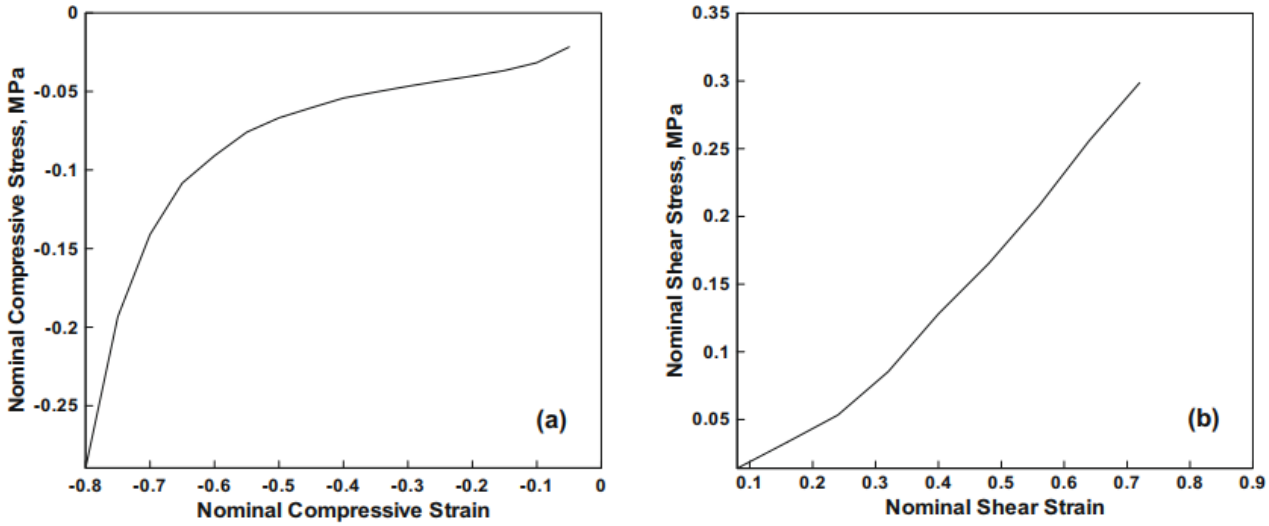

Fig. 68. Relationship between the stress and strain based on experimental data under different loading conditions (Grujicic *et al.*, 2009)

Later, the testing data were taken into finite element interface to evaluate the Ogden hyper-elastic coefficients of the strain energy potential equation using the curve fitting technique. The evaluated values of the coefficients from that study were:

$\mu 1 = 164.861$ kPa, $\alpha 1 = 8.88413$, $\beta 1 = 0.0$,

$\mu 2 = 0.023017$ kPa, $\alpha 2 = 4.81798$, $\beta 2 = 0.0$.

The same investigation explored the material properties further to the visco-elastic level by using the same curve fitting method in finite element. The values of the coefficients for the time dependent shear modulus function were given as:

$G1 = 0.3003$, $\tau 1 = 0.010014$ s,

G2 = 0.1997 and Ƭ2 = 0.10020 s

Material modelling of the polyurethane foam (Ju *et al.,* 2013) described the hyper-elastic, visco-elastic, polynomial and stress formulations for the foam properties. Visco-hyperelastic constitutive model for characterizing the behavior of polyurethane foam (Ju *et al.,* 2014) used different Ogden hyper-elastic coefficients for three different kinds of foams. The used coefficient values are given in Table 19.

Table 19. Ogden coefficients used for hyper-elastic foams (Ju *et al.,* 2014)

		μ_1	α_1	μ_2	α_2	μ_3	α_3
Foam A	Test 1	2.81	1.66	-2.80	1.61	3.1 E-3	38.28
	Test 2	9.22	1.64	-9.21	1.63	2.8 E-3	38.23
	Test 3	12.06	1.64	-12.05	1.63	3.0 E-3	38.21
Foam B	Test 1	9.27	1.63	-9.26	1.62	1.1 E-3	23.64
	Test 2	11.66	1.61	-11.65	1.61	1.1 E-3	17.74
	Test 3	7.27	1.63	-7.26	1.63	8.5 E-4	45.75
Foam C	Test 1	11.13	1.76	-11.112	7.15	9.5 E-4	21.73
	Test 2	9.86	1.76	-9.85	1.76	6.9 E-4	21.53
	Test 3	10.54	1.88	-10.53	1.87	2.4 E-4	27.62

The same investigation extended further to describe the values of the coefficients used in polynomial method. Table 20 is showing these coefficient values.

Table 20. Polynmial coefficients used for hyper-elastic foams (Ju *et al.,* 2014)

		C10	C01	C11	C20	C02	D1	D2
Foam A	Test 1	-2.02	1.22	-3.8 E-2	-0.221	5.6 E-3	1.182	0.251
	Test 2	-1.44	0.86	-2.9 E-2	-0.151	4.2 E-3	0.879	0.205

		C10	C01	C11	C20	C02	D1	D2
	Test 3	-1.83	1.11	-3.4 E-2	-0.199	5.1 E-3	1.069	0.232
Foam B	Test 1	-0.29	0.17	-6.9 E-3	-0.026	10 E-4	0.203	0.054
	Test 2	-0.23	0.13	-5.7 E-3	-0.021	8.3 E-4	0.168	0.045
	Test 3	-0.05	0.03	-2.6 E-3	-0.001	3.6 E-4	0.069	0.023
Foam C	Test 1	-0.27	0.15	-6.4 E-3	-0.023	9.2 E-4	0.184	0.052
	Test 2	-0.15	0.08	-4.6 E-3	-0.011	6.5 E-4	0.131	0.041
	Test 3	-0.07	0.04	-2.6 E-3	-0.028	3.7 E-4	0.076	0.026

Finite element modelling of the hyper-elastic soft foams (Schrodt, 2005) defined the Ogden parameter values for the different scenarios and optimized the parameter values for numerical and finite element applications. The optimized parameters are given in Table 21.

Table 21. Ogden coefficients used for hyper-elastic soft foams (Top) and optimized Ogden coefficients used for hyper-elastic soft foams (Bottom) (Schrodt, 2005)

	Mid-Point		Interval	
	N=1	N=2	N=1	N=2
$\mu_1 = \mu$ (MPa)	0.857 E-02	0.481 E-02	0.831 E-02	0.479 E-02
$\alpha_1 = \alpha$	0.198 E02	0.198 E02	0.198 E02	0.198 E02
$\beta_1 = \beta$	0.105 E-01	0.145 E-01	0.109 E-01	0.139 E-01
μ_2 (MPa)		0.360 E-02		0.351 E-02
α_2		0.198 E02		0.197 E02
β_2		0.650 E-02		0.657 E-02

	Mid-Point		Interval	
	N=1	N=2	N=1	N=2
	Numeric Fit		FE Fit	
μ (MPa)	0.831 E-02		0.907 E-02	
α	0.198 E02		0.213 E02	
β	0.109 E-01		0.849 E-01	

The values of the stress and strain inside the seat cushion foam material with respect to the different strain rates (Zhang *et.al*., 1998) were shown through tabular data as presented in Table 22, where both the quasi-static and dynamic load scenarios had been taken into account.

Table 22. Stress-strain behaviour of polyurethane foam with respect to strain rate (Zhang *et.al*., 1998)

Quasi-Static		Dynamic			
8.00 E3		4.00 E3		2.29 E3	
Eng. Strain	Stress (MPa)	Eng. Strain	Stress (MPa)	Eng. Strain	Stress (MPa)
0.00000	0.00000	0.00000	0.00000	0.00000	0.00000
0.04213	0.00615	0.05170	0.00923	0.04595	0.00862
0.12830	0.01108	0.13596	0.01354	0.12638	0.01508
0.21638	0.01292	0.22021	0.01538	0.22596	0.01754
0.30255	0.01446	0.30255	0.01662	0.28723	0.01877
0.38681	0.01600	0.38489	0.01846	0.36766	0.02092
0.47489	0.01785	0.46723	0.02138	0.45000	0.02508
0.56298	0.02231	0.55149	0.02831	0.53234	0.02969

Quasi-Static		Dynamic			
8.00 E3		4.00 E3		2.29 E3	
Eng. Strain	Stress (MPa)	Eng. Strain	Stress (MPa)	Eng. Strain	Stress (MPa)
0.65106	0.03154	0.63383	0.03708	0.61277	0.04123
0.73915	0.04677	0.71809	0.05277	0.69511	0.05523
0.83106	0.07692	0.80234	0.08200	0.77936	0.09446
0.88085	0.1200	0.85021	0.12000	0.81574	0.12000

Based on the knowledge gathered from the past literatures on the seat foam materials, hyper-elastic Ogden material properties (N=2) have been assigned to the seat foam for this research work. Striving for the best outcomes from the simulation, visco-elastic material properties have also been assigned to the seat foam based on the time dependent and instantaneous shear modulus functions. The values of all the coefficients taken into account for the simulation of car seat, are outlined in Table 23.

Table 23. Hyper-elastic and visco-elastic parameters used

Hyper-elastic parameters					
μ_1	0.00481 MPa	α_1	19.8	β_1	0.01450
μ_2	0.00360 MPa	α_2	19.8	β_2	0.00650
Visco-elastic parameters					
G_1	0.3003	τ_1	0.010014 s		
G_2	0.1997	τ_2	0.10020 s		

4.3.2. Density

Mechanical properties of the polyurethane foam at low temperature had been inspected at 295K, 111K, 76K and 4K by National Bureau of Standards, USA (Arvidson *et al.*, 1983) using the foam density value of 64 Kg/ m^3. Modelling of the car seat cushion (Haan, 2002) considered the density of the polyurethane foam as 67 Kg/m^3. Best performance of the polyurethane foam was assessed (Jarfelt and Chemeng, 2006) using different foam types with variable cell sizes and the ideal densities of all types of foams were outlined as shown in Table 24.

Table 24. Densities of different types of polyurethane foams (Jarfelt and Chemeng, 2006)

	Foam	Density (Kg/ m^3)	Cell Size (mm)*
A	Rigid foam	64	0.26-0.31
B	Rigid foam	55	0.29-0.31
C	Microcellular rigid	68	0.15-0.25
D	Microcellular semi-flexible	66	0.12-0.15
E	Microcellular semi-flexible	72	0.10-0.15
F	Microcellular semi-flexible	57	0.18-0.22

* Measured in two perpendicular directions

The study on the Poisson's ratio of the seat cushion foam material (Lowe and Lakes, 2000) mentioned the foam density in the range of 32 Kg/ m^3 to 64 Kg/ m^3 to be the most comfortable for human body.

Thesis on auxetic polyurethane foam (Yousif, H. I. Y., 2012) had taken into account the density value of the polyurethane foam as 27 Kg/m^3, while the automotive comfort study (Milivojevich *et al.*, 1999) described the regional density values of the car seat foams as

37 Kg/m^3, 47 Kg/m^3 and 52 Kg/m^3 for North America, Europe and Japan, respectively. Visco-elastic material modelling (Ju *et al.,* 2013) considered the density of the flexible polyurethane foam as 28 Kg/m^3.

After careful assessment of all the foam density values mentioned in the past related research works, rigid foam has been chosen for this simulation task and the density value of the car seat foam material has been taken as 64 Kg/ m^3.

4.3.3. Poisson's Ratio

Modern industries have been trying to develop car seat foam material which will bulge in inward direction and exhibit the negative Poisson's ratio. One of the cutting edge technologies (Lowe and Lakes, 2000) on the car seat cushion showed that the cushion polymer of density 18 Kg/m^3 with a compression ratio of 2.2, had a Poisson's ratio of -0.13, while the polymer of density 25 Kg/m^3 with a compression ratio of 3.4, had a Poisson's ratio of -0.26.

Practically, the car seat foam materials react mostly under the compression effects without any sideway restraints, hence, the lateral strain and longitudinal strain are not co-related to each other. Taking into account this fact, the computational analysis of car seat along with human body (Grujicic *et al.*, 2009) considered the Poisson's ratio as 0. Finite element modelling of the car seat (Haan, 2002) and design process of seat cushion (Camprubí *et.al*, 2007) made of polyurethane materials ignored the Poisson's ratio, too.

So, the effect of the Poisson's ratio can be ignored and in this finite element simulation of the car seat, the value of Poisson's ratio has been considered as 0.

4.3.4. Temperature Gradient

Though the polyurethane foam properties vary with respect to the surrounding temperature, this simulation work has been assumed to have constant thermal conditions

throughout the short span of simulation running period. Hence, no effect due to the temperature change has been considered.

4.4. Analysis Details in ABAQUS for the Car Seat

4.4.1. Analysis Steps

4.4.1.1. Step 1: Initial

First step is the base state of the simulation, where the car seat material properties and boundary conditions have been applied.

4.4.1.2. Step 2: Static General

Second step is the static general step, where the deformations are evaluated. The main aims of the simulation of the car seat are to verify the feasibilities of the material properties assigned and gain a knowledge about the suitability of the developed car seat for the next comprehensive simulation phase for entire car seat and human assembly. Hence, the simulation has been set to run for 1 second in this step.

4.4.2. Boundary Conditions

The following boundary conditions have been applied to the car seat:

a. Bottom side of the car seat cushion - Fixed.
b. Backrest of the car seat cushion - Angular fore-aft movement is allowed around the seat pivot point, but sidewise movements of the backend of the backrest are not allowed from the initial position.
c. Headrest of the car seat cushion - Angular fore-aft movement is allowed around the connecting point to the backrest, but sidewise movements of the backend of the headrest are not allowed from the initial position.

4.4.3. Acceleration and Load

The force obtained in Section 3.6.4, has been applied to the car seat in the horizontal direction. The load cause of male human body of 77.3 Kg mass, has been applied to the car seat in the vertical direction. All the forces have been applied to the estimated contact surface areas between human and seat.

The estimated contact surfaces and boundary conditions are presented in Fig. 69.

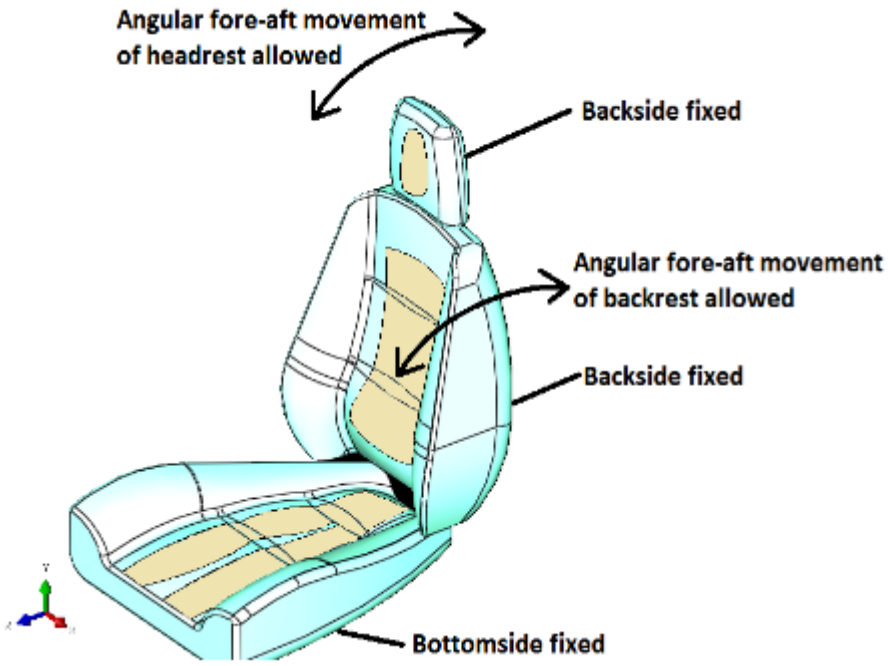

Fig. 69. Estimated contact surfaces and boundary conditions

All the forces have been implemented as equally distributed loads on the relevant surface areas.

4.4.4. Element type and Mesh

For this analysis, ten-node tetrahedral element - C3D10 has been used for mesh generation. The C3D10 element is suitable for generating mesh for general purpose by

utilizing four integration points. The meshed body is shown in Fig. 70. Mesh refinement has been optimized based on the capability of the computer hardware system.

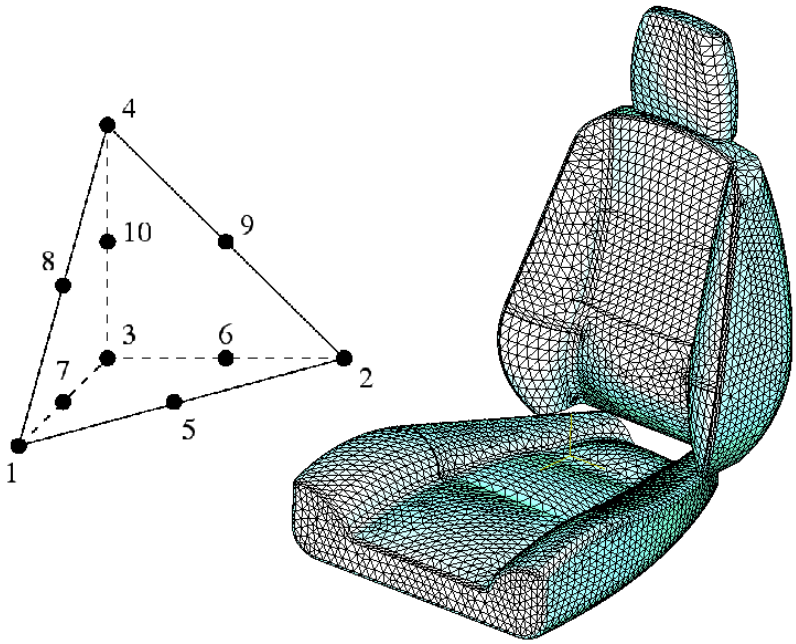

Fig. 70. 10-node tetrahedral element and mesh generated model of car seat

4.5. Results

A 64 bit standard laptop with RAM of 6 GB, Windows XP operating system and two number of dual-core 2.1 GHz Intel(R) Pentium(R) CPU B950 has been used to complete the simulation task. The simulation was set to run for 1 second. The ABAQUS solver took around 2 wall clock hours to run the simulation and yield results. The displacement values at the points of interest have been extracted from the result.

4.5.1. Displacement responses at the point of interest

The vertical displacement responses with respect to simulation time at the center of the seat cushion, center of the backrest and center of the headrest have been measured from the simulation result and detailed in Table 25.

Table 25. Measured values of vertical displacements for all the designated areas of seat

Time (Sec)	Displacement (mm)		
	Headrest	Backrest	Cushion
0.00	0.00000	0.00000	0.00000
0.10	-0.19578	-0.29578	-0.34578
0.20	-0.51223	-0.61223	-0.66223
0.35	-1.03514	-1.13514	-1.25514
0.58	-1.97724	-2.07724	-2.23724
0.91	-4.17513	-4.27513	-4.55513
1.00	-4.98838	-5.08838	-5.79838

The responses of all the segments have been outlined through graphs in Fig. 71, Fig. 72 and Fig. 73.

4.5.1.1. Response at Headrest

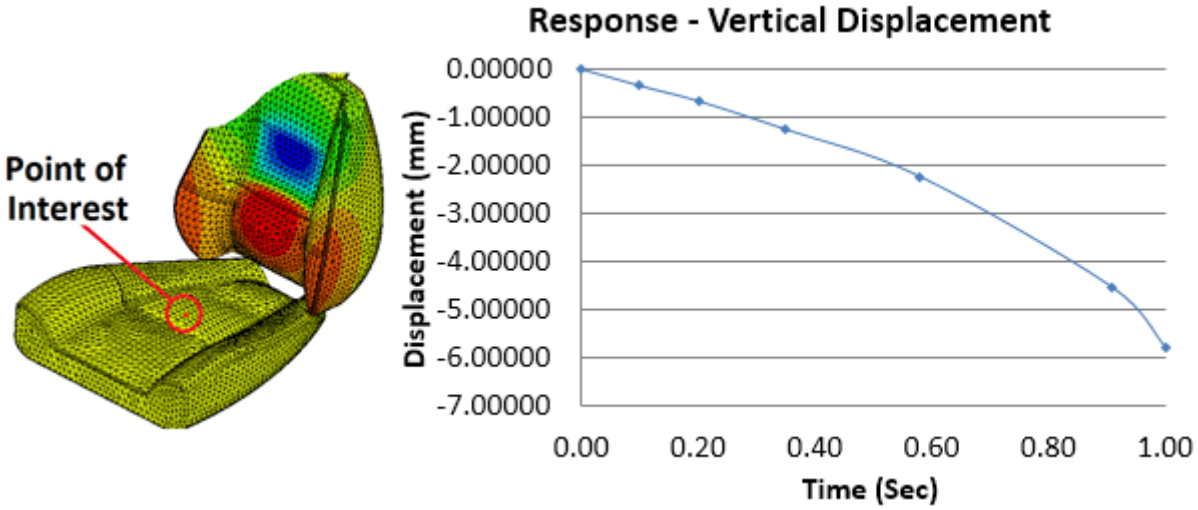

Fig. 71. Displacement response at headrest

4.5.1.2. Response at Backrest

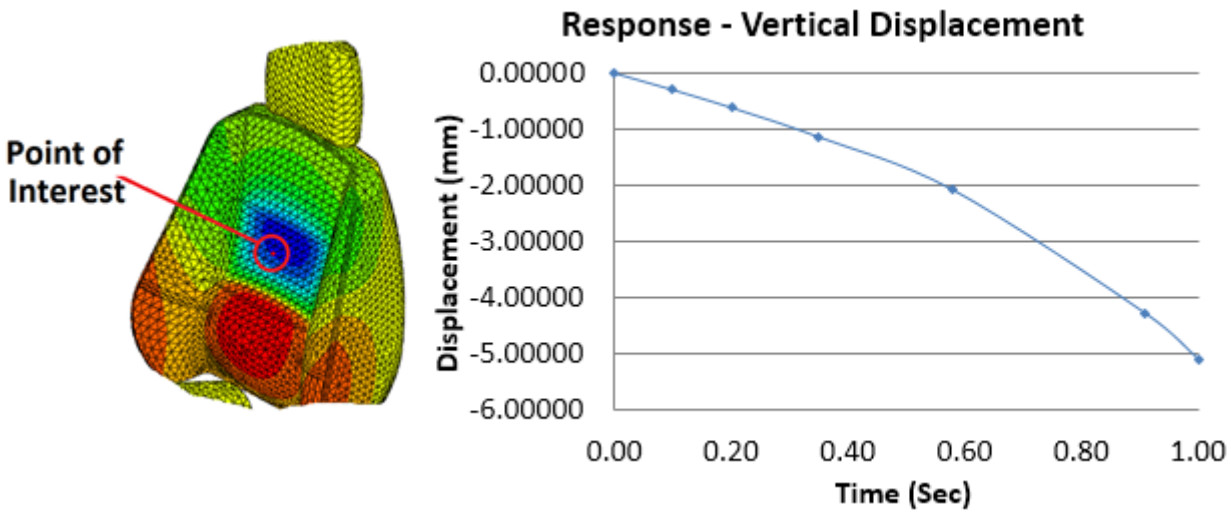

Fig. 72. Displacement response at backrest

4.5.1.3. Response at Cushion

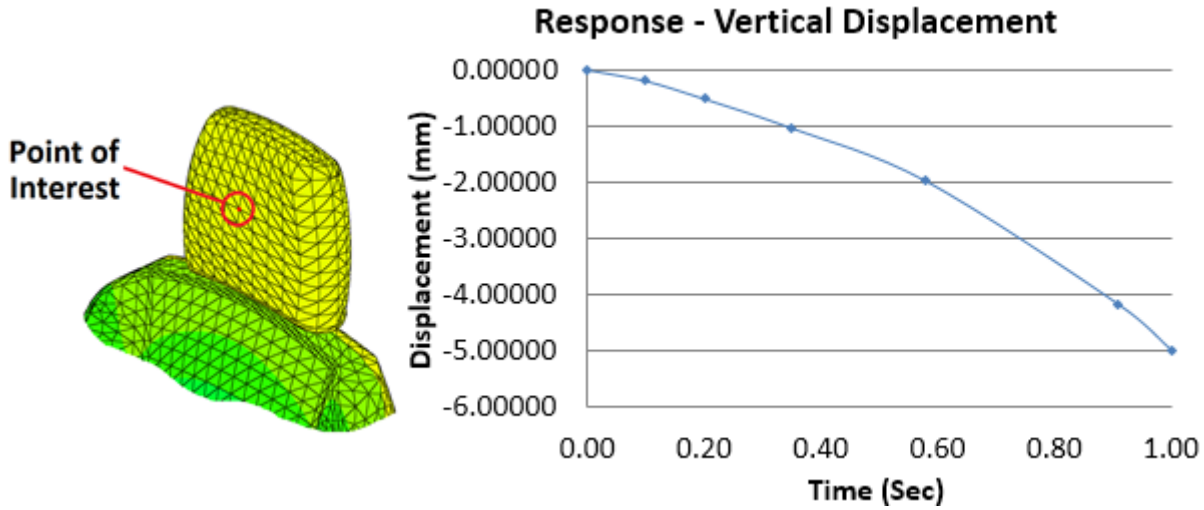

Fig. 73. Displacement response at seat cushion

4.6. Discussion on the Simulation of Car Seat

The results are showing justified levels of displacement values considering the simulation running time was only for 1 second. The maximum displacements for the headrest, backrest and seat cushion are 4.98838 mm, 5.08838 mm and 5.79838 mm, respectively.

The main aims of this simulation work of the car seat were to check the practicalities of the assigned hyper-elastic and visco-elastic material properties and understand the suitability of the modelled car seat for the next comprehensive simulation stage of combined seat-human assembly. The detailed non-linear analysis will be carried out for longer span of time period in the next simulation stage where the car seat will be assembled with the human body by means of the contact mechanism.

From the outputs of the unique simulation work, it is clear that the finite element method can effectively be used to establish simulation model of car seat. The boundary conditions, material properties and load conditions used in this simulation, have worked faultless providing convincing results. So, the purpose of this car seat simulation study became successful and this car seat simulated model can be taken to further advanced level in association with the human body.

CHAPTER 5

SIMULATION MODEL DEVELOPED FOR COMBINED HUMAN BODY AND CAR SEAT

The posture of the car seated human body is one of the key factors to define the safety and comfort of the occupant inside the moving car. Parts of the automobile seat are adjustable to provide the comfortable sitting postures to human bodies of different shapes and sizes. The smallest size of the human is 5^{th} percentile female body, while the biggest size is applicable for the 95^{th} percentile male body and the car seats should be adjustable to cope with this range of smallest and biggest sizes. The contact between the seat and the human body plays important role for the vibration transmission and the level of vibration generated inside the car seated human body is a function of many parameters including shapes, sizes, masses etc. of human body and the adjusted final posture of the seat.

For the vibration to be generated inside human body within the permissible ranges, suitable contact between the seat and human to be assigned in the simulation environment. To develop an effective simulation model for the human body and car seat, it is required to define comfortable sitting postures of the human portions in touch with the seat. The sitting posture and human-seat interfaces are primarily tuned by the

orientations of the human body segments, primarily; head, elbow, shoulder, torso, hip joint, ankle and knee.

Once the postures for the seat and human body are confirmed, the contact mechanisms in between all the mating surfaces need to be defined to get the vibration output data as accurate as possible. The polyurethane foam material of the seat is non-linear in nature and the human body segments are constructed by the ellipsoidal bodies with the damping and calculated stiffness parameters inside. So, the addition of the contact mechanisms makes the entire simulation more robust and time consuming and the chance for the entire simulation to get failed increases while all the complex factors are combined together. Hence, the real challenges of this simulation of the human body with car seat are to define the real life input parameters, place the human body in suitable posture, assign contact mechanisms at human-seat interfaces and obtain the desirable outputs within justified span of simulation running time.

5.1. Past works on Human Posture on Automotive Seat and Assembling Technique of Human Body and Automotive Seat Together

The sitting posture of the human body inside a car and the orientations of the seat segments should be in compliance with the industrial guidelines. General ergonomics principles, anthropometry and biomechanics, ergonomics of human-system interaction and ergonomics of the physical environment are elaborated in the standards ISO/TC 159/SC 1, ISO/TC 159/SC 3, ISO/TC 159/SC 4 and ISO/TC 159/SC 5, respectively.

Past research works on the human body bio-dynamics and car seat using different techniques have already been explored in the previous chapters. So, this section is mainly focusing on the earlier investigations related to the human posture on an automotive seat and the assembling technique of the human and automotive seat together.

A bio-dynamic model of human body was simulated (Himmetoglu *et al.*, 2009) for providing the rear impact solution using MSC Visual Nastran 4D-2001, where the sitting postures and the seat angles were determined from the photograph of a car seated human body. That simulation study further extended the research to define the contact mechanism between the human body and car seat, but was restricted to assign only a single value of frictional co-efficient. Later, the model was taken to MATLAB interface to determine the contact interfaces more efficiently assuming the bodies were rigid in nature. Initially, the model in MATLAB was developed for the human torso, but afterwards was capable of simulating the other portions of human body, namely; back and buttocks. The contact surfaces were split into different rectangular or trapezoidal areas. The seated human model and the contact surfaces utilized during that whole investigation, are shown in Fig. 74.

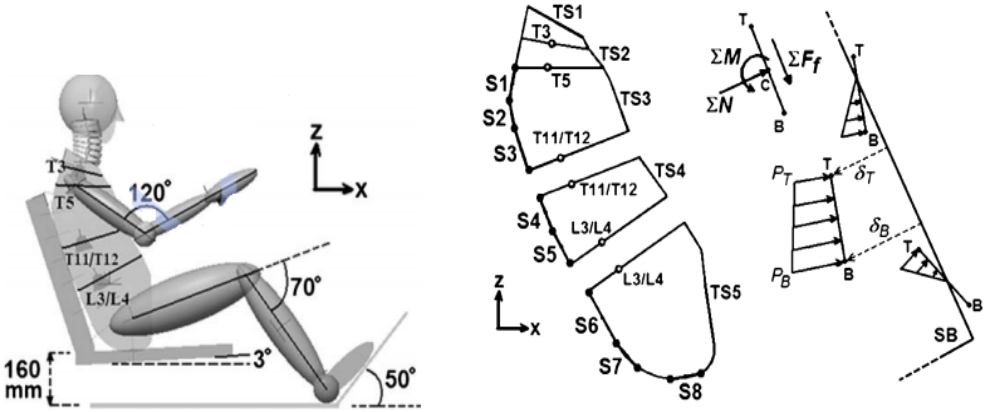

Fig. 74. Sitting posture (left) and contact definition (right) (Himmetoglu *et al.*, 2009)

The same study recorded the desired simulation results at 50m, 89ms, 100ms, 150ms, 200ms, 250ms and 300ms.

In the event of exploring the effect of seat posture on the human ergonomics (Kovacevc *et al.*, 2010), an anticipated data table for the seat position along with the dimensions of human occupant body was presented as shown in Fig. 75.

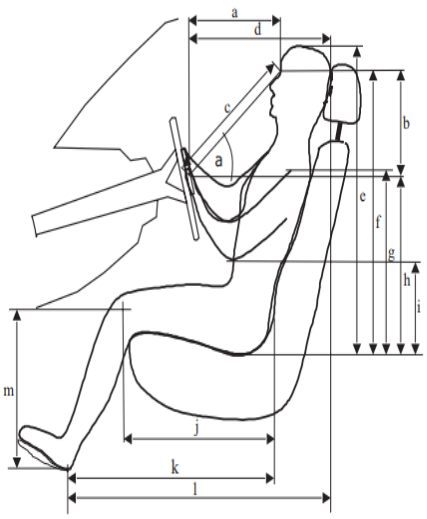

Sizes according to Fig. 1	Anthropometric measurements in females (cm)			Anthropometric measurements in males (cm)			Average (cm)
	Body height (cm)						
	155	165	175	175	185	195	175
a	38.4	38.3	38.7	39.4	39.7	39.8	39.1
b	14.8	14.8	15.0	15.2	15.7	16.9	15.4
c	34.6	34.8	35.3	35.3	36.6	38.1	35.8
d	47.4	47.5	47.7	48.2	48.4	48.4	47.9
e	78.2	83.7	88.0	88.3	93.7	98.1	88.3
f	69.1	72.2	76.1	76.3	82.6	88.4	77.5
g	51.3	54.4	56.6	60.9	62.4	64.9	58.4
h	50.5	50.5	50.5	50.5	50.5	50.5	50.5
i	20.4	21.7	24.3	24.0	24.7	24.0	23.2
j	44.0	45.7	48.8	48.1	50.3	52.5	48.2
k	52.4	52.6	53.2	53.3	53.5	53.4	53.1
l	57.7	58.1	58.5	58.8	59.6	59.8	58.8
m	39.9	43.2	45.5	45.4	47.8	50.7	45.4

Fig. 75. Anthropometric measurements of car seated human body (Kovacevc *et al.*, 2010)

Simulation of the sitting process of the driver inside a car (Mircheski *et al.*, 2014) analysed the comfort of the human body by considering the fixed positions of eye, hip, hand and heel. The same study adopted the optimized orientations for the different portions of the human body for running the simulation using the software tool RAMSIS. The optimized angles and driver posture are shown in Fig. 76.

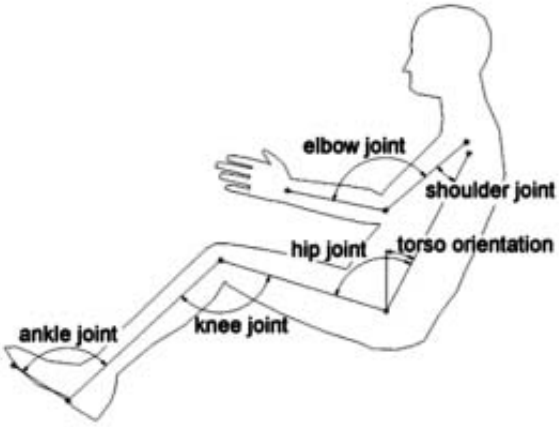

Torso orientation	27°
Angle of shoulder joint	22°
Angle of elbow joint	127°
Angle of hip joint	99°
Angle of knee joint	119°
Angle of ankle joint	103

Fig. 76. Optimized angles of driver body portions for comfortable sitting posture inside a car (Mircheski *et al.*, 2014)

Similar kinds of simulation models focusing on the comfort levels of the human body and car seat were developed using finite element method in few other studies (Grujicic *et al.*, 2009; Konosu, 2003; Murakami *et al.*, 2004; Hartung *et al.*, 2004; Mergl *et al.*, 2004; Verver *et al.*, 2004), where the interaction between the human body and automotive seat had been taken into account.

Simulation study on riding comfort was carried out using one dimensional Modelica software and three dimensional finite element tool (Choi *et al.*, 2017) where both the lumped mass and finite element methods were implemented. The entire human body, as shown in Fig. 77, was divided into fourteen different segments and the contacts with the seat and other automotive components were established. Later, vibration excitement levels were extracted from the simulation.

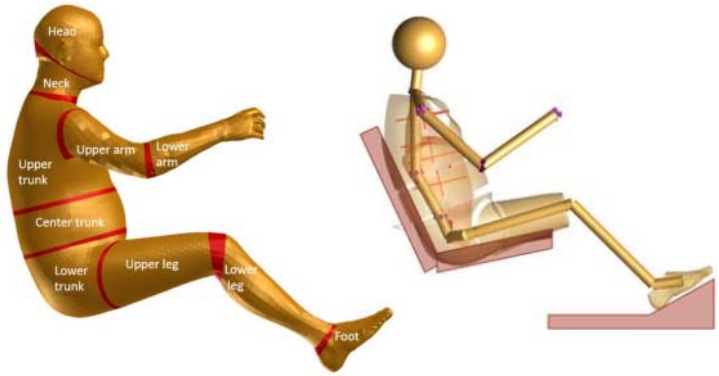

Fig. 77. Model of human body made of fourteen segments and sitting comfort analysis (Choi *et al.*, 2017)

Sensitivity study on the vertical vibration (Verver, M.M., 2004) stated that the damping and stiffness parameters of the seat cushion would greatly influence the seat-to-human vibration transmission and the final level of vibration inside the human body would be a function of the vertical acceleration. That investigation placed a spring-dashpot system under the seat to understand the effect of vibration transmission. The seated human body and the spring-dashpot system underneath are presented in Fig. 78.

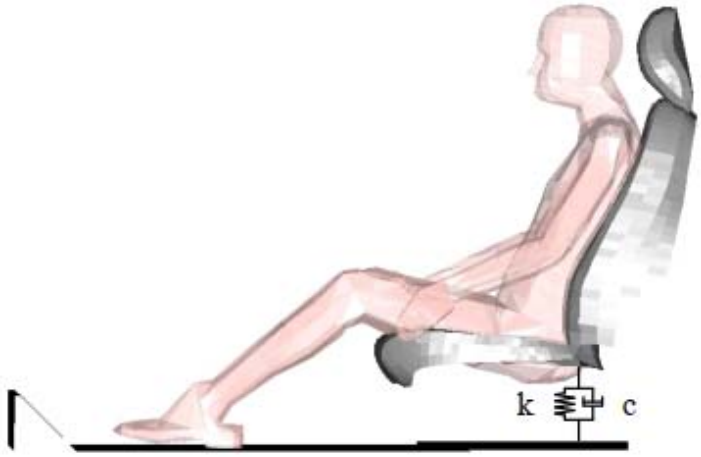

Fig. 78. Simulation set up of seated human body for the sensitivity study on vertical vibration (Verver, M.M., 2004)

From the literature survey on the assembly set up of human body and car seat, it can be concluded that the seat-human assembly can be manipulated in terms of position and orientation depending on the aspects of the investigation. Each of the simulations for the vibration transmission, sensitivity, rear impact and sitting comfort had considered different approach for assembling the human and automotive seat. Hence, in this research work, for the simulation set up of the assembled human body and car seat, the postures can be assigned to the seat-human assembly tallying with the real life operating scenario.

5.2. Preparation of CAD Assembly of the Car Seat and Human Body

The CAD model of the male human of 77.3 kg mass established in the Section 3.4.2 has been assembled with the CAD model of the car seat developed in Section 4.2. The orientations of the male human body have been kept same as described in Section 3.4.1. The seat portions have been adjusted in a way that the human model fits to the seat and creates suitable mating surfaces as per real life sitting condition.

3D CAD software Solidworks has been used to construct the entire assembly as presented in Fig. 79. In the CAD assembly, careful initiative has been taken to avoid any interference between the human body and the seat to evade any undesirable complexity in solving simulation.

Fig. 79. Established human-seat assembly

5.3. Setting up Simulation Model in Finite Element Environment for Human-Seat Assembly

The human-seat CAD assembly has been imported to finite element software ABAQUS in parasolid format. Fig. 80 shows the human-seat assembly imported into ABAQUS.

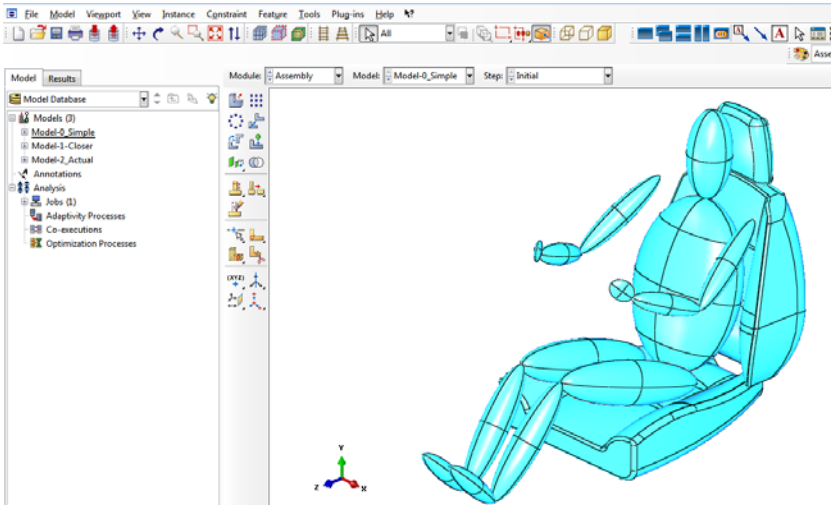

Fig. 80. Imported model in finite element environment

5.3.1. Analysis Details used from the Past Chapters

Comprehensive documentations have been outlined in CHAPTER 3 and CHAPTER 4 related to the estimations and calculations of the different simulation parameters for the human body and car seat. Table 26 is showing the relevant sections of the CHAPTER 3 and CHAPTER 4, referred for the necessary parameters used in this simulation of the combined human body and car seat.

Table 26. Summary of the simulation parameters used from previous chapters

Part/ assembly	Simulation parameters	Reference section
Human Body	Human segment masses	3.1
	Dimensions for human segments	3.2
	Human sitting position	3.4.1
	Densities of segments	3.5.1
	Axial and lateral Young's moduli	3.5.2
	Axial and lateral stiffness values	3.5.3
	Poisson's ratio	3.5.4
	Damping co-efficient and damping ratio	3.5.5
	Connection between human segments	3.6.1
	Boundary conditions for the hands and legs	3.6.3
	Element and mesh	3.6.5
Car Seat	Seat dimensions	4.2
	Seat material	4.3.1
	Density	4.3.2
	Poisson's ratio	4.3.3
	Boundary conditions	4.4.2
	Element and mesh	4.4.4
Human and Car Seat Assembly	Analysis steps	3.6.2
	Loading conditions	3.6.4

5.3.2. Establishing Contact Mechanism between Human Body and Car Seat

The contacts between the mating bodies have been assigned, once the sitting posture of the human body and the orientation of the car seat portion are finalized in the simulation environment.

Most of the earlier contact interface related bio-dynamic investigations in the automotive sector, were carried out mainly on the surfaces in-between the seat cushion and human lower parts. Assembly of seat cushion and human buttock was analysed (Paul *et al.*, 2012), where the buttock was made from the impression of maximum possible human size of 95th percentile male human. The seat cushion was made of layers of rigid steel and neoprene materials. The simulation was carried out in ANSYS Workbench 13 and the pressure distribution at the interface of human buttock and seat cushion had been measured. The seat model was established in accordance with Ford engineering specification CETP 01.10-L-401. The outputs from that simulation are shown in Fig. 81 with coloured contour.

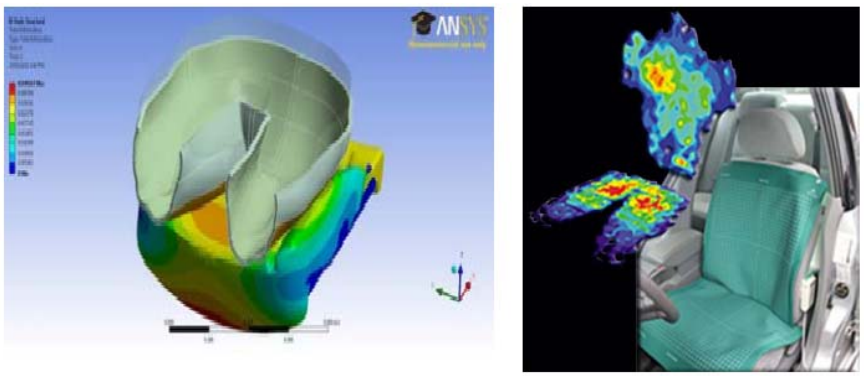

Fig. 81. Two layered seat cushion with the human buttock indenter (left) and pressure measurement (right) (Paul *et al.*, 2012)

Similar kind of simulations using the interactions between the car seat and human portions were developed by few other studies (Grujicic *et al.*, 2009; Konosu, 2003; Murakami *et al.*, 2004) for gaining knowledge on comfortable human orientation. Pressure at the contact interface of human body and seat was measured successfully while

studying the sitting comfort (Andreoni *et al.*, 2002; Siefert *et al.*, 2008). The analysis of the sitting process (Mircheski *et al.*, 2014) modelled the full human body, though, had taken into account only the human buttocks and seat cushion for assembling purpose. The seat was simulated with the impressions of the buttocks of 50th and 80th percentile male human bodies and the pressure distributions on the contact surfaces were measured from simulation results as detailed in Fig. 82. Later, the simulation results were verified with the testing data.

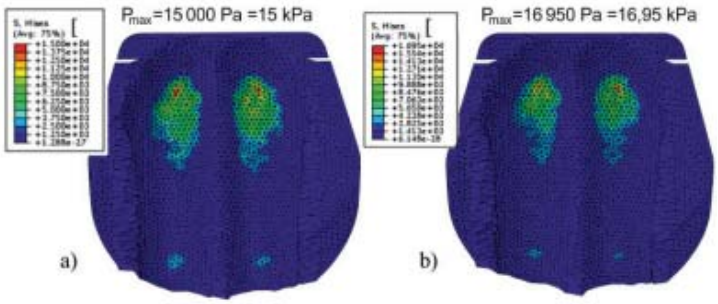

Fig. 82. Pressure distributions at the interfaces of human buttocks and seat cushion (Mircheski *et al.*, 2014)

Simulation study on riding comfort (Choi *et al.*, 2017) used one dimensional Modelica software and three dimensional finite element tool to investigate the contact between seat cushion and human thighs. Unique approach had been taken by defining two dimensional polygon to polygon contact in one dimensional lumped mass environment. The model layouts of that study are given in Fig. 83. Further investigation was carried on for the pressure distributions at the mating interfaces in relaxed and stressed states of human thighs.

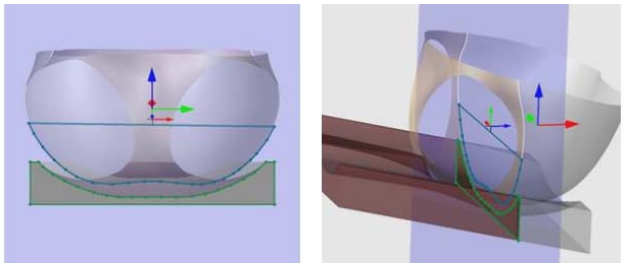

Fig. 83. Two dimensional contact in one dimensional lumped mass system (Choi *et al.*, 2017)

A three dimensional human body model was developed along with a foam made seat model (Zhang, 2014) in finite element environment, where contacts were established between the human body and seat by avoiding any kind of penetration. The main aim of that research work was to find out the vibration transmissibility from seat to human body and for that purpose the contacts were assigned at the backrest-human back and cushion-human buttocks interfaces. A dummy simulation model was also established using portions of a manikin attached to the seat by means of surface to surface contacts. Fig. 84 shows both the simulation models from that study.

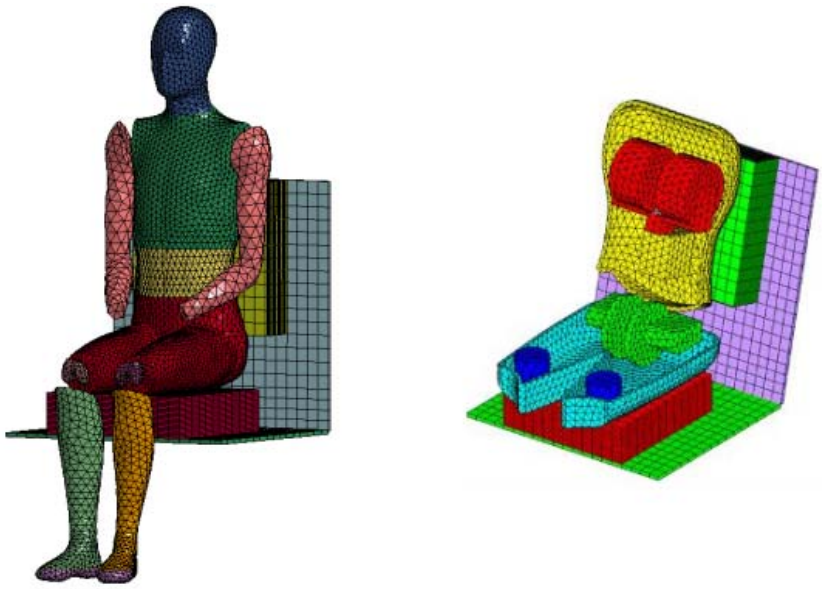

Fig. 84. Simulation of human body and car seat (left), simulation of manikin and car seat (right) (Zhang, 2014)

Simulation of the contact pressure distributions on the mating surfaces between human bottom portions and car seat (Verver, M.M., 2004) assumed that the coefficient of friction would be related to changes in the shear stresses at the mating surfaces. That investigation conducted a comparative study on the contact pressures with variable length, width and thickness of the seat cushion. All the case scenarios taken into account during that research work, are shown in Fig. 85.

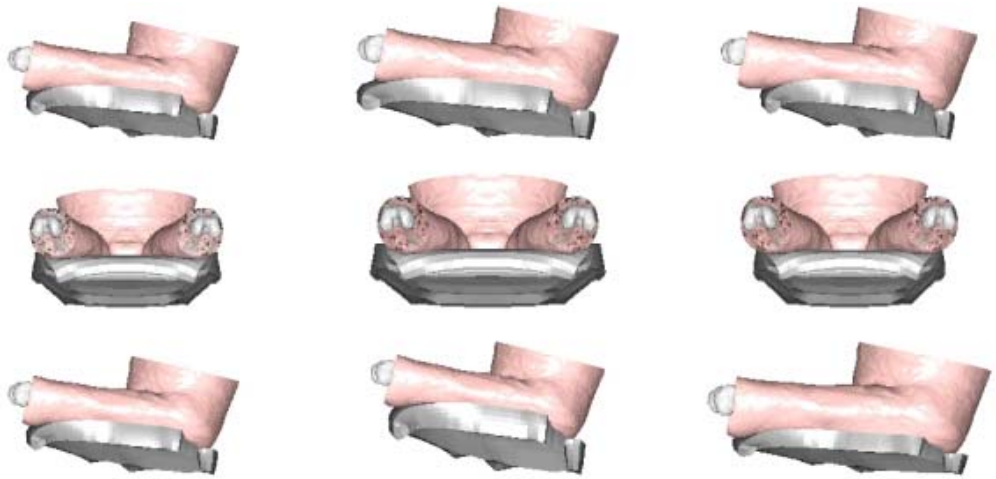

Fig. 85. Contact establishment between the human thigh and seat cushion (Top- variable length, middle- variable width, bottom- variable thickness) (Verver, M.M., 2004)

Review of the past research works on the contact mechanism between human body and car seat outlined an idea that the precise enough material properties need to be defined for the pressure or stress distribution related problems, while rigid bodies can be assigned as materials for the vibration transmission related investigations. Most of the past works strived to minimise the number of contact surfaces in order to reduce the complexity of the simulated system.

In the finite element tool ABAQUS, the contact between the bodies is designated by the master and slave surfaces and defined either by node to surface or surface to surface contact formulation. The advantage of the surface to surface formulation is that the master surface can't penetrate inside the slave surface and as a result, the simulation gives more accurate results (ABAQUS User's manual version 6.3).

The contact formulation also depends on the characteristics of the sliding nature. The sliding can be finite or small and a comprehensive overview of both types of sliding has been presented in Table 27.

Table 27. Contact formulation characteristics (ABAQUS User's manual version 6.3)

Characteristics	Contact formulation			
	Node to surface		Surface to surface	
	Finite sliding	Small sliding	Finite sliding	Small sliding
Account for shell thickness by default	No	Yes	Yes	Yes
Allow self-contact	Yes	No	Yes	No
Allow double sided surfaces	Slave surface only	No	Yes	No
Surface smoothing by default	Some smoothing of master surface	Yes for anchor points, each constraint uses flat approximation of master surface	No	No for anchor points, each constraint uses flat approximation of master surface
Default constraint enforcement method	Augmented Lagrange method for 3D self-contact; otherwise, direct method	Direct method	Penalty method	Direct method

Characteristics	Contact formulation			
	Node to surface		Surface to surface	
	Finite sliding	Small sliding	Finite sliding	Small sliding
Ensure moment equilibrium for offset reference surfaces with friction	No	No	Yes	Yes

The theoretical formulation and algorithm of the contact interaction are based on the pure penalty, Lagrange, multi-point or beam concept. The concept of contact surfaces and types of contact formulation are explained in Fig. 86.

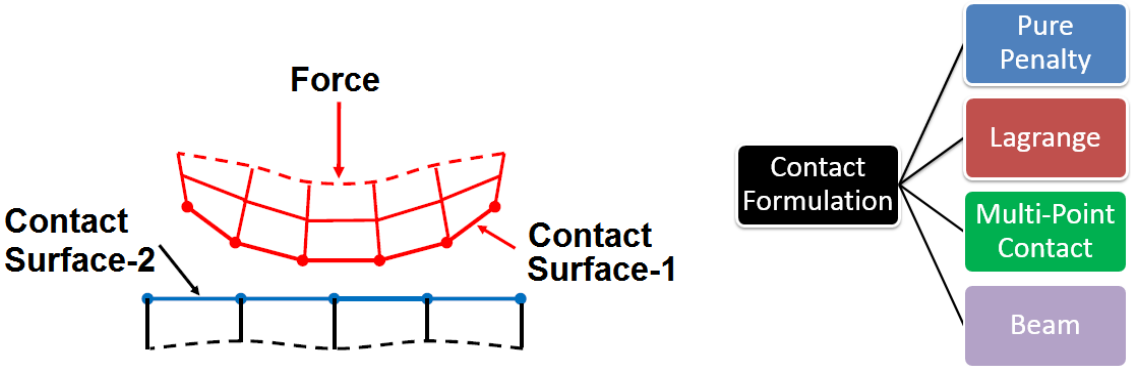

Fig. 86. Concept of contact between surfaces (left) and types of contact formulations (right)

Pure penalty and augmented Lagrange formulations are derived from the penalty based contact formulation and used for most of the non-linear solid bodies. Pure penalty method is based on the stiffness only while the augmented Lagrange considers some extra factor for the penetration. Normal Lagrange theory considers the chattering effects which assumes the gap between the surfaces is either open or closed. Multi-point contact formulation takes into account the bonded and no separation scenarios while, the beam type formulation considers only the bonded scenario mainly for massless elements. Fig.

87 is providing a clear picture of the working principles of pure penalty and pure Lagrange formulations inside the simulation solving system.

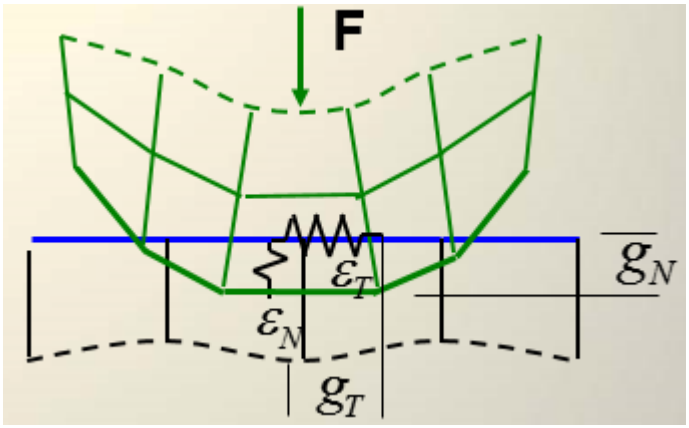

Fig. 87. Diagram explaining pure penalty and pure Lagrangian method (ANSYS, Inc. Manual, 2004)

The contact formulation can be established in the form of virtual work. For the pure penalty method:

$$\delta\Psi = \int_V \sigma^T \cdot \delta\varepsilon \, dV + \int_\Gamma \left(\varepsilon_N \cdot g_N \cdot \delta g_N + \varepsilon_T \cdot g_T \cdot \delta g_T \right) dA \qquad \text{(Eq. 5.1)}$$

While, for the pure Lagrangian method:

$$\delta\Psi = \int_V \sigma^T \cdot \delta\varepsilon \, dV + \int_\Gamma \left(\lambda_N \cdot \delta g_N + \lambda_T \cdot \delta g_T \right) dA \qquad \text{(Eq. 5.2)}$$

Where,

Ψ = virtual work

σ = stress

ε = displacement related to penetration

V = volume

g = displacement related to penetratio

A = area

λ = extra term for Lagrangian method cause of no penetratio

For the pure Lagrangian method, the conditions are:

$g_N \geq 0$	Ensure no penetration
$\lambda_N \leq 0$	Ensure compressive contact force/ pressure
$g_N \lambda_N = 0$	No contact $\lambda_N = 0$, gap is non zero Contact $g_N = 0$, contact force is non zero

To accomplish the simulation in most efficient way and get the desired results, the pros and cons of different kinds of contact mechanisms have been consulted with the database of SAS IP, Inc. and outlined in Table 28.

Table 28. Advantages and disadvantages of different contact formulation methods (SAS IP, Inc.)

Pure penalty	Augmented Lagrange	Normal Lagrange	MPC	Beam
Good convergence behaviour (few equilibrium iterations)	Additional equilibrium iterations needed if penetration is too large	Additional equilibrium iterations needed if chattering is present	Excellent convergence behaviour (one equilibrium iteration)	
Sensitive to selection of normal contact stiffness	Less sensitive to selection of normal	No normal contact stiffness is required		N/A

Pure penalty	Augmented Lagrange	Normal Lagrange	MPC	Beam
	contact stiffness			
Contact penetration is present and uncontrolled	Contact penetration is present but controlled to some degree	Usually penetration is near-zero	No penetration	Penetration is minimal with a stiff enough material definition
Useful for any type of contact behaviour			Only bonded and no separation behaviour	Bonded only
Iterative or direct solvers can be used		Only direct solver can be used	Iterative or direct solvers can be used	
Symmetric and asymmetric contact available		Asymmetric contact only		N/A
Contact detection at integration points		Contact detection at nodes		N/A

After a thorough review of all the contact mechanisms and relevant contact formulations, the multi-point bonded contact with no separation has been identified as the most effective one to take account the effects of a range of deformations. Hence, this contact mechanism has been assigned to the mating surfaces between the human body and car seat in conjunction with “tie-up” constraints during this course of simulation study. Fig.

88 shows the “tie-up” constraints assigned in-between mating parts of human body and car seat inside the finite element tool ABAQUS. This constraining method restricts the rotational degrees of freedom on the mating surfaces.

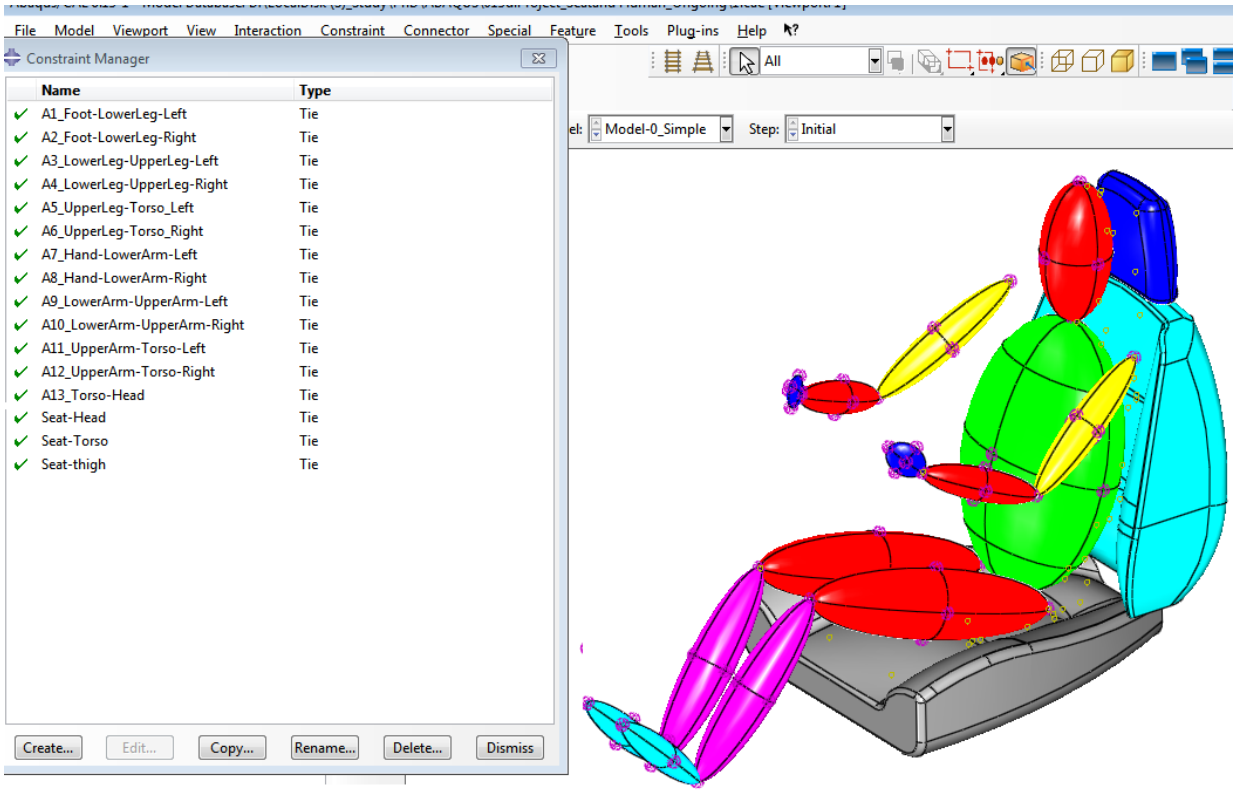

Fig. 88. “Tie-up” constraints details for creating interactions

Attempts have also been made to run the simulation by assigning other types of contact mechanism between the human body and car seat, though, cause of the limitation of the computer hardware, the simulation solver got terminated prematurely without displaying any output data.

5.4. Results

A 64 bit standard laptop with RAM of 6 GB, Windows XP operating system and two number of dual-core 2.1 GHz Intel(R) Pentium(R) CPU B950 have been utilized to

complete the simulation task. The simulation was set to run for 10 seconds. The ABAQUS solver took around 27 wall clock hours to run the simulation and yield results.

Efforts had been made to run the simulation for 60 seconds. But cause of the limitation of the computer system, the simulation process was unable to get solved and sudden termination of ABAQUS solver occurred. The acceleration responses and displacement values at the points of interest have been extracted from the results.

5.4.1. Acceleration responses at the points of interest

This simulation based study aims to focus on the vertical vibration. So, vertical acceleration responses with respect to simulation time at the designated points of head, chest, waist, upper arm, lower arm, thigh, leg, headrest, backrest and cushion have been measured from the simulation result and detailed in Table 29.

Table 29. Measured values of vertical accelerations for the human body and car seat

Time (Sec)	Acceleration (mm/sec^2) - Human segment							Acceleration (mm/sec^2) - Seat		
	Head	Chest	Waist	Upper Arm	Lower Arm	Thigh	Leg	Headrest	Backrest	Cushion
0.0	0.00	0.00	0.00	0.00	0.00	0.00	0.00	0.00	0.00	0.00
0.1	-0.11	0.15	0.13	0.03	0.19	0.19	-0.02	-0.18	0.24	0.31
0.2	0.65	0.36	0.38	0.00	0.26	0.26	-0.02	0.90	0.50	0.36
0.3	-0.14	0.03	0.01	-0.02	0.14	0.14	0.02	-0.18	0.04	0.17
0.4	-0.55	0.00	-0.06	-0.02	0.08	0.08	0.07	-0.93	-0.01	0.14
0.5	1.19	0.48	0.51	0.02	0.17	0.17	0.09	2.33	0.94	0.34
0.6	-0.30	0.11	0.08	0.01	0.18	0.18	0.05	-0.60	0.21	0.36
0.7	-0.39	-0.06	-0.09	-0.03	0.15	0.15	0.07	-0.65	-0.09	0.24

Time (Sec)	Acceleration (mm/sec^2) - Human segment							Acceleration (mm/sec^2) - Seat		
	Head	Chest	Waist	Upper Arm	Lower Arm	Thigh	Leg	Headrest	Backrest	Cushion
0.8	0.71	0.29	0.31	-0.04	0.07	0.07	0.11	0.98	0.40	0.10
0.9	-0.06	0.26	0.26	0.03	0.26	0.26	0.16	-0.07	0.32	0.32
1.0	-0.04	0.02	0.00	0.01	0.21	0.21	0.22	-0.07	0.04	0.36
1.1	-0.14	0.06	0.04	0.02	0.06	0.06	0.21	-0.28	0.13	0.11
1.2	0.59	0.39	0.40	0.02	0.14	0.14	0.26	1.19	0.77	0.27
1.3	0.13	0.14	0.13	-0.02	0.25	0.25	0.25	0.22	0.23	0.41
1.4	-0.83	-0.11	-0.17	0.00	0.22	0.22	0.26	-1.14	-0.15	0.30
1.5	1.05	0.42	0.46	0.02	0.08	0.08	0.31	1.29	0.51	0.10
1.6	0.10	0.22	0.22	-0.01	0.08	0.08	0.27	0.16	0.38	0.13
1.7	-0.63	-0.10	-0.15	0.00	0.24	0.24	0.27	-1.23	-0.19	0.47
1.8	0.54	0.21	0.23	-0.01	0.19	0.19	0.20	1.09	0.43	0.38
1.9	0.15	0.34	0.33	-0.05	0.07	0.07	0.22	0.25	0.56	0.11
2.0	0.10	0.08	0.06	0.01	0.18	0.18	0.30	0.14	0.12	0.25
2.1	-0.31	-0.01	-0.04	0.03	0.19	0.19	0.23	-0.38	-0.01	0.23
2.2	0.36	0.35	0.35	0.01	0.15	0.15	0.15	0.61	0.59	0.25
2.3	0.60	0.25	0.26	-0.01	0.09	0.09	0.06	1.17	0.49	0.18
2.4	-0.93	-0.16	-0.21	-0.01	0.22	0.22	0.07	-1.86	-0.32	0.44
2.5	0.55	0.31	0.32	0.02	0.27	0.27	0.13	0.91	0.50	0.45
2.6	0.50	0.32	0.34	0.03	0.10	0.10	0.08	0.69	0.45	0.14

Time (Sec)	Acceleration (mm/sec^2) - Human segment							Acceleration (mm/sec^2) - Seat		
	Head	Chest	Waist	Upper Arm	Lower Arm	Thigh	Leg	Headrest	Backrest	Cushion
2.7	-0.56	-0.07	-0.12	-0.03	0.02	0.02	0.02	-0.68	-0.09	0.02
2.8	0.26	0.13	0.12	0.00	0.25	0.25	-0.01	0.44	0.22	0.43
2.9	0.15	0.36	0.35	-0.01	0.23	0.23	0.02	0.30	0.70	0.44
3.0	0.35	0.17	0.17	-0.04	0.10	0.10	0.04	0.70	0.33	0.21
3.1	-0.27	-0.04	-0.07	0.00	0.08	0.08	-0.03	-0.45	-0.07	0.13
3.2	-0.05	0.26	0.25	0.03	0.20	0.20	-0.07	-0.06	0.35	0.28
3.3	0.87	0.34	0.38	0.00	0.20	0.20	-0.04	1.06	0.41	0.24
3.4	-0.73	-0.12	-0.18	-0.01	0.14	0.14	0.03	-1.23	-0.21	0.24
3.5	0.09	0.18	0.16	0.00	0.11	0.11	0.07	0.18	0.35	0.22
3.6	0.68	0.38	0.40	0.04	0.26	0.26	0.04	1.36	0.76	0.53
3.7	-0.45	0.00	-0.05	0.01	0.12	0.12	0.06	-0.74	0.00	0.21
3.8	0.13	0.06	0.04	0.00	0.06	0.06	0.10	0.18	0.08	0.08
3.9	0.15	0.32	0.32	-0.01	0.20	0.20	0.14	0.19	0.39	0.25
4.0	0.36	0.25	0.25	-0.03	0.26	0.26	0.18	0.62	0.42	0.45
4.1	-0.16	-0.03	-0.05	0.00	0.12	0.12	0.17	-0.32	-0.06	0.23
4.2	-0.26	0.15	0.13	0.00	0.06	0.06	0.22	-0.53	0.29	0.13
4.3	0.97	0.40	0.43	0.00	0.13	0.13	0.24	1.60	0.66	0.21
4.4	-0.56	-0.03	-0.08	0.01	0.30	0.30	0.29	-0.77	-0.04	0.41
4.5	-0.27	0.05	0.02	-0.02	0.16	0.16	0.34	-0.33	0.06	0.19

Time (Sec)	Acceleration (mm/sec^2) - Human segment							Acceleration (mm/sec^2) - Seat		
	Head	Chest	Waist	Upper Arm	Lower Arm	Thigh	Leg	Headrest	Backrest	Cushion
4.6	0.89	0.38	0.41	0.00	0.07	0.07	0.27	1.50	0.65	0.12
4.7	-0.38	0.10	0.06	0.04	0.21	0.21	0.26	-0.74	0.20	0.41
4.8	-0.09	0.00	-0.01	0.02	0.19	0.19	0.20	-0.18	-0.01	0.39
4.9	0.25	0.24	0.25	0.01	0.12	0.12	0.24	0.42	0.40	0.20
5.0	0.42	0.32	0.33	-0.03	0.13	0.13	0.29	0.58	0.45	0.18
5.1	-0.10	0.02	0.01	-0.01	0.21	0.21	0.23	-0.13	0.03	0.25
5.2	-0.50	0.03	-0.01	0.02	0.19	0.19	0.20	-0.85	0.05	0.32
5.3	1.05	0.42	0.45	0.00	0.05	0.05	0.14	2.05	0.82	0.09
5.4	-0.23	0.10	0.08	-0.04	0.10	0.10	0.14	-0.46	0.21	0.19
5.5	-0.71	-0.07	-0.13	0.02	0.32	0.32	0.13	-1.17	-0.12	0.53
5.6	0.91	0.34	0.37	-0.01	0.16	0.16	0.06	1.25	0.46	0.22
5.7	-0.08	0.21	0.21	-0.01	0.08	0.08	0.03	-0.10	0.26	0.09
5.8	-0.23	-0.02	-0.04	0.03	0.12	0.12	0.02	-0.39	-0.03	0.20
5.9	0.12	0.15	0.14	0.03	0.26	0.26	0.02	0.23	0.30	0.51
6.0	0.43	0.38	0.39	-0.02	0.19	0.19	0.01	0.85	0.75	0.39
6.1	0.20	0.11	0.10	-0.01	0.09	0.09	-0.01	0.32	0.18	0.15
6.2	-0.73	-0.07	-0.13	-0.01	0.14	0.14	-0.01	-1.01	-0.09	0.19
6.3	0.78	0.37	0.40	0.03	0.25	0.25	-0.02	0.95	0.46	0.30
6.4	0.30	0.24	0.25	-0.01	0.06	0.06	-0.05	0.51	0.41	0.10

Time (Sec)	Acceleration (mm/sec^2) - Human segment							Acceleration (mm/sec^2) - Seat		
	Head	Chest	Waist	Upper Arm	Lower Arm	Thigh	Leg	Headrest	Backrest	Cushion
6.5	-0.86	-0.14	-0.20	-0.03	0.11	0.11	-0.03	-1.67	-0.27	0.22
6.6	0.63	0.25	0.28	-0.01	0.21	0.21	0.03	1.26	0.51	0.43
6.7	0.14	0.31	0.31	-0.01	0.22	0.22	0.10	0.22	0.51	0.36
6.8	-0.11	0.01	-0.01	0.01	0.09	0.09	0.09	-0.15	0.02	0.12
6.9	0.01	0.07	0.05	0.03	0.10	0.10	0.10	0.01	0.09	0.12
7.0	0.16	0.37	0.36	0.01	0.22	0.22	0.15	0.27	0.62	0.37
7.1	0.50	0.20	0.21	0.00	0.27	0.27	0.18	0.97	0.39	0.52
7.2	-0.67	-0.12	-0.17	-0.01	0.07	0.07	0.21	-1.34	-0.24	0.14
7.3	0.36	0.28	0.29	0.01	0.10	0.10	0.17	0.60	0.47	0.16
7.4	0.64	0.36	0.38	0.02	0.23	0.23	0.21	0.88	0.50	0.32
7.5	-0.79	-0.13	-0.18	-0.01	0.17	0.17	0.33	-0.96	-0.16	0.21
7.6	0.41	0.17	0.17	-0.02	0.09	0.09	0.32	0.69	0.28	0.16
7.7	0.25	0.37	0.36	-0.05	0.16	0.16	0.29	0.49	0.71	0.31
7.8	-0.08	0.07	0.05	0.01	0.20	0.20	0.20	-0.15	0.14	0.40
7.9	0.03	0.01	-0.01	0.04	0.17	0.17	0.23	0.05	0.02	0.28
8.0	-0.02	0.31	0.30	-0.02	0.06	0.06	0.31	-0.02	0.42	0.08
8.1	0.63	0.28	0.30	-0.01	0.17	0.17	0.25	0.77	0.34	0.21
8.2	-0.58	-0.11	-0.15	0.02	0.31	0.31	0.20	-0.98	-0.18	0.52
8.3	0.04	0.17	0.16	-0.01	0.10	0.10	0.15	0.08	0.33	0.20

Time (Sec)	Acceleration (mm/sec^2) - Human segment							Acceleration (mm/sec^2) - Seat		
	Head	Chest	Waist	Upper Arm	Lower Arm	Thigh	Leg	Headrest	Backrest	Cushion
8.4	0.96	0.44	0.48	0.03	0.07	0.07	0.18	1.92	0.89	0.13
8.5	-0.75	-0.06	-0.12	0.02	0.19	0.19	0.20	-1.24	-0.09	0.31
8.6	0.11	0.08	0.06	0.00	0.23	0.23	0.11	0.16	0.10	0.31
8.7	0.49	0.36	0.38	-0.03	0.12	0.12	0.05	0.60	0.45	0.15
8.8	-0.02	0.14	0.13	-0.03	0.08	0.08	0.01	-0.03	0.24	0.14
8.9	-0.10	-0.01	-0.04	0.02	0.19	0.19	0.00	-0.19	-0.03	0.37
9.0	-0.16	0.21	0.20	0.03	0.24	0.24	0.01	-0.31	0.41	0.48
9.1	0.82	0.34	0.37	-0.03	0.05	0.05	0.01	1.35	0.56	0.09
9.2	-0.44	-0.03	-0.08	-0.01	0.18	0.18	0.00	-0.60	-0.05	0.24
9.3	-0.41	0.05	0.02	0.02	0.24	0.24	-0.02	-0.50	0.06	0.29
9.4	1.22	0.47	0.51	0.01	0.19	0.19	-0.04	2.06	0.79	0.32
9.5	-0.45	0.06	0.02	0.02	0.06	0.06	-0.02	-0.88	0.13	0.12
9.6	-0.26	-0.01	-0.03	0.02	0.13	0.13	0.01	-0.43	-0.01	0.27
9.7	0.53	0.31	0.32	-0.03	0.24	0.24	0.04	0.73	0.42	0.40
9.8	0.16	0.22	0.22	-0.01	0.21	0.21	0.04	0.20	0.27	0.28
9.9	-0.05	0.01	0.00	-0.01	0.01	0.01	0.09	-0.09	0.02	0.01
10.0	-0.43	0.09	0.05	0.00	0.17	0.17	0.17	-0.85	0.18	0.29

The acceleration responses of all the human and car seat segments have been outlined through graphs in Fig. 89, Fig. 90, Fig. 91, Fig. 92, Fig. 93, Fig. 94, Fig. 95, Fig. 96, Fig. 97 and Fig. 98.

5.4.1.1. Response at Head

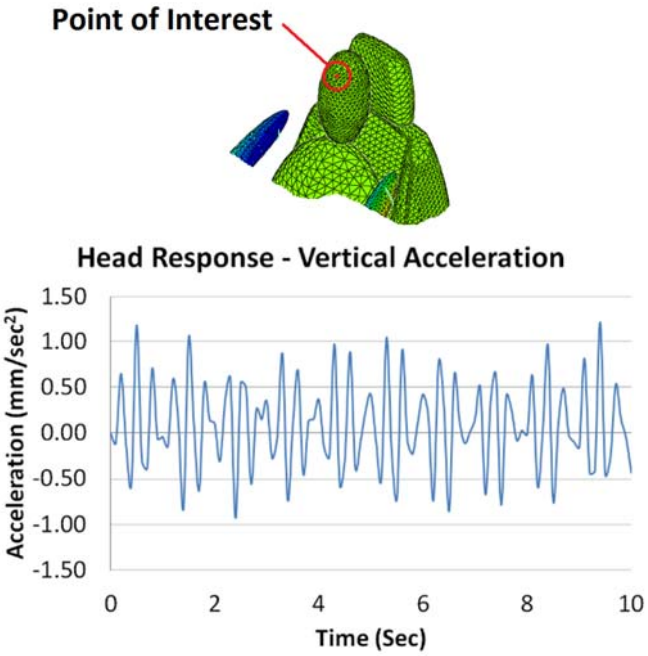

Fig. 89. Acceleration response at head

5.4.1.2. Response at Chest

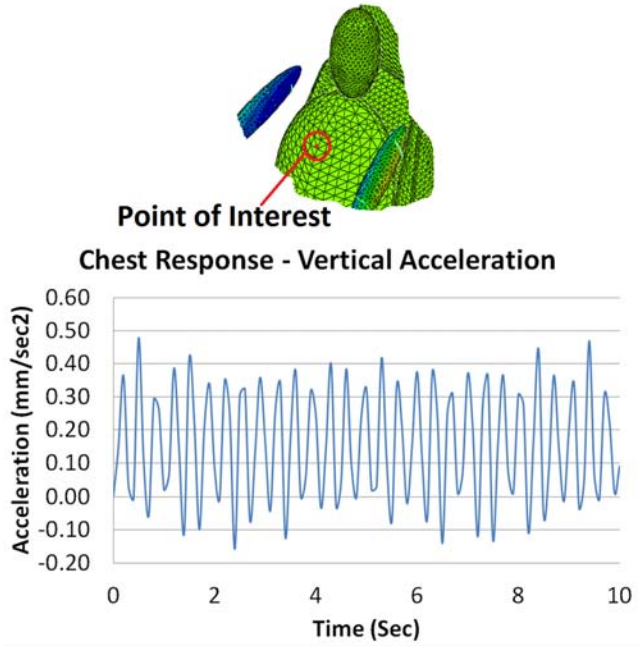

Fig. 90. Acceleration response at chest

5.4.1.3. Response at Waist

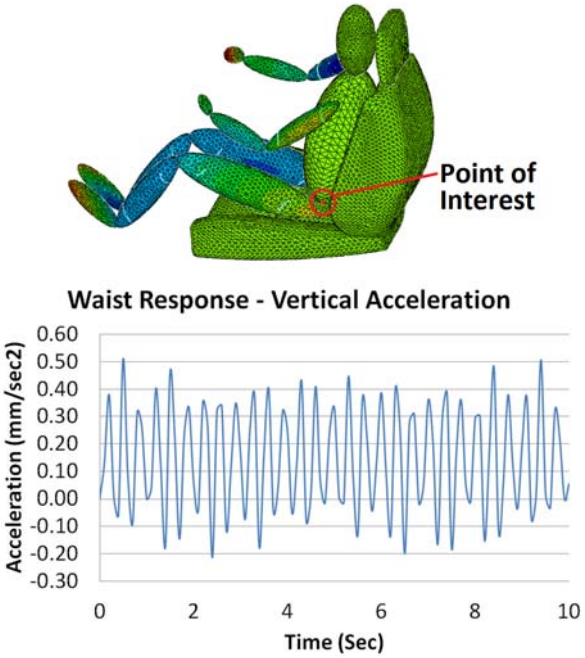

Fig. 91. Acceleration response at waist

5.4.1.4. Response at Upper Arm

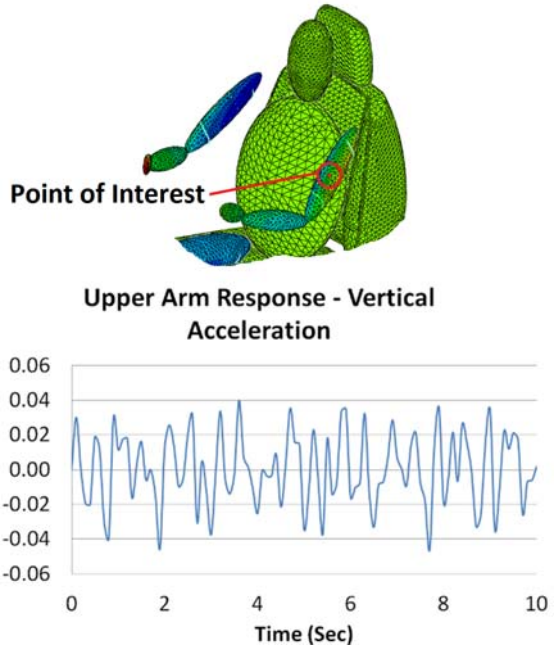

Fig. 92. Acceleration response at upper arm

5.4.1.5. Response at Lower Arm

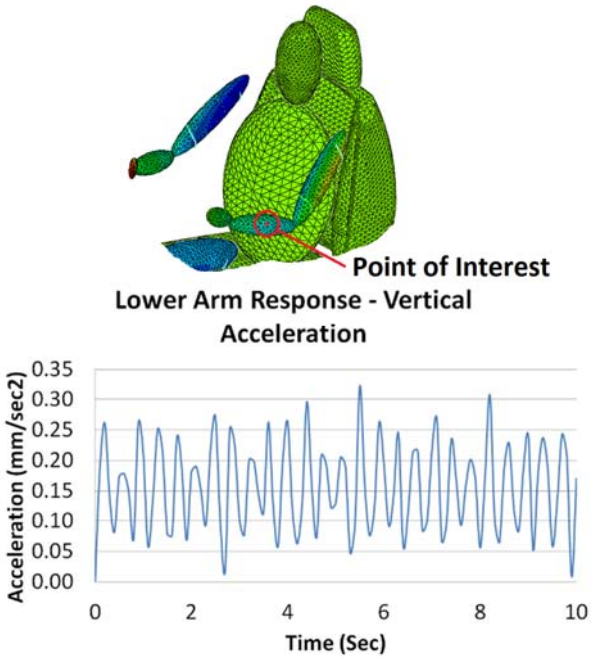

Fig. 93. Acceleration response at lower arm

5.4.1.6. Response at Thigh

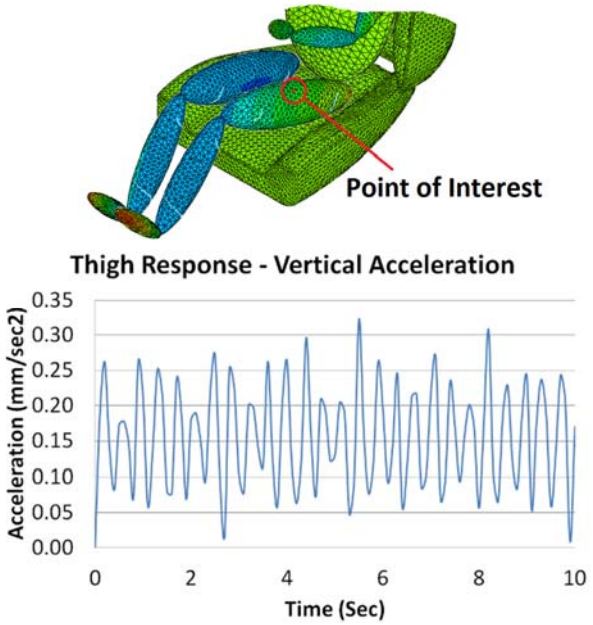

Fig. 94. Acceleration response at thigh

5.4.1.7. Response at Leg

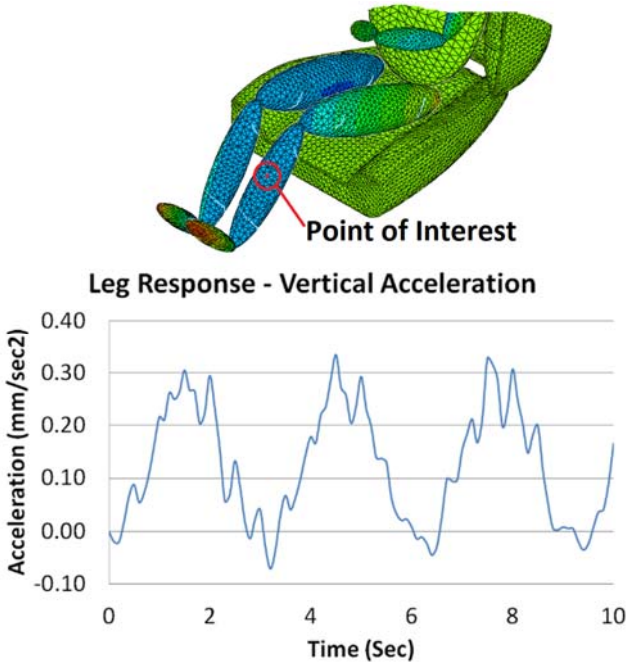

Fig. 95. Acceleration response at leg

5.4.1.8. Response at Headrest

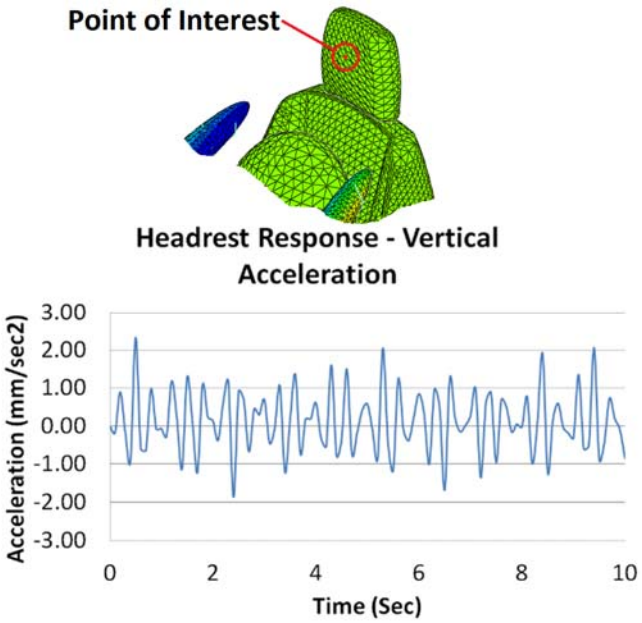

Fig. 96. Acceleration response at headrest

5.4.1.9. Response at Backrest

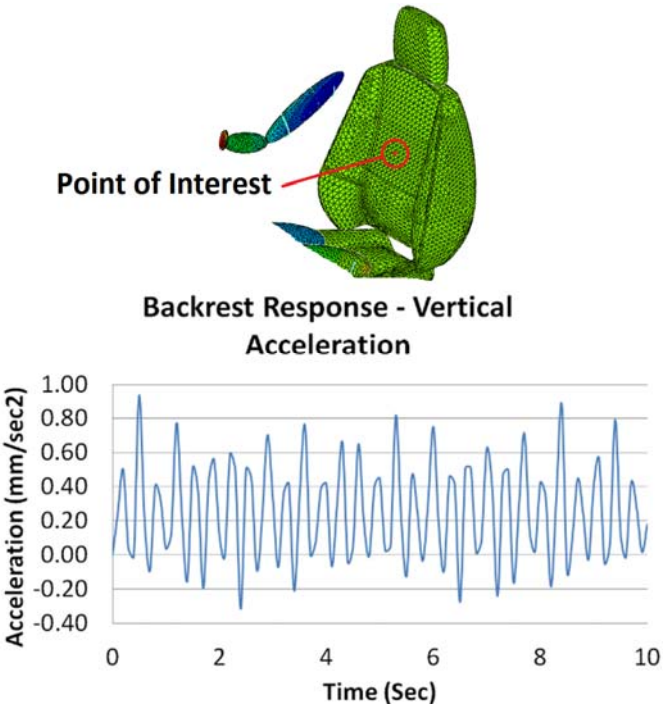

Fig. 97. Acceleration response at backrest

5.4.1.10. Response at Cushion

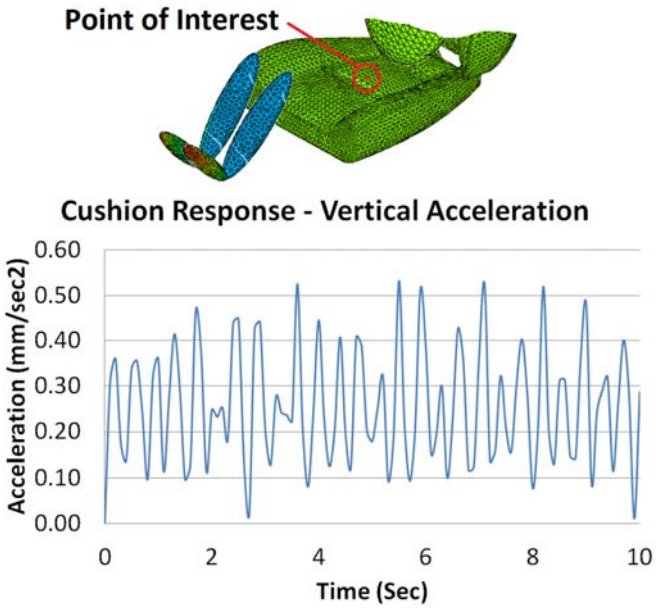

Fig. 98. Acceleration response at cushion

5.4.2. Displacement responses at the points of interest

The measured vertical displacement values with respect to simulation time at the designated points of head, chest, waist, upper arm, lower arm, thigh, leg, headrest, backrest and cushion are shown in Table 30.

Table 30. Measured values of vertical displacements for the human body and car seat

Time (Sec)	Displacement (mm) - Human segments							Displacement (mm) - Seat		
	Head	Chest	Waist	Upper Arm	Lower Arm	Thigh	Leg	Headrest	Backrest	Cushion
0.0	0.000000	0.000000	0.000000	0.000000	0.000000	0.000000	0.000000	0.000000	0.000000	0.000000
0.1	0.000000	0.000001	0.000001	0.000000	0.000000	0.000000	0.000000	0.000001	0.000001	0.000000
0.2	0.000002	0.000002	0.000002	0.000000	0.000000	0.000000	0.000002	0.000002	0.000003	0.000000
0.3	0.000004	0.000006	0.000006	0.000001	0.000001	0.000000	0.000004	0.000004	0.000006	0.000000
0.4	0.000007	0.000010	0.000010	0.000001	0.000001	-0.000001	0.000008	0.000010	0.000014	-0.000001
0.5	0.000011	0.000015	0.000015	0.000002	0.000002	-0.000001	0.000012	0.000016	0.000022	-0.000002
0.6	0.000016	0.000022	0.000022	0.000002	0.000002	-0.000002	0.000018	0.000023	0.000033	-0.000002
0.7	0.000021	0.000030	0.000030	0.000003	0.000003	-0.000002	0.000024	0.000026	0.000038	-0.000003
0.8	0.000028	0.000039	0.000040	0.000004	0.000004	-0.000003	0.000031	0.000033	0.000046	-0.000003
0.9	0.000035	0.000050	0.000050	0.000005	0.000005	-0.000003	0.000040	0.000039	0.000056	-0.000004
1.0	0.000043	0.000061	0.000062	0.000007	0.000007	-0.000004	0.000049	0.000060	0.000085	-0.000006
1.1	0.000052	0.000074	0.000075	0.000008	0.000008	-0.000005	0.000060	0.000076	0.000108	-0.000007
1.2	0.000062	0.000088	0.000089	0.000009	0.000009	-0.000006	0.000071	0.000093	0.000133	-0.000009
1.3	0.000073	0.000104	0.000105	0.000011	0.000011	-0.000007	0.000083	0.000091	0.000130	-0.000009
1.4	0.000085	0.000120	0.000121	0.000013	0.000013	-0.000008	0.000096	0.000100	0.000142	-0.000010

Time (Sec)	Displacement (mm) - Human segments							Displacement (mm) - Seat		
	Head	Chest	Waist	Upper Arm	Lower Arm	Thigh	Leg	Headrest	Backrest	Cushion
1.5	0.000097	0.000138	0.000139	0.000015	0.000015	-0.000009	0.000111	0.000109	0.000155	-0.000011
1.6	0.000111	0.000157	0.000159	0.000017	0.000017	-0.000011	0.000126	0.000154	0.000218	-0.000015
1.7	0.000125	0.000178	0.000179	0.000019	0.000019	-0.000012	0.000142	0.000182	0.000259	-0.000018
1.8	0.000140	0.000199	0.000201	0.000021	0.000021	-0.000014	0.000159	0.000210	0.000299	-0.000020
1.9	0.000156	0.000222	0.000224	0.000024	0.000024	-0.000015	0.000178	0.000195	0.000277	-0.000019
2.0	0.000173	0.000246	0.000248	0.000026	0.000026	-0.000017	0.000197	0.000203	0.000289	-0.000020
2.1	0.000191	0.000271	0.000273	0.000029	0.000029	-0.000018	0.000217	0.000214	0.000305	-0.000021
2.2	0.000209	0.000297	0.000300	0.000032	0.000032	-0.000020	0.000238	0.000291	0.000413	-0.000028
2.3	0.000229	0.000325	0.000328	0.000034	0.000034	-0.000022	0.000260	0.000333	0.000474	-0.000032
2.4	0.000249	0.000354	0.000357	0.000038	0.000038	-0.000024	0.000283	0.000374	0.000531	-0.000036
2.5	0.000270	0.000384	0.000387	0.000041	0.000041	-0.000026	0.000308	0.000338	0.000480	-0.000033
2.6	0.000292	0.000415	0.000419	0.000044	0.000044	-0.000028	0.000333	0.000344	0.000488	-0.000033
2.7	0.000315	0.000448	0.000451	0.000047	0.000047	-0.000030	0.000359	0.000355	0.000504	-0.000034
2.8	0.000339	0.000482	0.000485	0.000051	0.000051	-0.000033	0.000386	0.000471	0.000669	-0.000045
2.9	0.000364	0.000517	0.000521	0.000055	0.000055	-0.000035	0.000414	0.000530	0.000753	-0.000051
3.0	0.000389	0.000553	0.000557	0.000059	0.000059	-0.000038	0.000443	0.000584	0.000829	-0.000056
3.1	0.000416	0.000590	0.000595	0.000063	0.000063	-0.000040	0.000473	0.000519	0.000738	-0.000050
3.2	0.000443	0.000629	0.000634	0.000067	0.000067	-0.000043	0.000504	0.000521	0.000739	-0.000050
3.3	0.000471	0.000669	0.000674	0.000071	0.000071	-0.000045	0.000536	0.000530	0.000752	-0.000051
3.4	0.000500	0.000710	0.000716	0.000075	0.000075	-0.000048	0.000569	0.000695	0.000987	-0.000067
3.5	0.000530	0.000752	0.000759	0.000080	0.000080	-0.000051	0.000603	0.000772	0.001097	-0.000075
3.6	0.000560	0.000796	0.000802	0.000084	0.000084	-0.000054	0.000638	0.000841	0.001194	-0.000081

Time (Sec)	Displacement (mm) - Human segments							Displacement (mm) - Seat		
	Head	Chest	Waist	Upper Arm	Lower Arm	Thigh	Leg	Headrest	Backrest	Cushion
3.7	0.000592	0.000841	0.000848	0.000089	0.000089	-0.000057	0.000674	0.000740	0.001051	-0.000071
3.8	0.000624	0.000887	0.000894	0.000094	0.000094	-0.000060	0.000711	0.000734	0.001043	-0.000071
3.9	0.000658	0.000934	0.000942	0.000099	0.000099	-0.000064	0.000748	0.000740	0.001051	-0.000071
4.0	0.000692	0.000983	0.000991	0.000104	0.000104	-0.000067	0.000787	0.000961	0.001366	-0.000093
4.1	0.000727	0.001033	0.001041	0.000109	0.000109	-0.000070	0.000827	0.001060	0.001505	-0.000102
4.2	0.000763	0.001084	0.001092	0.000115	0.000115	-0.000074	0.000868	0.001144	0.001625	-0.000110
4.3	0.000800	0.001136	0.001145	0.000120	0.000120	-0.000077	0.000910	0.000999	0.001420	-0.000096
4.4	0.000837	0.001189	0.001199	0.000126	0.000126	-0.000081	0.000953	0.000984	0.001398	-0.000095
4.5	0.000876	0.001244	0.001254	0.000132	0.000132	-0.000085	0.000996	0.000985	0.001399	-0.000095
4.6	0.000915	0.001300	0.001310	0.000138	0.000138	-0.000088	0.001041	0.001271	0.001806	-0.000123
4.7	0.000955	0.001357	0.001368	0.000144	0.000144	-0.000092	0.001087	0.001393	0.001978	-0.000134
4.8	0.000996	0.001415	0.001427	0.000150	0.000150	-0.000096	0.001134	0.001494	0.002123	-0.000144
4.9	0.001038	0.001475	0.001487	0.000156	0.000156	-0.000100	0.001182	0.001298	0.001843	-0.000125
5.0	0.001081	0.001536	0.001548	0.000163	0.000163	-0.000104	0.001230	0.001271	0.001805	-0.000123
5.1	0.001125	0.001598	0.001611	0.000169	0.000169	-0.000109	0.001280	0.001265	0.001797	-0.000122
5.2	0.001169	0.001661	0.001674	0.000176	0.000176	-0.000113	0.001331	0.001625	0.002308	-0.000157
5.3	0.001215	0.001725	0.001739	0.000183	0.000183	-0.000117	0.001382	0.001771	0.002515	-0.000171
5.4	0.001261	0.001791	0.001806	0.000190	0.000190	-0.000122	0.001435	0.001891	0.002687	-0.000183
5.5	0.001308	0.001858	0.001873	0.000197	0.000197	-0.000126	0.001489	0.001635	0.002323	-0.000158
5.6	0.001356	0.001926	0.001942	0.000204	0.000204	-0.000131	0.001543	0.001594	0.002265	-0.000154
5.7	0.001405	0.001996	0.002012	0.000212	0.000212	-0.000136	0.001599	0.001580	0.002244	-0.000153
5.8	0.001455	0.002066	0.002083	0.000219	0.000219	-0.000140	0.001655	0.002021	0.002871	-0.000195

Time (Sec)	Displacement (mm) - Human segments							Displacement (mm) - Seat		
	Head	Chest	Waist	Upper Arm	Lower Arm	Thigh	Leg	Headrest	Backrest	Cushion
5.9	0.001505	0.002138	0.002155	0.000227	0.000227	-0.000145	0.001713	0.002195	0.003117	-0.000212
6.0	0.001557	0.002211	0.002229	0.000234	0.000234	-0.000150	0.001772	0.002335	0.003317	-0.000225
6.1	0.001609	0.002286	0.002304	0.000242	0.000242	-0.000155	0.001831	0.002011	0.002857	-0.000194
6.2	0.001662	0.002361	0.002380	0.000250	0.000250	-0.000160	0.001892	0.001954	0.002776	-0.000189
6.3	0.001716	0.002438	0.002458	0.000259	0.000259	-0.000166	0.001953	0.001930	0.002742	-0.000186
6.4	0.001771	0.002516	0.002536	0.000267	0.000267	-0.000171	0.002016	0.002461	0.003496	-0.000238
6.5	0.001827	0.002595	0.002616	0.000275	0.000275	-0.000176	0.002079	0.002664	0.003783	-0.000257
6.6	0.001884	0.002676	0.002697	0.000284	0.000284	-0.000182	0.002144	0.002825	0.004013	-0.000273
6.7	0.001941	0.002757	0.002780	0.000292	0.000292	-0.000187	0.002209	0.002426	0.003447	-0.000234
6.8	0.002000	0.002840	0.002863	0.000301	0.000301	-0.000193	0.002276	0.002351	0.003339	-0.000227
6.9	0.002059	0.002924	0.002948	0.000310	0.000310	-0.000199	0.002343	0.002315	0.003289	-0.000223
7.0	0.002119	0.003010	0.003034	0.000319	0.000319	-0.000205	0.002411	0.002944	0.004182	-0.000284
7.1	0.002180	0.003096	0.003121	0.000328	0.000328	-0.000210	0.002481	0.003178	0.004514	-0.000307
7.2	0.002242	0.003184	0.003210	0.000338	0.000338	-0.000216	0.002551	0.003268	0.004642	-0.000325
7.3	0.002304	0.003273	0.003300	0.000347	0.000347	-0.000222	0.002622	0.003457	0.004910	-0.000278
7.4	0.002368	0.003363	0.003391	0.000357	0.000357	-0.000229	0.002695	0.002960	0.004204	-0.000269
7.5	0.002432	0.003455	0.003483	0.000366	0.000366	-0.000235	0.002768	0.002860	0.004062	-0.000264
7.6	0.002498	0.003548	0.003576	0.000376	0.000376	-0.000241	0.002842	0.002809	0.003990	-0.000335
7.7	0.002564	0.003642	0.003671	0.000386	0.000386	-0.000247	0.002918	0.003563	0.005060	-0.000361
7.8	0.002631	0.003737	0.003767	0.000396	0.000396	-0.000254	0.002994	0.003835	0.005448	-0.000381
7.9	0.002699	0.003833	0.003864	0.000407	0.000407	-0.000260	0.003071	0.003934	0.005589	-0.000326
8.0	0.002768	0.003931	0.003963	0.000417	0.000417	-0.000267	0.003150	0.004151	0.005896	-0.000314

Time (Sec)	Displacement (mm) - Human segments							Displacement (mm) - Seat		
	Head	Chest	Waist	Upper Arm	Lower Arm	Thigh	Leg	Headrest	Backrest	Cushion
8.1	0.002837	0.004030	0.004062	0.000427	0.000427	-0.000274	0.003229	0.003546	0.005037	-0.000308
8.2	0.002908	0.004130	0.004163	0.000438	0.000438	-0.000281	0.003309	0.003418	0.004856	-0.000390
8.3	0.002979	0.004231	0.004266	0.000449	0.000449	-0.000288	0.003390	0.003350	0.004758	-0.000419
8.4	0.003051	0.004334	0.004369	0.000460	0.000460	-0.000295	0.003472	0.004240	0.006022	-0.000442
8.5	0.003124	0.004438	0.004474	0.000471	0.000471	-0.000302	0.003556	0.004555	0.006470	-0.000377
8.6	0.003198	0.004543	0.004579	0.000482	0.000482	-0.000309	0.003640	0.003597	0.005109	-0.000363
8.7	0.003273	0.004649	0.004687	0.000493	0.000493	-0.000316	0.003725	0.004548	0.006460	-0.000355
8.8	0.003349	0.004756	0.004795	0.000504	0.000504	-0.000323	0.003811	0.004882	0.006934	-0.000449
8.9	0.003425	0.004865	0.004905	0.000516	0.000516	-0.000331	0.003898	0.005138	0.007298	-0.000482
9.0	0.003503	0.004975	0.005015	0.000528	0.000528	-0.000338	0.003986	0.004378	0.006219	-0.000493
9.1	0.003581	0.005086	0.005127	0.000539	0.000539	-0.000346	0.004075	0.004210	0.005980	-0.000518
9.2	0.003660	0.005199	0.005241	0.000551	0.000551	-0.000353	0.004165	0.004116	0.005846	-0.000442
9.3	0.003740	0.005312	0.005355	0.000563	0.000563	-0.000361	0.004256	0.005197	0.007382	-0.000424
9.4	0.003821	0.005427	0.005471	0.000576	0.000576	-0.000369	0.004348	0.005570	0.007912	-0.000415
9.5	0.003903	0.005543	0.005588	0.000588	0.000588	-0.000377	0.004441	0.005690	0.008081	-0.000523
9.6	0.003985	0.005661	0.005706	0.000600	0.000600	-0.000385	0.004535	0.005978	0.008491	-0.000561
9.7	0.004069	0.005779	0.005826	0.000613	0.000613	-0.000393	0.004630	0.005086	0.007224	-0.000589
9.8	0.004153	0.005899	0.005947	0.000626	0.000626	-0.000401	0.004726	0.004883	0.006935	-0.000451
9.9	0.004238	0.006020	0.006069	0.000639	0.000639	-0.000409	0.004823	0.004766	0.006770	-0.000568
10.0	0.004324	0.006142	0.006192	0.000652	0.000652	-0.000417	0.004921	0.006009	0.008535	-0.000626

The displacement values of all the human and car seat segments have been outlined graphically in Fig. 99 and Fig. 100.

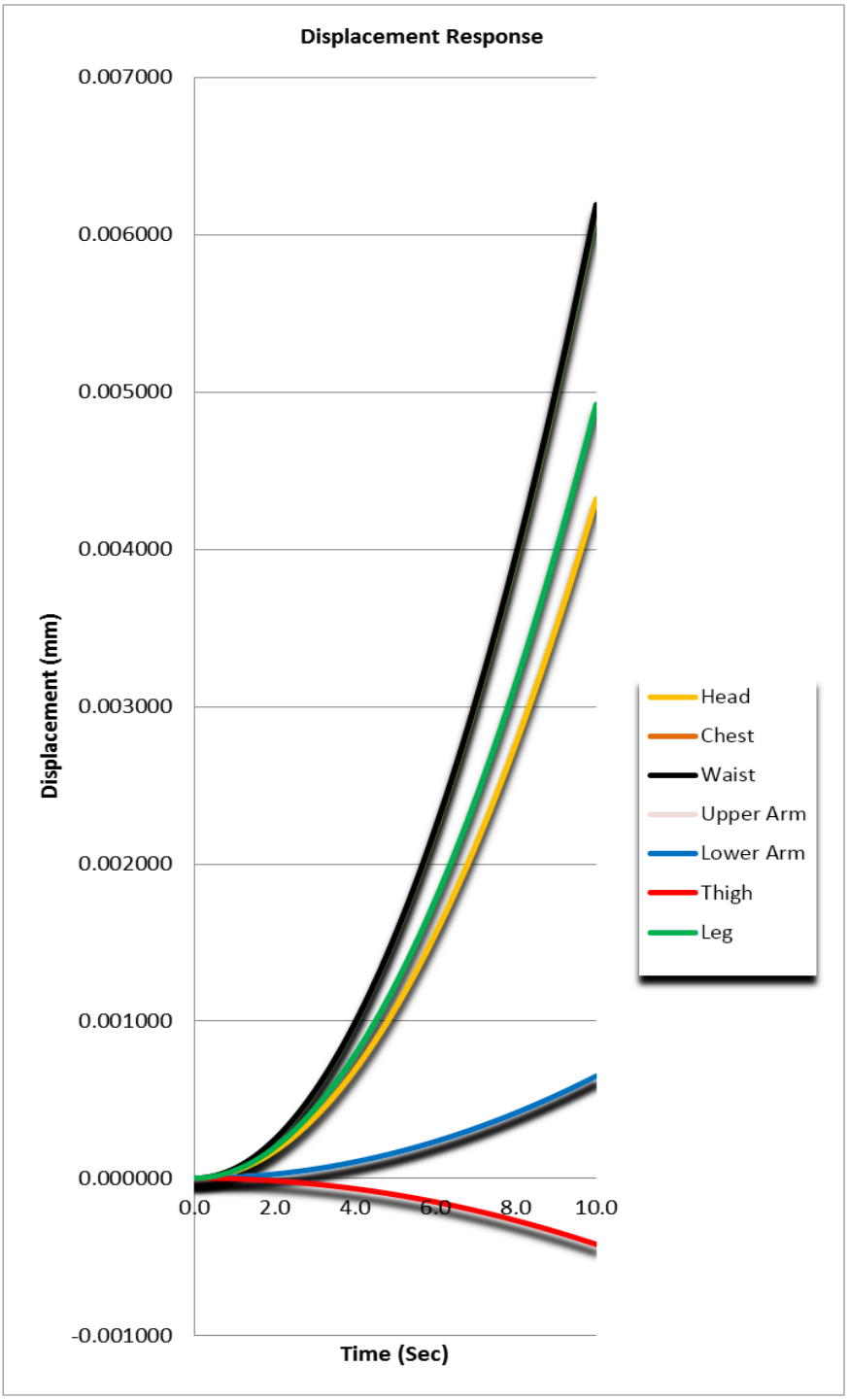

Fig. 99. Displacement responses at different segments of human body

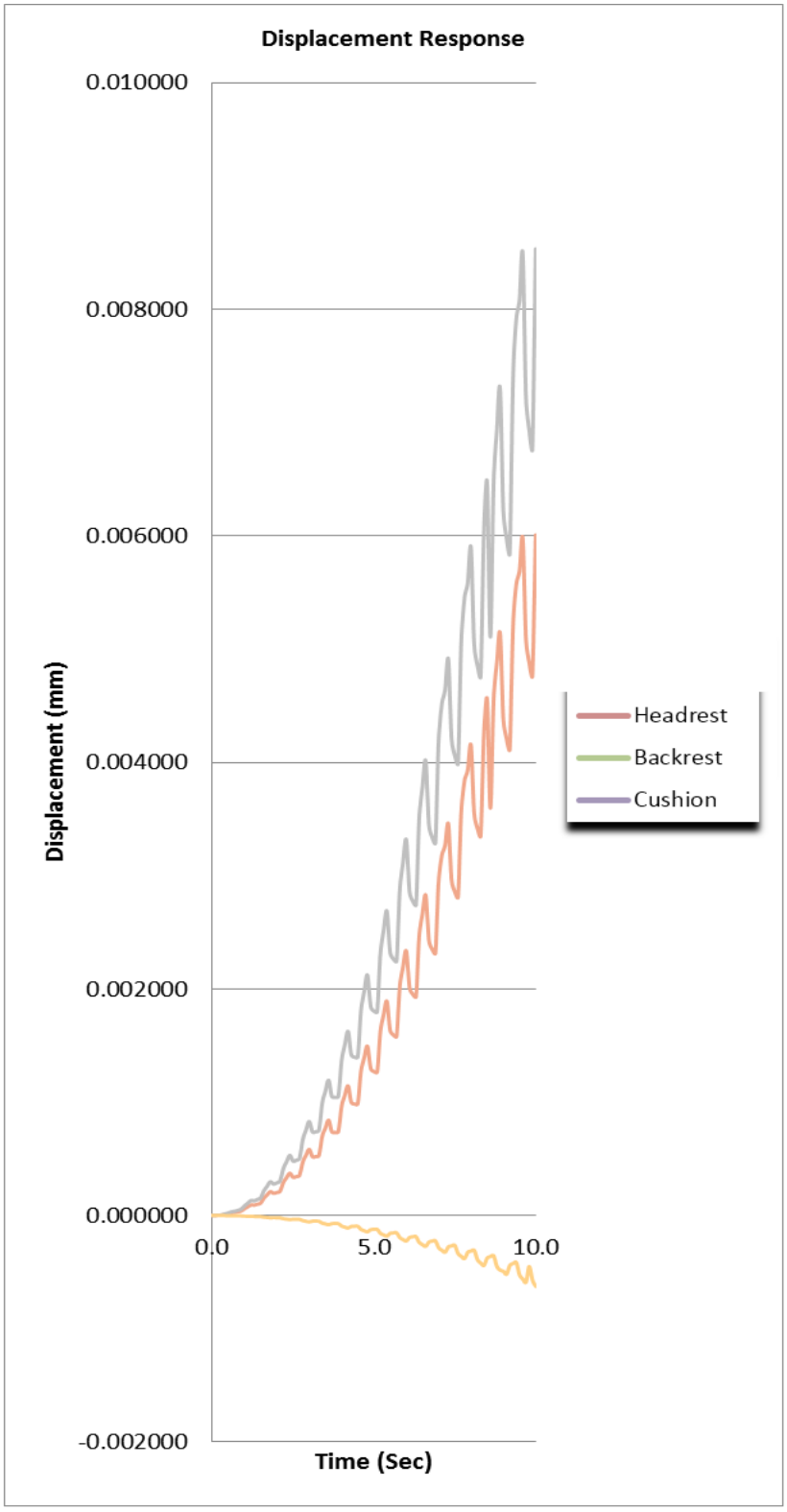

Fig. 100. Displacement responses at different segments of car seat

5.4.3. Frequencies at the points of interest

The frequencies of all the human and car seat segments have been calculated and given in Table 31.

Table 31. Calculated values of frequencies for all the human and car seat segments

Time (Sec)	Frequency (Hz) - Human segments							Frequency (Hz) - Seat		
	Head	Chest	Waist	Upper Arm	Lower Arm	Thigh	Leg	Headrest	Backrest	Cushion
0.0	0.00	0.00	0.00	0.00	0.00	0.00	0.00	0.00	0.00	0.00
0.1	79.16	77.94	73.32	108.37	270.12	337.34	31.67	90.95	89.54	387.57
0.2	97.66	61.32	62.31	2.68	159.62	199.35	16.29	105.64	66.34	215.64
0.3	30.51	12.19	7.29	28.94	78.31	97.80	9.92	31.84	12.72	102.06
0.4	44.92	3.52	11.96	21.96	44.55	55.64	14.50	49.53	3.89	61.35
0.5	52.83	28.08	28.92	17.04	51.86	64.77	13.44	61.22	32.54	75.06
0.6	22.02	11.06	9.80	11.61	43.88	54.81	8.77	25.43	12.77	63.28
0.7	21.63	6.91	8.69	15.42	34.17	42.68	8.70	24.85	7.94	49.03
0.8	25.50	13.71	14.19	15.47	20.71	25.86	9.40	27.58	14.83	27.98
0.9	6.63	11.57	11.44	11.95	35.49	44.33	10.19	6.91	12.07	46.26
1.0	4.79	3.05	0.66	6.77	28.77	35.93	10.56	5.29	3.36	39.62
1.1	8.29	4.70	3.53	7.51	13.71	17.13	9.47	9.61	5.45	19.85
1.2	15.53	10.53	10.70	6.96	19.14	23.90	9.68	17.94	12.16	27.60
1.3	6.75	5.84	5.51	6.11	24.06	30.05	8.73	7.76	6.71	34.52
1.4	15.71	4.81	6.03	2.33	20.66	25.81	8.33	17.00	5.21	27.92
1.5	16.55	8.73	9.15	5.30	11.69	14.60	8.36	17.27	9.11	15.24
1.6	4.70	6.00	5.98	2.97	10.80	13.48	7.34	5.18	6.62	14.87
1.7	11.27	3.75	4.54	0.15	17.89	22.35	6.88	13.06	4.35	25.90
1.8	9.92	5.21	5.38	4.12	15.01	18.74	5.70	11.45	6.02	21.64
1.9	4.91	6.22	6.16	7.01	8.59	10.72	5.65	5.65	7.15	12.32
2.0	3.87	2.96	2.50	3.47	13.23	16.53	6.16	4.18	3.20	17.88

Time (Sec)	Frequency (Hz) - Human segments							Frequency (Hz) - Seat		
	Head	Chest	Waist	Upper Arm	Lower Arm	Thigh	Leg	Headrest	Backrest	Cushion
2.1	6.40	0.77	1.95	4.76	12.94	16.17	5.22	6.67	0.81	16.87
2.2	6.60	5.46	5.47	3.34	10.97	13.70	4.05	7.28	6.02	15.11
2.3	8.12	4.40	4.52	2.64	8.30	10.36	2.35	9.41	5.10	12.01
2.4	9.72	3.36	3.90	1.86	12.17	15.20	2.50	11.23	3.88	17.55
2.5	7.19	4.49	4.59	3.57	12.99	16.23	3.31	8.26	5.16	18.64
2.6	6.57	4.44	4.54	4.25	7.62	9.51	2.53	7.11	4.81	10.29
2.7	6.69	2.03	2.56	4.03	3.06	3.82	1.08	6.98	2.12	3.99
2.8	4.43	2.62	2.49	1.53	11.18	13.97	0.95	4.88	2.89	15.40
2.9	3.24	4.19	4.12	2.42	10.21	12.75	1.20	3.76	4.86	14.78
3.0	4.76	2.76	2.75	4.02	6.66	8.32	1.53	5.50	3.19	9.60
3.1	4.08	1.35	1.77	0.66	5.62	7.02	1.23	4.68	1.56	8.07
3.2	1.61	3.22	3.15	3.58	8.74	10.92	1.89	1.74	3.49	11.81
3.3	6.83	3.58	3.76	1.30	8.41	10.50	1.31	7.12	3.74	10.96
3.4	6.06	2.10	2.50	2.17	6.87	8.58	1.17	6.69	2.32	9.46
3.5	2.10	2.44	2.34	0.92	6.02	7.51	1.68	2.43	2.83	8.71
3.6	5.55	3.48	3.56	3.46	8.88	11.09	1.28	6.41	4.02	12.81
3.7	4.39	0.25	1.17	1.45	5.96	7.44	1.54	5.04	0.28	8.55
3.8	2.29	1.26	1.07	0.63	3.98	4.97	1.89	2.48	1.36	5.37
3.9	2.43	2.94	2.94	1.71	7.17	8.96	2.21	2.54	3.07	9.35
4.0	3.65	2.52	2.53	2.47	8.00	10.00	2.40	4.03	2.78	11.02
4.1	2.39	0.90	1.14	0.34	5.21	6.51	2.26	2.77	1.04	7.54
4.2	2.96	1.84	1.74	0.89	3.72	4.65	2.54	3.42	2.13	5.37
4.3	5.55	2.99	3.09	0.84	5.16	6.44	2.57	6.38	3.43	7.40
4.4	4.12	0.76	1.30	1.35	7.72	9.64	2.77	4.46	0.82	10.43
4.5	2.80	0.96	0.57	2.02	5.52	6.90	2.92	2.92	1.01	7.20
4.6	4.96	2.74	2.81	0.65	3.65	4.56	2.58	5.47	3.02	5.03

Time (Sec)	Frequency (Hz) - Human segments							Frequency (Hz) - Seat		
	Head	Chest	Waist	Upper Arm	Lower Arm	Thigh	Leg	Headrest	Backrest	Cushion
4.7	3.16	1.37	1.09	2.49	6.05	7.56	2.45	3.67	1.59	8.76
4.8	1.53	0.21	0.49	1.63	5.72	7.15	2.14	1.76	0.25	8.25
4.9	2.48	2.04	2.05	1.54	4.46	5.57	2.25	2.85	2.35	6.39
5.0	3.13	2.31	2.33	2.31	4.50	5.62	2.46	3.39	2.50	6.08
5.1	1.52	0.58	0.31	1.36	5.54	6.92	2.14	1.59	0.61	7.22
5.2	3.29	0.69	0.45	1.82	5.23	6.53	1.94	3.63	0.76	7.20
5.3	4.67	2.48	2.55	0.81	2.57	3.21	1.59	5.42	2.87	3.72
5.4	2.14	1.22	1.05	2.23	3.59	4.48	1.56	2.48	1.41	5.17
5.5	3.71	1.00	1.32	1.53	6.44	8.05	1.49	4.26	1.15	9.25
5.6	4.12	2.10	2.19	1.31	4.49	5.61	1.01	4.46	2.28	6.07
5.7	1.22	1.64	1.62	0.97	3.03	3.78	0.73	1.28	1.71	3.94
5.8	2.00	0.49	0.72	1.97	3.72	4.64	0.57	2.20	0.54	5.12
5.9	1.40	1.34	1.27	1.97	5.42	6.77	0.58	1.62	1.56	7.84
6.0	2.63	2.08	2.10	1.32	4.57	5.71	0.35	3.04	2.40	6.59
6.1	1.76	1.10	1.04	1.03	3.11	3.89	0.44	2.02	1.27	4.46
6.2	3.34	0.85	1.18	0.87	3.78	4.72	0.38	3.62	0.92	5.10
6.3	3.39	1.97	2.04	1.78	4.90	6.12	0.55	3.54	2.06	6.39
6.4	2.08	1.57	1.58	1.12	2.38	2.97	0.75	2.29	1.73	3.28
6.5	3.44	1.17	1.39	1.74	3.23	4.04	0.60	3.99	1.36	4.68
6.6	2.91	1.55	1.62	0.88	4.36	5.45	0.59	3.37	1.79	6.29
6.7	1.33	1.69	1.68	0.79	4.33	5.41	1.06	1.53	1.94	6.22
6.8	1.18	0.33	0.36	0.75	2.68	3.35	1.03	1.27	0.36	3.62
6.9	0.36	0.78	0.65	1.53	2.89	3.61	1.02	0.37	0.82	3.76
7.0	1.38	1.76	1.73	0.75	4.17	5.21	1.27	1.52	1.95	5.74
7.1	2.40	1.28	1.30	0.15	4.54	5.68	1.37	2.79	1.49	6.58
7.2	2.76	0.98	1.15	0.83	2.27	2.83	1.45	3.23	1.14	3.27

Time (Sec)	Frequency (Hz) - Human segments							Frequency (Hz) - Seat		
	Head	Chest	Waist	Upper Arm	Lower Arm	Thigh	Leg	Headrest	Backrest	Cushion
7.3	2.00	1.48	1.50	1.02	2.66	3.32	1.27	2.10	1.55	3.81
7.4	2.62	1.65	1.69	1.23	4.08	5.10	1.41	2.74	1.73	5.52
7.5	2.86	0.98	1.15	0.71	3.43	4.28	1.73	2.92	1.00	4.47
7.6	2.04	1.09	1.09	1.10	2.50	3.13	1.68	2.50	1.33	3.45
7.7	1.58	1.59	1.58	1.74	3.22	4.02	1.58	1.87	1.89	4.66
7.8	0.86	0.69	0.57	0.94	3.59	4.49	1.29	1.01	0.81	5.18
7.9	0.53	0.29	0.25	1.50	3.24	4.05	1.38	0.56	0.31	4.65
8.0	0.38	1.41	1.37	1.07	1.85	2.31	1.57	0.36	1.35	2.50
8.1	2.37	1.32	1.37	0.56	3.20	4.00	1.40	2.34	1.31	4.17
8.2	2.25	0.82	0.96	1.12	4.22	5.27	1.25	2.70	0.98	5.81
8.3	0.58	1.01	0.98	0.62	2.42	3.03	1.05	0.76	1.33	3.51
8.4	2.82	1.61	1.67	1.20	1.90	2.37	1.15	3.38	1.93	2.74
8.5	2.46	0.57	0.83	0.91	3.19	3.98	1.19	2.62	0.61	4.57
8.6	0.95	0.65	0.57	0.25	3.46	4.33	0.89	1.05	0.72	4.68
8.7	1.95	1.41	1.43	1.30	2.48	3.10	0.60	1.83	1.32	3.23
8.8	0.38	0.88	0.82	1.14	2.06	2.57	0.19	0.41	0.94	2.83
8.9	0.84	0.26	0.43	0.90	3.04	3.80	0.13	0.96	0.30	4.40
9.0	1.07	1.02	1.00	1.28	3.39	4.24	0.23	1.35	1.29	4.96
9.1	2.41	1.30	1.35	1.27	1.57	1.96	0.18	2.85	1.54	2.06
9.2	1.74	0.40	0.61	0.72	2.84	3.55	0.17	1.92	0.44	3.73
9.3	1.67	0.49	0.29	1.00	3.27	4.08	0.34	1.57	0.46	4.16
9.4	2.85	1.48	1.53	0.73	2.89	3.60	0.45	3.06	1.59	4.42
9.5	1.71	0.54	0.28	0.96	1.59	1.99	0.37	1.98	0.63	2.36
9.6	1.29	0.18	0.37	0.85	2.37	2.96	0.20	1.35	0.19	3.47
9.7	1.82	1.16	1.19	1.03	3.17	3.96	0.45	1.91	1.22	4.16
9.8	0.99	0.98	0.97	0.53	2.88	3.60	0.47	1.02	1.00	3.98

Time (Sec)	Frequency (Hz) - Human segments							Frequency (Hz) - Seat		
	Head	Chest	Waist	Upper Arm	Lower Arm	Thigh	Leg	Headrest	Backrest	Cushion
9.9	0.57	0.22	0.07	0.49	0.58	0.72	0.69	0.70	0.27	0.68
10.0	1.59	0.61	0.47	0.26	2.57	3.21	0.92	1.89	0.72	3.41

The frequencies of all the human and car seat segments with respect to simulation time have been outlined through graphs in Fig. 101 and Fig. 102.

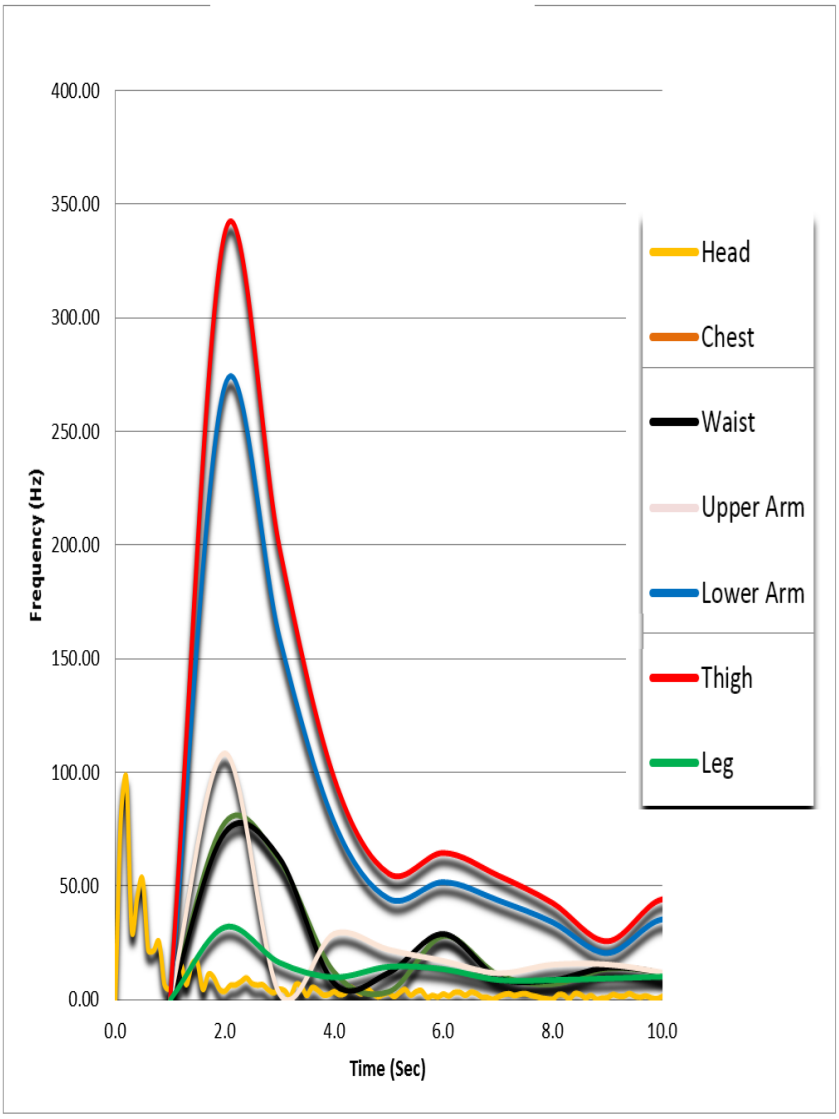

Fig. 101. Frequencies at different segments of human body

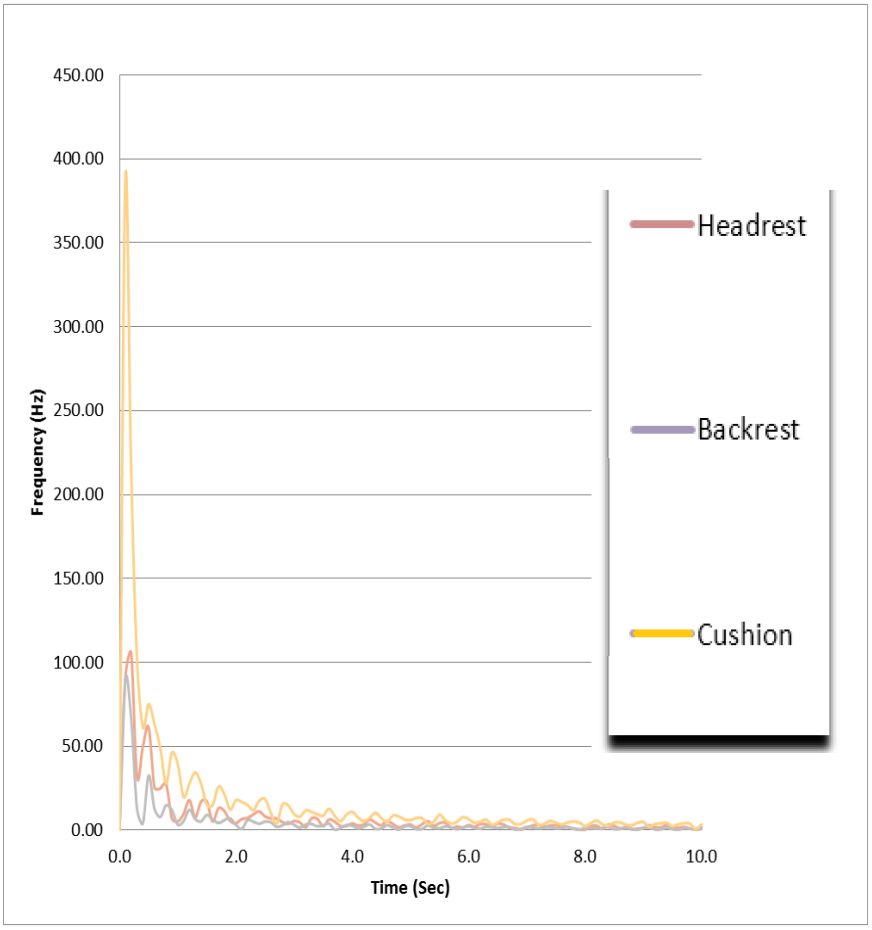

Fig. 102. Frequencies at different segments of car seat

The average frequencies of all the human and car seat segments are presented in Table 32.

Table 32. Average frequencies of all the human and car seat segments

Segments	Average frequency of human segment (Hz)
Head	7.10
Chest	4.13
Waist	4.18
Upper Arm	4.01

Segments	Average frequency of human segment (Hz)
Lower Arm	12.92
Thigh	16.13
Leg	3.20
Headrest	7.91
Backrest	4.61
Cushion	18.00

5.5. Discussion on the Unique Simulation Technique

Health, safety and comfort of the car seated human body is related directly to the level of frequency generated inside the human body. Hence, the frequencies of the respective simulated accelerations have been evaluated to check the compatibility of the simulation results with the human health, safety and comfort.

The results from this simulation are showing justified levels of frequencies, compared to the permissible range of frequencies for each of the human body segments obtained from past relevant research studies. During the investigation of the vibro-acoustic system (Cempel, 1989), the natural frequency ranges for different human organs were evaluated as per Table 33.

Table 33. Natural frequencies of different human organs (Cempel, 1989)

Human organ	Frequency of resonance (Hz)
Head	4-5
Jaw	6-8
Eyes	60-90
Chest organs	5-9
Upper limb	3

Human organ	Frequency of resonance (Hz)
Stomach organs	4.5-10
Bladder	10-18
Pelvis	5-9
Muscles	13-20
Liver	3-4

In general, the industrial standards and international guidelines recommend that the maximum permissible level of natural frequency inside human body to be lower than 20 Hz. Earlier biodynamic investigation on the human body (Zengkang et al., 2013) showed that the range of the natural frequencies of the human portions under the effects of vertical vibration would be in between 0.5 Hz and 20 Hz. Similar kind of study on the human portions exhibited the maximum possible resonating frequency values of 5 Hz, 8 Hz, 90 Hz, 9 Hz, 3 Hz, 10 Hz, 18 Hz, 9 Hz, 20 Hz and 4 Hz for head, jaw, eyes, chest, upper limb, stomach, bladder, pelvis, muscles and liver, respectively. Transmission of vibration between the car seat and hip had been observed (Mansfield and Griffin, 2000) using twelve number of objects sitting on seat without support. The resonating frequency was found to be 4 Hz, while the peak values of frequency were in-between 8 Hz and 9 Hz. Assessment of transmission of acceleration from seat to human lumbar spine (Panjabi *et al*., 1986) found the resonating frequency in-between 4 Hz and 5 Hz, while the study on the seat to head transmissibility (Zimmerman and Cook, 1997) found the resonating frequency as 5 Hz. First and second natural frequencies for the entire human body were evaluated as 5 Hz and 8 Hz- 9 Hz during the inspection of mode shape along with acceleration transmission between human trunk and seat (Kitazaki and Griffin, 1997; Kitazaki and Griffin, 1998). Examination of resonating characteristics of the entire human body under the influence of vertical vibration inside a standard car (Verver, 2004) found the natural frequency as 5 Hz. International standard ISO 5892 (2001) mentioned the resonating frequency magnitude of 5 Hz for the seat to head transmissibility in normal sitting stance without the seat backrest.

The simulation results are showing that the average frequency values at seat headrest, seat backrest and seat cushion as 7.91 Hz, 4.61 Hz and 18.0 Hz, respectively; while for the head, chest, waist, upper arm, lower arm, thigh and leg, the values are 7.10 Hz, 4.13 Hz, 4.18 Hz, 4.01 Hz, 12.92 Hz, 16.13 Hz and 3.10 Hz, respectively. So, the frequency values of these human portions are lower compared to the frequencies of the adjacent car seat segments, which shows the sign of effective vibration transmission from seat to human body. Furthermore, it gives an indication of correct functionalities of the assigned material properties, calculated stiffness values, defined damping parameters, assigned contact mechanism, implemented boundary conditions and applied loads during the development of this unique simulation technique.

The simulation had been repeated few times by assigning different contact formulations including coefficients of friction, though, cause of the lack of adequate memory inside the computer, the ABAQUS solver got terminated after running for long time without yielding any output. So, no frictional coefficients were assigned for the contact mechanism and only the tie-up constrains had been used in this simulation.

Past research works on the similar biodynamic fields have suggested that the assignment of frictional coefficients would be useful for the stress or pressure distribution related simulation studies. As the current simulation methodology aims to find out the final frequency levels at different points of human body and car seat, the use of tie-up constrains instead of frictional coefficient doesn't affect the primary objective of this simulation based investigation.

This unique finite element simulation methodology for the entire assembly of human body and car seat using the calculated three dimensional stiffness values for human portions and the combined properties of viscoelastic and hyper-elastic materials for the seat polyurethane foam, has become successful.

CHAPTER 6

VIBRATION MEASUREMENT AND TEST DATA ACQUISITION

Vibration is induced into a system cause of its dynamic operating environment. Condition of a structure under the effect of vibration can be monitored through measuring the level of vibration transmitted into that structure. Vibration got plenty pros and cons and efforts have been made over last many years by scientists and researchers to minimise the disadvantages of vibration and utilize the advantages of the effects of vibration. The only way to control the vibration, is to measure it.

Vibration can be free, forced, damped or random and measured by means of acceleration, frequency or displacement. Vibration severity in the industrial machines has been standardized by international standard ISO 10816, while the monitoring of the human health exposed to vibration has been standardized by international standards ISO 5348, ISO 5805, ISO 8662, ISO 8727, ISO 10819, CR 1030-1, CR 1030-2 and ISO 5349-1. These standards provide the ideas of vibration measurements, human exposure to vibration, hand-arm vibration, design of machines exposed to vibration and effects of vibration on the human body.

This chapter describes the techniques used by researchers for measuring the vibration at various points of human-vehicle system functioning at different environments, the technologies used behind the vibration measuring systems and the latest available technologies for measuring vibration.

Testing data have been collected to validate the simulation results obtained in CHAPTER 5. A detailed assessment of the collected test data has also been carried out in this chapter.

6.1. Past works on Vibration Measurement at Human-Vehicle Interface

The discomfort for the human occupants inside an automotive mainly comes from the vibration transmitted from the vehicle to the human body. Level of discomfort can be minimised by designing the automotive to avoid the resonant frequencies of the human organs. To understand the level of vibration inside the car seat and human body, it is important to measure it by means of acceleration, frequency or displacement. Over last many years, efforts have been made to establish suitable experimental set up for measuring the vibration at different locations of the car seat and human body. Generally, the sensors along with digital display units have been utilized in most of the past laboratory and real-life testing techniques.

One manikin and twelve numbers of male human representatives with mean age of 38.5 years and mean body mass of 77.2 kg were taken into vibration testing laboratory for studying the seat dynamics (Zhang, 2014). The human bodies, as shown in Fig. 103, were postured in relax condition with the head touching the headrest of the seat. The fore-aft vibration was measured by recording the frequencies for a period of 120 seconds at six locations on the car seat and the frequencies were found to be in the range of 0.25 Hz to 40 Hz. HVLab data acquisition system with 8 channels was used to collect the data.

Fig. 103. Laboratory test set up for studying the seat dynamics (Zhang, 2014)

Experimental set up using mannequins and foam made car seat was established (Kim *et al.*, 2003) for measuring the vibrations at human head, seat backrest, human thigh, seat cushion and seat bottom structure. The frequencies obtained for the seat bottom structure were in the range of 3 Hz to 35 Hz, while for the human portions the frequencies were found to be in the range of 6.5 Hz to 8 Hz. Low-frequency Kistler, Type 8303 and Neuwghent SAA-1000 accelerometers were used along with a data acquisition module. The entire experimental set up is outlined in Fig. 104.

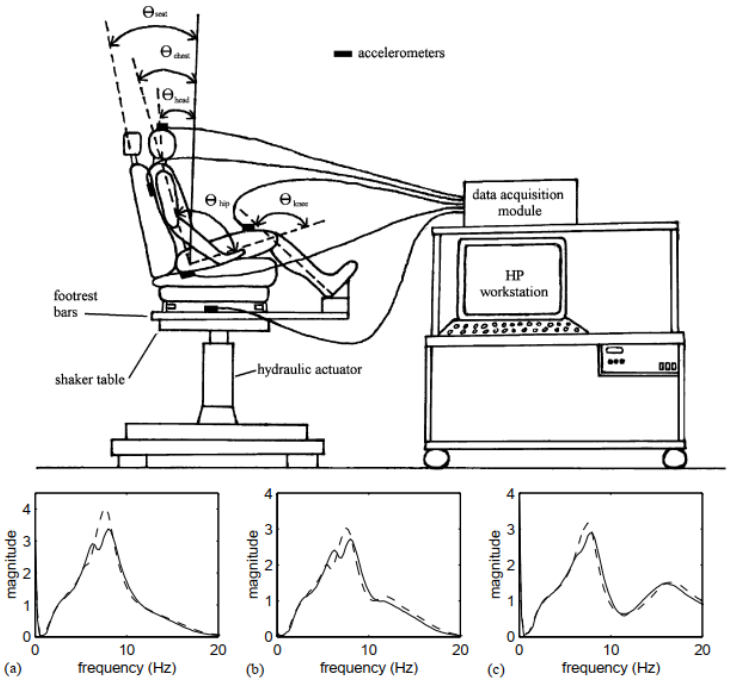

Fig. 104. Experimental set up for finding frequency and frequency graphs for seat bottom structure (a), backrest (b) and thigh (c) (Kim *et al.*, 2003)

Assessment of the vibration characteristics of the human-seat system (Cho and Yoon, 2001) measured the vibrations at the floor, hip, back and head. The system was excited with a random vibration of 1 m/sec^2 rms in vertical direction at the floor with the frequency range between 1 Hz to 25 Hz. Piezoelectric accelerometer type B&K 4504 was used to measure the output from that experiment. The used experimental set up is shown in Fig. 105.

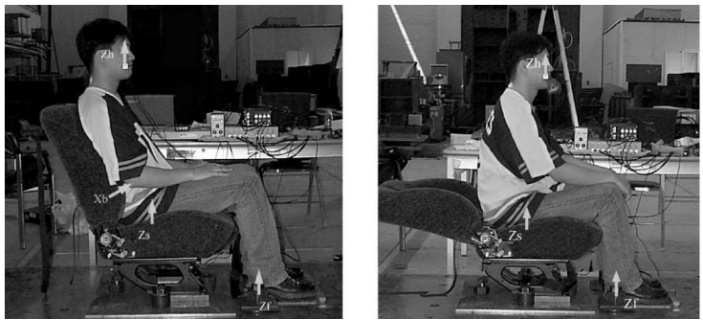

Fig. 105. Experimental set up for the vibration assessment of human-seat system (Cho and Yoon, 2001)

An air cushion seat was examined for the ride quality improvement (Hong *et al.*, 2003), where a capacitive type sensor Xsensor™ was used for analyzing the pressure distributions on the seat cushion and seat backrest as presented in Fig. 106.

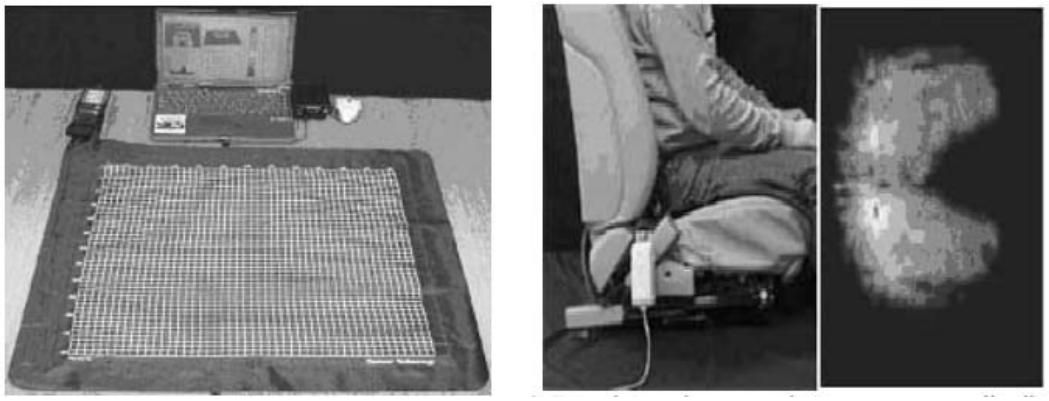

Fig. 106. Experimental set up for measuring the pressure distributions on car seat parts (Hong *et al.*, 2003)

Vehicle vibration based on the road conditions before and after reconstruction was practically tested (Lakušić *et al.*, 2011) by using Opel Vectra B1.8, 1.6V car and mounting the sensors on the wheel holder and chassis of the car. Sensors used for the wheel holder and chassis were Accelerometer Brüel & Kjær type 4508B1 (0.1 Hz – 8 kHz) and Accelerometer Brüel & Kjær type 4508B1 (0.1 Hz – 8 kHz), respectively. Other equipments used were data acquisition unit Brüel & Kjær PULSE, computer for data recording and post analysis, voice and video recorder etc. The analysed data gave the acceleration values at wheel holder and chassis of the vehicle. The outcomes along with the set up are shown in Fig. 107.

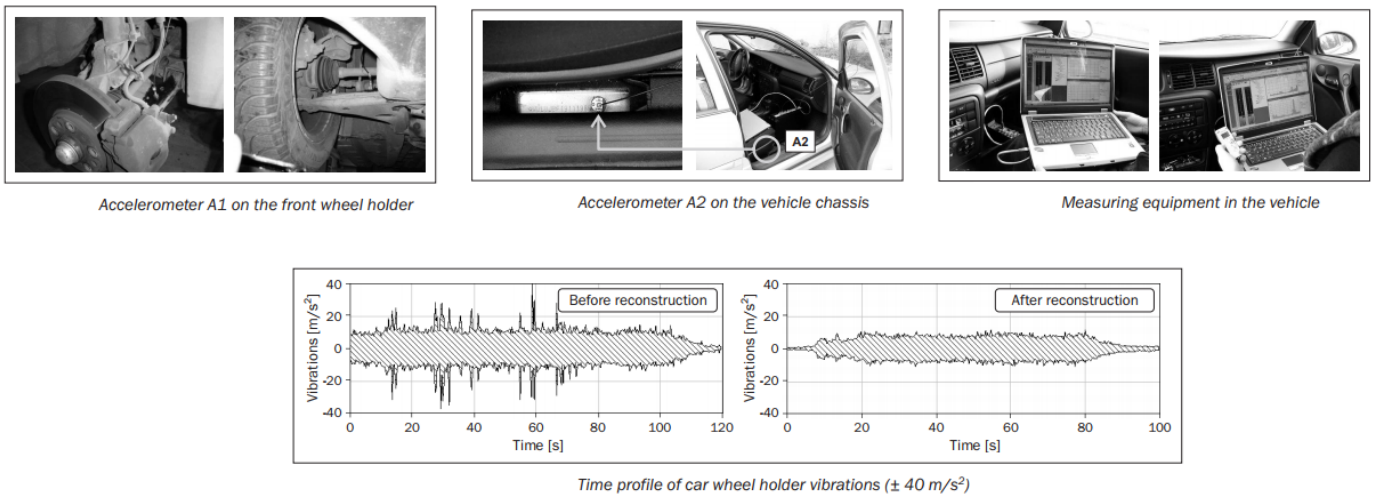

Fig. 107. On road vehicle vibration set up and results (Lakušić *et al.*, 2011)

Virtual real life operating condition of human and car seat was established in the laboratory (Ittianuwat *et al.*, 2014) for judging the vibration transmissions at various locations of the car seat and human body. Random vibration was generated inside a shaker table with a vibration magnitude of 1 m/sec^2 rms with a frequency range of 1 Hz to 100 Hz. Later, a car seat was placed at the top of the shaker table and the vibrations were measured at the seat frame, seat cushion and seat backrest. Tri-axial PCB 356A09 accelerometers were used for measuring the vibration and LMS SCADAS tool was used

for data acquisition. The results showed the vibration levels in the range of 1 Hz to 40 Hz. The comprehensive arrangement of that experimental work is shown in Fig. 108.

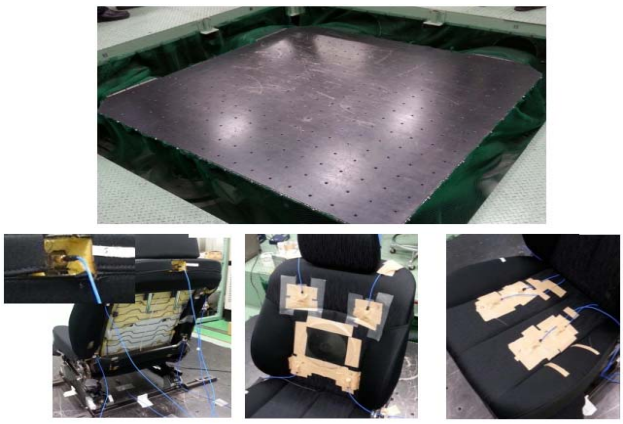

Fig. 108. Virtual vibration testing using shaker table and sensors (Ittianuwat *et al.*, 2014)

In vehicle vibration measurement system using sensors and vibration acquisition system (Stein *et al.*, 2011) followed the European directive 2002/44/EC, which regulates the limit of vibration transmission into human body in the workspace. The experiment was carried out in practical on-road operating environment. The sensors were mounted to the seat and connected to the data acquisition system as represented in Fig. 109. Two number of tri-axial ICP piezoelectric accelerometers were attached to the underside of the seat and a newly designed seat pad compatible to ISO 10326-1:1992 or EN 30326-1, had been placed on the seat surface. PCMCIA data acquisition system along with global positioning system had been used for collecting the necessary data. The speed of the car was maintained to be in between 10 km/hour and 15 km/hour and the acceleration spectrums were recorded.

Fig. 109. Set up for the on-road vibration measurement (Stein *et al.*, 2011)

Study on the transmission of the vibration into car seat backrest was carried out (Qui and Griffin, 2004) using a Ford Focus, Zetec, 2.0L, V817 LAR car operating at a speed between 35 miles/hour and 45 miles/ hour. One object of 80 kg mass and 183 cm height and another object of 70 kg mass and 173 cm height had been placed on the car seat in two different runs. One SAE pad with tri-axial accelerometers was mounted to the car seat backrest and four accelerometers were mounted at the four corners of the car seat base. The SAE pad was in compliance with the international standard ISO 10326-1 and the accelerometers used were the types of Entran EGCSY-240D and EGA-125F-10D/V10/L2M. The results from that experiment showed that the preliminary resonance for fore-aft transmissibility of the seat backrest occurred in between 4 Hz and 5 Hz. The conceptual seat model along with the mounted sensors and result plots are presented in Fig. 110.

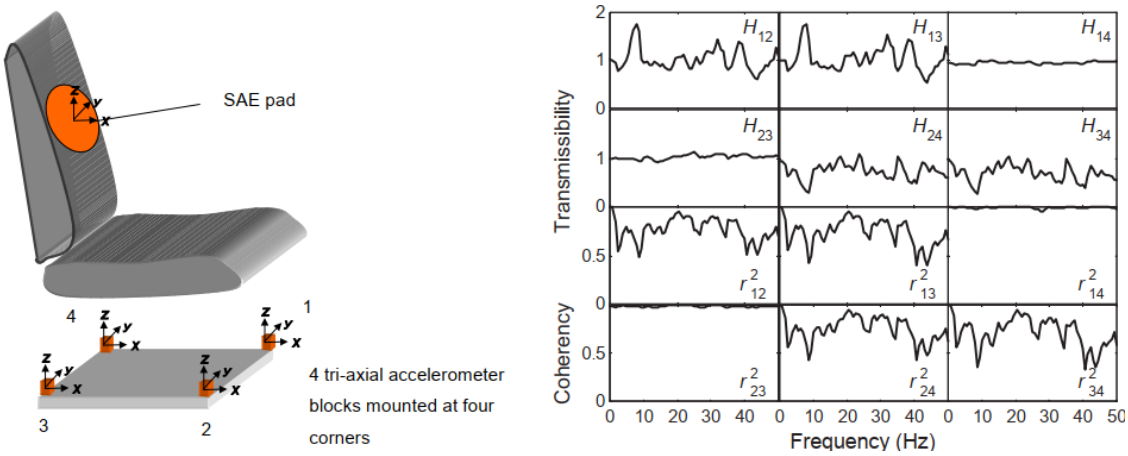

Fig. 110. Accelerometer mounted on car seat and the frequency levels (Qui and Griffin, 2004)

A vibration model for the human body and car seat was established in the laboratory to understand the benefit of modal dynamic analysis (Ruetzel, and Woelfel, 2005) where a dummy moving mass, named MEMOSIK was placed on the top of seat cushion and sensors were mounted at different locations of the seat. Transfer functions of the seat and

dummy model were evaluated. Fig. 111 is showing the set-up of the experiment and extracted results.

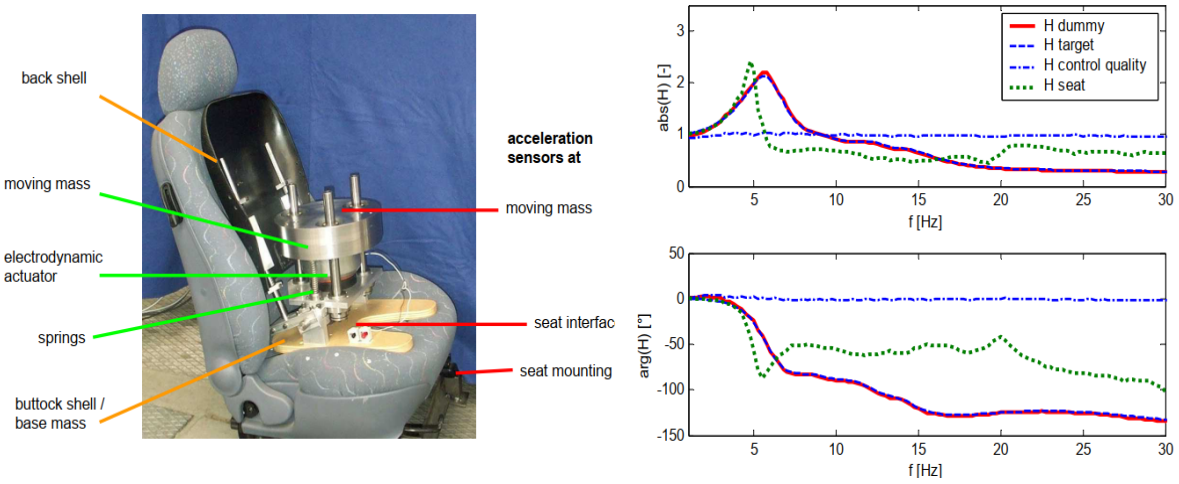

Fig. 111. Laboratory set up for human body vibration and the evaluated transfer functions (Ruetzel, and Woelfel, 2005)

Resonance of the human body cause of vertical vibration was investigated (Verver, 2004) in the laboratory by using human object, standard car seat and shaker platform as shown in Fig. 112. The human body was placed on a car seat and the entire human-seat assembly was positioned on a shaker platform which was excited by vertical vibration with variable acceleration. The rms magnitude of the used accelerations was 2.35 m/s^2. The vibration levels were measured at head and pelvis using the linear accelerometer Kistler 3803A/2G. The same experimental process was repeated using a rigid seat instead of standard car seat. That study concluded that no resonance frequency was found below 15 Hz in the car-human system.

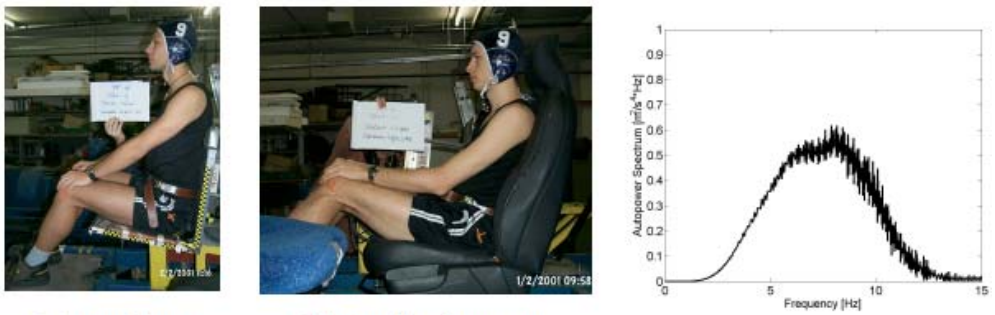

(a) Rigid seat *(b) Standard car seat*

Fig. 112. Laboratory set up for the resonance of human body and power spectral density (Verver, 2004)

From the past experimental works carried out on vibration measurement inside the human-car seat system, it is clear that the sensor and data acquisition system are the mandatory components for any kind of vibration measuring system. Depending on the aspect of a specific research work, different types of sensors and acquisition systems can be selected.

Mounting the sensors to the human body and car seat as per the vibration measuring guidelines, is also a vital factor while measuring the frequency, displacement or acceleration. Also, usage of multi-input data acquisition system in vibration measurement is advantageous, as it can acquire multiple outputs together from a single run, hence, time saving and accurate.

6.2. Vibration Measuring Techniques and Instruments

Vibration is an integral part of the dynamic industrial machines and accordingly, attempt to remove the unwanted effects of the vibration has become an essential task for the engineers and scientists. Vibration occurs cause of dynamic nature of a system and during the design process of any kind of machinery system, the vibration measurement using proper method has become one of the primary aspects in the modern industries. Vibration can be monitored by measuring frequency, acceleration or displacement and the level of

vibration can be quantified by peak, average or root mean square (rms) value. A typical vibration curve has been sketched in Fig. 113, which explains peak, average and root mean square values of vibration.

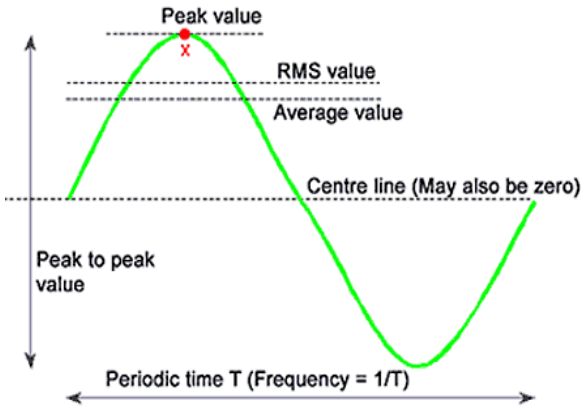

Fig. 113. Peak, average and rms values of vibration

Peak value signifies the maximum possible vibration level in the time period accounted, while the average value shows the mean of all the vibration magnitudes over the selected period of time. The rms value is the root mean square of all the vibration magnitudes, which takes into account both the time history and energy function.

The basic principles of any vibration measuring system are collecting the signal using sensor and signal conditioning system followed by passing the signal through an analogue filter, converting the analogue data to digital data, carrying out frequency analysis through digital filtering or fast Fourier transform, measuring the peak, average or rms data and post-processing the result to get desired chat or graph. The fundamentals of the vibration measurement procedure are explained with diagrams in Fig. 114.

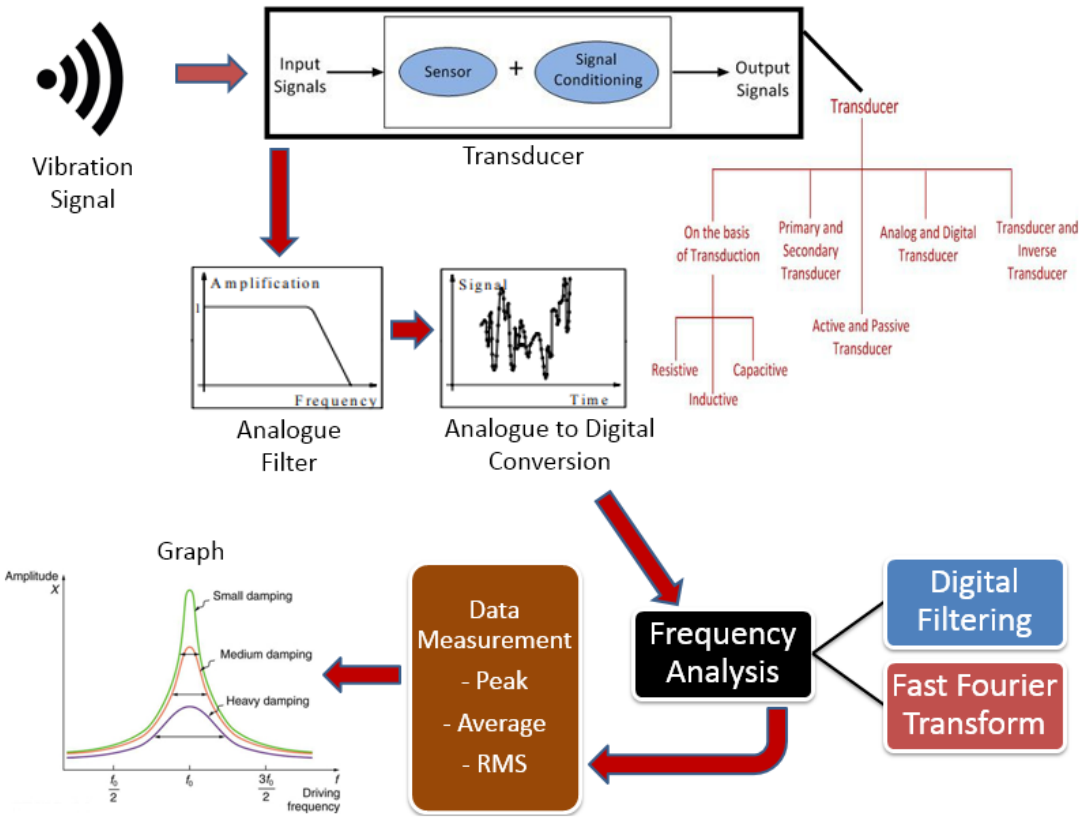

Fig. 114. Flow chart showing the processes involved in vibration measurement using digital sensor system

Accelerometer is the most common type of transducer used in the industries, inside of which an internal mass is connected to a piezoelectric cell through a spring element. Velocity transducer is used mainly for the rotating components in the industry, which got moving parts inside. Generally, velocity transducers are used for the measurement processes, which require less accuracy. Displacement transducer is made of internal movable and fixed parts and can directly be in touch with the moving or rotating object to measure vibration. Accelerometer and velocity transducer are designed to be mounted to the non-moving portion of a system, while the displacement transducer can be mounted to the moving object by establishing mating condition. Different types of transducers are presented in Fig. 115.

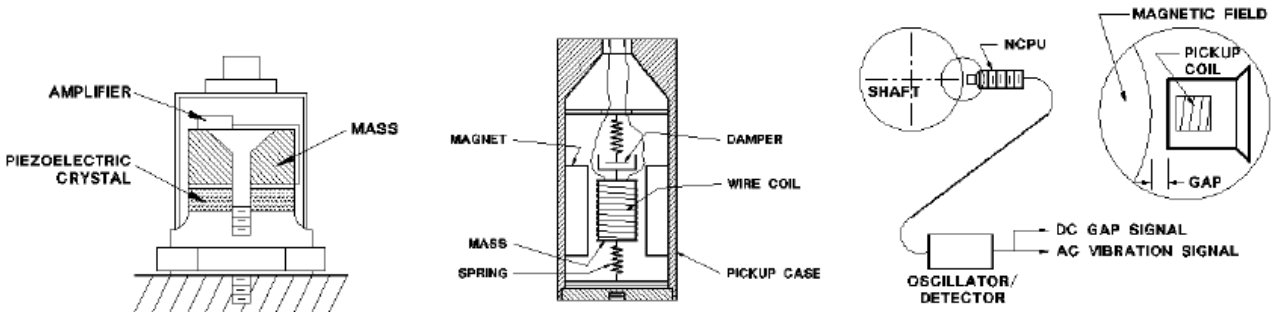

Fig. 115. Typical transducer diagrams, left- accelerometer, middle- velocity transducer, right- displacement transducer (Reliability Direct Store, 2018)

Modern industries have been evolved to develop the sensors with advanced technologies, which give the flexibility to the vibration measurement process to use portable, multiple output or hybrid instruments. Some of the technically advanced sensors have the in-built digital read out modules, which omit the necessity of robust data processing system and can be used for in-house experimental applications.

HAV Control Limited introduced HAVi Monitor (Hand Arm Vibration Indicator), a portable vibration measuring instrument, which can be used without any data acquisition system. Another three channel sensor with tri-axial accelerometer, Larson Davis HVM100 hand arm vibration meter, has been introduced by the same organization. Larson Davis HVM100 has been designed in compliance with ISO 8041 and got the in-built set up for measuring whole body vibration.

Pass^{TM} brought into the market a device named Extech SDL800 Vibration Meter, capable of measuring acceleration, velocity and displacement for the frequency range of 10 Hz to 1 kHz. Another instrument, Extech VB300 3 Axis G Force USB Datalogger by Pass^{TM}, is available in the market which can record the vibration data for a defined period of time in all the three axial directions.

Vibration measuring instrument with a smart screen, Tpi.9070 Smart Vibration Meter, has been introduced by Zoro, which can display the vibration signals on a screen with

colours. A highly sensitive instrument from Test Meter & Test Equipment Experts, named Tenmars ST-140 Vibration Meter is existing in the industry for measuring acceleration, displacement and velocity.

Fig. 116. Different kinds of portable vibration measuring systems for in-house application

Different kinds of portable and in-house vibration measuring units have been captured in Fig. 116.

Some organizations are solely dedicated to the vibration measurement systems with massive infrastructure to provide solutions for the vibration, acoustic and noise related problems. Usually these organizations use robust instruments with the facility of collecting multi-output data at a single point of time. m+p International is one of the reputed organizations and a pioneers for measuring vibration and noise inside various sorts of machineries in different industries. Another organization named Element, have been playing leading role for providing solutions in the fields of vibration and noise

control. Most of the third party companies have the provisions to give solutions for both the in-house and on-road systems. Few of the third party vibration measurement facilities are displayed in Fig. 117.

Fig. 117. Third party testing facilities, top - m+p International, bottom - Element

After the review of the past research works on vibration measurement and exploration of latest available technologies and instruments for vibration testing, it can be concluded that the vibration measurement can be accomplished at in-house laboratory, real-world on-road environment or third party facility. Each of the testing environments has got advantages and disadvantages on its own and summarized in Table 34.

Table 34. Advantages and disadvantages of different testing environments

	In-house lab testing	Practical/ on-road vehicle testing	Testing and measurement through third party facilities
Advantage	a. Set up can be used in for further development	a. Real life scenario b. No burden of set up c. Quick process d. Very accurate e. Can be used for wide variety of systems f. The process can be repeated many times as needed g. Very handy h. Less expensive	a. Advice from the 3rd party experts B. No burden of set up C. Quick process Accurate
Disadvantage	a. Less accurate b. Expensive c. Car seat mounting will be difficult d. Vibration platform will be just	a. More than one person should be involved during the process	a. Expensive

	In-house lab testing	Practical/ on-road vehicle testing	Testing and measurement through third party facilities
	a miniature of the real platform e. Time consuming		

6.3. Collection of Test Data

Few organizations expertise in the field of vibration measurement, had been contacted to obtain test results suitable for this simulation study.

m+p international is a Germany based business founded in 1980 and a worldwide provider of vibration related precise test and measurement solutions. m+p international agreed to help by providing the test data in brief format for a 50^{th} percentile male human body while driving, without violating their privacy policy and codes of conduct.

From the testing data, vertical accelerations with respect to time in micro-mm/sec² format and power spectrum densities with respect to frequency in logarithm of acceleration rms format were obtained. Along with collecting the testing data, efforts had been made to understand the details about the testing equipments, operating environment, mounting of the sensors, data acquisition tool and post-processing system. Based on the testing data obtained from m+p international, all the necessary informations are outlined in this section.

6.3.1. Instruments and Tools used

Information obtained from m+p international regarding the instruments and acquisition system used during the data collection, have been detailed in this section.

6.3.1.1. Measurement Device

NI 9234 Module with CompactDAQ Chassis was used as vibration measuring instrument, which got the capability of being connected to laptop through USB, Ethernet and Wi-Fi. An image of the measuring system NI 9234 Module has been captured from the database of National Instruments and is shown in Fig. 118.

Fig. 118. Vibration measuring instrument NI 9234 Module with CompactDAQ Chassis

The specifications of this product bundle have been taken from National Instrument's (NI) database and given here:

a. Measurement module and single space NI CompactDAQ chassis.
b. USB, Ethernet cable, Wi-Fi connection capability.
c. Optimized sampling rate= ±5 V input and 51.2 kS/s per channel.
d. 102 dB dynamic scale and 24-bit resolution.
e. IEPE signal monitoring, the range is from 0 or 2 mA.
f. AC/DC coupling capability with the AC coupling for 0.5 Hz.

6.3.1.2. Transducers

Transducer used for measurement was Dytran 3055 as displayed in Fig. 119. From the database of Dytran Instruments Inc, the specifications of the transducer have been summarized here:

a. Single axis IEPE.
b. Sensitivity from 10 to 500 mV/g.
c. TEDS capabilities.
d. 10–32 radial connector and 10–32 stud mounting capabilities.
e. Low noise JFET electronics.
f. Reliable performance in high humidity and dirty environments

Fig. 119. Vibration measuring transducer Dytran 3055

6.3.1.3. Data Processing System

The signal was processed through the "m+p Analyser", a strong and interactive software tool developed by m+p international. A screenshot of typical data signal displayed in "m+p Analyser" tool has been captured in Fig. 120.

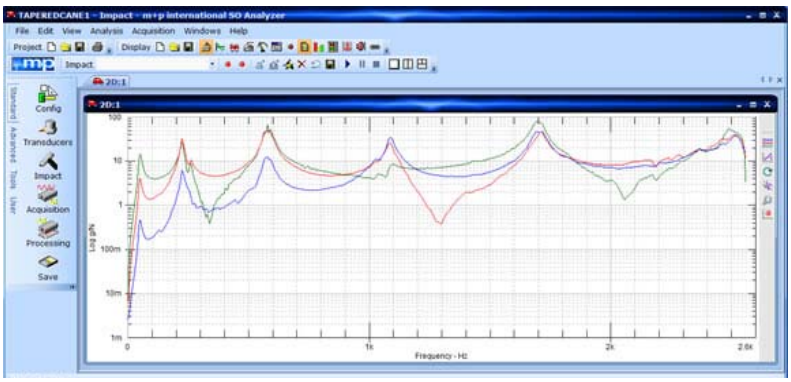

Fig. 120. Typical data signal displayed in "m+p Analyser" software tool

6.3.2. Measurement procedure

A standard hatchback car with a male human driver of 78 kg mass in seated condition was considered in the real life on-road operating condition. There was no visible sign of rough road condition and the driving speed was maintained at 30-35 miles/ hour for around 60 seconds. To have the maximised effect of vibration on the collected data, maximum gear system used in the car was third gear.

The transducer Dytran 3055 was mounted to the various locations of the car seat and the male human driver with the help of adhesive plasters and the cable of the transducer was connected to the vibration measuring instrument NI 9234 module. The USB cable from the NI module was connected to a standard laptop where the signal was processed through "m+p Analyser" software tool. For handling the NI module and recording the data in laptop, an assisting person was sitting beside the driver.

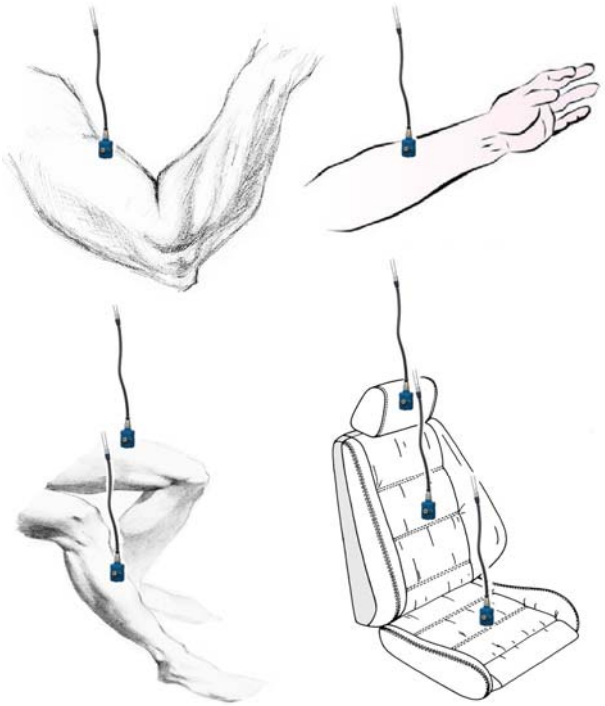

Fig. 121. Transducer mounting method for measuring vibration in vertical direction at various locations of human body and car seat

The aim of the measurement was to obtain the vibration related parameters in the vertical direction. So, the Dytran sensor was mounted at different points of human body and car seat in such a way that the axis of the sensor would always be in vertical direction. Fig. 121 is showing the ways of mounting the sensor at different locations of human body and car seat.

Fig. 122 shows the sample test set up of the driver human body, assistant body, transducer, measuring instrument and laptop with analyser.

Fig. 122. Sample test set up

6.3.3. Data received from Testing

Measurement of acceleration is the most effective way to assess the level of vibration as the acceleration of a dynamic object is one of the primary functions of the effect of vibration. The acceleration magnitude can be quantified by average, peak and rms values, though, the most common value used for measuring acceleration is the rms one, which is usually denoted as G_{rms}.

From the post processing system of vibration measuring unit, G_{rms} with respect to time data can be obtained, though these data set don't give idea about the frequency. Now a days, the modern industries are focusing on the rms value of the acceleration based on the

frequency domain, which calculates the Log of the magnitude value in terms of G_{rms}^2/Hz with respect to frequency, known as power spectrum density. Relationship between G_{rms} and power spectrum density can be described by Parseval's theorem. Equation 6.1 shows the formulation for transferring the data from time domain to the frequency domain using Parseval's theorem.

$$\int_{-\infty}^{\infty} h^2(t)\,dt = \int_{-\infty}^{\infty} \left(|H(f)|\right)^2 df \qquad \text{(Eq. 6.1)}$$

Where,
h(t) = Time dependent function
H(f) = Frequency dependent function

Test data obtained from m+p international, were containing the acceleration vs time and power spectrum density vs frequency plots for various locations of human body and car seat.

The raw testing data were received in .SOT format and using the temporary version of "m+p Analyser" software tool, the information required for this research work had been extracted. The raw vibration data plots from .SOT files are shown in Fig. 123, Fig. 124, Fig. 125, Fig. 126, Fig. 127, Fig. 128, Fig. 129, Fig. 130, Fig. 131 and Fig. 132.

6.3.3.1. Vibration data for Human Head

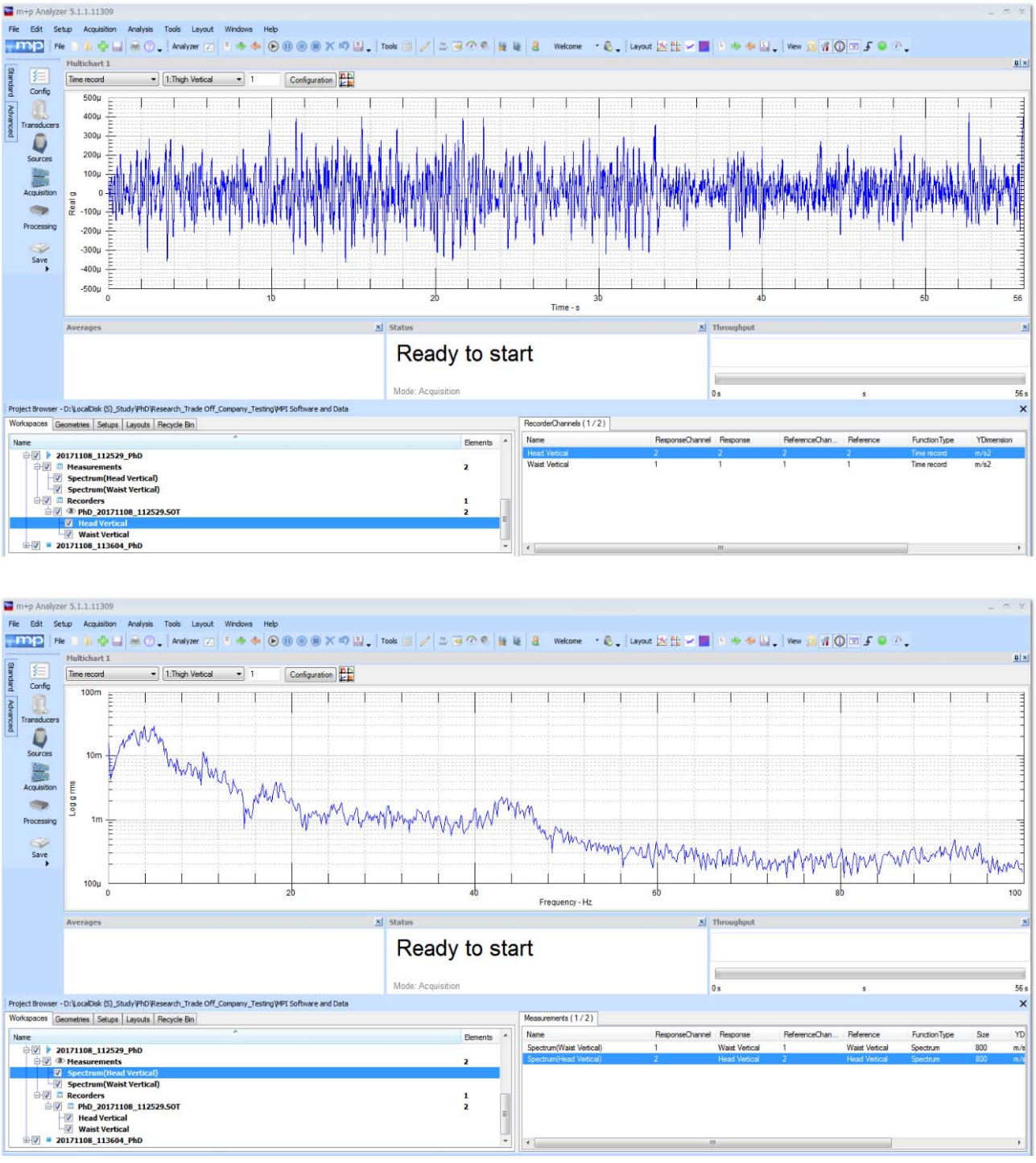

Fig. 123. Vibration data for human head (Top- acceleration vs time, bottom- power spectrum density vs frequency)

6.3.3.2. Vibration data for Human Chest

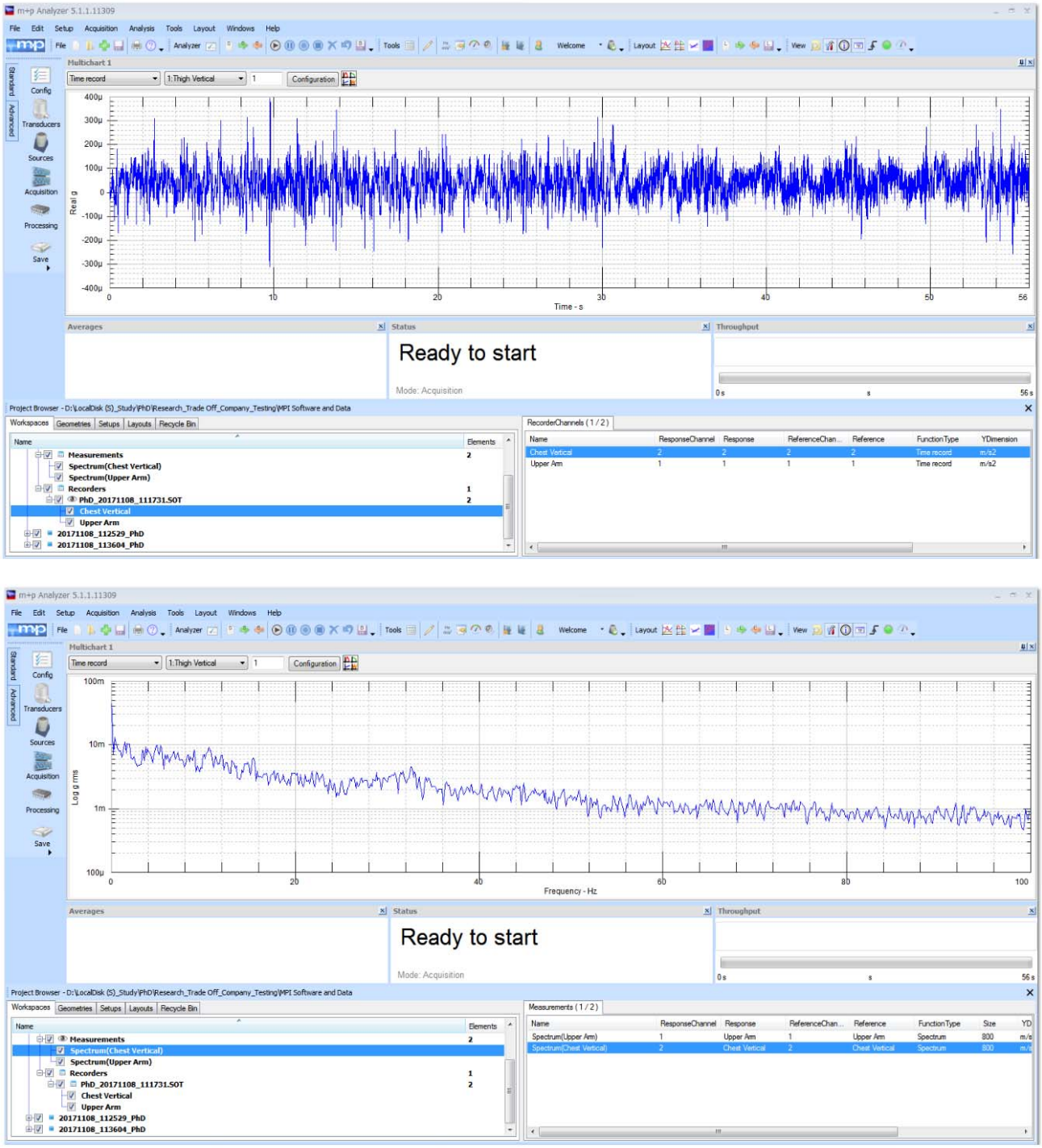

Fig. 124. Vibration data for human chest (Top- acceleration vs time, bottom- power spectrum density vs frequency)

6.3.3.3. Vibration data for Human Waist

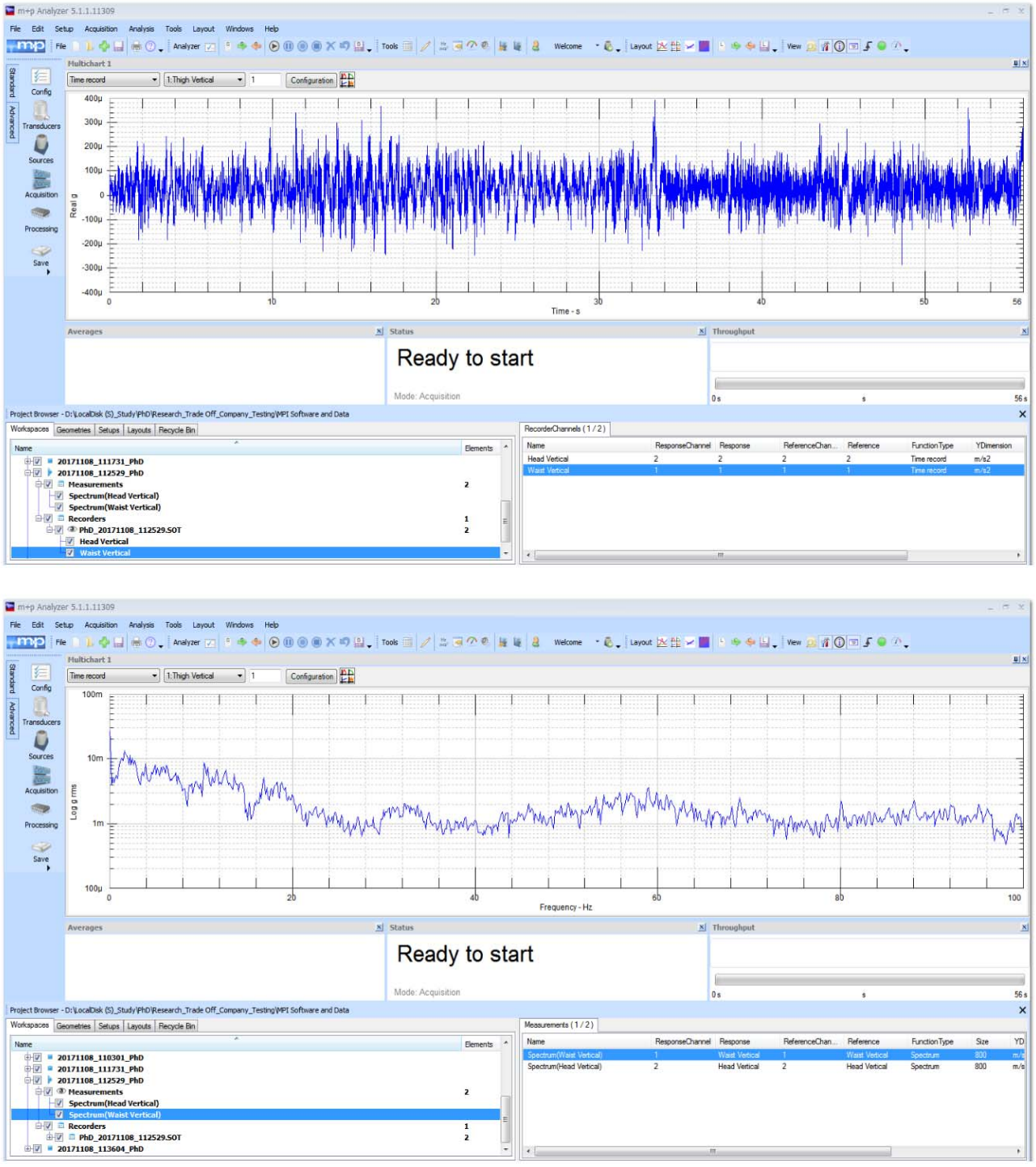

Fig. 125. Vibration data for human waist (Top- acceleration vs time, bottom- power spectrum density vs frequency)

6.3.3.4. Vibration data for Human Upper Arm

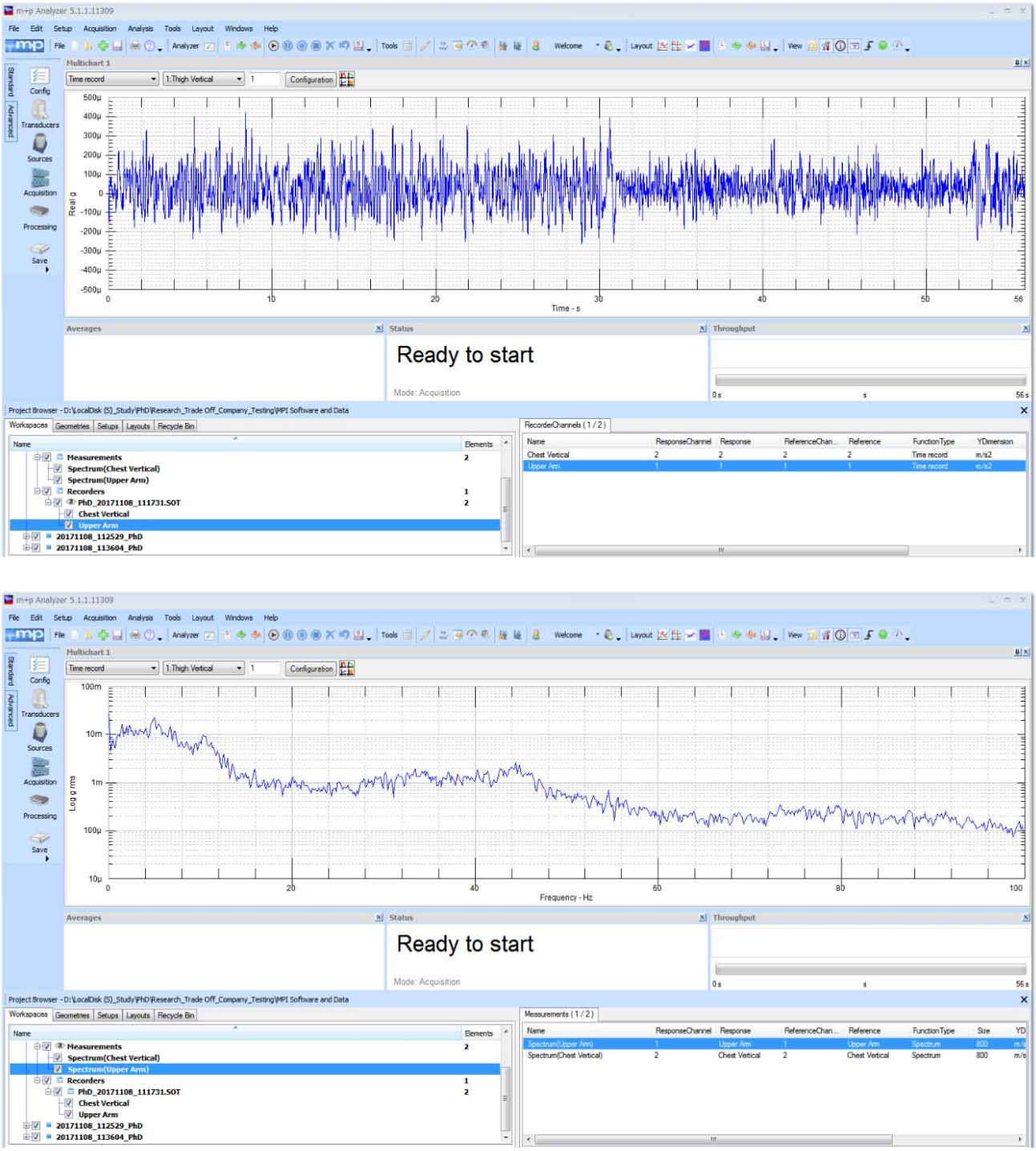

Fig. 126. Vibration data for human upper arm (Top- acceleration vs time, bottom- power spectrum density vs frequency)

6.3.3.5. Vibration data for Human Lower Arm

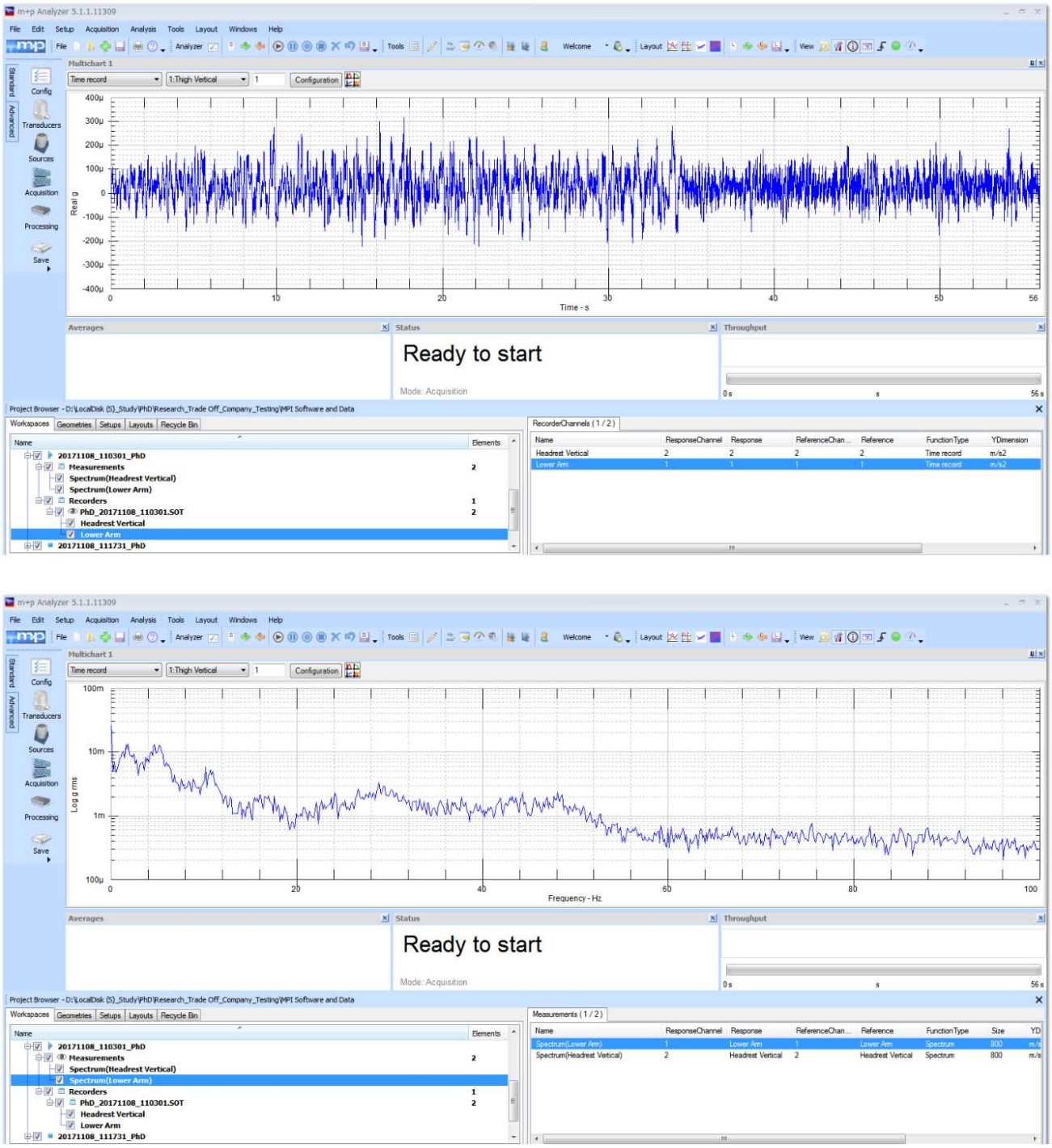

Fig. 127. Vibration data for human lower arm (Top- acceleration vs time, bottom- power spectrum density vs frequency)

6.3.3.6. Vibration data for Human Thigh

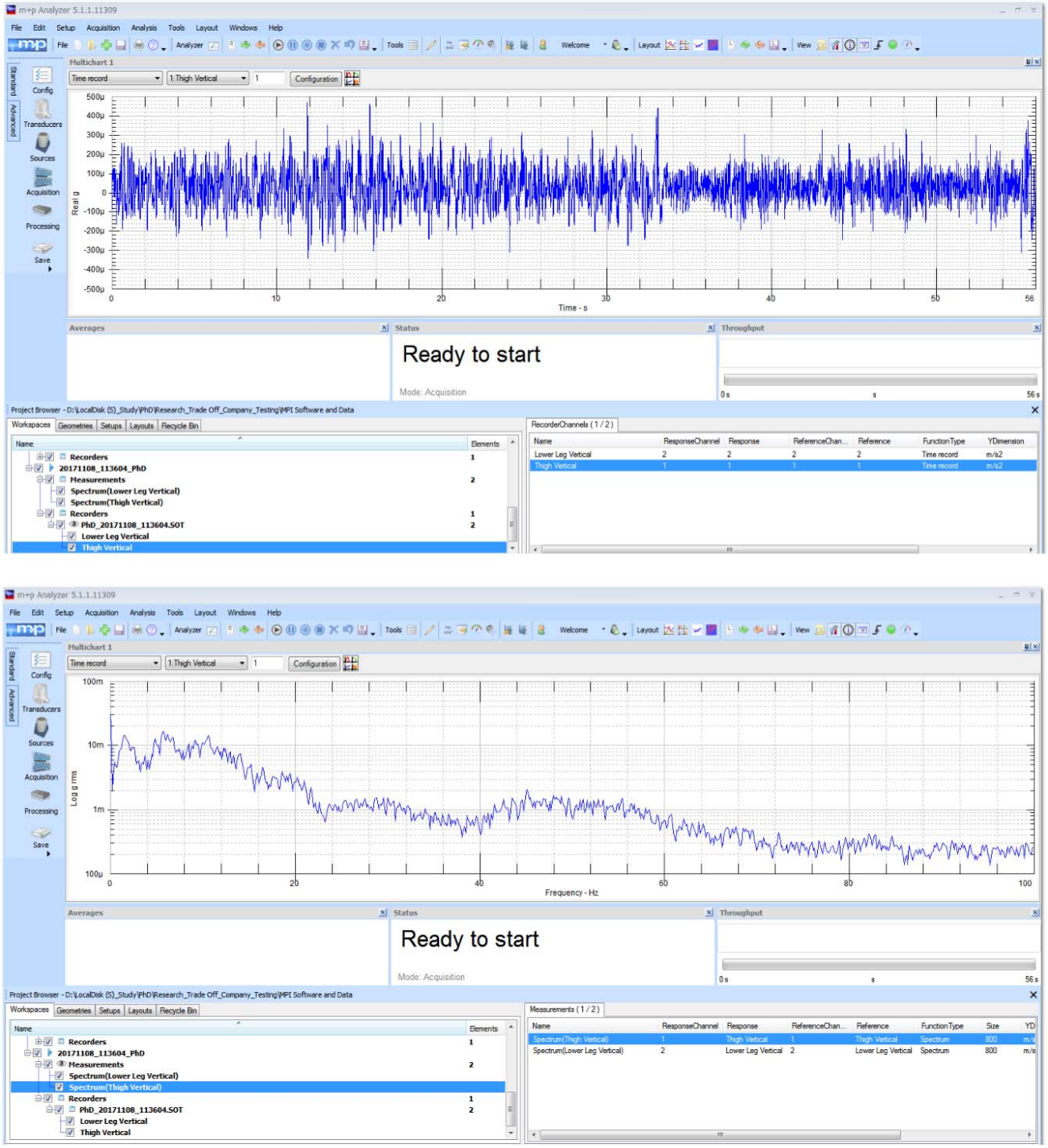

Fig. 128. Vibration data for human thigh (Top- acceleration vs time, bottom- power spectrum density vs frequency)

6.3.3.7. Vibration data for Human Leg

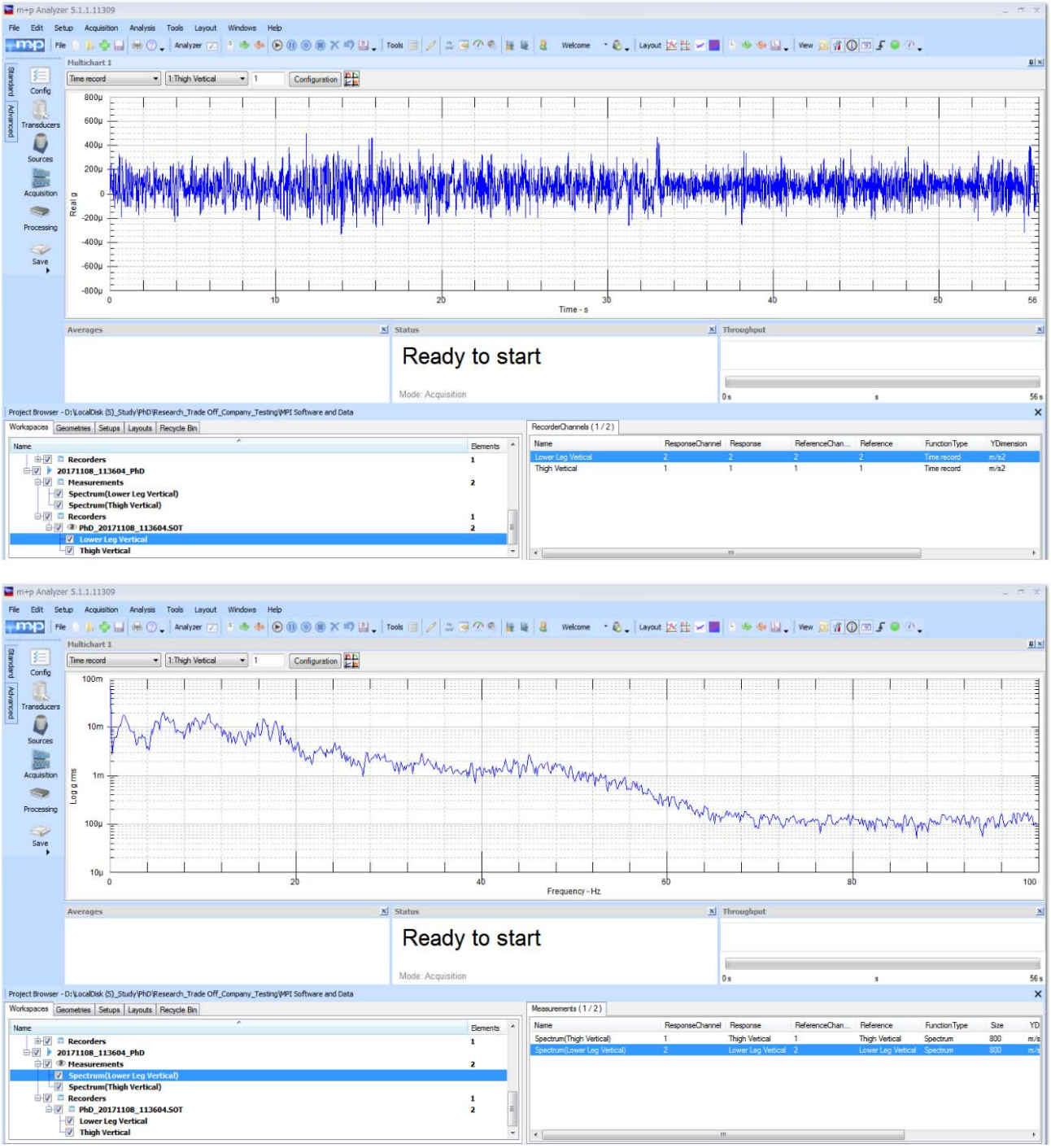

Fig. 129. Vibration data for human leg (Top- acceleration vs time, bottom- power spectrum density vs frequency)

6.3.3.8. Vibration data for Seat Headrest

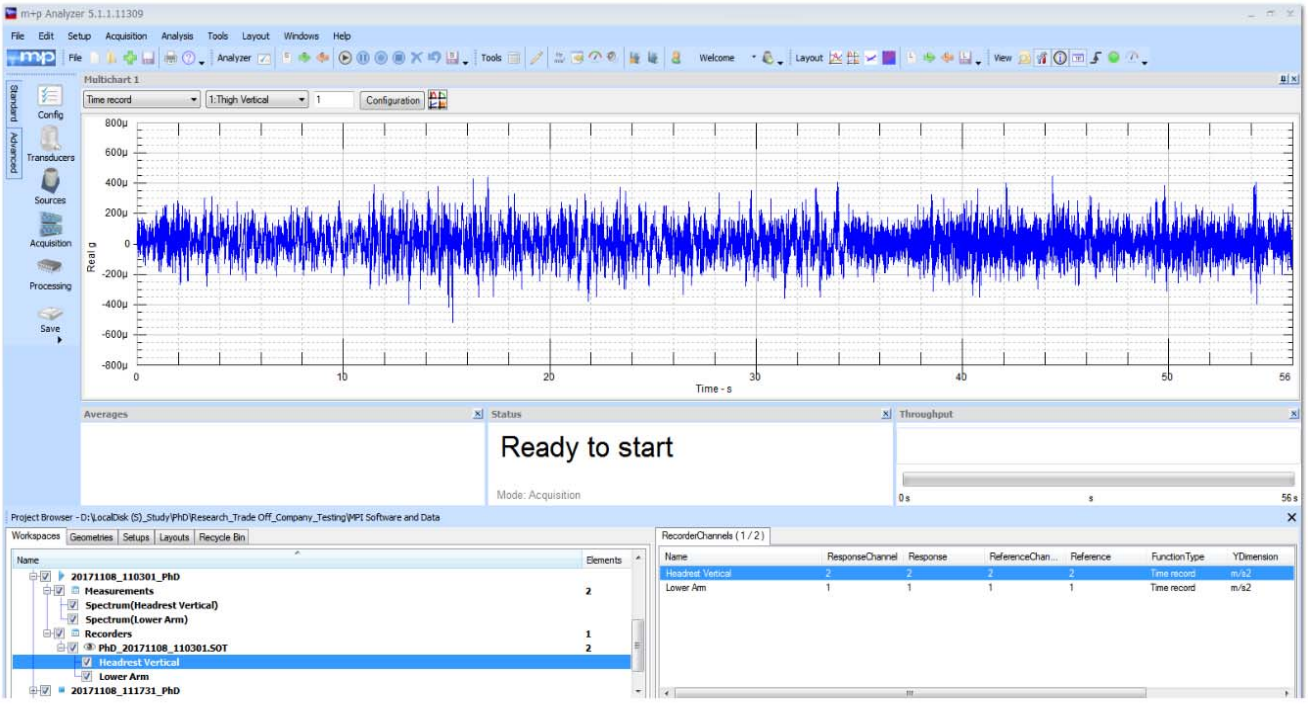

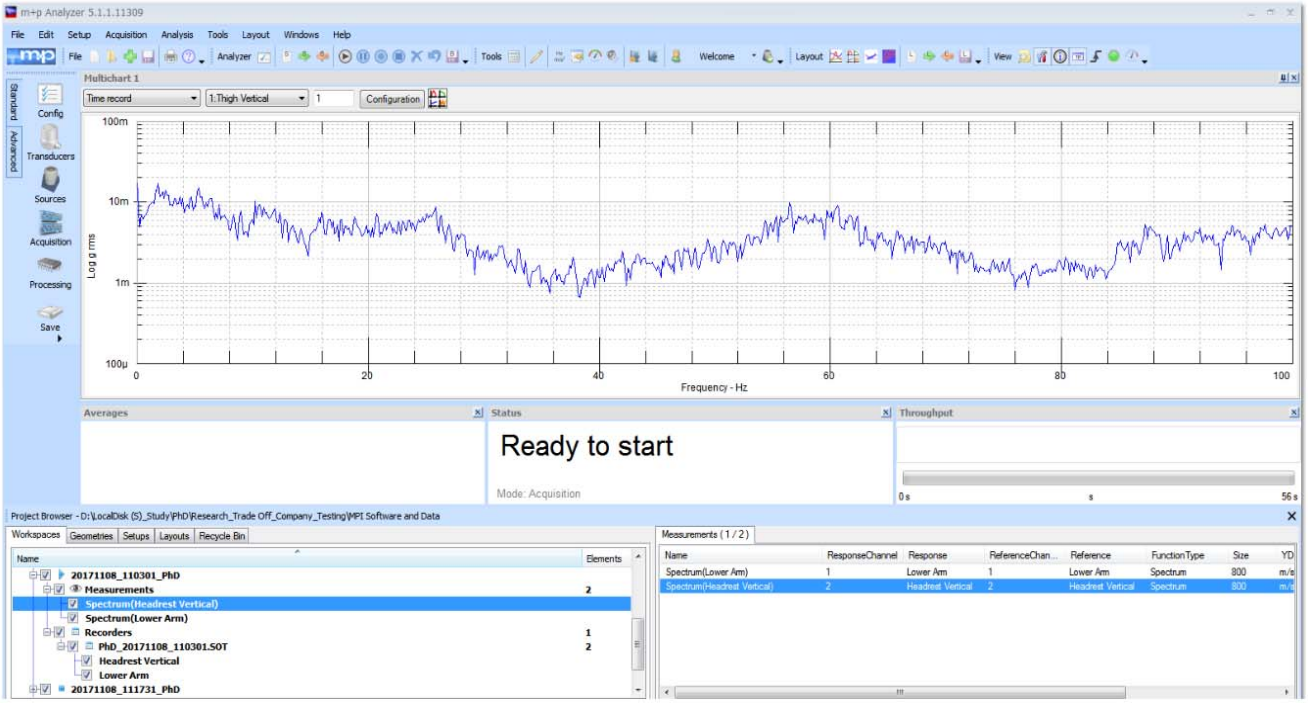

Fig. 130. Vibration data for seat headrest (Top- acceleration vs time, bottom- power spectrum density vs frequency)

6.3.3.9. Vibration data for Seat Backrest

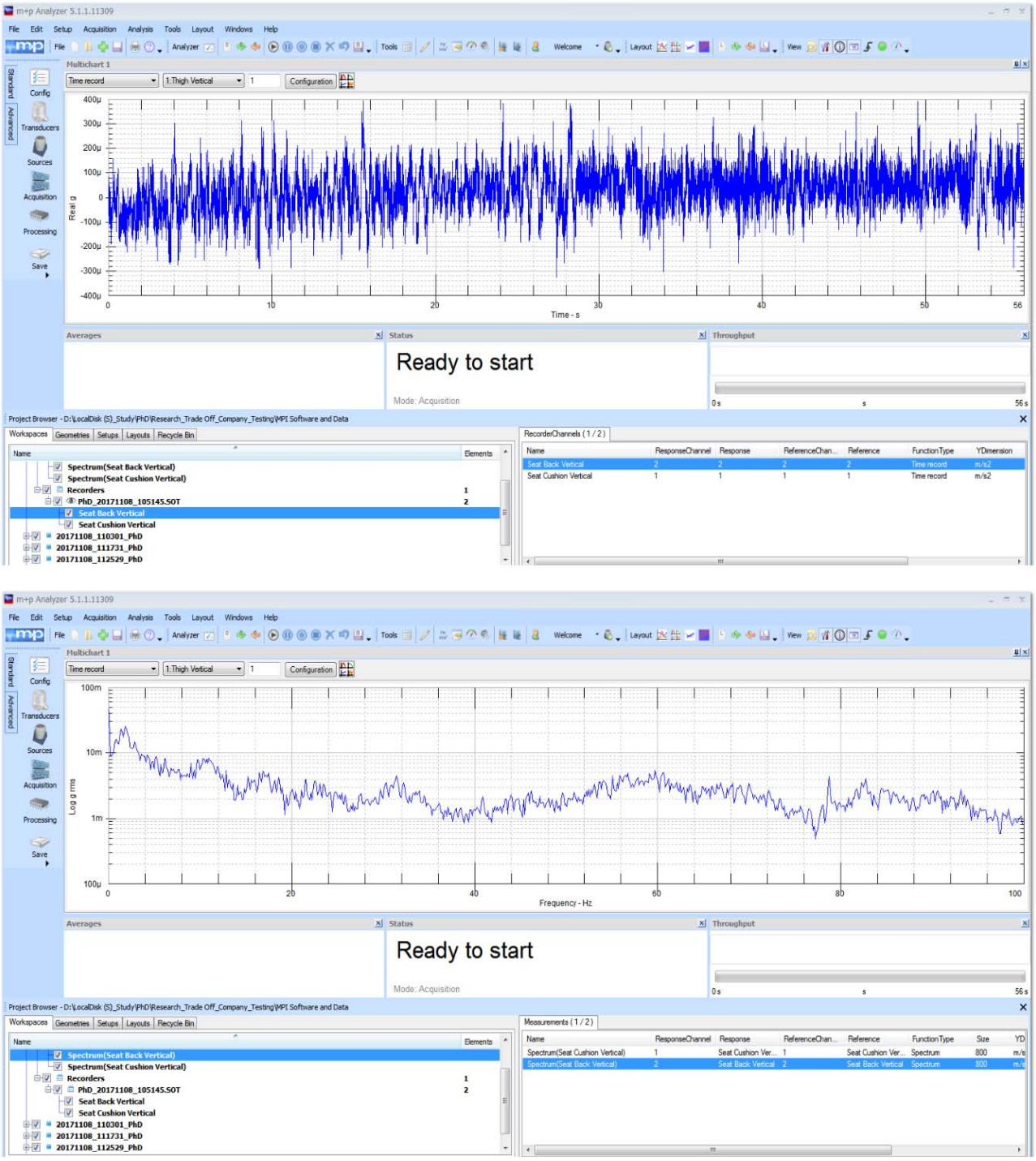

Fig. 131. Vibration data for seat backrest (Top- acceleration vs time, bottom- power spectrum density vs frequency)

6.3.3.10. Vibration data for Seat Cushion

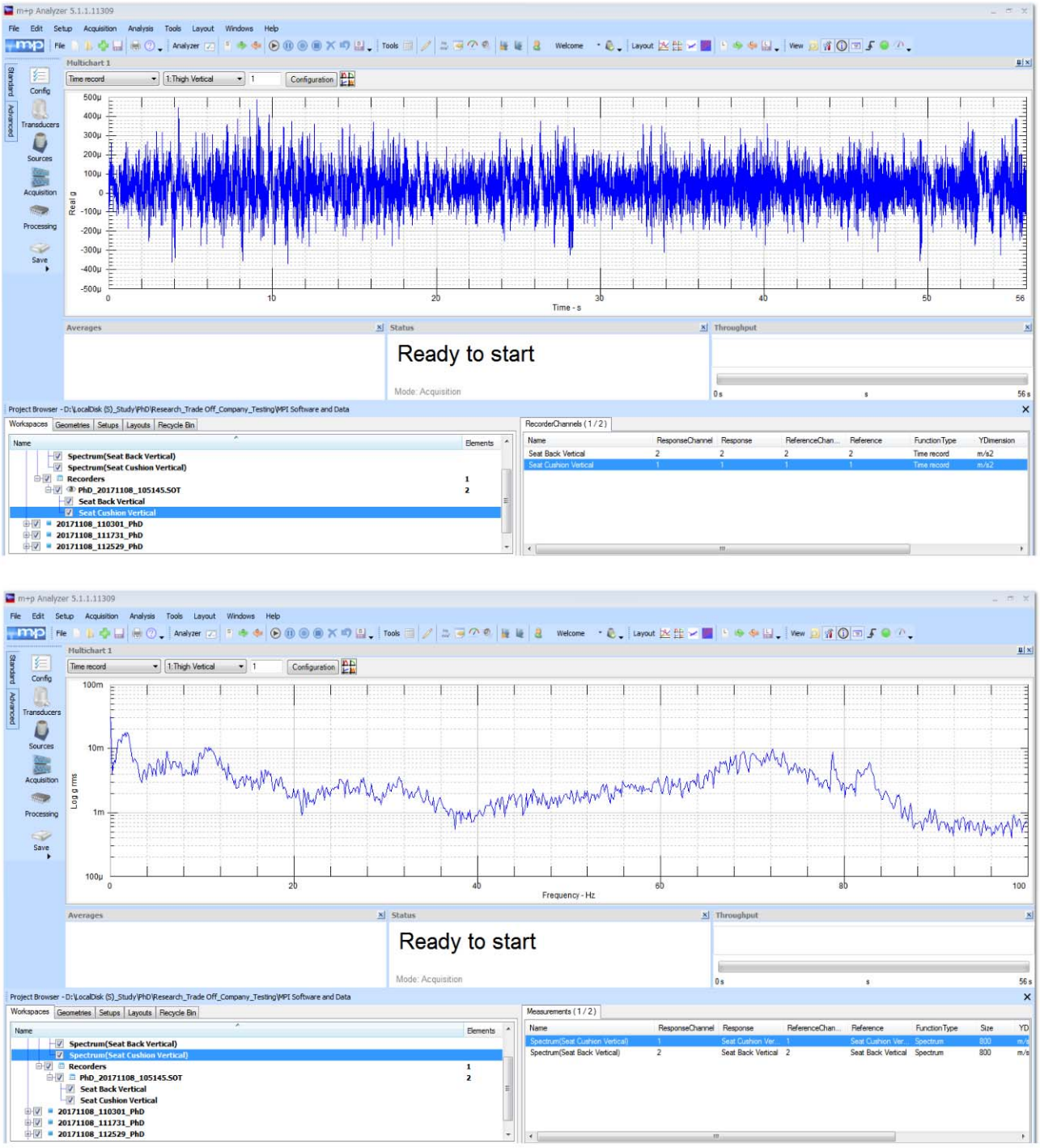

Fig. 132. Vibration data for seat cushion (Top- acceleration vs time, bottom- power spectrum density vs frequency)

6.3.4. Simplified Data Extracted from Raw Test Data

From the simulation results acceleration vs time, displacement vs time and frequency vs time data were received for initial 10 seconds of car operating condition. From the testing data acceleration vs time and power spectrum density vs frequency data had been obtained for initial 60 seconds of car operating condition.

Power spectral data can more clearly emphasize the vibration features, though there is no straight way to transfer the acceleration vs time data to the power spectral vs time data or vice versa. Hence, to make the comparison between simulation results and test data easier, the raw acceleration vs time data have been curtailed to initial 10 seconds and simplified using MS Excel tool. Fig. 133, Fig. 134, Fig. 135, Fig. 136, Fig. 137, Fig. 138, Fig. 139, Fig. 140, Fig. 141 and Fig. 142 are showing the simplified vertical acceleration vs time plots for initial 10 seconds for various portions of human body and car seat.

6.3.4.1. Simplified test data for Human Head

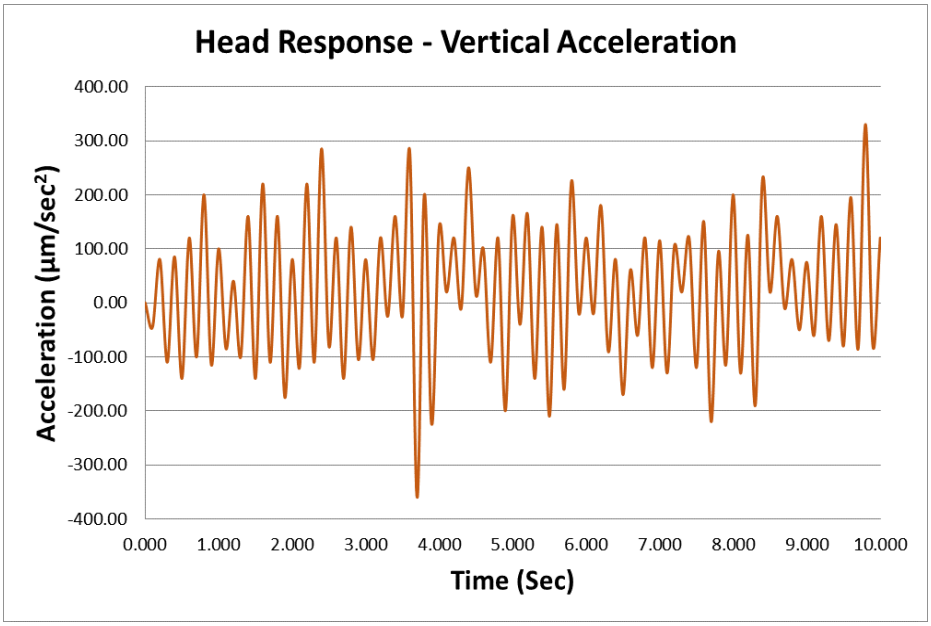

Fig. 133. Simplified test data for human head

6.3.4.2. Simplified test data for Human Chest

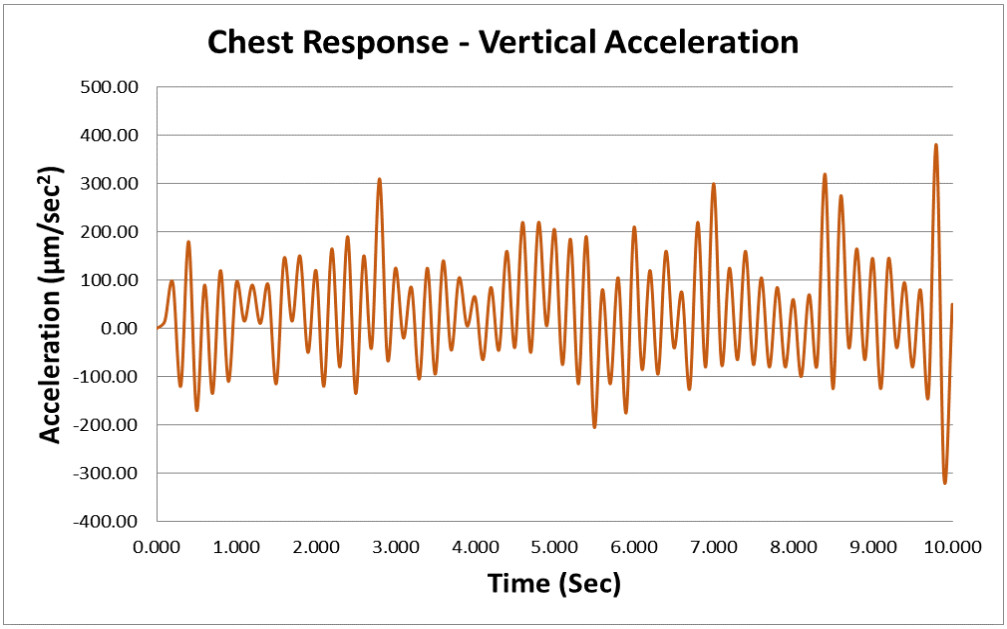

Fig. 134. Simplified test data for human chest

6.3.4.3. Simplified test data for Human Waist

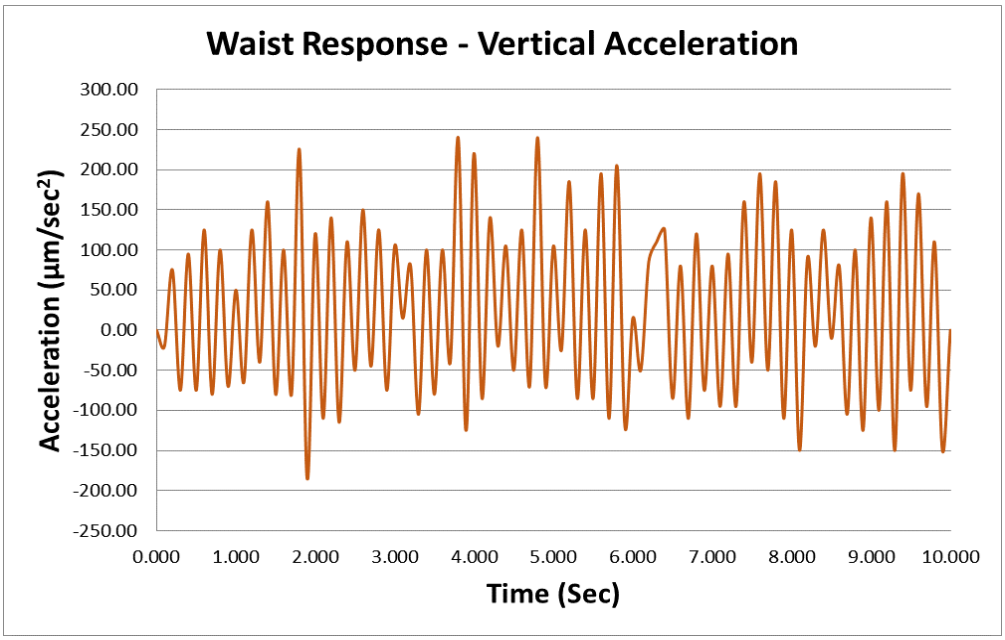

Fig. 135. Simplified test data for human waist

6.3.4.4. Simplified test data for Human Upper Arm

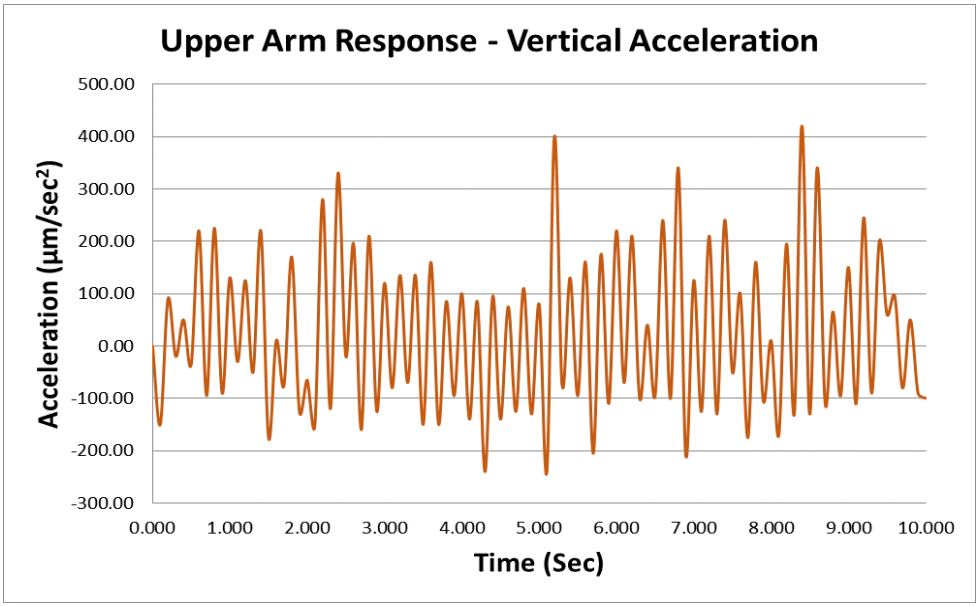

Fig. 136. Simplified test data for human upper arm

6.3.4.5. Simplified test data for Human Lower Arm

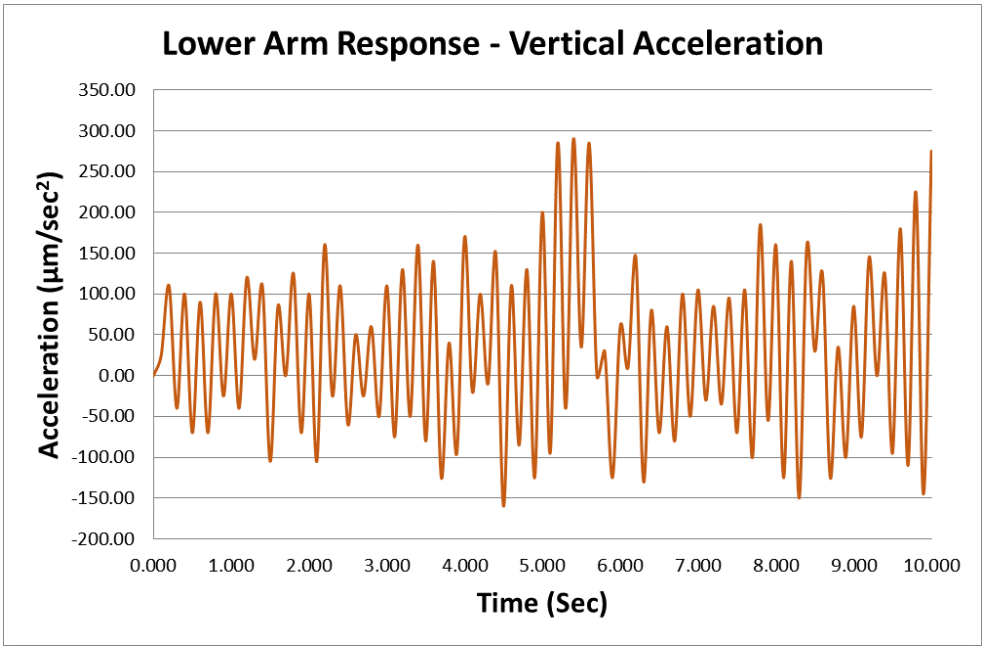

Fig. 137. Simplified test data for human lower arm

6.3.4.6. Simplified test data for Human Thigh

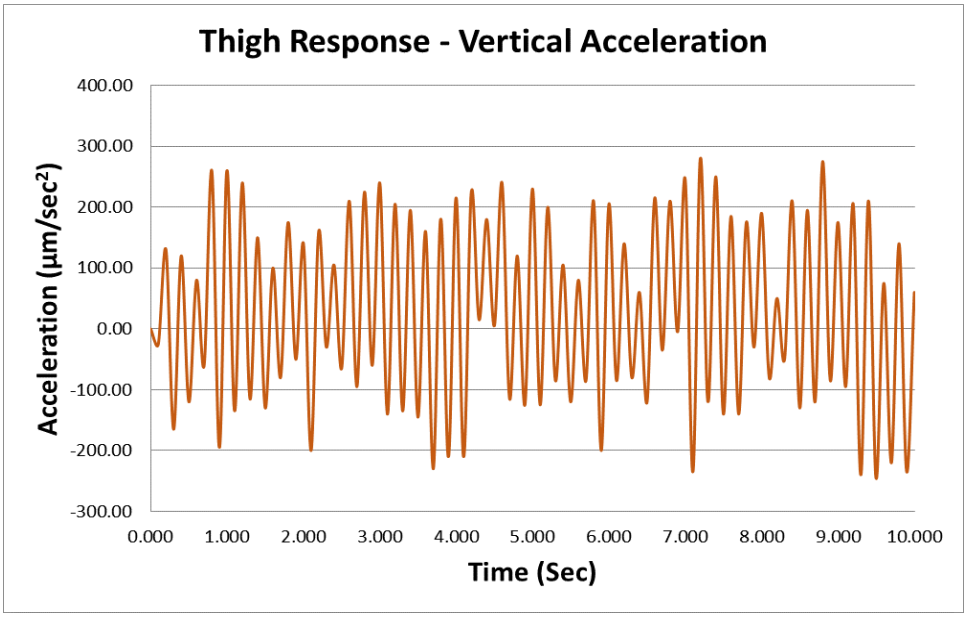

Fig. 138. Simplified test data for human thigh

6.3.4.7. Simplified test data for Human Leg

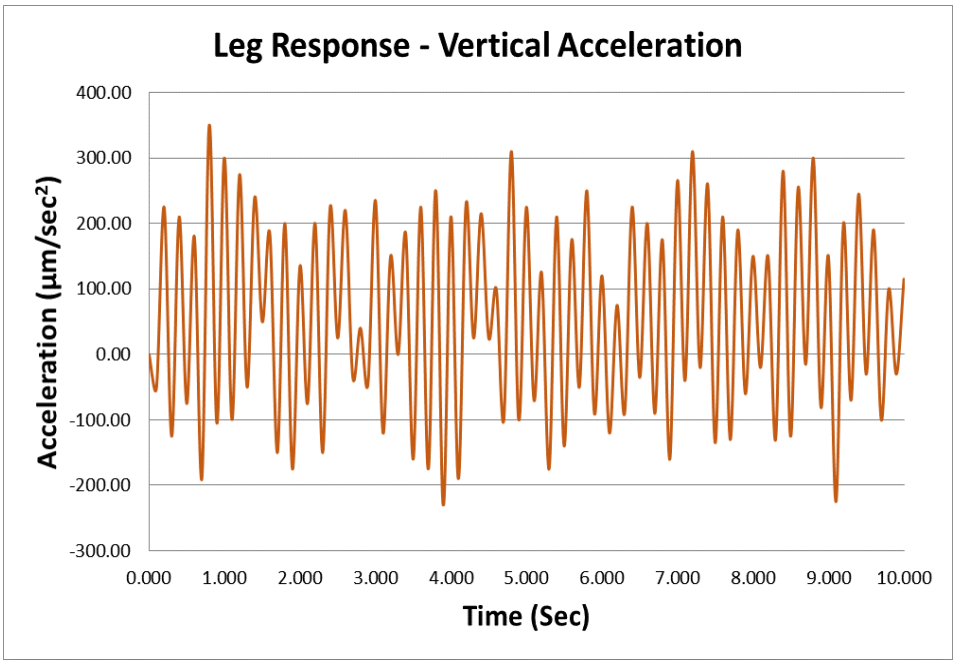

Fig. 139. Simplified test data for human leg

6.3.4.8. Simplified test data for Seat Headrest

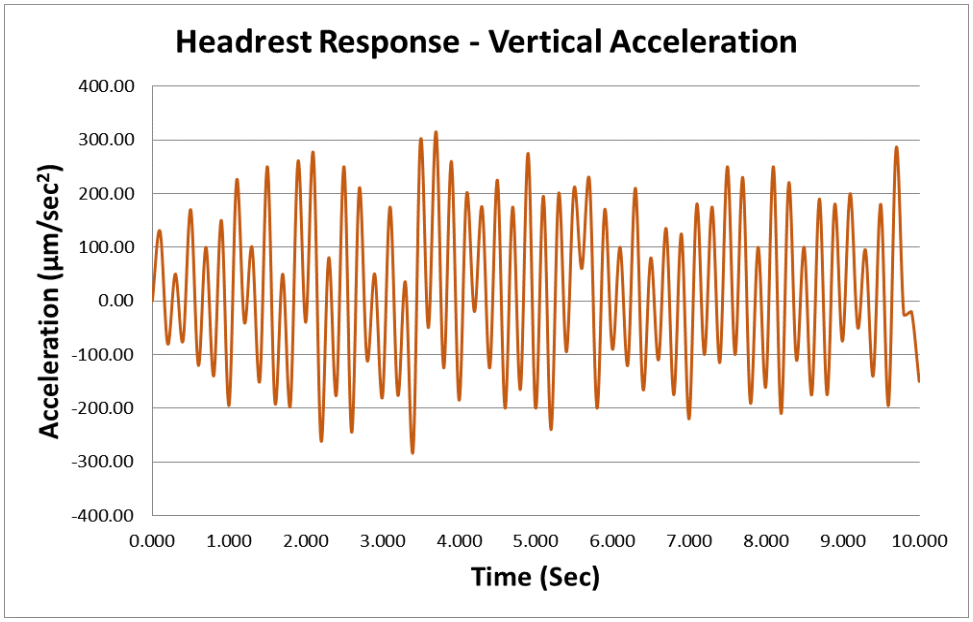

Fig. 140. Simplified test data for seat headrest

6.3.4.9. Simplified test data for Seat Backrest

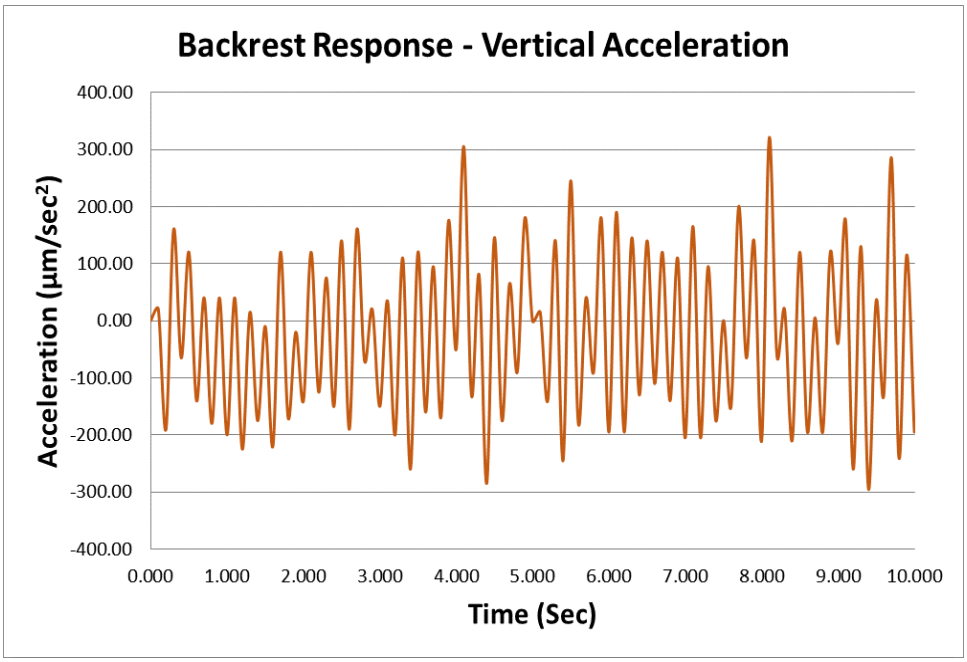

Fig. 141. Simplified test data for seat backrest

6.3.4.10. Simplified test data for Seat Cushion

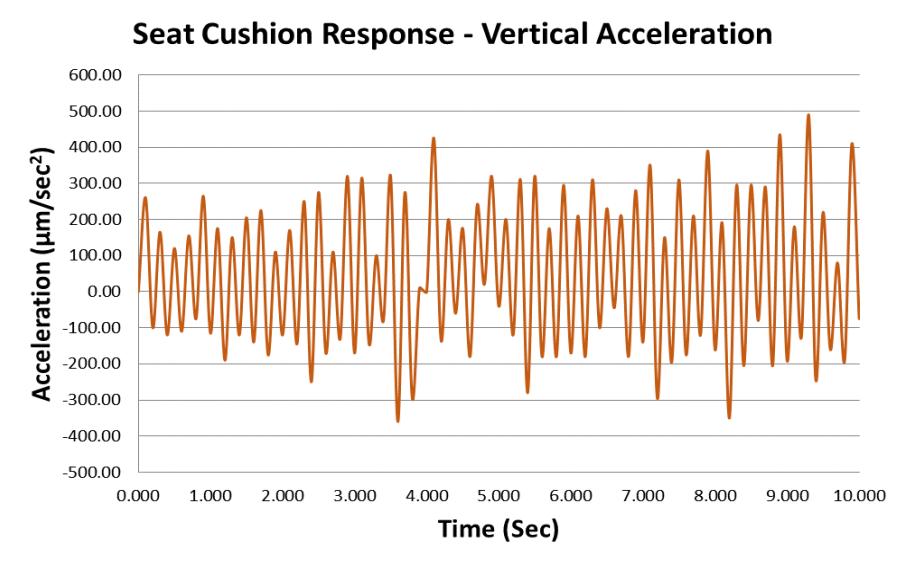

Fig. 142. Simplified test data for seat cushion

6.4. Discussion on the Vibration Measurement and Test Data Acquisition

The testing data had been collected for the initial 60 seconds after the car started moving from standstill condition. Cause of the inaccessibility of computer system with adequate hardware memory, the finite element simulation for the entire human body and car seat assembly had to be limited to initial 10 seconds. Hence, for the effective comparison of simulation outputs to the testing data ever an identical period of time, the testing data had been curtailed to initial 10 seconds and refined in convenient format.

For a car operating in normal condition on smooth terrain, the worst case vibration scenario occurs when the acceleration is at the highest level. From the literature survey carried out in CHAPTER 3 on the acceleration values of different types of cars, it can be stated that if the road surface doesn't get changed, the pick acceleration for a car occurs before initial 9-10 seconds. Hence, the processed test data and the simulation results for

initial 10 seconds are effective enough to assess the vibration characteristics at different locations of car seat and human body inside the dynamic car.

A comprehensive market research on the latest available technologies and instruments for measuring vibration has been accomplished. Testing data have been collected, filtered to appropriate format and condensed to match to the timeframe of finite element simulation. Therefore, the process of validating the simulation results by comparing to the testing data can be initiated.

CHAPTER 7

COMPARISON OF SIMULATION RESULTS AND TEST DATA

From the results of the finite element simulation, displacements, accelerations and frequencies in the vertical direction with respect to time were obtained in the formats of mm, mm/sec² and Hz, respectively. From the testing data, vertical accelerations with respect to time in micro-mm/sec² format and power spectrum densities with respect to frequency in logarithm of acceleration rms format were obtained.

Power spectrum data can be obtained from the finite element simulation by running the simulation through additional modules or by incorporating time-dependent kinematic excitation for non-linear systems. This process of extracting power spectrum data from finite element tool increases the complexity and robustness of the simulation set up by huge extent, which demands the simulation solving to be performed in a highly configured computer system. Also, transformation of power spectrum plots obtained from the testing data to the frequency vs time domain requires time consuming human effort to perform huge amount of numerical analysis. Hence, for the comparison purpose, vertical accelerations vs time data from the simulation results and testing data had been accounted. For convenient interpretation, all the vertical acceleration values from testing data have been transformed into mm/sec² format.

In the finite element simulation, efforts had been made to implement the best possible car operating scenarios to match to the real life test set up. It is obvious that the simulation set up conditions will differ from the practical vibration measurement scenarios, as all the real world parameters can't be assigned to the human body and car seat in the simulation environment. As a result, the output curves from the simulation plots will not coincide to the curves from the testing data. Thus, to compare the acceleration data, peak, average and rms values have been evaluated from both the simulation results and testing data, which are more feasible to recognize the matching range of the accelerations from both the set ups.

7.1. Comparison Matrix

A comparison matrix for the peak, average and rms values of vertical accelerations at different points of human body and car seat, has been detailed in Table 35.

Table 35. Comparison of vertical vibration in terms of acceleration

	Vertical vibration in terms of acceleration	Value from simulation result (mm/sec²)	Value from testing data (mm/sec²)
Human: Head	Peak	1.22	0.36
	Average	0.08	0.02
	rms	0.51	0.14
Human: Chest	Peak	0.48	0.38
	Average	0.16	0.03
	rms	0.23	0.14
Human: Waist	Peak	0.51	0.24
	Average	0.15	0.03
	rms	0.24	0.12

	Vertical vibration in terms of acceleration	Value from simulation result (mm/sec²)	Value from testing data (mm/sec²)
Human: Upper Arm	Peak	0.05	0.42
	Average	0.00	0.02
	rms	0.02	0.16
Human: Lower Arm	Peak	0.32	0.29
	Average	0.16	0.03
	rms	0.17	0.12
Human: Thigh	Peak	0.32	0.28
	Average	0.16	0.03
	rms	0.17	0.16
Human: Leg	Peak	0.34	0.35
	Average	0.12	0.06
	rms	0.16	0.17
Seat: Headrest	Peak	2.33	0.32
	Average	0.12	0.02
	rms	0.86	0.17
Seat: Backrest	Peak	0.94	0.32
	Average	0.26	-0.03
	rms	0.39	0.16
Seat: Cushion	Peak	0.53	0.49
	Average	0.26	0.04
	rms	0.29	0.22

7.2. Comparison Graphs

The compared data in the tabular format are beneficial to get the idea of the peak, average and root mean square values of the vertical accelerations, though the ranges of accelerations and respective fluctuations can be represented through comprehensive graphical format. Simulated and tested vertical accelerations for each of the segments of seated human body and car seat are plotted together by interactive segment-wise graphs in Fig. 143, Fig. 144, Fig. 145, Fig. 146, Fig. 147, Fig. 148, Fig. 149, Fig. 150, Fig. 151 and Fig. 152.

7.2.1. Human: Head

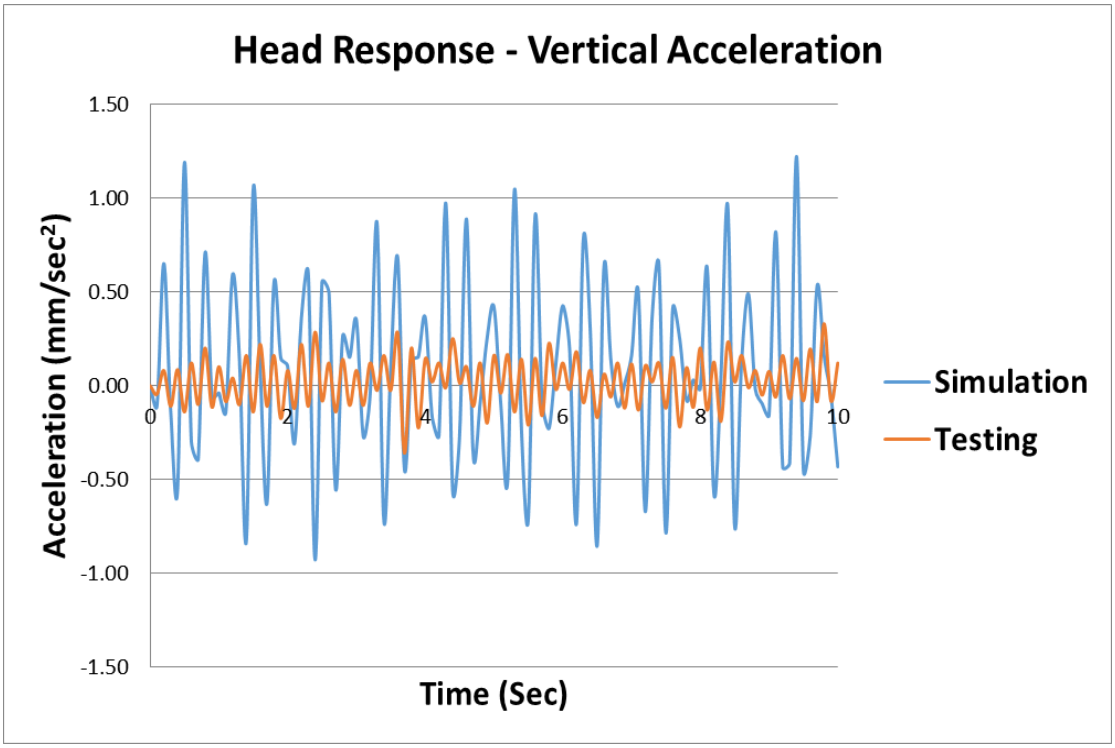

Fig. 143. Vertical accelerations of human head from simulation and testing

7.2.2. Human: Chest

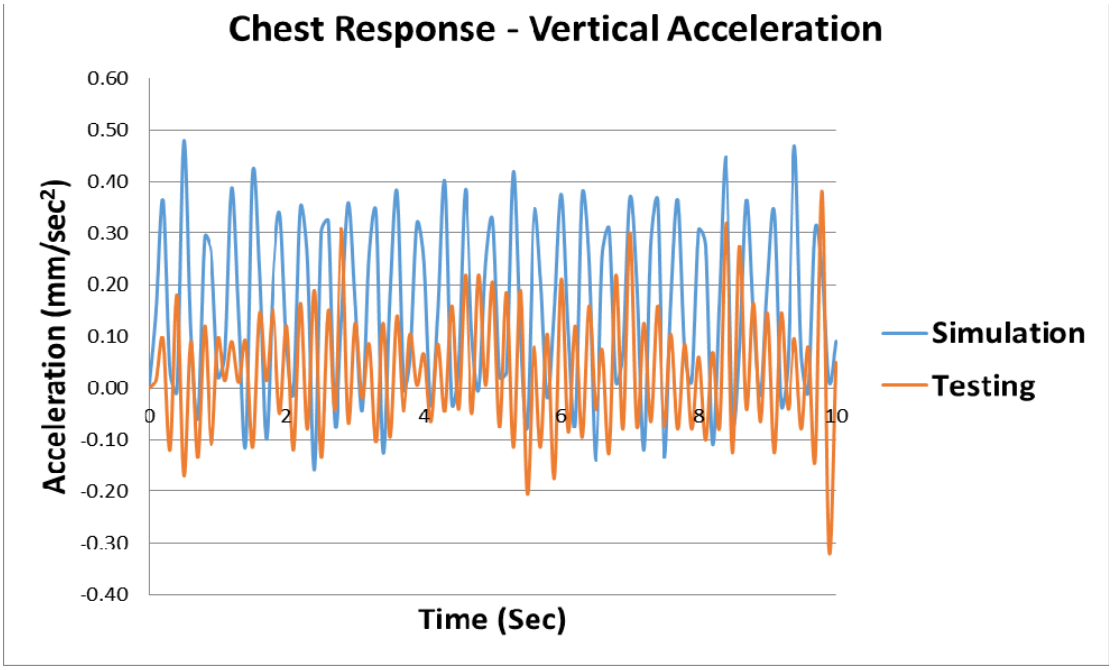

Fig. 144. Vertical accelerations of human chest from simulation and testing

7.2.3. Human: Waist

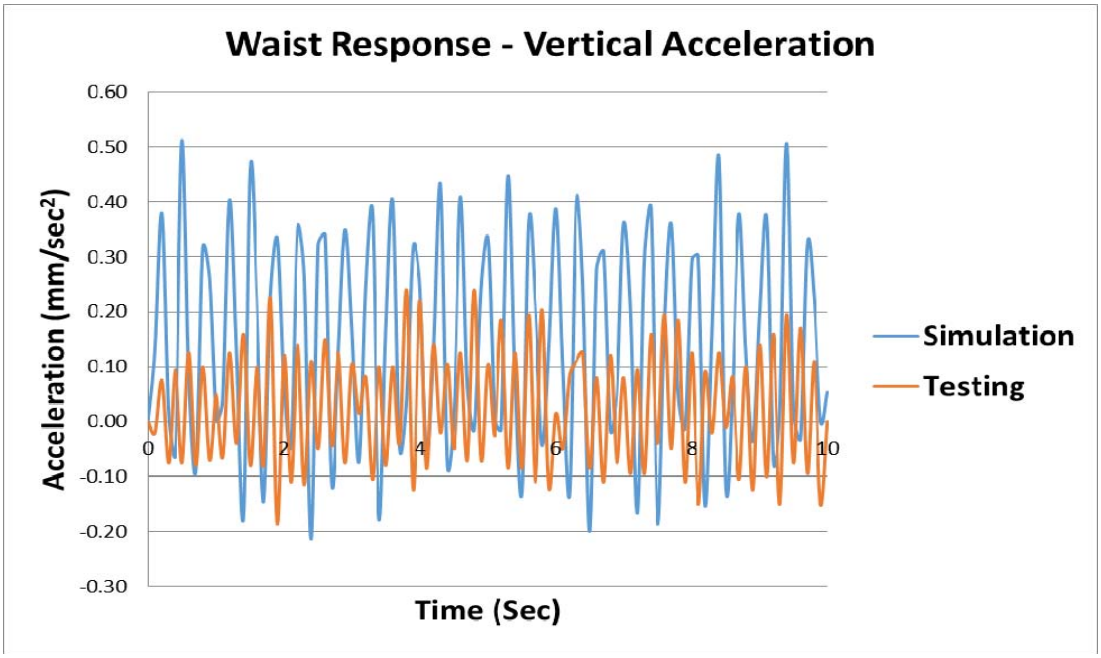

Fig. 145. Vertical accelerations of human waist from simulation and testing

7.2.4. Human: Upper Arm

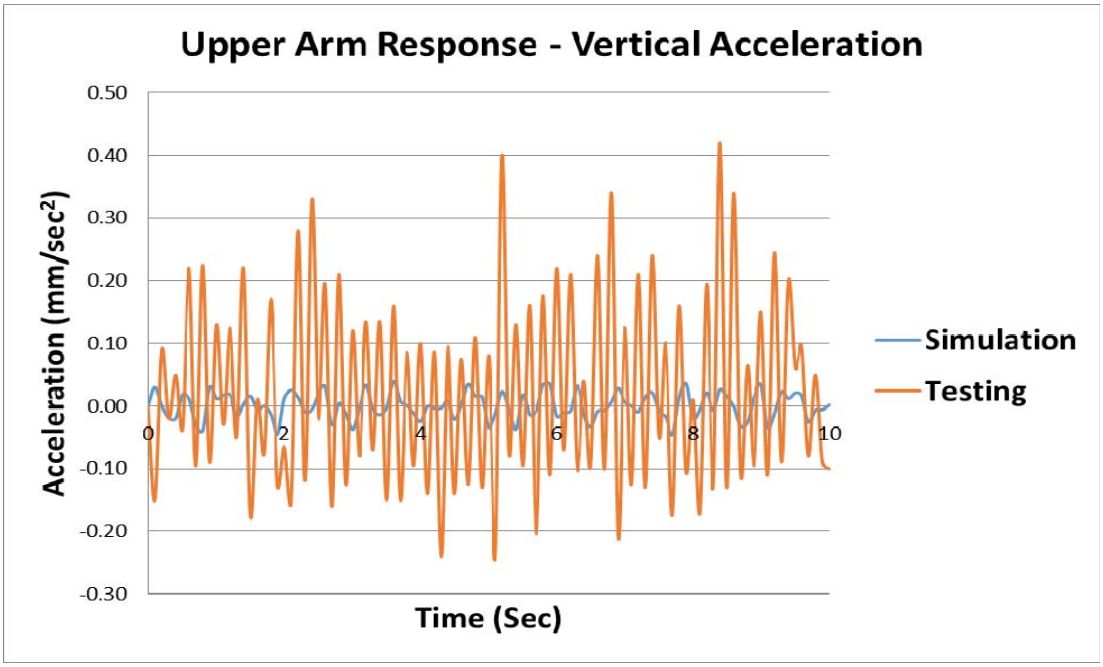

Fig. 146. Vertical accelerations of human upper arm from simulation and testing

7.2.5. Human: Lower Arm

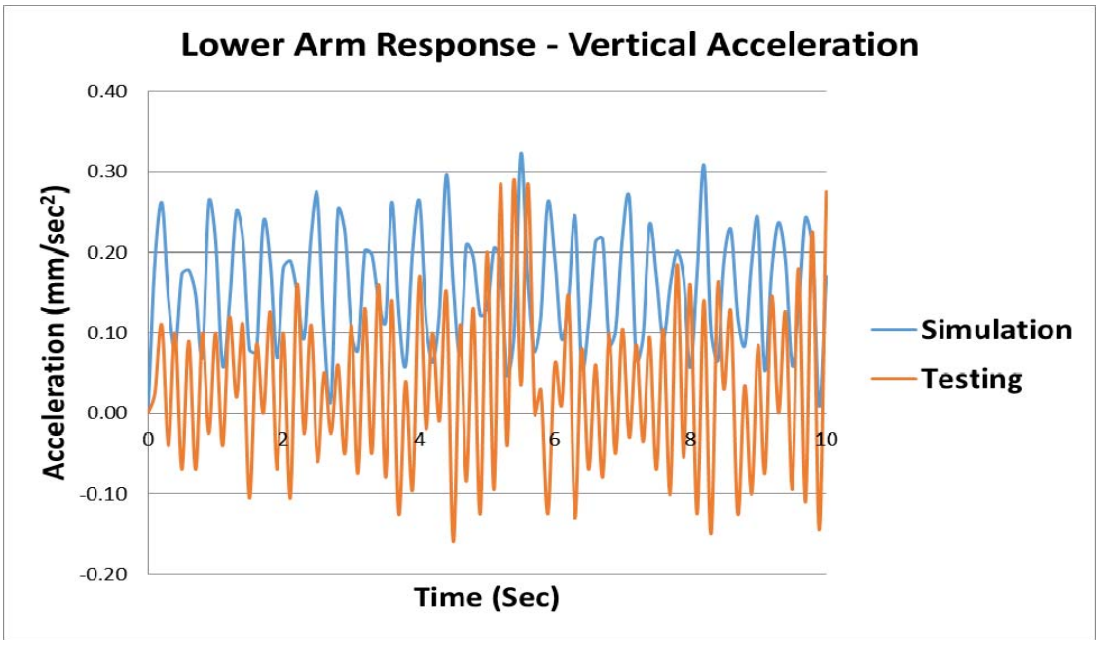

Fig. 147. Vertical accelerations of human lower arm from simulation and testing

7.2.6. Human: Thigh

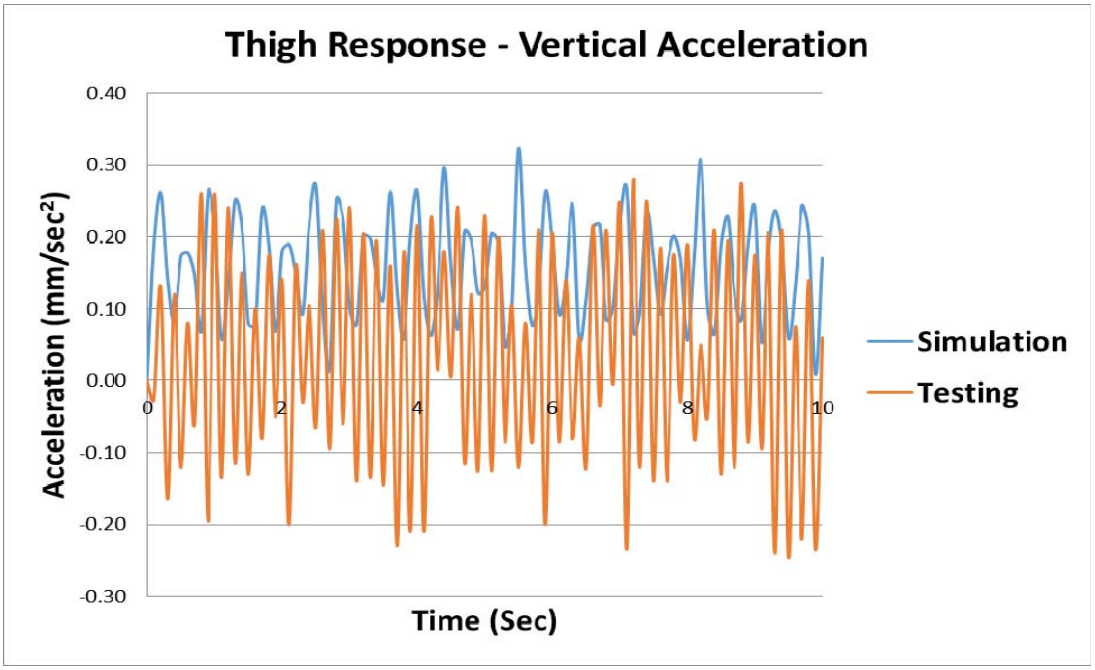

Fig. 148. Vertical accelerations of human thigh from simulation and testing

7.2.7. Human: Leg

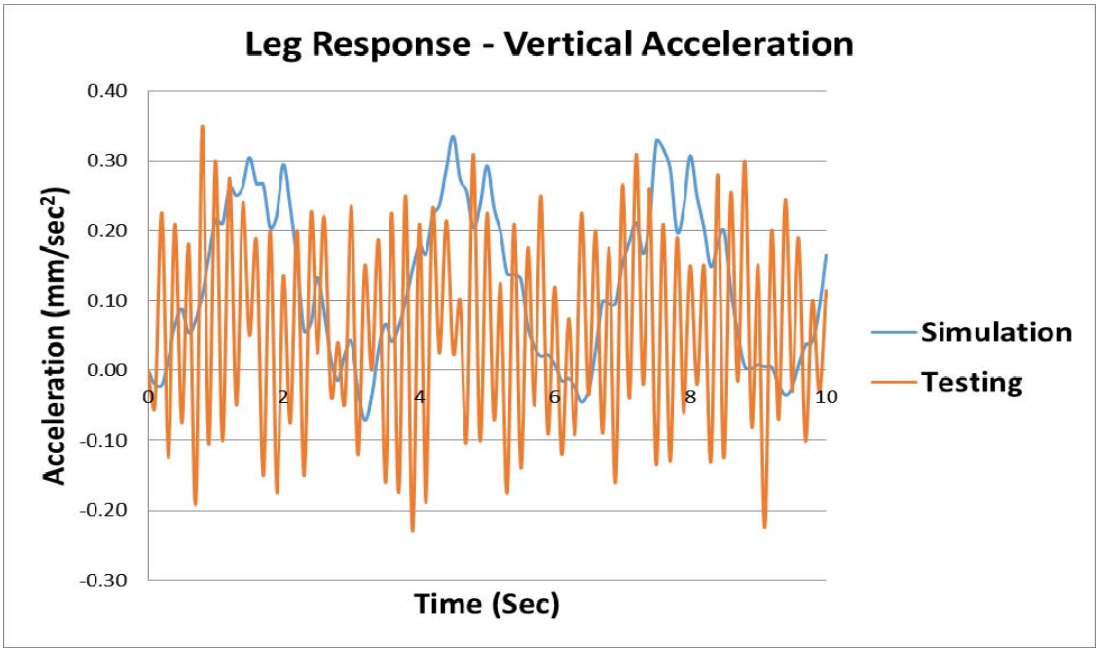

Fig. 149. Vertical accelerations of human leg from simulation and testing

7.2.8. Seat: Headrest

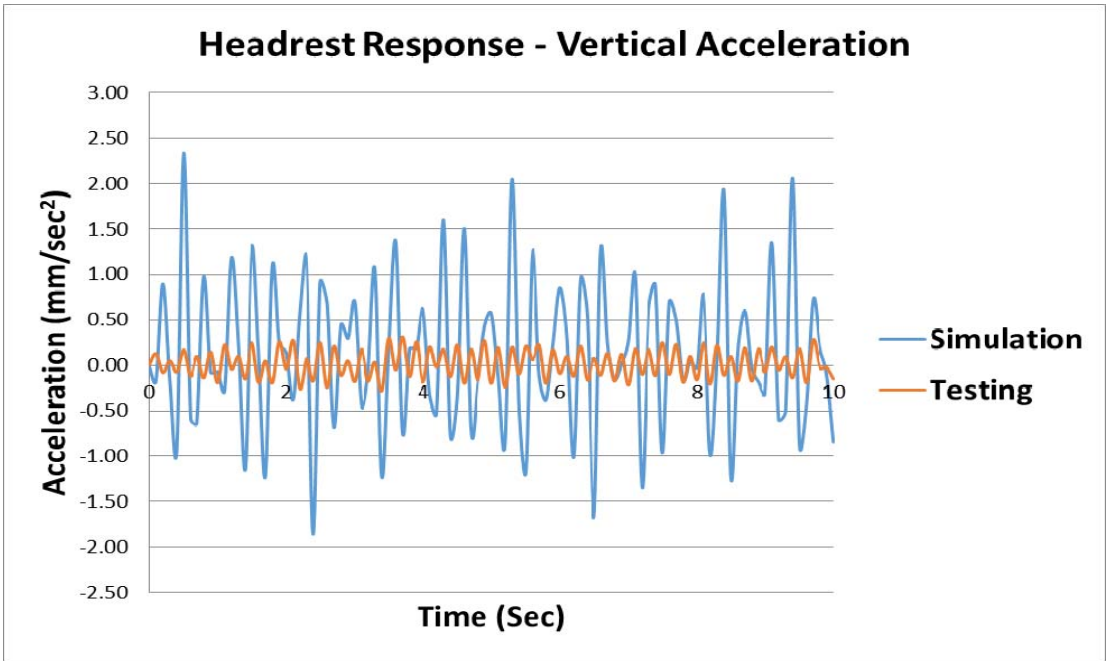

Fig. 150. Vertical accelerations of seat headrest from simulation and testing

7.2.9. Seat: Backrest

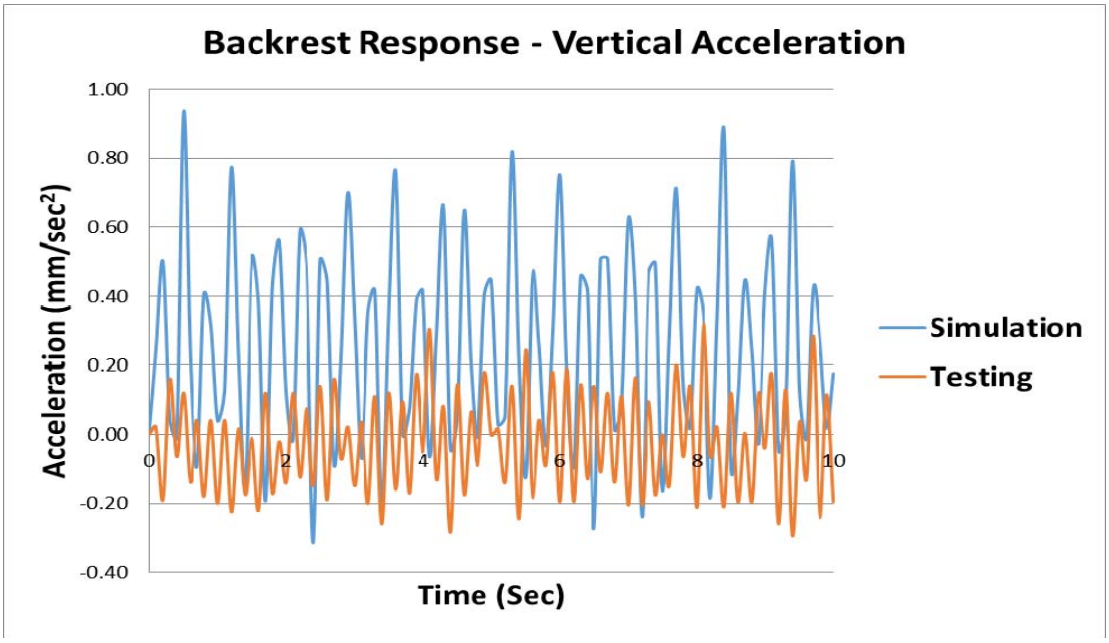

Fig. 151. Vertical accelerations of seat backrest from simulation and testing

7.2.10. Seat: Cushion

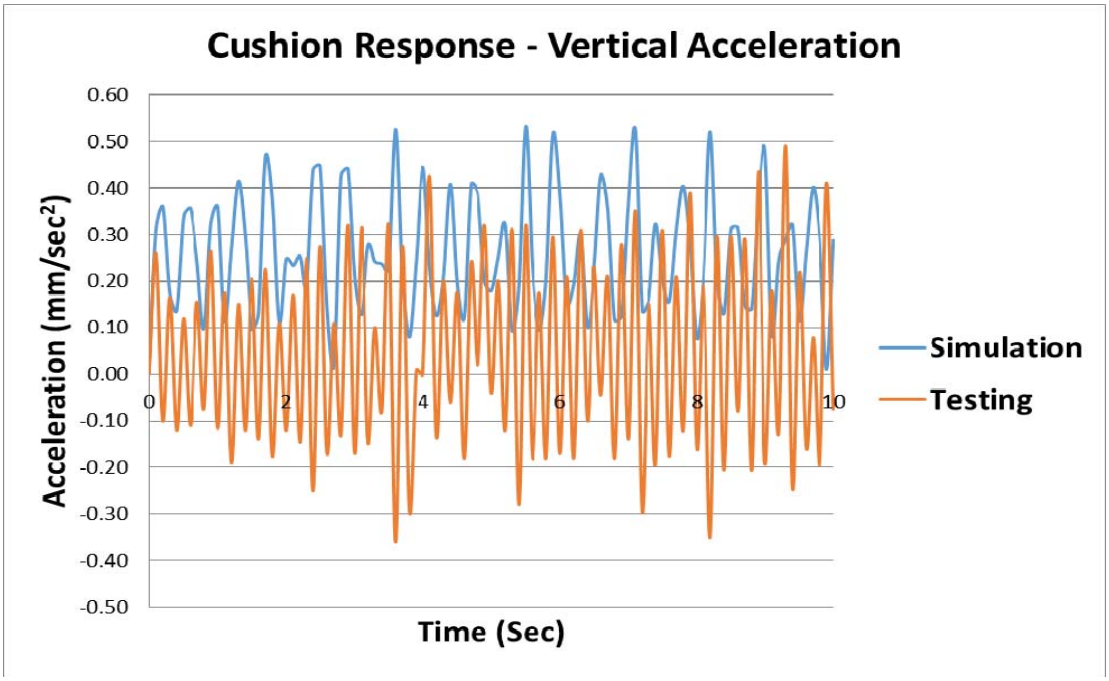

Fig. 152. Vertical accelerations of seat cushion from simulation and testing

7.3. Analytical Investigation of Simulation Results and Test Data

All the tables and charts clearly show that the simulation results are more conservative than those of obtained from the test data. Comparative data for the human head, human waist, human upper arm, seat headrest and seat backrest are being shown through graphs in Fig. 143, Fig. 145, Fig. 146, Fig. 150 and Fig. 151, respectively. From these graphs, it is observed that the upper and lower peak limits of the vertical accelerations from the testing data are well below the respective limits from the simulation results.

Comparative data of vertical accelerations for the human chest, human lower arm, human thigh and seat cushion are represented by graphs in Fig. 144, Fig. 147, Fig. 148 and Fig. 152, respectively, where the upper limit points from testing data are below the respective

points from simulation results, while the lower limit magnitudes from testing data exceed the respective values from simulation results.

Comparative assessment of vertical accelerations for the human leg is shown in the graph of the Fig. 149, where both the lower and upper limits from the simulation results are lower than respective limits from testing data.

It is further observed that if the absolute peak values are considered irrespective of the positive or negative magnitudes, then almost all the vertical acceleration values from the simulation results are higher than those of obtained from the corresponding testing data.

In the computer based simulation of the entire car seat and human body, a number of key parameters had been assigned, namely, mass specific stiffness values, estimated damping co-efficients, Young's moduli of the ellipsoidal human portions, realistic boundary conditions, input loads, contact interfaces and simulation steps as explained in detail in the Section 3.5, Section 3.6, and Section 5.3. In contrast, the data gathered from the testing set up were primarily based on signal processing system of the instruments used. To clarify the theoretical perception behind this fact, an elementary spring-dashpot-mass structure has been sketched in Fig. 153, which represents the human pelvis and a car seat cushion.

The transfer function of the signal processing system for this spring-dashpot-mass structure is denoted by the Equation 7.1.

$$H(s) = \frac{c_p \cdot s + k_p}{m_p \cdot s^2 + c_p \cdot s + k_p} \qquad \text{(Eq. 7.1)}$$

Where,

c_p = Damping value

k_p = Stiffness value

m_p = Mass of the human body pelvis

s = Transformation function of Laplace domain

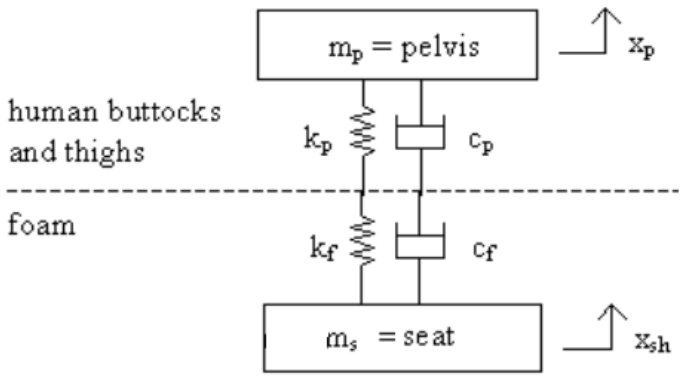

Fig. 153. Spring-damper-mass system representing human and car seat

From the simple Laplace transform formulation of the Equation 7.1, it is understood that for any amount of vibration input applied to the seat cushion, the output vibration at the human pelvis will be a function of the Laplace frequency domain. Also, minimum variation in the mass, stiffness or damping parameter, can greatly influence the final output level of vibration.

In the computerized ABAQUS simulation, efforts had been made to implement the human muscle and bone properties, seat material parameters and vehicle operating conditions as realistic as possible, though, mismatches between the simulation parameters and real life operating environment are unavoidable. As the results from the finite element simulation are more conservative in natures compared to the outputs from test data, the described unique simulation methodology can successfully be implemented to anticipate the final levels of vibration inside the car seated human body and car seat to optimize the design process of human-car seat system.

7.4. Discussion on Comparison of Simulation Results and Test Data

The combined car seat and human body assembly is very complex and robust system where numerous numbers of factors are associated and each of the factors on its own can influence the output behaviour of the system. Car class, seat type, seat orientation, human posture, road terrain, accelerating time, speed, seat foam properties, human portion properties, etc. all play significant roles to define and control the vibration inside the human-car seat assembly. Moreover, in this piece of simulation work, the vibration generated from car engine and road terrain have not been taken into account. If the engine vibration and road surface are considered, the final vibration data from the simulation will inevitably be tuned.

Slight alteration in any of the input parameters of the human-car seat bio-dynamic system can influence the final level of vibration by huge amount, hence, the variations between the simulation results and testing data are inevitable. Variations in the outcomes of the simulation and experimental studies cause of changes in input parameters, had been reported by many earlier biodynamic investigations. Standard and rigid car seat had been taken into account to investigate (Verver, 2004) the vibration transmission between the car seat and human body and concluded that the output level of vertical vibration inside the seat and human body would greatly be influenced by the vertical excitation. Frequency responses were found to be variable with respect to different human bodies and the reasons for those variations were cause of changes in the sitting postures and contact interfaces. Works in the similar biodynamic fields (Griffin, 1990; Pope *et al*., 1990; Zimmer; Kitazaki and Griffin, 1998 and Cook, 1997) outlined the effects of human sitting posture on the vertical vibration. Resonating frequency was reported (Griffin, 1990) to be higher for more inclined car seat in backward directions. Three kinds of seat foam materials had been used for analysis of car seat cushion (Pope *et al,* 1990) and it was reported that the first natural frequency would be lower for the seat with softer foam material. Contact interfaces between the car seat cushion and human thigh area along with the sitting orientation had been examined (Kitazaki and Griffin, 1998) thoroughly

and it was concluded that the increment in the contact surface area between the seat and human thigh would lower the axial stiffness underneath the human pelvis because of the non-linear relationship between the excited force and deflection. Investigations on the seat-human assembly (Hinz and Seidel, 1987; Panjabi *et al*., 1986; Mansfield and Griffin, 2000) exhibited the alterations in the vibration transmissions and acceleration data with different human representatives of variable sizes, shapes and sitting orientations. Studies on vibration transmission (Kitazaki and Griffin, 1998; Zimmerman and Cook, 1997) showed that the variations in the human pelvis location and human posture could change the frequency response and transfer function of the seat-human assembly. Biodynamic experimental study on vibration (Griffin, 1990) repeated the testing process for several times using the same human object with identical test set up. The output vibration levels for all the test runs were different from each other.

The ranges of the frequencies obtained from the computerized simulation results are lower than the permissible frequency limit of 20 Hz for the human organs. Most of the vertical acceleration values from simulation are higher in magnitudes than those received from testing data. The magnitudes of the acceleration data from simulation can further be lowered by applying prospective remedies suggested in past vibration related research works (Griffin, 1990; Pope *et al*., 1990; Zimmer; Kitazaki and Griffin, 1998 and Cook, 1997). Regardless of the reasonable amount of mismatches between the simulation results and testing data, it can be concluded that this simulation methodology can successfully be implemented to anticipate the frequency levels at different points of human body and car seat to optimize the human health, safety and comfort level.

CHAPTER 8

GUIDELINE FOR IMPLEMENTING THE UNIQUE SIMULATION TECHNIQUE IN RELEVANT INDUSTRIES

Upon completion of the validation process of the simulation results with testing data, it can be stated that through some manipulations on the simulation set up, this unique technique can successfully be implemented to similar kinds of transportation industries to judge the level of vibrations inside the seat and its occupant.

This chapter describes the step by step instructions for using this unique simulation methodology for the seat and human body assembly in other relevant industries. Each section of this chapter is elaborating the specific guidelines to be followed for anticipating the level of vibration inside human body and seat in an effective way.

8.1. Required General Reference Documents

Table 36 is showing the international standards to be referred to in this guideline, which are prerequisites for accomplishing all the steps successfully to obtain the output data as accurate as possible. It is recommended to refer to the latest available version of each of the documents.

Some of these documents are related to in-field practical measurement of the vibration, though can be useful to understand the vital locations of the vibration measurement inside the simulated model.

Table 36. International standards related to vibration measurement

Reference number	Document number	Document title
[1]	ISO/TC 159/SC 1	General ergonomics principles
[2]	ISO/TC 159/SC 3	Anthropometry and biomechanics
[3]	ISO/TC 159/SC 4	Ergonomics of human-system interaction
[4]	ISO/TC 159/SC 5	Ergonomics of the physical environment
[5]	ISO 5348	Mechanical vibration and shock — Mechanical mounting of accelerometers
[6]	ISO 5805	Mechanical vibration and shock — Human exposure — Vocabulary
[7]	ISO 8662	Hand-held portable power tools — Measurement of vibrations at the handle.

Reference number	Document number	Document title
[8]	ISO 8727	Mechanical vibration and shock — Human exposure - Biodynamic coordinate systems
[9]	ISO 10819	Mechanical vibration and shock — Hand-arm vibration - Method for the measurement and evaluation of the vibration transmissibility of gloves at the palm of the hand
[10]	CR 1030-1	Hand-arm vibration — Guidelines for vibration hazards reduction - Part 1: Engineering methods by design of machinery
[11]	CR 1030-2	Hand-arm vibration — Guidelines for vibration hazards reduction - Part 2: Management measures at the workplace
[12]	CR 12349	Mechanical vibration — Guide to the health effects of vibration on the human body
[13]	ISO 5349-1	Mechanical vibration — Measurement and evaluation of human exposure to hand-transmitted vibration

8.2. Required Equipments and Tools

The equipments and the software tools needed to execute the entire simulation process, are listed in Table 37.

Table 37. Equipments and tools required

	Equipment/ tool name	Example/ preference
[1]	Computer	Preferably a workstation with minimum 64 GB memory and adequate graphics display capability.
[2]	Cad modelling package	Solidworks, Inventor, CATIA, I-Deas, Unigraphics NX, Creo or Solidedge etc. (Depends on the infrastructure and facilities of the organization)
[3]	Finite element package	ABAQUS CAE, ANSYS Workbench etc. (Depends on the infrastructure and facilities of the organization)

8.3. Assessing Operating Medium and type of Seat

The transportation medium can either be the road, water or air and carriage system can either be bus, tram, railway, ship or plane etc. Section 8.1 describes the general reference documents for vibration measurement, though each industry has its own standards based on the criteria of operating system and aspects of the safety and comfort levels. Hence, it is recommended to follow these industry specific reference documents along with the general reference documents for conducting the simulation process.

Step	Description
1	Classify the type of the industry e.g. transportation, railway, water or aviation and the type of transportation medium e.g. car, bus, truck, train, aeroplane, helicopter, ship, boat etc. from Fig. 154.  Fig. 154. Various mediums of transportation
2	The transportation medium can be categorized into different classes and it is necessary to select the correct class of the vehicle. For example, the car model can be of different models and specifications e.g. mini, medium, large, executive, luxury, coupe, sedan, sports etc. as shown in Fig. 155. 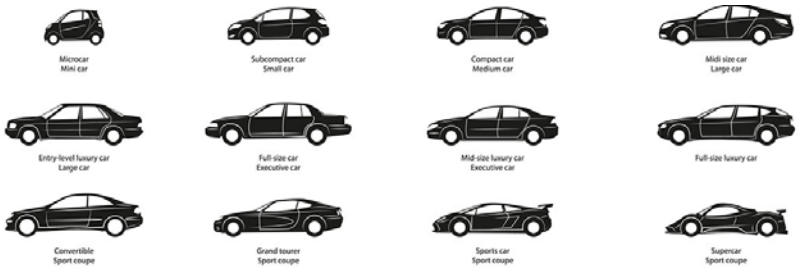 Fig. 155. Different classes of the car Similar way, the water transportation medium can be classified into boat, ship, cruise etc. and aviation carriage medium can be classified into plane, helicopter etc.
3	Based on the transportation medium and its class, the seats for passengers and

Step	Description
	drivers are also get changed and depending on the type of application, the proper seat type to be chosen. An example of different kinds of seats are shown in Fig. 156.  Fig. 156. Typical seats for car, train and airplane (left to right)

8.4. Assessing Operating Environment

The transportation medium can be designed for the normal, harsh, accidental or sporty operating condition. Simulation parameters will drastically be different between the slow speed standard medium and the high speed sports medium. Acceleration, speed and frequency coming from the vehicle engine will be different for each case scenarios.

Step	Description
1	Classify the type of the operation for the medium.
2	Find the maximum possible acceleration value during the initial pick up period, as this value of acceleration will be used to carry out the simulation in worst case scenario.
3	Calculate the operating frequency of the engine of the medium. This frequency value can be evaluated from the engine speed through simple numerical transformation.

Step	Description
4	Calculate or estimate the maximum possible vibration caused by the navigation path condition.
5	NOTICE **Notice:** In case of road transportation, special precaution to be taken while calculating the maximum possible vibration. Maximum possible vertical displacement of the vehicle tyre due to bad road condition to be considered.
6	NOTICE **Notice:** In case of water transportation, addition to acceleration and frequency input, the translations and orientations in three directions should be considered. Six parameters namely, surge, saw, heave, pitch, roll and yaw, as shown in Fig. 157, play vital roles in any water transportation medium. So, maximum possible translations and orientations to be calculated prior to carrying out the simulation. 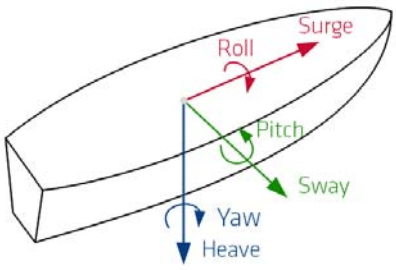 Fig. 157. Degrees of Freedom for water transportation system
7	Other relevant industry or organization specific document for assessing operating environment to be followed, if any.

8.5. Constructing CAD Model of Human Body

The human sizes and masses fall in a range of 5th percentile female mass to 95th percentile male mass. Shapes and sizes of human body vary with respect to age, gender, geographical location and many other factors. Anthropometric or handbook data to be consulted to find out the parameters of the human body and three dimensional CAD assembly of the human body should be established.

Step	Description
1	Select the type of human body to be analysed through the simulation.
2	Measure the mass of the human body to be analysed. From the total mass, the mass of each segment to be calculated by following the procedure shown in Section 3.1 or the relevant industrial or organizational rules.
3	Follow the country-wise standard anthropometric handbook relevant to the optimized design process and select the dimensions of the human parts. NOTICE **Notice:** The anthropometric dimensions change from one country to another. For example, 50th percentile European male and 50th percentile Asian male have different dimensions of the same segment.
4	Represent human segments through ellipsoidal bodies. The procedure mentioned in the Section 3.3 to be followed.
5	Define the posture of the human body. Depending on the transportation seat type, personal comfort level and ergonomic standards, the posture of the human model to be optimized.
6	Establish three dimensional assembly of human body using accessible CAD

Step	Description
	tool.
7	 Fig. 158. Typical human body represented by ellipsoidal segments NOTICE **Notice:** The entire CAD model of human body to be parametrically constructed such that it can be amended anytime cause of the changes in the system requirements. A typical human body modelled for analysis purpose is shown in Fig. 158.

8.6. Constructing CAD Model of Transportation Seat

Transportation seat specifications vary from one class to other. Standard seat dimensions and specifications are available from the seat manufacturers, though, the adjusted orientations and relevant angles differ for different human bodies. Three dimensional CAD model of the transportation seat must comply with the ergonomic standards and be optimized for health and safety of the occupying passenger or driver.

Step	Description
1	Select the type of transportation seat associated to the occupant human body.
2	Get the specifications of the seat from manufacturer or in-house facilities.

Step	Description
3	Define the inclination of the seat. Relevant company guidelines or ergonomic standards to be followed.
4	Establish three dimensional assembly of seat using accessible CAD tool.
5	 Fig. 159. Typical transportation seat model NOTICE **Notice:** The three dimensional CAD assembly of the transportation seat to be parametrically constructed such that it can be modified anytime during the design process. A typical transportation seat modelled for analysis purpose is shown in Fig. 159.

8.7. Setting Up Assembly for Human Body and Transportation Seat

It is preferable to be consistent to use the same CAD tool throughout the modelling and assembling processes of human body and seat. Use of different CAD packages for different stages can lead to lose the parametric features of the models and assembly.

Step	Description
1	Import the CAD models of the human body and transportation seat into the assembly module of accessible CAD tool.
2	Assemble both the bodies based on the interior arrangement of the transportation medium. In case of analysis of the human driver, position of hand at the steering and position of leg at the pedals vary with different types of transportation mediums and classes. In case of analysis of the passenger, the movements of the legs and hands can be ignored.
3	Both the bodies should be placed as per real life mating condition, without any interference or direct contact. NOTICE **Notice:** Special precaution to be taken while assembling to avoid any interference or direct contact. Any interference and direct contact may produce undesirable errors while the assembly will be taken into the finite element environment. A typical human-seat assembly for analysis purpose is shown in Fig. 160.
4	 Fig. 160. Typical human-seat assembly

8.8. Evaluation of Analysis Parameters prior to Simulation

Inevitable parameters for the human body segments and transportation seat need to be evaluated or selected before entering to the simulation environment.

Step	Description
1	Calculate the densities of all the human portions.
2	From the reliable source of references, Young's moduli of the human bone and muscle to be selected as shown in the Section 3.5.2.
3	Calculate the axial and transverse Young's moduli for the human segments using the formulation and methodology shown in Section 3.5.2.
4	Calculate the axial and transverse stiffness values for the human segments using the formulation and methodology shown in Section 3.5.3.
5	Chose the Poisson's ratio for human segments as accurate as possible. Section 3.5.4 can be followed to get the idea of choosing Poisson's ratio.
6	Choose the damping ratio and damping co-efficient values for human parts as realistic as possible. To consider the worst case scenario, Section 3.5.5 can be followed.
7	Select the proper type of the seat material, either nylon, polyester, alcantara, vinyl, faux leather or leather.
8	Select the parameter values of the hyper-elastic material. Section 4.3.1 can be followed as reference. NOTICE **Notice:** It is recommended to consider Ogden hyper-elastic methodology and select parameters up to second order $\mu 1$, $\alpha 1$, $\beta 1$, $\mu 2$,

Step	Description
	α2 and β2.
9	Select the parameter values of the viscoelastic material. Section 4.3.1 can be followed as reference. NOTICE **Notice:** It is recommended to consider polynomial co-efficients G1, Ƭ1, G2 and Ƭ2.
10	Density of the seat foam material to be chosen depending on the type of foam material as mentioned in Section 4.3.2.
11	Chose the Poisson's ratio for seat foam as accurate as possible. Section 4.3.3 can be followed to get the idea of choosing Poisson's ratio.
12	NOTICE **Notice:** Temperature gradient of the seat foam to be defined in case of operating in abnormal and harsh condition.
13	Calculate the acceleration or force to be applied based on the operating environment and type of application of the transportation medium. Section 3.6.4 can be used as a reference if necessary.

8.9. Simulation Set Up and Running the Analysis

Standard finite element tool like ABAQUS Workbench, ANSYS CAE or any other recommended finite element software tool to be used for setting up the simulation environment.

Step	Description
1	Import the entire human body and seat assembly to the finite element environment. NOTICE **Notice:** The best option for importing the CAD model to finite element environment is using the parasolid format.
2	Remove all the redundant edges and surfaces, if any, to simplify the models.
3	Assign the material properties and densities to all the human segments and transportation seat foam obtained from Section 8.8.
4	Assign the stiffness and damping values of the human segment obtained from Section 8.8.
5	Assess the contact surfaces between the human body and seat. Assign the contact mechanism selecting the most relevant formulation from Section 5.3.2. NOTICE **Notice:** Multi-point bonded contact with no separation is the best option, though different contact mechanism can be used depending on the configuration of the computer hardware.
6	Assign the boundary conditions and constrains as accurate as possible. Degrees of freedom for each of the segments to be chosen carefully.
7	Apply the loading condition by means of acceleration or force obtained from Section 8.8.
8	Incorporate the frequency appearing from the engine vibration and navigational path obtained from Section 8.4.

Step	Description
9	In case of ABAQUS, the loading conditions to be assigned in different steps. For the natural frequency of the entire system, linear perturbation step to be used and for dynamic analysis, modal dynamic step to be used. All the loading conditions and input frequency to be applied at modal dynamic step. 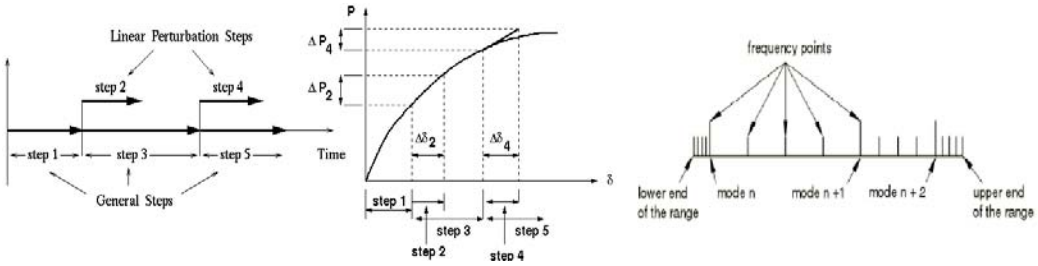 Fig. 161. ABAQUS CAE steps In case of ANSYS Workbench, separate modules can be created to establish a step by step hierarchy. 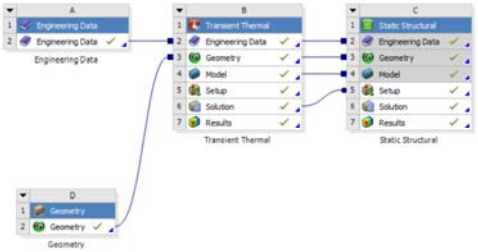 Fig. 162. ANSYS Workbench hierarchy Typical ABAQUS and ANSYS analysis steps are shown in Fig. 161 and Fig. 162, respectively. For any other finite element tool, proper sequences of hierarchy or steps to be followed as necessary.
10	Mesh all the bodies following the meshing guidelines for different types of operating condition, surface contact and material properties. NOTICE **Notice:** It is recommended to use ten-node tetrahedral

Step	Description
	element C3D10 for the simulation using ABAQUS. In case of ANSYS Workbench, the areas of interest to be refined with higher mesh densities.
11	Depending on the capability of the computer system used, set the simulation running time in between 10 seconds and 60 seconds.

8.10. Simulation Result: Output and Extracted Data

Approaches used and the facility available inside the simulation tool lead the type of the data to be extracted from the simulation. The basic intention is to know the vertical accelerations, vertical displacements and frequency levels which can be obtained directly or through other sources of output.

Step	Description
1	Evaluate the vertical accelerations and vertical displacements at the designated points of human body and transportation seat. For human body, the locations should ideally be head, chest, upper arm, lower arm, waist, thigh and leg. For seat, the locations should ideally be center of the headrest, center of the backrest and center of the cushion,
2	From the mathematical relationships between the frequency, displacement and acceleration; frequency with respect to time should be evaluated.
3	Check if the frequency levels are under the permissible limit of human organs as mentioned in the industrial standards or organization manual. For reference, Section 5.5 can be followed.

Step	Description
4	**NOTICE** **Notice:** If the obtained frequencies are not falling within the permissible ranges of natural frequencies of human body portions, the procedures from the Section 8.3 to Section 8.10 to be repeated after adjusting and assessing the system in a different way. The input parameters to be tuned for revising the simulation.

8.11. Discrepancy Log

During the entire simulation process any kind of error, troubleshooting and possible remedy should be recorded for future improvement of the simulation project.

Discrepancy Occurred During Procedure		**Yes** ☐	**No** ☐
	Name of Simulation In-Charge	**Date**	
Section no. / Step no.	**Discrepancy/Corrective Action**	**Name**	**Date**

8.12. Personnel Involved

A table should be used to record all the personnel involved during the simulation process. The main person to organize the simulation or the lead person of the simulation project, should be listed in the first row.

Employee No.	Name (Print)
	(Simulation In-Charge)

8.13. Approval of Simulation

Simulation results should be checked, verified and approved by the qualified and knowledgeable personnel.

Signatures below verifies that: ☐ The Simulation is according to standards, guideline and other relevant reference document. ☐ A discrepancy log has been created, filled out and documented.	
Simulation In-Charge	
Name (Print)	
Date and Signature	
Approver	
Name (Print)	
Date and Signature	

8.14. Support Center

In case of any kind of help or assistance needed for conducting the simulation process, contact details of expertise are provided below:

Contact Details

Postal address
Purnendu Mondal/ Subramaniam Arunachalam
School of Architecture, Computing & Engineering
University of East London (Docklands Campus)
London E16 2RD, UK

Contact details
E-mail: u1619864@uel.ac.uk, purnendu.mondal@yahoo.com, s.arunachalam@uel.ac.uk
Mobile: +44(0)7578738922

CHAPTER 9

DISCUSSION, CONCLUSION AND SCOPE OF IMPROVEMENT

The aim this research study was to develop a finite element simulation methodology to predict the final level of vibration inside the car seated human body and car seat in dynamic condition. Numerous research works to establish comprehensive simulation set up for car-human system had been carried out over in past decades, though those investigations focused only on very specific area of the entire human-car assembly. So, initiative has been taken during this course of research work to fill up the gaps in the pre-existing technologies by offering a novel finite element simulation technique to predict the final level of vibrations at different locations of entire human-car seat system to assess and optimize the health, comfort and safety of car seated human body. The expensive and time consuming real life vibration measuring procedure can be omitted in various industries by accurate anticipation of the final level of vibration data inside human body though the implementation of this novel simulation methodology.

Detail discussion have been carried out in CHAPTER 1 on the objectives and findings of this research work along with representing critical review of literatures and matrix based comparison table of past investigations. The objectives of this simulation based study were literature review and critical analysis of various existing simulation technologies for

judging the vibration inside automotive-human system, establishing simulated models for human body, car seat and human-car seat assembly, validating simulation results with testing data and finally, proposing a guideline to implement the developed simulation tool in similar industries.

Research questions outlined in CHAPTER 1, are based on the finding of the best suitable technique for finite element simulation, procedure in simulation model for optimizing the car seated human health, comfort and safety, accuracy of simulation results compared to test data, limitations of the computerized finite element simulation and implementation of the developed simulation technique in similar industries.

This chapter is summarizing the of findings from the different simulation phases, validation of simulation results by comparing to test data and deviations of simulation results from test data, general procedure to implement this simulation methodology in similar industries, overall conclusion and finally, scope of improvement to take this novel simulation methodology to further advanced level.

9.1. Finite Element Simulations and Responses of Human Body, Car Seat and Human-Car Seat Assembly under the Effect of Vertical Vibration

Biodynamic responses of the human body, car seat and human-car seat assembly under the effects of vertical vibration had been investigated by developing simulation based models in CHAPTER 2, CHAPTER 3, CHAPTER 4 and CHAPTER 5.

9.1.1. Lumped Mass Parameter Method: Manual Intervention

Before carrying out the detailed finite element simulation for the human body and car seat, a preliminary theory based mathematical model using Mathcad formulations had

been developed for human body constructed only by head and torso. Lumped mass parameter method had been utilized to establish that experimental model and the first two natural frequencies and mode shapes of the human body had been extracted. The masses of the head and torso and stiffness value in between those two bodies had been taken from the detailed evaluation of human parameters carried out in CHAPTER 3.

The lumped mass method is simple and effective way to obtain the fundamental frequencies and mode shapes in bi-directional plane, though addition of more degrees of freedom in three dimensional environment restricts the capability of this method because of the limitation of human competency in solving numerous number of complex equations manually. For the lumped mass model with higher number of degrees of freedom, mathematical tool like FORTRAN or MATLAB is used to solve the equations of the system. Furthermore, this method assumes that the human portions are made of rigid point masses, though, in reality the human portions are constructed of non-uniformly distributed masses and the properties for all the human segments are dissimilar from each other.

Detail literature review in CHAPTER 1 showed that last many years numerous investigations had been conducted using this lumped mass parameter method to analyse various kinds of biodynamic problems. Thus, developing the simulation of human body using this technique will have very less chance to have innovative outcome. Cause of the enormous development in the computer technology over last few decades, lumped mass parameter method aided by manual calculation has become almost obsolete to be used for analyzing complex mechanical systems.

9.1.2. Combination of Lumped Mass Parameter and Finite Element Methods in Three-Dimensional Space: Computerized Simulation

Detail discussion in the CHAPTER 2 on the lumped mass parameter and finite element methods clearly stated that the lumped mass parameter is well-organized for the assessment of the mode shape related queries, while finite element analysis is more suitable for judging the portion-wise human behaviour under the effect of vibration. Based on the literature studies in CHAPTER 1 and CHAPTER 2, initiative had been taken to simulate a car seated three-dimensional human body using lumped mass method in finite element environment.

A three dimensional CAD model of seated human body inside a car had been taken from open source web database, Grabcad to carry out the experimental simulation work as described in Section 2.2. Raw data collection from open source, measurement of human portions in three dimensional space, assignment of co-ordinate system to measure the locations of human portions, mounting the connecting points of human portion in finite element space, calculation of masses of human segments, average masses of lumped parameters, lumped mass connections, axial stiffness values, modal displacement and graphical plots of vertical displacements are shown in Fig. 28, Fig. 29, Table 4, Fig. 30, Table 5, Table 6, Fig. 31, Table 7, Table 8 and Fig. 32, respectively. Boundary condition had been incorporated to hands, legs, head and pelvis as realistic as possible and linear perturbation frequency analysis under free vibration had been conducted.

The resonating frequencies obtained from this experimental work are of very low magnitudes compared to the realistic permissible ranges of natural frequencies described in Section 5.5. The reasons behind the very low levels of natural frequency values can be pointed out as:

- Free vibration has been considered during the simulation task. If the entire lumped mass model would be excited under the effect of force vibration as per the real life

driving condition, the natural frequencies would be much higher than those of obtained from the experimental work.

- Only the human body has been taken into account without the car seat. Association of car seat by means of modeling another lumped mass model inside the simulation space, would definitely yield much higher levels of natural frequencies.
- Only unidirectional stiffness parameters have been used in the simulation and no damping factor have been considered. Assignment of three dimensional stiffness parameters along with the damping co-efficients would certainly exhibit higher levels of resonating frequencies.

From the outcome of this miniature simulation study, it is obviously clear that combination of lumped mass parameter and finite element methods can be used for carrying out bio-dynamic vibrational analysis. The main disadvantage of this methodology is that the actual shapes and sizes of the human portions can't be represented, hence, lacking the real life feasibility.

9.1.3. Unique Bio-Dynamic Model Developed for Seated Human Body inside a Car: Finite Element Simulation

After conducting the basic experimental simulation studies using lumped mass parameter and finite element methods, a unique approach had been taken to generate bio-dynamic three dimensional model of car seated 50^{th} percentile male human body of 77.3 kg mass, as explained in CHAPTER 3.

The extracted human segmental mass data are presented in Table 9 and Table 10 of Section 3.1, while human segmental dimensions had been obtained from anthropometric databases as shown in Table 11 of Section 3.2. For simplification, the human segments had been represented through ellipsoidal entities. The advantages and numerical

philosophy of representing human portions through ellipsoidal bodies had been outlined in Section 3.3. Later, in Section 3.4 a CAD model had been established using Solidworks modeling tool for the car seated human body based on a real life visual image of 50^{th} percentile male human. The three dimensional, age and shape specific stiffness parameters for all the ellipsoidal bodies had been calculated using the formulations of composite materials. The established human model had been imported into finite element environment and bone-muscle material properties, three dimensional stiffness parameters, damping co-efficient, boundary conditions and loads had been assigned to the human segments.

Explorations and evaluations of many parameters were necessary to produce effective simulation model for the human body. Detailed methods of obtaining the densities of the human portions, axial and lateral young's moduli of the human segments, axial and lateral stiffness values of the body segments, Poisson's ratios, damping co-efficients along with damping ratios, contact interactions, analysis steps, boundary conditions, loads, element types and results are discussed in Section 3.5.1, Section 3.5.2, Section 3.5.3, Section 3.5.4, Section 3.5.5, Section 3.6.1, Section 3.6.2, Section 3.6.3, Section 3.6.4, Section 3.6.5 and Section 3.7, respectively.

The unique natures of this simulation methodology can be listed as:

- Modelling the human portions through ellipsoidal segments to evaluate size and shape specific three dimensional stiffness data.
- Constructing the ellipsoids with composite formulations for achieving realistic bone-muscle properties.
- Representing the entire human body through ellipsoidal objects which eventually helps the finite element simulation to simplify the entire human model to yield desired result data within a reasonable amount of simulation solving time.

The simulation of the human body under forced vibration ran successfully yielding acceleration and displacement data in the vertical direction. From the obtained data set, frequency values had been evaluated, which were very close to the acceptable ranges of frequencies for human organs as explained in Section 3.8.

Earlier studies, handbooks, standards and literatures showed the permissible ranges of frequencies for human portions in between 0.5 Hz and 20 Hz, while this bio-dynamic simulation displayed the minimum frequency value of 0.93 Hz at leg and maximum frequency value of 4.7 Hz at thigh. The displacements obtained from the simulation are higher than the expected levels and the potential reason behind it can be identified as absence of car seat in the simulation set up. Association of foam made car seat underside of the human thigh area will definitely show lower magnitudes of displacement values. Although, this simulation methodology worked flawless, still, further improvement is possible to get more accurate vibration data by involving car seat in the simulation environment and assigning material properties to seat polyurethane foam.

9.1.4. Development of Car Seat Model: Finite Element Simulation

CHAPTER 4 outlined the development of a car seat made of polyurethane foam material. The car seat had been modelled in Solidworks modeling tool after performing detailed research on the types and dimensions of the existing car seats in the industry. Besides the comprehensive survey of literatures on the similar fields, automotive seat design database from Ricaro had been consulted.

To model the material properties of polyurethane foam as realistic as possible, both the hyper-elastic and visco-elastic formulations had been implemented. Ogden model with N=2 and second order Prony series had been applied for hyper-elastic and visco-elastic properties , respectively as shown in Table 23.

The main aims of this simulation work of the car seat were to verify the feasibilities of the assigned visco-elastic and hyper-elastic material properties and get an idea of the suitability of the car seat model to fit with the modelled human body in CHAPTER 3. Because of this fact, the metallic frame underneath the seat had been ignored and the underside of the seat cushion had been made to be fixed.

The loads had been implemented on the estimated contact surfaces between the human body and respective mating portions of the car seat. The details of the loading and boundary conditions have been explained in Section 4.4.3. Other necessary parameters and analysis set ups had been elaborated in Section 4.3 and Section 4.4, respectively.

Vertical displacements at different location of the car seat were evaluated from the simulation results. The maximum displacement values at headrest, backrest and cushion had been found to be 4.98838 mm, 5.08838 mm and 5.79838 mm, respectively.

The simulation of car seat model shows that:

- Both the hyper-elastic and visco-elastic properties can be assigned together to the polyurethane foam material of car seat for getting effective results from finite element simulation.
- The levels of displacements are convincing over short period of simulation running time. Longer span of simulation running time will obviously display more accurate displacement magnitudes.
- The car seat model can be associated to the human body developed in CHAPTER 3 for carrying out comprehensive analysis on car seated human bio-dynamics.

9.1.5. Combined Human Body and Car Seat: A Comprehensive Finite Element Simulation

The car seated bio-dynamic model of 50th percentile male human body developed in CHAPTER 3 had been united to the car seat model established in CHAPTER 4. Afterwards, a comprehensive finite element based simulation had been accomplished in CHAPTER 5 for predicting the final levels of vibrations inside the portions of human body and car seat. Main challenges during the association of the human model to the car seat, were faced as:

- Defining the suitable contact mechanisms between the ellipsoidal human portions and car seat.
- Implementing the real life driving conditions as realistic as possible along with precise boundary conditions.
- Assigning the acceptable posture of human body and orientation of car seat.
- Setting up the simulation by avoiding unnecessary complexity to run and complete the robust finite element analysis within justified time limit.
- Obtaining the desirable outputs at the locations of interest for evaluating the effects of vertical vibration on car seat and human body.

Techniques for assembling human driver body and car seat were studied from anthropometry based configurations, biomechanics of seated human, ergonomics principles and relevant international standards in Section 5.1. Simulation parameters had been identified from the detailed investigations carried out in CHAPTER 3 and CHAPTER 4. A summary of all the implemented simulation parameters have been presented in Table 26.

Different kinds of contact interfaces had been studied from earlier research studies and ABAQUS CAE manual as explained in Section 5.3.2. All types of contact formulations along with their pros and cons had been summarized in Table 27 and Table 28.

Theoretical formulations along with the associated algorithms of the contact interactions for pure penalty, Lagrange, multi-point and beam concepts, had been observed in detail and multi-point bonded contact with no separation had been recognized as the most suitable formulation to be assigned between human body and car seat.

The simulation had been set to run from standstill condition of the car to a definite accelerating period. Efforts were made to run the simulation for initial 60 seconds, though, cause of the limitation of the computer capability to solve robust problem, the simulation running time had to limit to initial 10 seconds. The vertical accelerations and displacements at various points of human driver and car seat had been extracted from the simulation results and recorded through tables and graphs in Section 5.4. Later, the frequency values at different points of human body and car seat portions were evaluated as detailed in Section 5.4.3. The average frequency magnitudes obtained for head, chest, waist, upper arm, lower arm, thigh, leg, seat headrest, seat backrest and seat cushion were 7.10 Hz, 4.13 Hz, 4.18 Hz, 4.01 Hz, 12.92 Hz, 16.13 Hz, 3.20 Hz, 7.91 Hz, 4.61 Hz and 18.0 Hz, respectively. The observed key features of this unique simulation phase can be highlighted as:

- Frequency magnitudes of human segments are lower than those of the mating car seat portions, which is a clear indication of the effective vibration transmission from foam made car seat to human body. Moreover, it gives a sign of correct functionalities of the calculated three dimensional stiffness values, assigned material properties, defined damping parameters, allocated contact mechanism, implemented boundary conditions and applied loads inside the unique simulation set up.
- Obtained frequency values are falling within the ranges of permissible natural frequencies for human organs as per the past references detailed in Section 5.5.
- During the assignment of contact mechanism, approaches had been taken to implement different types of contact mechanisms by allocating frictional co-

efficients. But, cause of the lack of adequate hardware memory in the available computer system, the simulation got terminated prematurely without yielding any output data. Past simulation studies on the similar biodynamic fields reported that the assignment of frictional co-efficient would be beneficial for stress or pressure distribution related problems. Furthermore, the goal of this novel simulation based study mainly lies in the domain of predicting final levels of vibration data inside car seat and human segments. Therefore, application of tie-up constrains at the interfaces of human body and car seat, as detailed in Section 3.6.1 and Section 5.3.2, must not have any impact on the primary aim and outcome of this study.

Assignments of calculated three dimensional stiffness values to the human ellipsoidal segments and combined hyper-elastic and viscoelastic material properties to the car seat polyurethane foam performed flawless inside the simulation system. Hence, the finite element based unique bio-dynamic simulation methodology became successful to anticipate the final levels of vibration inside human body and car seat portions.

9.2. Validation of Simulation Results: Deviations from the Test Data

Testing data had been collected from m+p international for a 50^{th} percentile male human driver under the condition similar to simulated environment, as detailed in CHAPTER 6. NI 9234 Module with CompactDAQ Chassis and Dytran 3055 transducer had been used as instruments for measuring the vertical acceleration with respect to time and power spectrum density with respect to frequency at different segments of human driver and car seat. The raw testing data were received in .SOT format, which were later operated in "m+p Analyser" software tool to extract the necessary data plots in graphical format. The simulation results were obtained for initial 10 seconds of accelerating period, while the testing data had been gathered for initial 60 seconds. To compare the simulation results to

the testing data over an identical period of timeframe, the acceleration data from testing had been simplified and curtailed to initial 10 seconds as described in Section 6.3.4.

A comparison matrix highlighting the peak, average and rms values of vertical accelerations obtained from both the simulation results and testing data, has been represented in Table 38. The contrasts between the vertical accelerations received from simulation results and testing data have been graphically detailed in Section 7.2.

In the finite element simulation, efforts had been made to implement the vehicle operating conditions, human bone and muscle properties and seat foam material parameters as practical as possible, though, mismatches in-between the simulation results and testing data are inevitable. The potential reasons for mismatches have been discussed in detail in Section 7.3 and Section 7.4.

The absolute deviations of the simulation results from the testing data for the peak, average and rms magnitudes of vertical accelerations have been recorded in Table 38.

Table 38. Deviations of the simulation results from the testing data

Segment	Vertical vibration in terms of acceleration	Absolute deviation between accelerations from simulation and testing (mm/sec²)
Human: Head	Peak	0.86
	Average	0.06
	RMS	0.37
Human: Chest	Peak	0.10
	Average	0.13
	RMS	0.09
Human: Waist	Peak	0.27
	Average	0.12

Segment	Vertical vibration in terms of acceleration	Absolute deviation between accelerations from simulation and testing (mm/sec²)
Human: Upper Arm	RMS	0.12
	Peak	0.37
	Average	0.02
Human: Lower Arm	RMS	0.14
	Peak	0.03
	Average	0.13
Human: Thigh	RMS	0.05
	Peak	0.04
	Average	0.13
Human: Leg	RMS	0.01
	Peak	0.01
	Average	0.06
Seat: Headrest	RMS	0.01
	Peak	2.01
	Average	0.10
Seat: Backrest	RMS	0.69
	Peak	0.62
	Average	0.29
Seat: Cushion	RMS	0.23
	Peak	0.04
	Average	0.22
	RMS	0.07

Inside the finite element environment stiffness values, damping co-efficients, Young's moduli of the human parts, boundary conditions, load circumstances, contact mechanism and simulation steps had been allocated as explained in detail in the Section 3.5, Section

3.6, Section 5.3.1and Section 5.3.2. In contrast, testing data received from the real life vibration measurement process are greatly dependent on the signal processing system of the instruments used.

The reasons of the deviations occurred, have been theoretically investigated and explained in Section 7.3. The hypothetical clarification clearly showed that any minute amendment in any of the simulation parameters could alter the final output level of vibration by a great extent. Thus, the deviations between the results from computerized analysis and testing data are obvious. Similar kinds of mismatches have been found in past similar research studies as detailed in Section 7.4.

It has been observed in Section 7.3 that the results from the computerized analysis are more conservative in natures compared to the data gathered from testing. Hence, regardless of the justified amounts of mismatches between the values from simulation and testing, it can be concluded that this unique simulation methodology can successfully be implemented to anticipate the final levels of vibration inside the car seated human body and car seat to optimize the health, safety and comfort of human-car seat system.

9.3. Guideline for implementing this Unique Simulation Methodology in similar Industries

The outlined unique simulation methodology can effectively be implemented to similar kinds of industrial sectors to anticipate the final vibration levels inside human body portions, though manipulations and adjustments will be required in the execution process of simulation depending on the type of industry. Comprehensive stepwise instructions have been provided in CHAPTER 8 to use this unique simulation technique in other relevant fields. General international standards mentioned in Table 36 and basic equipments detailed in Table 37, can be followed regardless of the industry type, though, usage of industry specific guidelines and facilities will be more preferable. The main

challenges to utilize this unique simulation technique in other relevant industries can be pointed as:

- Assessing the operating medium e.g. car, bus, truck, train, aeroplane, helicopter, ship, boat etc. as detailed in Section 8.3.
- Assessing the operating environment as elaborated in Section 8.4.
- Assessing the type of seat as explained in Section 8.3

Starting from establishing CAD models for human body and seat up to the simulation post-processing, an all-inclusive industrial instruction has been provided through Section 8.5, Section 8.6, Section 8.7, Section 8.8, Section 8.9 and Section 8.10.

9.4. Overall Conclusions

This section draws the conclusions of the overall research work carried out in conjunction with the research questions highlighted in Section 1.1.6.

A unique finite element based simulation model has been developed for a car seated 50^{th} percentile male human driver in dynamic condition to predict the final levels of vibration at different locations of human body and car seat. The unique features of this simulation methodology are characterised as representing human portions through ellipsoidal bodies, assigning shape specific stiffness data to human segments, predicting final vibration data at various points of entire human-car seat assembly and eliminating the necessity of practical vibration measurement. For the car seat foam material both the hyper-elastic and viscoelastic properties had been assigned together and preferred contact mechanism at seat-human interfaces were allocated.

Prior to initiating the research study on the unique simulation methodology, different other methods e.g., theory based mathematical model using lumped mass method,

combination of lumped mass and finite element methods etc. had been explored and experimentally verified in CHAPTER 2. After comprehensive exploration of the existing technologies and critical literature review of the earlier investigations in the similar fields, a combination of most suitable practices have been implemented to develop the unique biodynamic simulation methodology for the car seated human body.

Frequency magnitudes at the various segments of human body and car seat had been evaluated from the simulation results to assess the effects of vertical vibration on the car seated human body. The obtained frequency values were appearing to be within the allowable ranges of natural frequencies of human organs as prescribed by ergonomic standards and explored by earlier biodynamic investigations. The frequency related past biodynamic research works have been detailed in Section 5.5, which show the evidence of the acceptability of the frequencies obtained from this unique simulation model. The input parameters of the simulation set up can be tuned as per recommendations given by other case studies in Section 7.4 to lower the frequency levels, hence, to optimize the health, comfort and safety of car seated human body.

Comparisons between the data received from finite element simulation and vibration testing are shown in CHAPTER 7. The validation process are based on the vertical accelerations values obtained from simulation and testing. For head, waist, upper arm, headrest and backrest the peak limits of simulation outcomes are higher than the corresponding limits of testing data. For chest, lower arm, thigh and cushion the upper limits of simulation results are higher than respective upper limits of testing data, while simulation bottom peaks are lower than respective testing data lower peaks. For human leg both the lower and upper peaks of testing data are higher than corresponding simulation results. Mismatches in-between the simulation results and testing data are unavoidable as cited by other similar research outcomes presented in Section 7.4. Absolute deviations of the simulation results from the testing data have been presented in Table 35 and the potential reasons for deviations have been clarified in Section 7.3 and Section 7.4. It has been observed that the vertical acceleration values from the finite

element simulation are more conservative in natures compared to the vertical acceleration values from practical testing, though, the frequencies related to the corresponding acceleration values from simulation are falling within the permissible ranges of natural frequencies of human body portions. This unique simulation methodology is yielding satisfactory results, however, the deviations between simulation outcomes and testing data can be minimised by further fine tunings of the simulation input parameters as described in Section 7.4.

Efforts had been made to run the simulation for initial 60 seconds by assigning contact mechanisms with frictional coefficients to mating the surfaces between human body and car seat. But, cause of the inadequacy of computer hardware memory, the simulation solver got terminated prematurely without providing any output. Therefore, the main challenges during the simulation phases were to run it in a standard configured computer system and obtain the desired results within reasonable timeframe. To avoid the necessity of highly advanced computer hardware system, the simulation set up had been made to be as non-robust as possible. For that purpose, human model had been simplified by constructing its parts through ellipsoidal bodies and tie-up constraints had been implemented to perform the contact mechanisms in between mating surfaces without the need of frictional coefficient. Furthermore, the running time of the simulation had been restricted to initial 10 seconds after the cars started moving from standstill state. The simplified simulation model worked flawless and provided all the data of interest without compromising the aim of this unique simulation based biodynamic research study.

This unique simulation methodology can be implemented in other similar industries with minor manipulations in the simulation set up conditions. The main challenges will be to assess the type of automotive, operating environment and type of seat. An industrial guideline containing step by step instructions has been prepared in CHAPTER 8 to execute this unique simulation technique in other relevant industries to anticipate vibration data as different points of human-seat assembly.

9.5. Scope of Improvement

This unique finite element based simulation technique accounts the vibration only in the vertical direction. For the economic commuting cars, the vibration primarily comes from the vertical direction, hence, this simulation methodology is very useful to monitor the vibration levels inside the standard cars. For the sport or racer type cars, the fore-aft vibration plays huge role on the health, safety and comfort of the human occupants inside. In case of accidental scenarios, the sidewise vibration needs to be assessed for the car to offer sufficient safety to the driver and passengers. For the completeness of this unique simulation system, it will be beneficial to consider vibrations in fore-aft and lateral directions, too. Combination of vertical, fore-aft and lateral vibrations will obviously provide a more realistic and comprehensive simulation set up, which can be implemented on any type of car and predict more accurate vibration data.

This simulation considers the vibration to be generated from the initial accelerating period of the car operating in smooth terrain. Practically, the car engine will contribute extra vibration and additional jerking from the interfaces of tyres and road will also appear, especially for the rough road surfaces. Incorporation of engine excitation and road surface condition is recommended to improve this finite element simulation to further advanced level.

To avoid the complexity in the simulation environment, efforts have been made to minimise the number of contact interfaces. To achieve this, the metallic frames underneath the car seat and car body structure have been ignored and fixed boundary condition has been implemented at the underside of the modelled seat. For more effective vibration transmission from the car body to seat through the metallic frame, it is advised to model the car body frame and metallic frame underneath the seat.

Currently, each human portion has been modelled using single ellipsoidal body to calculate the shape and size specific three dimensional stiffness data. It is recommended

to split each of the human ellipsoidal segments into multiple smaller ellipsoids to form real anatomical human geometry and evaluate the three dimensional stiffness parameters for each of the smaller ellipsoids separately. This method will involve time consuming manual efforts, however, eventually will yield very accurate stiffness values for the human portions.

Cause of the inaccessibility of the computer system with adequate hardware memory, the simulation running time has been limited to initial 10 seconds. It suggested to run this unique finite element simulation set up in a highly configured computer system for 60 seconds to investigate the vibration outcomes in more detail.

REFERENCES

Abbas, W., Abouelatta, O.B., El-Azab, M., Elsaidy, M. and Megahed, A.A. (2010). Optimization of Biodynamic Seated Human Models using Genetic Algorithms. *Scientific Research*, 2, pp. 710-719.

Adams, D., Morgan, G.B., Nghi, T., Salloum, M.J. and O'Bannon, T. (1999). Creating a biofidelic seating surrogate. *SAE Conference*, 1999-01-0627.

Ahmadian, M., Seigler, T.M., Clapper D. and Sprouse, A. (2002). Alternative test methods for long term dynamic effects of vehicle seats. *SAE Conference,* 2002-01-3082.

Alderson, K. L., Webber, R.S. and Evans, K.E. (2000). Novel variation in the microstructure of auxetic microporous ultra high molecular weight polyethylene, Part 2: Mechanical properties, *Polymer Engineering & Science*, 40 (8), pp.1906-1914.

American Society for Testing Materials. (2003). D3574 – 01. Standard Test Methods for Flexible Cellular Materials. *In Annual Book of ASTM Standards. ASTM International, West Conshohocken, PA*.

American Society for Testing Materials. (2008). D4168-95. Standard test methods for transmitted shock characteristics of foam-in-place cushioning materials. *In Annual Book of ASTM Standards. ASTM International, West Conshohocken, PA*.

American Society for Testing Materials. (2007). D5024: Standard test methods for plastics: Dynamic mechanical properties: In compression. *In Annual Book of ASTM Standards. ASTM International, West Conshohocken, PA*.

American Society for Testing Materials. (2009). D5112-98. Standard test method for vibration (horizontal linear motion) test of products. *In Annual Book of ASTM Standards. ASTM International, West Conshohocken, PA*.

American Society for Testing Materials. (2010). D3580-95. Standard test methods for vibration (vertical linear motion) test of products. *In Annual Book of ASTM Standards. ASTM International, West Conshohocken, PA*.

References

American Society for Testing Materials. (2011). D1596-97. Standard test method for dynamic shock cushioning characteristics of packaging material. *In Annual Book of ASTM Standards. ASTM International, West Conshohocken, PA*.

Amirouche, F. M. L. and Ider. S. K. (1988). Simulation and analysis of a biodynamic human model subjected to low accelerations – a correlation study. *Journal of Sound and Vibration*, 123 (4), pp. 281–292.

Andreoni, G., Santambrogio, G.C., Rabuffetti, M. and Pedotti, A, (2002). Method for the analysis of posture and interface pressure of car drivers. *Applied Ergonomics*, 33, pp.511–522.

Arvidson, J. M., Sparks, L. L. and Guobang, C. (1983). National Bureau of Standards. *Tensile, compressive and shear properties of a 65-kg/m3 polyurethane foam at low temperatures*.

Ashby, P. (1975) Ergonomics handbook 1: Human factors design data: Body size and strength. Pretoria: Tute Publication.

automotive.com/uploads/media/Schumacher_0_1311324313_rec_gp_am_gb.pdf [Accessed 22 Mar. 2018].

Bader, D.L. and Bowker, P. (1983). Mechanical characteristics of skin and underlying tissues in vivo. *Biomaterials*, 4, pp. 305-308.

Baik, S., Lee, J. and Suh, J. (2003). A study on the characteristics of vibration in seat system. *SAE Paper*, 3.

Banks, H., Negash, G. and Gaitens, M. (2007). Multiscale considerations in modeling of nonlinear elastomers. *International Journal for Computational Methods in Engineering Science and Mechanics*, 8(2), pp. 53-62.

Bansal, H. (2013). Mathematical validation of Eigen values and Eigen vectors of different human body segments in sitting posture. *MEng. Thesis, Thapar University*.

Basri, B, and Griffin, M. J. (2011).The vibration of inclined backrests: perception and discomfort of vibration applied normal to the back in the x–axis of the body, *Journal of Sound and Vibration*, 330, pp. 4646–4659.

Batt, G. (2013). Primary Resonance Behavior of Expanded Polymer Cushion Material under Low-Intensity Harmonic Excitations. *A Dissertation Presented to the Graduate School of Clemson University*, pp. 17-21.

Benson, B.R., Smith, G.C., Kent, K.W. and Monson, C.R. (1996). Effects of seat stiffness in out-of-position occupant response in rear-end collisions. *Proceedings of the 40th Stapp Car Crash Conference 1996*, SAE no 962423. pp 331-344.

References

Berkson, M.H., Nachemson, A. and Schultz, A.B. (1979). Mechanical properties of the human lumbar spine motion segments – Part II: Responses in compression and shear; influence of gross morphology. *Journal of Biomechanical Engineering*, 101, pp 53-57.

Besnault, B., Guillemot, H., Robin, S., Lavaste, F. and Le Coz, J-Y. (2008). A parametric finite element model of the human pelvis. *Proceedings of the 42nd STAPP Car Crash Conference*, SAE paper no 983147, pp. 33- 46.

Boileau, P.E. and Rakheja, S. (1998). Whole-body vertical biodynamic response characteristics of the seated vehicle driver measurement and model development. *International Journal of Industrial Ergonomics*, 22, pp. 449-472.

Bosboom, E.M.H., Hesselink, M.K.C., Oomens, C.W.J., Bouten, C.V.C., Drost, M.R. and Baaijens, F.P.T. (2001). Passive transverse mechanical properties of skeletal muscle under in vivo compression. *Journal of Biomechanics*, 34, pp. 1365-1368.

Boshuizen, H.C., Bongers, P.M. and Hulshof, C.T. (1992). Self reported back pain in forklift truck and freight container tractor drivers exposed to whole body vibrations. *Spine*, 17(1), pp. 59-65.

Bovenzi, M. and Zaidini, A. (1992). Self-reported low back pain symptoms in urban bus drivers exposed to whole body vibrations. *Spine*, 17(9), pp. 1048-1059.

Bovenzi, M. and Hulshof, C.T.J. (1998). An updated review of epidemiologic studies on the relationship between exposure to whole-body vibration and low back pain. *Journal of Sound and Vibration*, 215 (4), pp. 595-612.

Brooks, R. M. (2012). Acceleration characteristics of vehicles in rural Pennsylvania. *IJRRAS*, 12 (3), pp. 449-453.

Brienza, D., Chung, K., Brubaker, C., Wang, J., Karg, T. and Lin, C. (1996). A system for the analysis of seat pressure support surfaces using surface shape control and simultaneous measurement of applied pressures. *IEEE transactions on rehabilitation engineering*, 4(2), pp. 103-113.

Brosh T. and Arcan, M. (2000). Modeling the body/chair interaction – an integrative experimental–numerical approach. *Clinical Biomechanics*, 15, pp. 217-219.

Brouwn, G.G. (2000). Postural control of the human arm. *PhD-thesis*, *Delft University of Technology*.

Brown, N. & Keeley, S. (1997). *Asking the Right Questions: A Guide to Critical Thinking.* Pearson: London, ISBN: 0131829939.

Bubb, H. and Estermann, S. (2000). Influences of forces on comfort feeling in vehicles. *SAE Conference*, SAE no 2000-01-2171.

References

Buck, B. and Woelfel, H. P. (1998). Dynamic Three-Dimensional Finite Element Model of a Sitting Man with a Detailed Representation of the Lumbar Spine and Muscles. *Computer Methods in Biomechanics and Biomedical Engineering*, 2, pp. 379-386, 1998.

Burdzik, R. and Konieczny, L. (2014). Vibration Issues in Passenger Car. *Silesian University of Technology*, 9(3), p. 83-90.

Caddock, B.D. and Evans, K.E. (1989). Microporous materials with negative Poisson's ratio: I. Microstructure and mechanical properties, *Journal of Physics*, 22(12), pp. 1877-1882.

Camprubí, N. and Rueda, F. (2007). Comfort Evaluationof Foam SeatsUsing Realistic Simulation. Advanced Design & Analysis Division.

Camprubí, N., Rueda, F. and Alonso, I. (2007). Numerical Simulation in the Design Process of Foam Seats for the Automotive Industry. *ABAQUS Users' Conference*, pp. 1-15.

carsoda.com, (2017). *Steering Wheels Size Chart*. [online] Available at: https://www.carsoda.com/blogs/news/92683075-steering-wheels-size-chart [Accessed 9 Oct. 2017].

Cempel, C. (1989). Applied vibroacustic. *PWN*, Warsaw.

Cengiz, T.G. (2014). A pilot study for defining characteristics of Turkish women via anthropometric measurements. *Work*, 49 (4), pp. 713–722.

Chaffm, D.B. and Anderson, G.B. (1991). Occupational Biomechanics (2nd ed.), Wiley-Interscience, New York, NY.

Chan, N. and Evans. (1997). Microscopic examination of the microstructure and deformation of conventional and auxetic foams, *Journal of Materials Science*, 32 (21), pp.5725-5736.

Chagnon, G., Marckmann, G., Verron, E., Gornet, L., Charrier, P. and Ostoja-Kuczynski, E. (2002). A new modelling of the Mullins effect and the viscoelasticity of elastomer based on a physical approach. *Proceedings of the International Rubber Conference*. Prague, Czech Republic.

Chen, E.J., Novakofski, J., Jenkins, W. K.and O'Brien, W.D. (1996). Young's Modulus Measurements of Soft Tissues with Application to Elasticity Imaging. *IEEE transactions on ultrasonics, ferroelectrics, and frequency control*, 43(1), pp. 191-194.

Cheung, M. and Zhang, M. (2006). Finite Element Modeling of the Human Foot and Footwear. *ABAQUS Users' Conference*, pp. 145-159.

Cho, Y. and Yoon, Y. S. (2001). Biomechanical model of human on seat with backrest for evaluating ride quality. *International Journal of Industrial Ergonomics*, 27 (2001), pp. 331–345.

Cho, Y., Yoon, Y. S. and Park, S.J. (2000). Determination of seat sponge properties with estimated biodynamic model. *SAE Conference 2000*, SAE no 2000-01-0640.

Choi, H. Y., Han, M, Hirao, A. and Matsuoka, H. (2017). Virtual Occupant Model for Riding Comfort Simulation. *Proceedings of the 12th International Modelica Conferenc*e. pp. 27-34.

Chow, W.W. and Odell, E.I. (1978). Deformations and stresses in soft body tissues of a sitting person. *Journal of Biomechanical Engineering*, 100, pp. 79-87.

Corbridge, C, Griffin, M.J, and Harborough, P. (1989). Seat dynamics and passenger comfort. *Institute of Mechanical Engineers Part F: Journal of Rail and Rapid Transit*, 203, pp. 57–64.

Cottrell, S. (2005). *Critical Thinking Skills*. Palgrave: Basingstoke; ISBN: 1-4039-9685-7.

Crichton, M. L., Chen, X., Huang, H. and Kendall, M. A. F. (2013). Elastic modulus and viscoelastic properties of full thickness skin characterised at micro scales. *Biomaterials*, 34, pp. 2087-2097.

Cunningham, A., Huygens, E. and Leenslag, J. W. (1994). MDI comfort cushioning for automotive applications, *Cellular Polymers*, 13 (6), pp. 461–472.

Czysz, H. J. (1986). Experimentelle Untersuchungen an Polyurethan-Integralweichschaum zur Bestimmung von Kennwerten zu Berechnungsgrundlagen. *PhD Thesis, Universitat der Bundeswehr Hamburg*.

Dabnichki, P.A., Crocombe, A.D. and Hughes, S.C. (1994). Deformation and stress analysis of supported buttock contact. *Proceedings of the Institution of Mechanical Engineers*, *Journal of Engineering in Medicine*, 208, pp. 9-17.

Dae-Eun Hyun, Seung-Hyun Yoon, Myung-Soo Kim, and Bert Juttler. (2003). Modeling and Deformation of Arms and Legs Based on Ellipsoidal Sweeping. *Proceedings of the 11th Pacific Conference on Computer Graphics and Applications*.

Dalstra, M., Huiskes, R. and Erning, L. (1995). Development and validation of a three dimensional finite element model of the pelvis bone. *Journal of Biomechanical Engineering*, 117, pp. 272-278.

Delleman, N.J. (1999). Working postures – prediction and evaluation. *PhD-thesis, Vrije Universiteit, Amsterdam (The Netherlands)*.

References

Deng, R., Davies. P. and Bajaj, A. K. (2002). Flexible polyurethane foam modelling and identification of viscoelastic parameters for automotive seating applications. *Journal of Sound and Vibration*, 264, pp. 391–417.

Duthie, G. M., Pyne, D. B., Hopkins, W. G., Livingstone, S. and Hooper, S. L. (2006). Anthropometry profiles of elite rugby players: quantifying changes in lean mass. *Br J Sports Med*, 40, pp. 202-207.

Ebe, K. and Griffin, M.J. (1994). Effect of polyurethane foam on dynamic sitting comfort. *Proceedings of Inter Noise 94, Yokohama, Japan*, pp. 9338926.

Ebe, K. and Griffin, M.J. (2001). Factors affecting static seat cushion comfort. *Ergonomics*, 44, pp. 901–921.

Ehlers, W. and Markert, B. (2001). Viscoelastic polyurethane foams at finite deformations. *Trends in Computational Structural Mechanics*, (2001), pp. 249–256.

element.com, (2018). *Element's Official Website*. [online] Available at: https://www.mpihome.com/en/industries/automotive.html [Accessed 13 Jul. 2018].

El-Khatib, A. and Guillon, F. Lumbar (2001). Intradiscal pressure and whole-body vibration –first results. *Clinical Biomechanics*, 16(1), pp. S127-S134.

Evans, K.E. (1990). Tailoring the negative Poisson's ratio, *Chemical Ind*., 20, pp.654-657.

Evans, K.E., Nkansah, M.A., Hutchinson, I.J. and Rogers, S.C. (1991). Molecular network design, *Nature*, 353, pp.124.

Ezenwa, B. and Yeoh, H. T. (2011). Multiple vibration displacements at multiple vibration frequencies stress impact on human femur computational analysis. *Journal of Rehabilitation Research & Development*, 48(2), pp. 179-189.

Fairley, T.E. and Griffin, M.J. (1986). A test method for the prediction of seat transmissibility. *Society of Automotive Engineers International Congress and Exhibition*, 860047.

Fairley, T.E. and Griffin, M.J. (1989). The apparent mass of the seated human body: vertical vibration. *Journal of Biomechanics*, 22(2), pp. 81–94.

Fairley, T.E. and Griffin, M.J. (1990). The apparent mass of the seated human body in the fore–and–aft and lateral direction. *Journal of Sound and Vibration*, 139(2), pp. 299–306.

Fang, B. (2013). CAE Methods on Vibration-Based Health Monitoring Of Power Transmission Systems. *A Thesis Presented to The Faculty of California Polytechnic State University*, pp. 50-88.

Fritz, M. (2000). Description of the relation between the forces acting in the lumbar spine and whole-body vibrations by means of transfer functions. *Clinical Biomechanics*, 15, pp. 234-240.

Frost III, B.L., Hubbard, R.P. and Boughner, R.L. (1997). Development of back contours for automobile seat design. *SAE Conference*, SAE no 970590.

Fung, Y.C. (1968). Foundations of Solid Mechanics, Prentice-Hall.

Gibson, L.J. and Ashby, M.F. (1988). Cellular Solids: Structure and Properties, Pergamn Press, London.

Gibson, L. J., Ashby, M. F., Schajer, G. S. and Robertson, C. I. (1982). The mechanics of two dimensional cellular materials, *Proceedings of The Royal Society of London*, 382, pp.25-42.

Gordon, C. C., Churchill, T., Clauser, C. E., Bradtrniller, B., McConville, J. T., Tebbetts, I. and Walker, R. A. (1989).1988anthropometric survev of U.S. Army personnel: Methods and summary statistics. Final report (NATICWR- 891027).Natick, MA: U.S. Army Natick Research, Development and Engineering Center.

Gottlieb, G. L., Agarwal, G. C. and Penn, R. (1978). Sinusoidal oscillation of the ankle as a means of evaluating the spastic patient. *J Neurol Neurosurg Psychiatry*, 41(1), pp. 32-39.

Grandjean, E. (1980). Sitting posture of car drivers from the point of view of ergonomics. In D.J. Oborne and J.A. Levis (eds.), Human Factors in Transport Research. *User Factors: Comfort, the Environmentand Behaviour*, 2, pp. 205-213. New York: Academic Press.Gyi, D.E. and Porter, J.M. (1999). Interface pressure and the prediction of car seat discomfort. *Applied Ergonomics*, 30, pp. 99-107.

Green, A. E. and Adkins, J. E. (1970). Oxford University Press. *Large Elastic Deformations*, 2nd Ed.

Griffin, M. J. (1990). Handbook of human vibration. Academic press, *London: Academic Press Limited*. ISBN 0–12–303040–4.

Griffin, M. J. (2001). The validation of biodynamic models, *Clinical Biomechanics*, 16, pp. 81-92.

Grujicic, M., Pandurangan, B., Arakere, G., Bell, W.C., He, T. and Xie, X. (2009), Seat-cushion and soft-tissue material modeling and a finite element investigation of the seating comfort for passenger-vehicle occupants. *Materials and Design*, 30, pp. 4273-4285.

Grujicic, M., Bell, W. C., Arakere, G. and Haque, I. (2009). Finite element analysis of the effect of up-armouring on the off-road braking and sharp-turn performance of a high-

mobility multi-purpose wheeled vehicle. *Proceedings of The Institution of Mechanical Engineers Part D-journal of Automobile Engineering - PROC INST MECH ENG D-J AUTO. 223. 1419-1434. 10.1243/09544070JAUTO1187*.

Guo, L.X., Zhang, Y.M. and Zhang, M. (2011). Finite Element Modeling and Modal Analysis of the Human Spine Vibration Configuration. *IEEE Transactions on Biomedical Engineering*, 58(10), pp. 2987-2990.

Haan, R. (2002). FE model of a car seat. *Netherlands Organisation for Applied Scientific Research*, pp. 9-12.

Harsha, S. P., Desta, M., Prashanth, A. S. and Saran, V. H. (2014). Measurement and bio-dynamic model development of seated human subjects exposed to low frequency vibration environment. *International Journal of Vehicle Noise and Vibration*, 10 (1-2), pp. 1-24.

Hartmann, S.; Haupt, P. and Tschope, T. (2001). Parameter identification with a direct search method using finite elements. *Constitutive Models for Rubber II*, pp. 249–256.

Hartung, J., Mergl, C., Henneke, C., Madrid-Dusik, R and Bubb, H. (2004). Measuring Soft Tissue Compliance of the Human Thigh. SAE Technical Paper Series 2004-01-2158.

havcontrol.co.uk, (2018). *HAV Control Limited's Official Website*. [online] Available at: https://www.havcontrol.co.uk/havi-hand-arm-vibration-monitor.html?gclid=EAIaIQobChMI1Lvego6d3AIVSLDtCh3muAEPEAQYASABEgIXF_D_BwE [Accessed 13 Jul. 2018].

havcontrol.co.uk, (2018). *HAV Control Limited's Official Website*. [online] Available at: https://www.havcontrol.co.uk/larson-davis-hvm100-hav-meter.html [Accessed 13 Jul. 2018].

Hellman, A. (2008). Simulation of complete vehicle dynamics using FE code Abaqus. *MSc Thesis- Luleå University of Technology*, pp. 19-31.

Hendriks, F.M., Brokken, D., Oomens, C.W.J., Baaijens, F.P.T. and Horsten, J.B.A.M. (2003). A Numerical-experimental method to characterise the non-linear mechanical behaviour of human skin. *Skin Research and Technology*, 9, pp. 274-283.

Hertzberg, H.T.E. (1972). The human buttocks in sitting: pressures, patterns and palliatives. *SAE Conference*, SAE no 720005.

Hilyard, N. C., Collier, P. and Care, C. M. (1984). Influence of mechanical properties of cellular plastic cushioin materials on ride comfort. *Conference on 'Dynamics in Automotive Engineering' held at Cranfield Institute of Technology*, Cranfield, Bedford.

Himmetoglu, S., Acar, M., Bouazza-Marouf, K. and Taylor, A. (2009). A multi-body human model for rear-impact simulation. *Proceedings of the IMechE, Part D: Journal of Automobile Engineerin*g, 223(5), pp. 623-638.

Hin, B., Blüthner, R., Menzel, G., Rützel, S., Seidel, H. and Wölfel, H. P. (2006). Apparent mass of seated men – Determination with single– and multi–axis excitations at different magnitudes. *Journal of Sound and Vibration*, 298, pp. 788–809.

Hinz, B., Bluethner, R., Menzel, G. and Seidel, H. (1993). Estimation of disc compression during transient whole-body vibration. Clinical Biomechanics, 9(4), pp. 263-271.

Hinz, B. and Seidel, H. (1987). The non-linearity of the human body's dynamic response during sinusoidal whole body vibration. *Industrial Health*, 25, pp. 169-181.

Hinz, B., Seidel, H., Braeuer, D., Menzel, G., Bluethner, R. and Erdman, U. (1988). Examination of spinal column vibrations: a non-invasive approach. *European Journal of Applied Physiology*, 57, pp. 707-713.

Holmlund, P., Lundstrom, R. and Lindberg, L. (2000). Mechanical impedance of the human body in vertical direction. *Applied Ergonomics*, 31 (4), pp. 415–422.

Hong, K.T., Hwang, S.H. and Hong, K.S. (2003). Automotive Ride-Comfort Improvement with an Air Cushion Seat. *SICE Annual Conference*, 1(3), pp. 2043-2048.

Horst, M.J. (2002). Human head neck response in frontal, lateral and rear end impact loading – modelling and validation. *PhD-thesis, Eindhoven University of Technology*.

Houghton, T. J. C. (2003). The effect of backrest inclination on the transmission of vertical vibration through an antomotive seat. In: *Processdings of the 38th UK conference on the human response to vibration*, 17–19 September, Institute of Naval Medicine, Gosport, England.

Huang, Y. and Griffin, M. J. (2006). Effect of voluntary periodic muscular activity on nonlinearity in the apparent mass of the seated human body during vertical random whole–body vibration. *Journal of Sound and Vibration*, 298 (3), pp. 824–840.

Hu, H., Li, Z., Yan, J., Xiao, H., Duan, J. and Zenga, Li. (2007). Anthropometric measurement of the Chinese elderly living in the Beijing area. *Journal of Industrial Ergonomics*, 37(4), pp. 303-311.

Huang, Y. and Griffin, M. J. (2008). Non–linear dual–axis biodynamic response of the semi–supine human body during vertical whole–body vibration. *Journal of Sound and Vibration*, 312 (1–2), pp. 296–315.

References

Hubbard, R.P., Haas, W.A., Boughner, R.L., Canole, R.A. and Bush, N.J. (1993). New biomechanical models for automobile seat design. SAE Technical Paper Series 930110.

Hulshof, C. and Zanten, B.V. (1987). Whole-body vibration and low back pain. A review of epidemiologic studies. *International Archives of occupational and Environmental Health*, 59, pp. 205-220.

Hilyard, N. C. (1982). Mechanics of Cellular Plastics. New York: Macmillan.

International Organization for Standardization. (1994). Mechanical vibration – aboratory method for evaluating vehicle seat vibration – Part 1: *Basic requirements. ISO10326–1*.

International Organisation for Standardization. (1997). Guide for the evaluation of human exposure to whole body vibration. *ISO 2631–1*.

International Organisation for Standardization. (2001). Mechanical vibration and shock—range of idealized values to characterise seated–body biodynamic response under vertical vibration. *ISO 5982*.

International Organisation for Standardization (2008) Flexible Cellular Polymeric Materials – Determination of Hardness (Indentation Technique). *ISO 2439*.

Ippili, R. K., Davies, P., Bajaj, A. K. and Hagenmeyer, L. (2008). Nonlinear multi–body dynamic model of seat–occupant system with polyurethane seat and H–point prediction. *International Journal of Industrial Ergonomics*, 38, pp. 368–383.

Ittianuwat, R, Fard, M. and Kato, K. (2014). The Transmission of Vibration at Various Locations on Vehicle Seat to Seated Occupant Body. *Inter-Noise*, pp. 1-12.

Jalil, N. A. A. and Griffin, M. J. (2007). Fore–and–aft transmissibility of backrests: Effect of backrest inclination, seat–pan inclination, and measurement location, *Journal of Sound and Vibration*, 299, pp. 99–108.

Jalil, N. A. A. and Griffin, M. J. (2007). Fore–and–aft transmissibility of backrests: Variation with height above the seat surface and non–linearity, *Journal of Sound and Vibration*, 299, pp. 109–122.

James, A. G. and Green, A. (1975). Strain energy functions of rubber. ii the characterization of filled vilcanisates. *Journal of Applied Polymer Science,* 19, pp. 2033–2058.

Jarfelt, U.; Ramnäs, O. (2006). Thermal conductivity of polyurethane foam Best performance. *Proceedings of the 10th International Symposium on District Heating and Cooling, Hannover, Germany*, 3–5 Sep; pp. 1–12.

Jhinkwan, A. and Singh, J. (2014). Design Specifications and Ergonomic Evaluation of Car Seat (A Review). *International Journal of Engineering Research & Technology (IJERT)*, 3 (5), pp. 611-613.

Joshi, G., Bajaj, A. K. and Davies, P (2010). Whole–body Vibratory Response Study Using a Nonlinear Multi–body Model of Seat–occupant System with Viscoelastic Flexible polyurethane Foam. *Industrial Health*, 48, pp. 663–674.

Ju, M.L., Jmal, H., Dupuis, R. and Aubry, E. (2013). Visco-hyperelastic model for polyurethane foam: comparison among Polynomial, Reduced polynomial, and Ogden models. In: *21ème Congrès Français de Mécanique*, 26 au 30 août, Laboratoire MIPS, Mulhouse, France.

Ju, M.L., Jmal, H., Dupuis, R. and Aubry, E. (2014). Visco-hyperelastic constitutive model for modeling the quasi-static behavior of polyurethane foam in large deformation. *Polymer Engineering and Science*, 55 (8), pp.1795-1804.

Kamalakar, G. B. and Mitra, A. c. (2017). Development and Analysis of Human Hand-Arm System Model for Anti-Vibration Isolators. *Materialstoday*, 5(2), pp. 3943-3952.

Kasra, M., Shirazi, A. and Drouin. A. (1992). Dynamics of human lumbar intervertebral joints. Experimental and finite-element investigations. *Spine*, 17(1), pp. 93-102.

Keegan, J. J. (1964). The medical problem of lumbar spine flattening in automobile seats. SAE Technical Paper 838A. New York, NY: Society of Automotive Engineers, Inc.

Kim, S.K., White, S.W., Bajaj, A.K. and Davies, P. (2003). Simplified models of the vibration of mannequins in car seats. *Journal of Sound and Vibration*, 264 (2003), pp. 49–90.

Kim, T., Cho, Y., Yoon, Y. and Park, S. (2001). Dynamic Ride Quality Investigation and DB of Ride Values for Passenger and RV Cars. *SAE Technical Paper*, 01, pp. 0384.

Kim, T. H., Kim, Y. T. and Yoon, Y. S. (2005). Development of a biomechanical model of the human body in a sitting posture with vibration transmissibility in the vertical direction. *Industrial Ergonomics*, 35 (9), pp. 817–829.

Kim, D., Yoon, W., Park, H., Kim, H. and Park, J. (2013). Measurement of dynamic viscoelastic properties of flexible polyurethane foam under compression for application to seat vibration analysis. *The Journal of the Acoustical Society of America*, 134, pp. 4103–4112

Kitazaki, S. and Griffin, M.J. (1995). A data correction method for surface measurement of vibration on the human body. *Journal of Biomechanics*, 28(7), pp. 885-890.

Kitazaki, S. and Griffin, M.J. (1997).A modal analysis of whole body vertical vibration, using a finite element model of the human body. *Journal of Sound and Vibration*, 200(1), pp. 83-103.

Kitazaki, S. and Griffin, M.J. (1998). Resonance behaviour of the seated human body and effects of posture. *Journal of Biomechanics*, 31(1998), pp. 143-149.

Kolich, M., Essenmacher, S. D. and McEvoy, J. T. (2005). Automotive seating: the effect of foam physical properties on occupied vertical vibration transmissibility. *Journal of Sound and Vibration*, 281, pp. 409–416.

Kondo, T. and Ito, Y. (2002). Predicting ride comfort on seat using explicit FEM code. SAEConference 2002, SAE no 2002-01-0779.

Konieczny, A. (2016). Analysis of Simplifications Applied in Vibration Damping Modelling for a Passive Car Shock Absorber. *Hindawi Publishing Corporation Shock and Vibration*, 2016(6182847), pp. 1-9.

Konosu, A. (2003). Development of a Biofidelic Human Pelvic FE-Model with Several Modifications onto a Commercial Use Model for Lateral Loading Conditions. SAE Technical Paper Series 2003-01-0163.

Kovacevc, S., Vucinic, J., Kirin, S. and Pejnovic, N. (2010). Impact of anthropometric measurements on ergonomic driver posture and safety. *Periodicum Biologorum*, 112 (1), pp. 51-54.

Lacquaniti, F., Licata, F. and Soechting, J. F. (1982). The mechanical behavior of the human forearm in response to transient perturbations. *Journal of Biological Cybernetics*, 44(1), pp. 35-46.

Lakes, R.S. (1987a). Foam structures with a negative Poisson's ratio, *Science*, 235, pp.1038-1040.

Lakes, R.S. (1987b). Polyhedron cell structure and method of making same, *Int. Patent Publication Number- WO88/00523*.

Lakes, R. S. and Lowe, A. (2000). "Negative Poisson's ratio foam as seat cushion material", *CellularPolymers*, 19, pp. 157-167.

Lakušić, S., Brčić, D. and Lakušić, V.T. (2011). Analysis of Vehicle Vibrations – New Approach to Rating Pavement Condition of Urban Roads. *Promet – Traffic&Transportation*, 23(6), pp. 485-494.

Leva, P. (1996). Adjustments to Zatsiorsky-Seluyanov's Segment Inertia Parameters. *Journal of Biomechanics*, 29 (9), pp. 1223-1230.

Lewis, C. H. and Griffin, M. J. (2002). Evaluating vibration isolation of soft seat cushions using an active anthropodynamic dummy. *Journal of Sound and Vibration*, 253, pp. 295–311.

Li, K., Zheng, L., Tashman, S., and Zhang, X. (2012). The inaccuracy of surface-measured model-derived tibiofemoral kinematics. *Journal of Biomechanics*, 45(15), pp. 2719-2723.

Liang, C. C. and Chiang, F. C. (2008). Modelling of a seated human body exposed to vertical vibrations in various automotive postures. *Industrial Health*, 46, pp. 125–167.

Liu, C., Qiu, Y. and Griffin, M. J. (2012). A finite–element model of the vertical in–line and fore–and–aft cross–axis apparent mass and transmissibility of the human body sitting on a rigid seat and exposed to vertical vibration. *Proceedings of the 47th UK conference on the human response to vibration*, 17–19 September, University of Southampton, Southampton, England.

Lo, L., Fard, M., Subic, A. and Jazar, R. (2013). Structural dynamic characterization of a vehicle seat coupled with human occupant. *Journal of Sound and Vibration*, 332, pp. 1141–1152.

Lowe, L. and Lakes, R. S. (2000). Negative Poisson's Ratio Foam as Seat Cushion Material. *Cellular Polymer*s, 19, pp. 157-167.

Macias, N., Quezada, A. D., Flores, M., Valencia, M. E., Denova-Gutiérrez, E,,Quiterio-Trenado, M., Gallegos-Carrillo, K., Barquera, S. and Salmerón, J. (2014). Accuracy of body fat percent and adiposity indicators cut off values to detect metabolic risk factors in a sample of Mexican adults. *BMC Public Health,* 14(1), 341 doi: 10.1186/1471-2458-14-341.

Majumder, J. (2014). Anthropometric dimensions among Indian males — A principal component analysis. *Euras J Anthropol*, 5(2), pp. 54−62.

Mansfeld, N.J. and Griffin, M.J. (2000). Non-linearities in apparent mass and transmissibility during exposure to whole-body vertical vibration. *Journal of Biomechanics*, 33(2000), pp. 933-941.

Mansfield, N. J. and Griffin, M. J. (2002). Effects of posture and vibration magnitude on apparent mass and pelvis rotation during exposure to whole–body vertical vibration. *Journal of Sound and Vibration*, 253 (1), 93 – 107.

Mansfield, N. J., Lundstrom, R., Lenzuni, P. and Nataletti, P. (2006). Effect of vibration magnitude, vibration spectrum and muscle tension on apparent mass and cross axis transfer functions during whole–body vibration exposure. *Journal of Biomechanics*, 39, pp. 3062–3070.

Mansfield, N. J. and Maeda, S. (2006). Comparison of the apparent masses and cross–axis apparent masses of seated humans exposed to single and dual–axis whole–body vibration. *Journal of Sound and Vibration*, 298 (3), pp. 841–853.

Marshall, R.J., Altamore, P.F. and Hartley, D. (2000). Dynamic analysis of crew seats and cockpit interiors. SAE Conference 2000, SAE no 2000-01-1674.

Massidda, M., Toselli. S., Brasili, P. and Caló, M. C. (2013). Somatotype of elite Italian gymnasts. *Collegium antropologicum - PubMed*, 37(3), pp. 853-857.

Matsumoto, Y. and Griffin, M. J. (1998a), Movement of the upper–body of seated subjects exposed to vertical whole–body vibration at the principal resonance frequency. *Journal of Sound and Vibration*, 215 (4), pp. 743 –762.

Matsumoto, Y. and Griffin, M. J. (1998b). Dynamic response of the standing human body exposed to vertical vibration: influence of posture and vibration magnitude. *Journal of Sound and Vibration*, 212 (1), pp. 85–107.

Matsumoto, Y., Griffin, M.J. (2001). Modelling the dynamic mechanisms associated with the principal resonance of the seated human body. Clinical Biomechanics, Vol. 16, No. 1, pp. S31-S44.

Matsumoto, Y. and Griffin, M. J. (2002) Non–linear characteristics in the dynamic responses of seated subjects exposed to vertical whole–body vibration, *Journal of Biomechanical Engineering*, 124, pp. 527 – 532.

McKee, C.T., Last, J. A., Russell, P. and Murphy, C.J. (2011). Indentation Versus Tensile Measurements of Young's Modulus for Soft Biological Tissues. *Tissue Engineering: Part B*, 17(3). pp. 155-164.

Mehar, A., Chandra, S. and Velmurugan, S. (2013). Speed and Acceleration Characteristics of Different Types of Vehicles on Multi-Lane Highways. *European Transport \ Trasporti Europei*, 55, pp. 1-12.

Mergl, C., Anton, T., Madrid-Dusik, R., Hartung, J., Librandi, A. and Bubb, H. (2004). Development of a 3D Finite Element Model of Thigh and Pelvis. SAE Technical Paper Series 2004-01-2132.

Milivojevich, A., Blair, G. R., Pageau, J. G. and Van-Heumen, J. D. (1999). Automtotive seating comfort; defining comfort properties in Polyurethane Foam. *Society of Automotive Engineering*, 01, pp. 1-10.

Mills N. J. (2007). Polymer Foams Handbook: Engineering and Biomechanics Applications and Design Guide. Butterworth-Heinemann.

References

Mills, N. J. and Gilchrist, A. (2000). Modelling the indentation of low density polymers foams. *Cellular Polymers*, 19, pp. 389–412.

Mircheski, I., Kandikjan, T. and Sidorenko, S. (2014). Comfort analysis of vehicle driver's seat through simulation of the sitting process. *Analiza udobnosti vozačeva sjedala simulacijom postupka sjedanja*, 21(2), pp. 291-298.

Mirzaali, M. J., Schwiedrzik, J. J., Thaiwichai, S., Best, J.P. and Michler, J. (2016). Mechanical properties of cortical bone and their relationships with age, gender, composition and microindentation properties in the elderly. *Bone*, 93, pp. 196-211.

Moens, C.C.M. and Horvath, I. (2002). Finite elements model of the human body: geometry and non-linear material properties. *Proceedings of the TMCE 2002*.

Muksian, R. and Nash, C. D. (1974). A model for the response of seated humans to sinusoidal displacements of the seat. *Journal of Biomechanics*, 9, pp. 339–342.

Murakami, D., Kitagawa, Y., Kobayashi, S., Kent, R. and Crandall, J (2004). Development and Validation of a Finite Element Model of a Vehicle. SAE Technical Paper Series 2004-01-0325.

Nawayseh, N. and Griffin, M. J. (2003). Non–linear dual–axis biodynamic response to vertical whole–body vibration, *Journal of Sound and Vibration*, 268, pp. 503 – 523.

Nawayseh, N. and Griffin, M. J. (2004). Tri–axial forces at the seat and backrest during whole–body vertical vibration. *Journal of Sound and Vibration*, 277 (1–2), pp. 309 – 326.

Nawayseh, N. and Griffin, M. J. (2005). Non–linear dual–axis biodynamic response to fore–and–aft whole–body vibration. *Journal of Sound and Vibration*, 282 (3–5), pp. 831–862.

Nawayseh, N. and Griffin, M. J. (2009). A model of the vertical apparent mass and the fore–and–aft cross–axis apparent mass of the human body during vertical whole–body vibration. *Journal of Sound and Vibration*, 319 (1–2), pp. 719–730.

Nesaragi, V.V., Maruthi, B.H., Chandru, B. T. and Kumar, D. (2014). Design and noise, vibration, harshness analysis of engine bonnet of the car. *Int. Journal of Engineering Research and Applications*, 4(7). pp. 5-11.

Nigam, S.P. and Malik, M. (1987). A Study on a Vibratory Model of a Human Body. *Journal of Biomechanical Engineering*, 109, pp. 148-153.

Ogden, R. W. (1972). Large deformation isotropic elasticity – On the correlation of theoryand experiment for incompressible rubberlike solids. *Proceedings of the RoyalSociety of London Series A*, 1972, 326, pp. 565–584.

Paddan, G. S. and Griffin, M. J. (1988a). The transmission of translational seat vibration to the head – I. Vertical seat vibration. *Journal of Biomechanics*, 21 (3), pp. 191–197.

Paddan, G. S. and Griffin, M. J. (1988b). The transmission of translational seat vibration to the head – II. Horizontal seat vibration. *Journal of Biomechanics*, 21 (3), pp. 199–206.

Paddan, G.S. and Griffin, M. J. (1998). A review of the transmission of translational seat vibration to the head. *Journal of Sound and Vibration*, 215(4), pp. 863-882.

Paddan, G. S. and Griffin, M. J. (2002). Effect of Seating on Exposures to Whole-Body Vibration in Vehicles. *Journal of Sound and Vibration*, 253(1), pp. 215-241.

Panjabi, M. M., Andersson, G. B. J., Jorneus, L., Hult, E. and Mattsson, L. (1986). In vivo measurement of spinal column vibrations. *Journal of Bone and Joint Surgery*, 68(5), pp. 695-702.

Panjabi, M.M., Oxland, T.R., Yamamoto, I. and Crisco, J.J. (1994). Mechanical behaviour of the human lumbar and lumbosacral as shown by three-dimensional loaddisplacement curves. *Journal of Bone and Joint Surgery*, 76-A (3).

Pankoke, S. and Siefert, A. (2008). Latest development in occupant simulation techniques related to seating comfort and human response and human response to vibration: finite element occupant model CASIMIR, *In: 43rd United Kingdom Conference on Human Responses to Vibration: Caterpillar Inc*, Leicester, England.

Pankoke, S., Buck, B. and Woelfel, H. P, (1998). Dynamic FE model of sitting man adjustable to body height, body mass, body posture used for calculating internal forces in the lumbar vertebral disks. *Journal of Sound and Vibration*, 215, pp. 827–839.

Pankoke, S., Hofmann, J. and Wölfel, H.P. (2001). Determination of vibration-related spinal loads by numerical simulation. *Clinical Biomechanics*, 16(1), pp. S45-S56.

Park, S. and Kim, C. (1997). The evaluation of seating comfort by objective measurements, SAE970595, SAE Conference.

Paul, G., Pendlebury, J. and Miller, J. (2012). The contribution of seat components to seat hardness and the interface between human occupant and a driver seat. *International Journal of Human Factors Modelling and Simulation (IJHFMS)*, 3(3/4), pp.378-397.

Pattern, W.N., Sha, S. and Mo, C. (1998). A Vibration Model of Open Celled Polyurethane Foam Automotive Seat Cushions. *Journal of Sound and Vibration*, 217(1), pp. 145-161.

Paul, G., Miller, J. and Pendlebury, J. (2013). A finite element model of seat cushion indentation with a soft tissue human occupant model. *Proceedings, 2nd International*

Digital Human Modeling Symposium, University of Michigan & Pennsylvania State University.

Pick, A. J. and Cole, D. J. (2005). Neuromuscular Dynamics in the Driver-Vehicle System. *Vehicle System Dynamics*, 00(00), pp. 1-10.

Pickles, A.P., Alderson, K.L. and Evans, K.E. (1996).The effects of powder morphology on the processing of auxetic polypropylene PP of negative Poisson's ratio, *Polymer Engineering & Science*, 36 (5), pp. 636-642.

Plagenhoef, S., Evans, F.G. and Abdelnour, T. (1983). Anatomical data for analyzing human motion. *Research Quarterly for Exercise and Sport*, 54, pp. 169-178.

Pope, M.H., Broman, H. and Hansson, T. (1989). The dynamic response of a seated subject on various cushions. *Ergonomics*, 32(10), pp. 1155-1166.

Pope, M.H., Broman, H. and Hanson, T. (1990). Factors affecting the dynamic response of the seated subject. *Journal of Spinal disorders*. 3(2), pp. 135-142.

Qiu, Y. and Griffin, M. J. (2003). Transmission of fore–aft vibration to a car seat using field tests and laboratory simulation, *Journal of Sound and Vibration*, 264(1), pp. 135–155.

Qiu, Y. and Griffin, M. J. (2004). Transmission of vibration to the backrest of a car seat evaluated with multi–input models, *Journal of Sound and Vibration*, 274(1–2), pp. 297–321.

Qiu, Y. (2007). A seat–occupant model for the prediction of backrest transmissibility in the fore–and–aft direction. *In: 42nd UK Conference on Human Responses to Vibration*, Southampton.

Qiu, Y. and Griffin, M. J. (2010). Biodynamic responses of the seated human body to single–axis and dual–axis vibration. *Industrial Health*, 48 (5), pp. 615–627.

Qiu, Y. and Griffin, M. J. (2011). Modelling the fore-and-aft apparent mass of the human body and the transmissibility of seat backrests. Vehicle System Dynamics: *International Journal of Vehicle Mechanics and Mobility*, 49(5), pp. 703-722.

Qiu, Y. and Griffin, M. J. (2012). Biodynamic Response of the Seated Human Body to Single–axis and Dual–axis Vibration: Effect of Backrest and Non–linearity. *Industrial Health*, 50, pp. 37–51.

Rakheja, S., Stiharu, I. and Boileau, P. (2002). Seated occupant apparent mass characteristics under automotive postures and vertical vibration. *Journal of Sound and Vibration*, 253 (1), pp. 57–75.

References

Rakheja, S., Stiharu, I., Zhang, H. and Boileau, P. (2006). Seated occupant interactions with seat backrest and pan, and biodynamic responses under vertical vibration. *Journal of Sound and Vibration*, 298, pp. 651–671.

recaro-automotive.com, (2018). *Recaro Automotive Seating's Official Website*. [online] Available at:-https://www.recaro.

Reed, M. P., Schneider, L. W. and Ricci, L. L. (1994). Survey of auto seat design recommendations for improved comfort. *UMTRI*, 6. pp. 5-10.

reliabilitydirectstore.com, (2018). *Reliability Direct Store's Official Website*. [online] Available at: https://www.reliabilitydirectstore.com/kb_results.asp?ID=26 [Accessed 13 Jul. 2018].

Rhimi. (2015). Virtual dummy for ergonomical analysis. [online] Grabcad. Available at: https://grabcad.com/library/dummy-car-seat-1 [Accessed 17 Jul. 2017].

Ruetzel, S. and Woelfel, H.P. (2005). *The Benefit of Modal Analysis for Whole Body Vibration Models*. Darmstadt: Darmstadt University of Technology- Conference & Exposition on Structural Dynamics, pp. 1-11.

Rusch, K. C. (1965). Dynamic Behaviour of Flexible Open-cell Foams. Ph. D. Thesis, Engineering, general, University of Akron.

Saha, P. N. (1985). Anthropometric characteristics among industrial workers in India. *Proceedings of International Symposium on Ergonomics in Developing Countries, Jakarta, Indonesia*, pp. 158-161.

Schrodt, M., Benderoth, G., Kuhhorn, A. and Silber. G. (2005). Hyperelastic Description of Polymer Soft Foams at Finite Deformations. *Technische Mechanik*, 25, pp. 162-173.

Seidel, H., Bluethner, R. and Hinz, B. (2001). Application of finite-element models to predict forces acting on the lumbar spine during whole body vibration. *Clinical Biomechanics*, 16(1), pp. S57-S63.

Setyabudhy, R. H., Ali, A., Hubbard, R. P., Beckett, C. and Averill, R. C. (1997). Measuring and Modeling of Human Soft Tissue and Seat Interaction. SAE International Congress and Exposition, 10.4271/970593.

sharcnet.ca, (2018). *SAS IP, Inc.'s Official Website*. [online] Available at: https://www.sharcnet.ca/Software/Ansys/16.2.3/en-us/help/wb_sim/ds_contact_theory.html [Accessed 25 May. 2018].

Siefert A., Pankoke, S. and Wölfel, H-P. (2008). Virtual optimisation of car passenger seats: Simulation of static and dynamic effects on drivers' seating comfort. *International Journal of Industrial Ergonomics*, 38, pp.410–424.

Silber, G and Then C. (2009). Numerical Analysis of the Interactions between Human Body Soft Tissue and Body Supports. *SIMULIA Customer Conference*, pp. 1-15.

Shan, C.W., Ghazali, M.I. and Idris, M.I. (2012). Improved Vibration Characteristics of Flexible Polyurethane Foam Via Composite Formation. *International Journal of Automotive and Mechanical Engineering*, 7, pp. 1031-1042.

Simo, B. (1986). On material representation and constitutive branching in finite compressible elasticity. *J. Mechanics of Solids*, 34(2), pp. 125–145.

Singh, R., Davies, P. and Bajaj, A.K. (2003). Estimation of the dynamical properties of polyurethane foam through use of Prony series. *Journal of Sound and Vibration*, 263(2003), pp. 1005-1043.

Singh, R., Davies, P. and Bajaj, A. K. (2003). Identification of nonlinear and viscoelastic properties of flexible polyurethane foam. *Nonlinear Dynamics*, 34, pp. 319–346.

Siefert, A., Pankoke, S. and Wolfel, H. P. (2008). Virtual optimisation of car passenger seats: Simulation of static and dynamic effects on drivers' seating comfort. *International Journal of Industrial Ergonomics*, 38, pp. 410–424.

Sitnik, L.J., Magdziak-Toklowicz, M., Wróbel, R. and Kardasz, P. (2013). Vehicle Vibration in Human Health. Journal of KONES Powertrain and Transport, 20(4), pp. 411-418.

Smith, S.D. (1997). Cushions and suspensions: predicting their effects on the biodynamic responses of humans exposed to vertical vibration. Heavy vehicle systems, *Int. J. of Vehicle Design*, 4(2-4), pp. 296-316.

Smith, S.D. (2000). Modeling differences in the vibration response characteristics of the human body. Journal of Biomechanics, 33, pp. 1513-1516.

Sonenblum, S.E., Sprigle, S.H., Cathcart, J.M. and Winder, R. J. (2015). 3D anatomy and deformation of the seated buttocks. *Journal of Tissue Viability*, 24, pp. 51-61.

Spyrou, L. A. and Aravas, N. (2011). Muscle and Tendon Tissues: Constitutive Modeling and Computational Issues. *Journal of Applied Mechanics*, 78, pp. 1-10.

Stein, G. J., Chmúrny, R. and Rosík, V. (2011). Compact Vibration Measuring System for in-vehicle Applications. *Measurement Science Review*, 11(5), pp. 154-159.

Stein, G.J., Múčka, P., Chmúrny, R., Hinzb, B. and Blüthner, R. (2007). Measurement and modelling of x-direction apparent mass of the seated human body–cushioned seat system. *Journal of Biomechanics*, 40, pp. 1493-1503.

References

Tamaoki, G. Yoshimura, T. and Nakai, K. (2005). Multi–body Dynamics Modelling of Seated Human Body under Exposure to Whole–Body Vibration. *Industrial Health*, 43, pp. 441–447.

Tang, C, Y., Chan, W. and Tsui, C.P. (2010). Finite Element Analysis of Contact Pressures between Seat Cushion and Human Buttock-Thigh Tissue. *Scientific Research*, 2, pp. 720-726.

test-meter.co.uk, (2018). *Test Meter & Test Equipment Experts's Official Website*. [online] Available at: https://www.test-meter.co.uk/tenmars-st-140-vibration-meter/?utm_source=google_shopping&gclid=EAIaIQobChMI1Lvego6d3AIVSLDtCh3muAEPEAQYFCABEgKfDPD_BwE [Accessed 13 Jul. 2018].

tester.co.uk, (2018). *PassTM's Official Website*. [online] Available at: https://www.tester.co.uk/extech-vb300-3-axis-g-force-usb-datalogger?fee=3&fep=3396&gclid=EAIaIQobChMI1Lvego6d3AIVSLDtCh3muAEPEAQYAyABEgKny_D_BwE [Accessed 13 Jul. 2018].

tester.co.uk, (2018). *PassTM's Official Website*. [online] Available at: https://www.tester.co.uk/extech-sdl800-vibration-meter-datalogger?fee=3&fep=3395&gclid=EAIaIQobChMI1Lvego6d3AIVSLDtCh3muAEPEAQYByABEgJwKvD_BwE [Accessed 13 Jul. 2018].

Tewari, V.K. and Prasad, N. (2000). Optimum seat pan and back-rest parameters for a comfortable tractor seat. Ergonomics, 43(2), pp. 167-186.

Thite, A. N. (2012). Development of a Refined Quarter CarModel for the Analysis of Discomfort due to Vibration. *Hindawi Publishing Corporation - Advances in Acoustics and Vibration*, 2012(863061), pp. 1-7.

Tiemessen, I. J., Hulshof, C. T. J. and Frings–Dresen, M. H. W. (2007). An overview of strategies to reduce whole–body vibration exposure on drivers: A systematic review. *International journal of industrial ergonomics*, 37, pp. 245–256.

Todd, B. A. and Thacker, J.G. (1194). Three-dimensional computer model of the human buttocks, in vivo. *The Journal of Rehabilitation Research and Development*, 31(2). pp. 111-119.

Toward, M. G. R. and Griffin, M. J. (2009). Apparent mass of the human body in the vertical direction: Effect of seat backrest. *Journal of Sound and Vibration*, 327, pp. 657–669.

Toward, M. G. R. and Griffin, M. J. (2010). Apparent mass of the human body in the vertical direction: Effect of a footrest and a steering wheel. *Journal of Sound and Vibration*, 329, pp. 1586–1596.

Toward, M. G. R. and Griffin, M. J. (2011a). Apparent mass of the human body in the vertical direction: inter–subject variability. *Journal of Sound and Vibration*, 330 (4), pp. 827–841.

Toward, M. G. R. and Griffin, M. J. (2011b). The transmission of vertical vibration through seats: Influence of the characteristics of the human body. *Journal of Sound and Vibration*, 330 (26), pp. 6526–6543.

Tufano, S. and Griffin, M. J. (2013). Nonlinearity in the vertical transmissibility of seating: the role of the human body apparent mass and seat dynamic stiffness. *Vehicle System Dynamics*, 51 (1), pp. 122–138.

Van den Bogert, P. A. J. and DeBorst, R. (1994). On the behaviour of rubberlike materials in compression and shear. *Arcive of. Applied Mechanics,* 64, pp. 136–146.

Verver, M.M. (2004). *Numerical tools for comfort analyses of automotive seating*. Eindhoven: Technische Universiteit Eindhoven, pp. 7-70.

Wagnac, E.L., Aubin, C.E., C and Dansereau, J. (2008). A new method to generate a patient-specific finite element model of the human buttocks. Biomed. Eng. *IEEE Trans*, 55(2), pp. 774-783.

Wan, Y. and Schimmels, J.M. (1995). A simple model that captures the essential dynamics of a seated human exposed to whole body vibration. *Advances in Bioengineering, ASME, BED*, 31, pp. 333-334.

Wang, H. and Zhang, D. (2004). Modeling and simulation with finite element method in vehicle seats. *Journal of Tongji University (Natural Science)*, 32 (7).

Wang, W., Rakheja, S. and Boileau, P. (2004). Effects of sitting postures on biodynamic response of seated occupants under vertical vibration. *International Journal of Industrial Ergonomics*, 34, pp. 289–306.

Wang, W., Rakheja, S. and Boileau, P. (2008). Relationship between measured apparent mass and seat–to–head transmissibility responses of seated occupants exposed to vertical vibration. *Journal of Sound and Vibration*, 314, pp. 907–922.

Wang, Y. and Cuitino, A. M. (2000). Three-dimensional nonlinear open-cell foams with large deformations. *Journal of the Mechanics and Physics of Solids*, 48, pp. 961–988.

Wardell, Gareth. (2007). Jaguar XK Coupe Review. *The Auto Channel*.

Warner, C.Y., Stother, C.E., James, M.B. and Decker, R.L. (1991). Occupant protection inrear-end collisions: II. The role of seat back deformation in injury reduction. *Proceedings of the 35stStapp Car Crash Conference 1991*, pp.379-390, SAE no912914.

Wei, L. and Griffin, M. J. (1998a). Mathematical models for the apparent mass of the seated human body exposed to vertical vibration. *Journal of Sound and Vibration*, 212 (5), pp. 855– 874.

Wei, L. and Griffin, M. J. (1998b). The prediction of seat transmissibility from measures of seat impedance. *Journal of sound and vibration*, 214 (1), pp. 121–137.

Wildman, E. C. (2000). Foundations of the Human Body. *Advanced human nutrition*, 1st ed.

Williamson, P. (2005). *Aspects of Simulation of Automobile Seating Using LS-Dyna 3D*. Bamberg: LS-DYNA Anwenderforum, pp. 53-60.

Wu, X., Rakheja, S. and Boileau, P.E. (1998). Study of human-seat interface pressure distribution under vertical vibration. *International Journal of Industrial Ergonomics*, 21, pp. 433-449.

Yousif, H. I. Y. (2012). Auxetic Polyurethane Foam (Fabrication, Properties and Applications). *MSc Thesis- Helwan University*, pp. 2-10.

Yun, M.H. Donges, L. and Freivalds, A. (1992). Using force sensitive resistors to evaluate the driver seating comfort. *Advances in Industrial Ergonomics and Safety*, 4, pp. 403-410.

Zengkang, G., Hillis, A.H. and Darling, J. (2013). Biodynamic modelling of seated human subjects exposed to whole-body vibration in both vertical and fore-and-aft directions. *Centre for Power Transmission and Motion Control*.

Zhang, J., Kikuchi, N., Li, V., Yee, A. and Nusholtz, G. (1998). Constitutive Modeling of Polymeric Foam Material Subjected to Dynamic Crash Loading. *International Journal of Impact Engineering*, 21(5), pp. 734-743.

Zhang, L. Z. and Dupuis, R. (2011). Measurement and identification of dynamic properties of flexible polyurethane foam. *Journal of Vibration and Control*, 17, pp. 517–526.

Zhang, L., Helander, M.G. and Drury, C.G. (1996). Identifying factors of comfort and discomfort in sitting. Human Factors, 38(3), pp. 377-389.

Zhang, X. (2014). Measurement and Modelling of Seating Dynamics to Predict Seat Transmissibility. *Thesis for the degree of Doctor of Philosophy- Institute of Sound And Vibration Research*, pp. 50-226.

Zhang, Y., Zhong, W., Zhu. H., Chen, Y., Xu, L. and Zhu, J. (2013). Establishing the 3-D finite element solid model of femurs in partial by volume rendering. *International Journal of Surgery*, 11, pp. 930-934.

Zheng, G., Qiu, Y. and Griffin. M. J. (2011). An analytic model of the in–line and cross–axisapparent mass of the seated human body exposed to vertical Vibration with and without a backrest. *Journal of Sound and Vibration*, 330, pp. 6509–6525.

Zengkang, G., Andrew J., Hillis, A.J. and Darling, J. (2013). Development of a Biodynamic Model of a Seated Human Body Exposed to Low Frequency Whole-body Vibration. 11th International Conference on Vibration ProblemsAt: Lisbon, Portugal.

Zimmermann, C. L. and Cook, T. M. (1997). Effects of vibration frequency and postural changes on human responses to seated whole-body vibration exposure. *Int Arch Occup Environ Health*, 69(3), pp. 165-79.

Zitzewitz, Paul. Merrill Physics Principles and Problems. New York: Glencoe, 1995: 91.

zoro.co.uk, (2018). *Zoro's Official Website*. [online] Available at: https://www.zoro.co.uk/shop/measuring-and-test-equipment/vibration-meters/9070-smart-vibration-meter/p/ZT1017797X?utm_campaign=pla-Measuring+%26+Test+Equipment+-+&utm_source=google&utm_medium=shopping-pla&utm_keyword=ZT1017797X&istCompanyId=6aa6787b-063e-4414-802d-129f235df603&istItemId=wtqixrlxqa&istBid=tztt&gclid=EAIaIQobChMI1Lvego6d3AIVSLDtCh3muAEPEAQYBCABEgL9PPD_BwE [Accessed 13 Jul. 2018].

APPENDIX A.
AUTHOR'S PUBLICATIONS

Journal Papers

Mondal, P. and Arunachalam, S. (2020). Unique Finite Element Modeling of Human Body inside Accelerating Car to predict Accelerations and Frequencies at Different Human Segments. *Applied Sciences, MDPI*, 10(5), pp. 1861 (16 Pages).

Mondal, P. and Arunachalam, S. (2020). Finite Element Modelling of Car Seat with Hyperelastic and Viscoelastic Foam Material Properties to Assess Vertical Vibration in Terms of Acceleration. *Engineering, Scientific Research Publishing*, Vol. 12(3), pp. 177-193.

Mondal, P. and Arunachalam, S. (2020). Modelling the Car Seated Human Body using Composite Ellipsoidal Bodies and Evaluation of Size and Shape Specific Stiffness Data for Various Human Segments. *SSRG International Journal of Mechanical Engineering, Seventh Sense Research Group®*, 7(2), pp. 26-32.

Mondal, P. and Arunachalam, S. (2020). Compact System for Measuring Vibration at Different locations of Car Seat and Human Driver in Dynamic Condition. *International Journal of Innovative Research in Science, Engineering and Technology*, 9(2), pp. 13669-13676.

Mondal, P. and Arunachalam, S. (2018). Vibration Study in Human-Car Seat System: Overview and a Novel Simulation Technique. *Journal of Material Sciences & Engineering, OMICS International*, 7(1), pp. 1000421 (5 Pages).

Conference Articles

Mondal, P. and Arunachalam, S. (2019). Vibration in car seat- occupant system: Overview and proposal of a novel simulation method. *AIP Conference Proceedings 2080*, 040003 (2019), pp. 040003-1 - 040003-8 (8 Pages).

APPENDIX B.
ABAQUS INPUT FILE FOR SIMULATION OF COMBINED HUMAN BODY AND CAR SEAT

*Heading
** Job name: Job-Final Model name: Model-0_Final
** Generated by: Abaqus/CAE 6.13-1
*Preprint, echo=NO, model=NO, history=NO, contact=NO
**
** PARTS
**
*Part, name=A_Head
*End Part
**
*Part, name=B_Torso
*End Part
**
*Part, name=C1_Arm-Upper_Left
*End Part
**
*Part, name=C2_Arm-Upper_Right
*End Part

```
**
*Part, name=D1_Arm-Lower_Left
*End Part
**
*Part, name=D2_Arm-Lower_Right
*End Part
**
*Part, name=E1_Hand_Left
*End Part
**
*Part, name=E2_Hand_Right
*End Part
**
*Part, name=F1_Upper-Leg_Left
*End Part
**
*Part, name=F2_Upper-Leg_Right
*End Part
**
*Part, name=G1_Lower-Leg_Left
*End Part
**
*Part, name=G2_Lower-Leg_Right
*End Part
**
*Part, name=H1_Foot_Left
*End Part
**
*Part, name=H2_Foot_Right
*End Part
```

```
**
*Part, name=Seat-Backrest
*End Part
**
*Part, name=Seat-Cushion
*End Part
**
*Part, name=Seat-Headrest
*End Part
**
**
** ASSEMBLY
**
*Assembly, name=Assembly
**
*Instance, name=H2_Foot_Right, part=H2_Foot_Right
*Node
      1,       -13.5,  -81.1750183,   947.150146
      2,       -63.5,  -102.741776,   968.716858
      3,       -63.5,  -174.866669,   853.458496
      4,       -63.5,   12.5166321,    1040.8418
      5,      -113.5,  -81.1750183,   947.150146
      6,       -63.5,  -59.6082611,   925.583374
      7,  -16.3632259,  -88.3684235,   954.343506
      8,  -23.3587856,  -94.0334549,   960.008545
      9,  -32.3830833,  -98.0563583,   964.031494
     10,  -42.3745422,  -100.722237,   966.697327
     11,  -52.8382492,  -102.245758,   968.220886
     12,       -63.5,  -109.507454,    961.83667
     13,       -63.5,  -116.155807,   954.843018
```

Appendix B

14, -63.5, -122.682129, 947.735413
15, -63.5, -129.079483, 940.511475
16, -63.5, -135.33812, 933.167053
17, -63.5, -141.44458, 925.695618
18, -63.5, -147.380203, 918.087891
19, -63.5, -153.118683, 910.330444

.....** Due to space constrain further list omitted**.....

*Nset, nset=m_Set-1, instance=H1_Foot_Left
4,
*Nset, nset=m_Set-2, instance=H2_Foot_Right
3,
*Nset, nset=m_Set-3, instance=G1_Lower-Leg_Left
4,
*Nset, nset=m_Set-4, instance=G2_Lower-Leg_Right
4,
*Nset, nset=m_Set-5, instance=F1_Upper-Leg_Left
5,
*Nset, nset=m_Set-6, instance=F2_Upper-Leg_Right
3,
*Nset, nset=m_Set-7, instance=E1_Hand_Left
5,
*Nset, nset=m_Set-8, instance=E2_Hand_Right
1,
*Nset, nset=m_Set-9, instance=D1_Arm-Lower_Left
3,
*Nset, nset=m_Set-10, instance=D2_Arm-Lower_Right
3,
*Nset, nset=m_Set-11, instance=C1_Arm-Upper_Left

3,
*Nset, nset=m_Set-12, instance=C2_Arm-Upper_Right
2,
*Nset, nset=m_Set-13, instance=A_Head
6,
*Nset, nset=_PickedSet89, internal, instance=H1_Foot_Left
4,
*Nset, nset=_PickedSet90, internal, instance=G1_Lower-Leg_Left
3,
*Nset, nset=_PickedSet91, internal, instance=H2_Foot_Right
3,
*Nset, nset=_PickedSet92, internal, instance=G2_Lower-Leg_Right
3,
*Nset, nset=_PickedSet93, internal, instance=G1_Lower-Leg_Left
4,
*Nset, nset=_PickedSet94, internal, instance=F1_Upper-Leg_Left
1,
*Nset, nset=_PickedSet95, internal, instance=G2_Lower-Leg_Right
4,
*Nset, nset=_PickedSet96, internal, instance=F2_Upper-Leg_Right
4,
*Nset, nset=_PickedSet97, internal, instance=F1_Upper-Leg_Left
5,
*Nset, nset=_PickedSet99, internal, instance=F2_Upper-Leg_Right
3,
*Nset, nset=_PickedSet116, internal, instance=B_Torso
14,
*Nset, nset=_PickedSet117, internal, instance=B_Torso
9,
*Nset, nset=_PickedSet118, internal, instance=E1_Hand_Left

5,
*Nset, nset=_PickedSet119, internal, instance=D1_Arm-Lower_Left
4,
*Nset, nset=_PickedSet120, internal, instance=E2_Hand_Right
1,
*Nset, nset=_PickedSet121, internal, instance=D2_Arm-Lower_Right
4,
*Nset, nset=_PickedSet122, internal, instance=D1_Arm-Lower_Left
3,
*Nset, nset=_PickedSet123, internal, instance=C1_Arm-Upper_Left
4,
*Nset, nset=_PickedSet124, internal, instance=D2_Arm-Lower_Right
3,
*Nset, nset=_PickedSet125, internal, instance=C2_Arm-Upper_Right
6,
*Nset, nset=_PickedSet126, internal, instance=C1_Arm-Upper_Left
3,
*Nset, nset=_PickedSet127, internal, instance=B_Torso
4,
*Nset, nset=_PickedSet128, internal, instance=C2_Arm-Upper_Right
2,
*Nset, nset=_PickedSet129, internal, instance=B_Torso
1,
*Nset, nset=_PickedSet130, internal, instance=B_Torso
3,
*Nset, nset=_PickedSet131, internal, instance=A_Head
6,
*Elset, elset=_m_Surf-14_S3, internal, instance=Seat-3-1
86, 218, 281, 2492, 4351, 4355, 4409, 4425, 4429, 10076, 10812, 10842, 11586, 12351, 12490, 12525

12640, 13283, 13344, 13540, 14289, 14341, 14473, 14657, 14919, 14976, 15053, 15068, 15087, 15107, 15119, 15149
15178, 15181, 15197, 15255, 15324, 15347, 15495, 15584, 15870, 16082, 16142, 16746, 17030, 17082, 17238, 17583
17891, 17907, 18153, 18182, 18209, 18239, 18350, 18404, 18417, 18446, 18453, 18468, 18505, 18513, 18558, 19290
19409, 19432, 19475, 19503, 19508, 19749, 19752, 19887, 19970, 20076, 20217, 20222, 20320, 20700, 20703, 20818
21325, 21355, 21377, 21410, 21440, 21457, 21626, 21676, 21883, 21906, 21914, 21927, 21957, 21982, 22018, 22031
22038, 22048, 22049, 22068, 22078, 22080, 22105, 22116, 22137, 22139, 22140, 22157, 22198, 22212, 22225, 22229
22235, 22236, 22304, 22598, 22602, 22615, 22715, 22716, 22724, 22729, 22743, 22759, 22762, 22763, 22764, 22765
22772, 22773, 22779, 22820, 22821, 22823, 22827, 22839, 22844, 22849, 22857, 22861, 22868, 22875, 22879, 22893
22908, 22930, 22940, 22942, 22946, 22951, 22984, 22987, 22990, 22991, 22992, 22997, 23000, 23004, 23008, 23009
23016, 23017, 23022, 23160, 23162, 23238, 23247, 24596, 24709, 24784, 25288, 25290, 25554, 25651, 26438, 26687
26691, 26784, 26786, 27713, 27715, 28486, 28487, 28867, 29296, 29297, 29543, 30451, 30454, 30587, 31506, 31702
31868, 32108, 32197, 32604, 32605, 32705, 32737, 32848, 33063, 33072, 33792, 33914, 34057, 34180, 34585, 34586
34645, 34649, 34854, 35145, 35216, 35337, 36000, 37177, 37672, 38410, 38411, 39158, 39332, 39335, 41071, 41735
41751, 41873, 41875, 42902, 42961, 48874
*Elset, elset=_m_Surf-14_S1, internal, instance=Seat-3-1
11694, 20058, 20168, 20233, 22196, 22867
*Elset, elset=_m_Surf-14_S4, internal, instance=Seat-3-1

Appendix B

14979, 18254, 18441, 18550, 19959, 20059, 21264, 21645, 21941, 32103, 34778, 41874, 46869

*Elset, elset=_m_Surf-14_S2, internal, instance=Seat-3-1

15035, 18396, 22146, 22177, 22733, 22863, 22872, 32513

*Surface, type=ELEMENT, name=m_Surf-14

_m_Surf-14_S3, S3

_m_Surf-14_S1, S1

_m_Surf-14_S4, S4

_m_Surf-14_S2, S2

*Elset, elset=_m_Surf-16_S3, internal, instance=Seat-2-1

268, 301, 422, 774, 860, 1091, 1506, 1509, 1598, 1601, 1790, 2161, 2295, 2301, 2365, 2447

2467, 2553, 2583, 2587, 2630, 2709, 2767, 2890, 2984, 3136, 3208, 3279, 3292, 3412, 3432, 3472

3473, 3495, 3515, 3523, 3555, 3586, 3587, 3598, 3633, 3638, 3646, 3653, 3657, 3671, 3678, 3686

3689, 3694, 3702, 3719, 3731, 3733, 3737, 3748, 3770, 3782, 3852

*Elset, elset=_m_Surf-16_S4, internal, instance=Seat-2-1

1224, 1237, 2317, 3718, 3726, 3730, 3773

*Elset, elset=_m_Surf-16_S2, internal, instance=Seat-2-1

2275, 2475, 2717, 3542, 3564, 3606, 3630, 3634, 3664, 3674, 3681, 3778

*Elset, elset=_m_Surf-16_S1, internal, instance=Seat-2-1

3415, 3696, 3706, 3766, 3800, 3841

.....** Due to space constrain further list omitted**.....

*Elset, elset=_s_Surf-14_S2, internal, instance=Seat-1-1

5283, 5287, 8458, 12258, 12723, 13940, 13942, 15594, 18719, 25044, 26501

*Elset, elset=_s_Surf-14_S3, internal, instance=Seat-1-1

5294, 7481, 11470, 12266, 12270, 12496, 13920, 13968, 14937, 14954, 14994, 15022, 15043, 15237, 15374, 15841
16008, 16013, 16016, 16045, 16110, 16134, 16626, 16824, 17037, 17043, 17682, 17867, 18225, 18242, 18283, 18722
18736, 18928, 23906, 24022, 25016, 25038, 25062, 25064, 25076, 25077, 25081, 25082, 25087, 25099, 25104, 25109
25110, 25114, 25117, 25129, 25133, 25140, 25144, 25155, 25157, 25164, 25179, 25182, 25185, 25186, 25197, 25199
25200, 25210, 25224, 25237, 25242, 25249, 25256, 25260, 25262, 25268, 25273, 25274, 25275, 25277, 25285, 25286
25292, 25296, 25299, 25301, 25308, 25319, 26944, 28817, 29120, 29655, 29658, 29660, 30055, 30822, 30823, 30825
31312, 31314, 31727, 31740, 32392, 34008, 34568, 34717, 35198, 35494, 36168, 36169, 39799, 41414, 41868, 42170
42532,
*Elset, elset=_s_Surf-14_S1, internal, instance=Seat-1-1
5432, 12501, 12726, 15346, 15907, 18231, 18342, 23989, 25142, 25153, 25214, 25254
*Elset, elset=_s_Surf-14_S4, internal, instance=Seat-1-1
14952, 15926, 16074, 18721, 22496, 22499, 23299, 25058, 25241, 34566, 42438, 47729
*Surface, type=ELEMENT, name=s_Surf-14
_s_Surf-14_S2, S2
_s_Surf-14_S3, S3
_s_Surf-14_S4, S4
_s_Surf-14_S1, S1
*Elset, elset=_s_Surf-16_S2, internal, instance=Seat-3-1
31, 4649, 5158
*Elset, elset=_s_Surf-16_S3, internal, instance=Seat-3-1
200, 3896, 4141, 4152, 4703, 4753, 4809, 4874, 4924, 4981, 5300, 5312, 5354, 5369, 5373, 5383

Appendix B

5385, 5392, 6036, 6264, 6268, 6270, 6278, 6286, 6304, 6314, 6343, 6346, 6356, 6363, 6365, 6368
6372, 6373, 6393, 6399, 6415, 6423, 6436, 6437, 6440, 6443, 6534, 8184, 8572, 9469, 11164, 11209
11255, 11277, 15644, 22433, 23028, 23032, 23384, 24612
*Elset, elset=_s_Surf-16_S4, internal, instance=Seat-3-1
37277,

.....** Due to space constrain further list omitted**.....

*Surface, type=ELEMENT, name=s_Surf-28
_s_Surf-28_S3, S3
_s_Surf-28_S1, S1
_s_Surf-28_S4, S4
_s_Surf-28_S2, S2
*Surface, type=NODE, name=_PickedSet89_CNS_, internal
_PickedSet89, 1.
*Surface, type=NODE, name=_PickedSet90_CNS_, internal
_PickedSet90, 1.
*Surface, type=NODE, name=_PickedSet91_CNS_, internal
_PickedSet91, 1.
*Surface, type=NODE, name=_PickedSet92_CNS_, internal
_PickedSet92, 1.
*Surface, type=NODE, name=_PickedSet93_CNS_, internal
_PickedSet93, 1.
*Surface, type=NODE, name=_PickedSet94_CNS_, internal
_PickedSet94, 1.
*Surface, type=NODE, name=_PickedSet95_CNS_, internal
_PickedSet95, 1.
*Surface, type=NODE, name=_PickedSet96_CNS_, internal

_PickedSet96, 1.
*Surface, type=NODE, name=_PickedSet97_CNS_, internal
_PickedSet97, 1.
*Surface, type=NODE, name=_PickedSet116_CNS_, internal
_PickedSet116, 1.
*Surface, type=NODE, name=_PickedSet99_CNS_, internal
_PickedSet99, 1.
*Surface, type=NODE, name=_PickedSet117_CNS_, internal
_PickedSet117, 1.
*Surface, type=NODE, name=_PickedSet118_CNS_, internal
_PickedSet118, 1.
*Surface, type=NODE, name=_PickedSet119_CNS_, internal
_PickedSet119, 1.
*Surface, type=NODE, name=_PickedSet120_CNS_, internal
_PickedSet120, 1.
*Surface, type=NODE, name=_PickedSet121_CNS_, internal
_PickedSet121, 1.
*Surface, type=NODE, name=_PickedSet122_CNS_, internal
_PickedSet122, 1.
*Surface, type=NODE, name=_PickedSet123_CNS_, internal
_PickedSet123, 1.
*Surface, type=NODE, name=_PickedSet124_CNS_, internal
_PickedSet124, 1.
*Surface, type=NODE, name=_PickedSet125_CNS_, internal
_PickedSet125, 1.
*Surface, type=NODE, name=_PickedSet126_CNS_, internal
_PickedSet126, 1.
*Surface, type=NODE, name=_PickedSet127_CNS_, internal
_PickedSet127, 1.
*Surface, type=NODE, name=_PickedSet128_CNS_, internal

_PickedSet128, 1.
*Surface, type=NODE, name=_PickedSet129_CNS_, internal
_PickedSet129, 1.
*Surface, type=NODE, name=_PickedSet130_CNS_, internal
_PickedSet130, 1.
*Surface, type=NODE, name=_PickedSet131_CNS_, internal
_PickedSet131, 1.
** Constraint: A1_Foot-LowerLeg-Left
*Tie, name=A1_Foot-LowerLeg-Left, adjust=yes
_PickedSet90_CNS_, _PickedSet89_CNS_
** Constraint: A2_Foot-LowerLeg-Right
*Tie, name=A2_Foot-LowerLeg-Right, adjust=yes
_PickedSet92_CNS_, _PickedSet91_CNS_
** Constraint: A3_LowerLeg-UpperLeg-Left
*Tie, name=A3_LowerLeg-UpperLeg-Left, adjust=yes
_PickedSet94_CNS_, _PickedSet93_CNS_
** Constraint: A4_LowerLeg-UpperLeg-Right
*Tie, name=A4_LowerLeg-UpperLeg-Right, adjust=yes
_PickedSet96_CNS_, _PickedSet95_CNS_
** Constraint: A5_UpperLeg-Torso_Left
*Tie, name=A5_UpperLeg-Torso_Left, adjust=yes
_PickedSet116_CNS_, _PickedSet97_CNS_
** Constraint: A6_UpperLeg-Torso_Right
*Tie, name=A6_UpperLeg-Torso_Right, adjust=yes
_PickedSet117_CNS_, _PickedSet99_CNS_
** Constraint: A7_Hand-LowerArm-Left
*Tie, name=A7_Hand-LowerArm-Left, adjust=yes
_PickedSet119_CNS_, _PickedSet118_CNS_
** Constraint: A8_Hand-LowerArm-Right
*Tie, name=A8_Hand-LowerArm-Right, adjust=yes

_PickedSet121_CNS_, _PickedSet120_CNS_
** Constraint: A9_LowerArm-UpperArm-Left
*Tie, name=A9_LowerArm-UpperArm-Left, adjust=yes
_PickedSet123_CNS_, _PickedSet122_CNS_
** Constraint: A10_LowerArm-UpperArm-Right
*Tie, name=A10_LowerArm-UpperArm-Right, adjust=yes
_PickedSet125_CNS_, _PickedSet124_CNS_
** Constraint: A11_UpperArm-Torso-Left
*Tie, name=A11_UpperArm-Torso-Left, adjust=yes
_PickedSet127_CNS_, _PickedSet126_CNS_
** Constraint: A12_UpperArm-Torso-Right
*Tie, name=A12_UpperArm-Torso-Right, adjust=yes
_PickedSet129_CNS_, _PickedSet128_CNS_
** Constraint: A13_Torso-Head
*Tie, name=A13_Torso-Head, adjust=yes
_PickedSet131_CNS_, _PickedSet130_CNS_
** Constraint: Seat-Head
*Tie, name=Seat-Head, adjust=yes
s_Surf-28, m_Surf-28
** Constraint: Seat-Torso
*Tie, name=Seat-Torso, adjust=yes
s_Surf-24, m_Surf-24
** Constraint: Seat-thigh
*Tie, name=Seat-thigh, adjust=yes
s_Surf-26, m_Surf-26
*End Assembly
*Amplitude, name=Amp-1
0.001, -0.1, 0.002, -0.25, 0.003, -0.45, 0.004, -0.5

Appendix B


```
0.005,  -0.06,  0.006,  -0.7,  0.007,  -0.8,  0.008,
-0.82
0.009,  -0.84,  0.01,  -0.861
**
** MATERIALS
**
*Material, name="A_Head including Neck"
*Density
 1.36231e-09,
*Elastic
 3006.01, 0.49
*Material, name=B_Torso
*Density
 1.01635e-09,
*Elastic
 3006.01, 0.49
*Material, name="C_Upper Arm"
*Density
 2.15631e-09,
*Elastic
 3006.01, 0.49
*Material, name="D_Lower Arm"
*Density
 1.94668e-09,
*Elastic
 3006.01, 0.49
*Material, name=E_Hand
*Density
 6.35495e-09,
*Elastic
```

```
 3006.01, 0.49
*Material, name="F_Upper Leg"
*Density
 1.22481e-09,
*Elastic
 3006.01, 0.49
*Material, name="G_Lower Leg"
*Density
 1.51112e-09,
*Elastic
 3006.01, 0.49
*Material, name=H_Foot
*Density
 1.25143e-09,
*Elastic
 3006.01, 0.49
*Material, name=Seat
*Density
 6.4e-11,
*Hyperfoam, n=2, moduli=LONG TERM
 0.00481,   19.8, 0.0036,   19.8, 0.0145, 0.0065
*Viscoelastic, frequency=PRONY
 0.3003,       0., 0.010014
 0.1997,       0.,   0.1002
**
** INTERACTION PROPERTIES
**
*Surface Interaction, name=Seat-Human-Contact
1.,
*Friction, rough
```

```
**
** BOUNDARY CONDITIONS
**
** Name: Foot Type: Displacement/Rotation
*Boundary
Set-15, 1, 1
Set-15, 2, 2
Set-15, 3, 3
Set-15, 5, 5
Set-15, 6, 6
** Name: Hand Type: Displacement/Rotation
*Boundary
Set-16, 1, 1
Set-16, 2, 2
Set-16, 3, 3
Set-16, 4, 4
Set-16, 6, 6
** Name: SeatCushionBottom Type: Displacement/Rotation
*Boundary
Set-48, 1, 1
Set-48, 2, 2
Set-48, 3, 3
Set-48, 4, 4
Set-48, 5, 5
Set-48, 6, 6
** ----------------------------------------------------------------
**
** STEP: A_NaturalFrequency
**
*Step, name=A_NaturalFrequency, nlgeom=NO, perturbation
```

```
*Frequency, eigensolver=Lanczos, acoustic coupling=off, normalization=displacement
25, , 50., , ,
**
** OUTPUT REQUESTS
**
*Restart, write, frequency=0
**
** FIELD OUTPUT: F-Output-1
**
*Output, field, variable=PRESELECT
*End Step
** ----------------------------------------------------------------
**
** STEP: B_Modal Dynamics
**
*Step, name="B_Modal Dynamics", nlgeom=NO, perturbation
*Modal Dynamic, continue=NO
0.001, 10.
*Modal Damping
1, 20, 0.2
**
** BOUNDARY CONDITIONS
**
** Name: Acceleration Type: Acceleration base motion
*Base Motion, type=ACCELERATION, dof=3, amplitude=Amp-2, scale=1.
1.40802e-07, -95.3873, -268.587
**
** LOADS
**
** Name: Load-3   Type: Gravity
```

Appendix B


```
*Dload
, GRAV, 981., 0., -1., 0.
**
** OUTPUT REQUESTS
**
**
** FIELD OUTPUT: F-Output-2
**
*Output, field
*Node Output
A, AT, TU, U, V
**
** HISTORY OUTPUT: H-Output-1
**
*Output, history, variable=PRESELECT
*End Step
```

APPENDIX C.
ABAQUS INPUT FILE FOR SIMULATION OF HUMAN BODY

```
*Heading
** Job name: Job-1 Model name: Model-1
** Generated by: Abaqus/CAE 6.13-1
*Preprint, echo=NO, model=NO, history=NO, contact=NO
**
** PARTS
**
*Part, name=A_Head
*Node
      1,  3.61502998e-07,   725.192749,   -252.52298
      2,          0.,   887.672546,  -188.256912
      3,        77.5,   731.610413,  -175.289154
      4,       -77.5,   731.610413,  -175.289154
      5,  -3.61503453e-07,   738.028015,  -98.0553284
      6,          0.,   575.548218,  -162.321396
      7,  3.59910501e-07,   739.715271,  -253.393555
      8,  3.55195539e-07,   754.262451,  -253.587967
      9,  3.47243173e-07,   768.802185,  -253.085251
     10,  3.35904446e-07,   783.297913,  -251.850357
     11,  3.2095366e-07,   797.705017,  -249.830963
```

12, 3.02067491e-07, 811.964844, -246.952713
13, 2.78793948e-07, 825.995117, -243.111496
14, 2.50504854e-07, 839.672241, -238.16188
15, 2.16331301e-07, 852.797913, -231.900452
16, 1.75101277e-07, 865.031128, -224.046768
17, 1.25407666e-07, 875.752869, -214.246628
18, 6.63420749e-08, 883.84375, -202.211594
19, 14.2237844, 885.021606, -188.036652
20, 26.8875351, 877.97937, -187.451477
21, 37.5418739, 868.139893, -186.633881
22, 46.3815804, 856.638611, -185.678192
23, 53.7084007, 844.119751, -184.637955
24, 59.7735863, 830.944824, -183.543213
25, 64.7634354, 817.327759, -182.411713
26, 68.8126297, 803.403198, -181.254684
27, 72.0181046, 789.261597, -180.079605
28, 74.4491272, 774.967163, -178.89183
29, 76.1541138, 760.568665, -177.695404
30, 77.1650085, 746.105103, -176.493576
31, 76.0108566, 730.358398, -190.35672
32, 71.6006622, 729.15448, -204.845261
33, 64.4388962, 728.044922, -218.197968
34, 54.8007774, 727.072449, -229.901718
35, 43.056694, 726.274292, -239.506729
36, 29.6579666, 725.681274, -246.643906
37, 15.1195011, 725.31604, -251.038956
38, -15.1194983, 725.31604, -251.038956
39, -29.6579666, 725.681274, -246.643906
40, -43.0566902, 726.274292, -239.506729
41, -54.8007736, 727.072449, -229.901718

42, -64.4388962, 728.044922, -218.197968
43, -71.6006622, 729.15448, -204.845261
44, -76.0108566, 730.358398, -190.356735
45, -77.1650085, 746.105103, -176.493576
46, -76.1541138, 760.568665, -177.695404
47, -74.4491272, 774.967163, -178.89183
48, -72.0181046, 789.261536, -180.07959
49, -68.8126297, 803.403198, -181.254669
50, -64.7634354, 817.327698, -182.411713
51, -59.7735939, 830.944824, -183.543213
52, -53.7084122, 844.11969, -184.637955
53, -46.3815956, 856.638611, -185.678192
54, -37.5418968, 868.139832, -186.633881
55, -26.8875618, 877.979309, -187.451477
.....** Due to space constrain further list omitted**.....
*Elset, elset=__PickedSurf114_S2, internal, instance=A_Head
1633, 1715, 3882, 4552, 4749, 4847, 4889, 5135, 5175, 5219, 5721, 5941, 5989, 6108, 6120, 7157
7231, 7264, 7650, 7903, 7995, 8392, 8451, 8620, 8647, 8729, 8942
*Elset, elset=__PickedSurf114_S4, internal, instance=A_Head
2299, 2435, 2850, 3069, 3212, 3235, 3953, 4076, 4360, 4453, 4846, 4897, 4951, 5522, 5593, 5709
5744, 5774, 5907, 6245, 6430, 6475, 7103, 7174, 7194, 7317, 7383, 7528, 7530, 7591, 7669, 7824
7940, 8258, 8339, 8466, 8468, 9132
*Elset, elset=__PickedSurf114_S1, internal, instance=A_Head
12, 1710, 2862, 3253, 3353, 4710, 4867, 8461, 8836, 8987, 9101, 9366, 9784
*Surface, type=ELEMENT, name=_PickedSurf114, internal
__PickedSurf114_S3, S3
__PickedSurf114_S2, S2

__PickedSurf114_S4, S4
__PickedSurf114_S1, S1
*Surface, type=NODE, name=_PickedSet89_CNS_, internal
_PickedSet89, 1.
*Surface, type=NODE, name=_PickedSet90_CNS_, internal
_PickedSet90, 1.
*Surface, type=NODE, name=_PickedSet91_CNS_, internal
_PickedSet91, 1.
*Surface, type=NODE, name=_PickedSet92_CNS_, internal
_PickedSet92, 1.
*Surface, type=NODE, name=_PickedSet93_CNS_, internal
_PickedSet93, 1.
*Surface, type=NODE, name=_PickedSet94_CNS_, internal
_PickedSet94, 1.
*Surface, type=NODE, name=_PickedSet95_CNS_, internal
_PickedSet95, 1.
*Surface, type=NODE, name=_PickedSet96_CNS_, internal
_PickedSet96, 1.
*Surface, type=NODE, name=_PickedSet97_CNS_, internal
_PickedSet97, 1.
*Surface, type=NODE, name=_PickedSet116_CNS_, internal
_PickedSet116, 1.
*Surface, type=NODE, name=_PickedSet99_CNS_, internal
_PickedSet99, 1.
*Surface, type=NODE, name=_PickedSet117_CNS_, internal
_PickedSet117, 1.
*Surface, type=NODE, name=_PickedSet118_CNS_, internal
_PickedSet118, 1.
*Surface, type=NODE, name=_PickedSet119_CNS_, internal
_PickedSet119, 1.

*Surface, type=NODE, name=_PickedSet120_CNS_, internal
_PickedSet120, 1.
*Surface, type=NODE, name=_PickedSet121_CNS_, internal
_PickedSet121, 1.
*Surface, type=NODE, name=_PickedSet122_CNS_, internal
_PickedSet122, 1.
*Surface, type=NODE, name=_PickedSet123_CNS_, internal
_PickedSet123, 1.
*Surface, type=NODE, name=_PickedSet124_CNS_, internal
_PickedSet124, 1.
*Surface, type=NODE, name=_PickedSet125_CNS_, internal
_PickedSet125, 1.
*Surface, type=NODE, name=_PickedSet126_CNS_, internal
_PickedSet126, 1.
*Surface, type=NODE, name=_PickedSet127_CNS_, internal
_PickedSet127, 1.
*Surface, type=NODE, name=_PickedSet128_CNS_, internal
_PickedSet128, 1.
*Surface, type=NODE, name=_PickedSet129_CNS_, internal
_PickedSet129, 1.
*Surface, type=NODE, name=_PickedSet130_CNS_, internal
_PickedSet130, 1.
*Surface, type=NODE, name=_PickedSet131_CNS_, internal
_PickedSet131, 1.
** Constraint: A1_Foot-LowerLeg-Left
*Tie, name=A1_Foot-LowerLeg-Left, adjust=yes
_PickedSet90_CNS_, _PickedSet89_CNS_
** Constraint: A2_Foot-LowerLeg-Right
*Tie, name=A2_Foot-LowerLeg-Right, adjust=yes
_PickedSet92_CNS_, _PickedSet91_CNS_

** Constraint: A3_LowerLeg-UpperLeg-Left
*Tie, name=A3_LowerLeg-UpperLeg-Left, adjust=yes
_PickedSet94_CNS_, _PickedSet93_CNS_
** Constraint: A4_LowerLeg-UpperLeg-Right
*Tie, name=A4_LowerLeg-UpperLeg-Right, adjust=yes
_PickedSet96_CNS_, _PickedSet95_CNS_
** Constraint: A5_UpperLeg-Torso_Left
*Tie, name=A5_UpperLeg-Torso_Left, adjust=yes
_PickedSet116_CNS_, _PickedSet97_CNS_
** Constraint: A6_UpperLeg-Torso_Right
*Tie, name=A6_UpperLeg-Torso_Right, adjust=yes
_PickedSet117_CNS_, _PickedSet99_CNS_
** Constraint: A7_Hand-LowerArm-Left
*Tie, name=A7_Hand-LowerArm-Left, adjust=yes
_PickedSet119_CNS_, _PickedSet118_CNS_
** Constraint: A8_Hand-LowerArm-Right
*Tie, name=A8_Hand-LowerArm-Right, adjust=yes
_PickedSet121_CNS_, _PickedSet120_CNS_
** Constraint: A9_LowerArm-UpperArm-Left
*Tie, name=A9_LowerArm-UpperArm-Left, adjust=yes
_PickedSet123_CNS_, _PickedSet122_CNS_
** Constraint: A10_LowerArm-UpperArm-Right
*Tie, name=A10_LowerArm-UpperArm-Right, adjust=yes
_PickedSet125_CNS_, _PickedSet124_CNS_
** Constraint: A11_UpperArm-Torso-Left
*Tie, name=A11_UpperArm-Torso-Left, adjust=yes
_PickedSet127_CNS_, _PickedSet126_CNS_
** Constraint: A12_UpperArm-Torso-Right
*Tie, name=A12_UpperArm-Torso-Right, adjust=yes
_PickedSet129_CNS_, _PickedSet128_CNS_

```
** Constraint: A13_Torso-Head
*Tie, name=A13_Torso-Head, adjust=yes
_PickedSet131_CNS_, _PickedSet130_CNS_
*End Assembly
**
** MATERIALS
**
*Material, name="A_Head including Neck"
*Density
 1.09267e-09,
*Elastic
 3006.01, 0.49
*Material, name=B_Torso
*Density
 8.15181e-10,
*Elastic
 3006.01, 0.49
*Material, name="C_Upper Arm"
*Density
 1.72951e-09,
*Elastic
 3006.01, 0.49
*Material, name="D_Lower Arm"
*Density
 1.56138e-09,
*Elastic
 3006.01, 0.49
*Material, name=E_Hand
*Density
 5.09711e-09,
```

Appendix C

*Elastic
3006.01, 0.49
*Material, name="F_Upper Leg"
*Density
9.8238e-10,
*Elastic
3006.01, 0.49
*Material, name="G_Lower Leg"
*Density
1.21202e-09,
*Elastic
3006.01, 0.49
*Material, name=H_Foot
*Density
1.00374e-09,
*Elastic
3006.01, 0.49
**
** BOUNDARY CONDITIONS
**
** Name: Foot Type: Displacement/Rotation
*Boundary
Set-15, 1, 1
Set-15, 2, 2
Set-15, 3, 3
Set-15, 4, 4
Set-15, 5, 5
Set-15, 6, 6
** Name: Hand Type: Displacement/Rotation
*Boundary

Set-16, 1, 1
Set-16, 2, 2
Set-16, 3, 3
Set-16, 4, 4
Set-16, 5, 5
Set-16, 6, 6
** Name: TorsoBack Type: Displacement/Rotation
*Boundary
Set-18, 1, 1
Set-18, 2, 2
Set-18, 3, 3
Set-18, 5, 5
Set-18, 6, 6
** Name: UpperLeg Type: Displacement/Rotation
*Boundary
Set-17, 1, 1
Set-17, 2, 2
Set-17, 4, 4
Set-17, 6, 6
** --
**
** STEP: A_NaturalFrequency
**
*Step, name=A_NaturalFrequency, nlgeom=NO, perturbation
*Frequency, eigensolver=Lanczos, acoustic coupling=on, normalization=displacement
100, , , , ,
**
** OUTPUT REQUESTS
**
*Restart, write, frequency=0

Appendix C


```
**
** FIELD OUTPUT: F-Output-1
**
*Output, field, variable=PRESELECT
*End Step
** ----------------------------------------------------------------
**
** STEP: B_Modal Dynamics
**
*Step, name="B_Modal Dynamics", nlgeom=NO, perturbation
*Modal Dynamic, continue=NO
0.01, 10.
*Modal Damping
1, 20, 0.2
**
** LOADS
**
** Name: Load-1   Type: Body force
*Dload
Set-46, BZ, -53.389
**
** OUTPUT REQUESTS
**
**
** FIELD OUTPUT: F-Output-2
**
*Output, field
*Node Output
A, AT, TU, U, V
**
```

```
** HISTORY OUTPUT: H-Output-1
**
*Output, history, variable=PRESELECT
*End Step
```